PhD Thesis

Energy Efficient Passenger Comfort in Underground Subway Environments

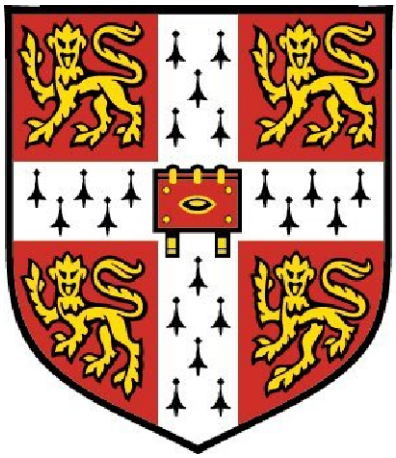

Adnan Mortada

Girton College

University of Cambridge

This dissertation submitted for the degree of

Doctor of Philosophy

December 2016

Acknowledgements

Since I first arrived to Cambridge 4 years ago, I've found myself considerably lucky to have received guidance, advice, and help from so many and so often. These four years have profoundly influenced my life choices and offered an enriching medium for both academic and professional development. I can only list a few names here, and I first start by thanking my supervisor Dr. Ruchi Choudhary.

In my view, she is the ideal supervisor. From the beginning of my research to the time I write these words, Dr. Choudhary has been incredibly supportive and dedicated, always allowing me the space and time to explore new ideas, both in the fields of engineering and beyond. More than that, she became a good friend in the process, and for that I am grateful.

I have to also thank my advisor, Professor Kenichi Soga for his simultaneous encouragement and guidance. It has been a great opportunity for me to learn from him over the last years, especially in the fields of geotechnics where his knowledge and expertise is unequivocal.

I have to also thank Per Sahlin, the CEO of EQUA in Sweden, for contributing IDA tunnel software for modeling the London Underground. I want to also thank EQUA's technical team for assisting me to get familiar with IDA tunnel at the beginning of my PhD.

Many thanks go to my colleagues in the Energy Efficient Cities Initiative, who have been a pleasure to work with over the years. In particular, special thanks to Yohei Kiguchi, Rebecca Ward, and Joris Doumouro who has helped tremendously in discussing the ideas and methods behind the Subway spaces simulations, not to mention being fantastic travel companions in Hyderabad and Turin.

I would also like to give thanks to my friends and college mates who have encouraged and supported me over the past four years and always offered encouragement. In particular Carlos, Jinan, Larissa, Fabio, Daniel, and Hanane who have been a consistent source of intellectual stimulation and enjoyment.

To my parents, Laila, Riad, and my brother Adriano: you have been patient not only with my absence but with the lack of phonecalls that came with it. I hope you understand that my family was often on my mind over the last years, though maybe I didn't show it as frequently as I could have. Thank you so much for having always been supportive of me.

Abstract

Underground subway systems provide an efficient high capacity public transportation method for commuters within dense urban areas. Passengers using underground subway systems are subjected to enclosed and crowded environments that must be controlled to maintain tolerable temperatures and ventilation.

Modern subway stations and trains are cooled using conventional air conditioning, providing acceptable levels of passenger comfort. However, deep and old subway systems suffer from overheating problems, because they were built before the invention of modern mechanical ventilation and air conditioning, resulting in passenger discomfort and health issues during summer conditions (Gilbey et al., 2011). These systems were not designed to handle the high numbers of passengers and train traffic in current congested cities such as London or New York. The oldest deep subway lines such as the London Underground (1863), Paris (1900), New York (1902), Berlin (1902) , and Moscow Metro (1935), commonly experience overheating problems (Griffiths, 2006). When high ambient temperatures are combined with heat rejected from train braking and passenger traffic, the temperatures of the tunnels and platforms rise substantially above tolerable levels. The London Underground, particularly the deep sections have become uncomfortable during summer due to congestion and poorly ventilated tunnels, where during the 2006 European heat wave, temperatures as high as 47 °C were recorded (Griffiths, 2006). Retrofitting old deep subway systems with air conditioning is often infeasible, because the tunnels only allow enough room for trains. Furthermore, heat rejected from air-conditioning in these narrow tunnel spaces could in fact further exacerbate the overheating problems.

As a result, temperatures in old subway tunnels (and surrounding ground) have increased over long term (Botelle et al., 2010). The shallow ground surrounding an old overheated subway system thus has a large potential of low enthalpy energy that can be used for low-grade heating and cooling purposes. Advances in ground source heat pump configurations makes it possible to consider extracting this geothermal energy in an efficient manner (Nicholson et al., 2014).

The objective of this thesis is to investigate the use of stand-alone standard closed loop vertical Ground Source Heat Exchangers (GHE) to extract excess heat from old and deep subway tunnels. Because vertical GHEs are physically and structurally independent of the underground subway structure, they can be positioned flexibly around the tunnels. Furthermore, vertical closed loop GSHP systems are standard in urban areas because they can be easily installed, do not require large spaces, and yield good system efficiency (Kavanaugh and Rafferty, 1997). In the UK, they

also qualify for subsidies under the UK Government's Renewable Heat Incentive Scheme (DECC, 2014a). To evaluate the potential of vertical GHEs for usefully extracting excess heat from the subway tunnels, one must be able to quantify the net gains: How much useful heat can be feasibly extracted from underground tunnels over a time period ? What is the optimal GHE set-up that could maximize heat extraction ? and what are the resulting temperature drops in the underground tunnels and platforms ?

This thesis presents a novel co-simulation framework designed to answer the above questions through simulation modelling. It couples a 1D model of a subway line with a 3D FEM model of vertical ground heat exchangers. The 1D subway model represents spatially averaged transient heat and air flows in the underground, while the FEM model simulates vertical close-loop GHEs next to the subway tunnels. The two models are co-simulated such that information is passed back and forth through a common temperature boundary layer at the outer tunnel walls until both models converge. As a result, the cooling effect of vertical GHEs on the underground climate is examined. In addition, the heat extraction rates of the GHEs placed next to the subway tunnels are compared with standard GHEs. Different arrangements and distances of the GHEs with respect to the tunnels are also examined to achieve the best heat extraction and cooling in the tunnels and stations simultaneously. Finally, partially insulated GHEs are investigated to provide for both heating and cooling demand, because the need to extract heat from the subway is most during the summer months, when demand from building is also for cooling.

As an illustrative study, the London Underground's Central line is selected as a representative of an old subway system that suffers from overheating and ventilation problems. The Central Line is one of the busiest line of the London Underground, and suffers from over heating problems particularly during summer conditions, where temperatures above 35 C have been recorded in some areas (Gilbey et al., 2011). Retrofitting the Central Line with vertical closed loop GHEs is investigated to examine its benefits both underground and overground: In addition to the cooling effect in the train tunnels, the heat extracted from the Central Line system is quantified against the heating demand of the surrounding buildings above the tunnels. It is shown that the GHEs enhance the passenger thermal comfort, while providing district heating to the buildings above.

Table of Contents

List of Figures

List of Nomenclature

IDA Tunnel Air Flow Model

Symbol	Description	Unit
a_v	Train Frontal Area	$[m^2]$
A_t	Area of a Segment	$[m^2]$
A_{tr}	Region Area	$[m^2]$
B_s	Buoyancy Forcing Function for a Ventilation Shaft Section	$[m^2/sec^2]$
${C_{Bt}}^+$	Total Head Loss Coefficient for Turning, Expansion, Contraction Losses, etc. for the case of a Positively Directed Flow at the Backward End of a Segment	$[-]$
${C_{Bt}}^-$	Total Head Loss Coefficient for Turning, Expansion, Contraction Losses, etc. for the case of a Negatively Directed Flow at the Backward End of a Segment.	$[-]$
C_{DvB}	Aerodynamic Drag Coefficient for Train Back	$[-]$
C_{DvF}	Aerodynamic Drag Coefficient for Train Front	$[-]$
C_D	Train Aerodynamic Drag Coefficient	$[-]$
${C_{Ft}}^+$	Total Head Loss Coefficient for Turning, Expansion, Contraction Losses, etc. for the case of a Positively Directed Flow at the Forward End of a Segment	$[-]$
${C_{Ft}}^-$	Total Head Loss Coefficient for Turning, Expansion, Contraction Losses, etc. for the case of a Negatively Directed Flow at the Forward End of a Segment	$[-]$
D_{vF}	Aerodynamic Drag on Front of Train	$[-]$
E	Surface Roughness	$[mm]$
f	Darcy-Weibach Friction Factor	$[-]$
f_t	Segment Darcy-Weibach Friction Factor	$[-]$
f_{tr}	Region Darcy-Weibach Friction Factor	$[-]$
F_S	Surface Forces	$[N]$
F_B	Body Forces	$[N]$
g	Gravitational Acceleration	$[m/sec^2]$
h_l	Major Head Losses	$[m^2/sec^2]$

h_{lm}	Minor Head Losses	$[m]$
h_T	Total Head Losses	$[m]$
H_x	Total Head at Point x or Node x	$[m]$
ΔH	Contribution to Total Head by Region	$[m]$
J	Change of H along a junction	$[m]$
K_{vB}	Coefficient Defined as the Change in Static Pressure Over the Back of the Train is Related to the Velocity Head Relative to the Back of the Train	$[-]$
K_{vF}	Coefficient Defined as the Change in Static Pressure Over the Front of the Train is Related to the Velocity Head Relative to the Front of the Train	$[-]$
K_x	Coefficient Defined as the Change in Static Pressure at Point x	$[-]$
l_t	Segment Length	$[m]$
l_{tv}	Train Length in Segment	$[m]$
l_v	Train Length	$[m]$
L	Length	$[m]$
L_t	Segment Length	$[m]$
P	Pressure	$[Pa]$
P_t	Segment Perimeter	$[m]$
P_v	Train Perimeter	$[m]$
Q_s	Volume Flow Rate of Air in a Section	$[m^3/sec]$
R	Gas Constant for Air	$[J/kg\,K]$
Re	Reynolds Number	$[-]$
T_o	Ambient Air Temperature	$[K]$
T_s	Section Air Temperature	$[K]$
U_v	Train Velocity	$[m/sec]$
V	Air Velocity	$[m/sec]$
V_t	Segment Air Velocity	$[m/sec]$
w_s	Section Forcing Function	$[m^2/sec^2]$
W	Weight Force	$[N]$
W_o	Weight per Unit Area of Ambient Column of Air	$[kg/m^2]$

W_s	Weight per Unit Area of Column of Air in a Ventilation Shaft Section	$[Kg/m^2]$
X_{α_1}	First Coefficient of Fitted Fan Curve	$[sec/m^7]$
X_{α_2}	Second Coefficient of Fitted Fan Curve	$[1/m^4]$
X_{α_3}	Third Coefficient of Fitted Fan Curve	$[1/m\,sec]$
X_{α_4}	Fourth Coefficient of Fitted Fan Curve	$[m^2/sec^2]$
z	Height	$[m]$
Z_s	Section Volume Flow Rate Inertial Term	$[1/m]$
ΔZ	The Contribution to the Section Inertial Term by Region	$[1/m]$
ρ	Density	$[kg/m^3]$
ρ_o	Ambient Air Density	$[kg/m^3]$
ρ_s	Segment Air Density	$[kg/m^3]$
λ_v	Train Darcy-Weisbach Friction Factor	$[-]$
$\Gamma_{s\alpha}$	Forcing Function Caused by Presence of Operational Fan in Ventilation Shaft	$[m^2/sec^2]$
σ_{tv}	Tunnel Blockage Ratio	$[-]$
Ω	Loop Forcing Function	$[m^2/sec^2]$
τ	Shear Stress	$[N/m^2]$
$\sum_{st}$	Summation Over all Segments in a Section	$[-]$
$\sum_{tr}$	Summation Over all Regions in a Segment	$[-]$

IDA Tunnel Heat Transfer Model

Symbol	Description	Unit
a	Train Frontal Area	$[m^2]$
$A_{ann.}$	Amplitude of Annual Air Temperature Fluctuation in the Tunnel	$[K]$
A_{Brake}	Heat Transfer Surface Area of Brake Unit	$[m^2]$
A_c	Convective Heat Transfer Area	$[m^2]$
A_{di}	Amplitude of Diurnal Temperature Fluctuation in the Tunnel	$[K]$
A_r	Radiative Heat Transfer Area	$[m^2]$
A_w	Wetted Surface Area of the Tunnel	$[m^2]$
A_{wi}	Tunnel Wall Surface Area in Segment i	$[m^2]$
C_{Brake}	Heat Capacity of Brake Unit	$[kJ/K]$
C_c	The Duty Cycle of the Compressor	$[\%]$
C_D	Train Aerodynamic Drag Coefficient	$[-]$
C_{m-g}	The Duty Cycle of the Motor Generator	$[\%]$
C_p	Specific Heat Capacity of Air	$[J/kg\,K]$
C_{Train}	Active Heat Capacity of Train Body	$[kJ/K]$
d_a	Distance to Accelerate to Maximum Speed	$[m]$
D_g	Specific Heat Capacity of Air	$[J/kg\,K]$
F_D	Aerodynamic Force Drag	$[N]$
F_M	Mechanical Resistance of Single Train Car	$[N]$
Gr_D	Grashof Number	$[-]$
$\bar{h}$	Average Convection Heat Transfer Coefficient	$[W/m^2K]$
h_c	Convection Heat Transfer Coefficient	$[W/m^2K]$
h_i	Convection Heat Transfer Coefficient at Segment i	$[W/m^2K]$
h_w	Convection Heat Transfer Coefficient for a Wetted Tunnel Surface	$[W/m^2K]$
h_{wi}	Convection Heat Transfer Coefficient for a Tunnel Wall at Segment i	$[W/m^2K]$
H_D	Convection Heat Transfer Coefficient for a Tunnel Wall at Segment i	$[kg_{water}/kg_{air}]$

H_i	Design Specific Humidity	$[kg_{water}/kg_{air}]$
i	Supplied Current to the Resistor Grids	$[A]$
I	Average Starting Current per Motor	$[A]$
k_x	Thermal Conductivity at Region x	$[W/m\,K]$
K_m	Kinetic Energy Coefficient	$[-]$
KE	Kinetic Energy of The Train at Maximum Speed	$[J]$
KE_{step1}	Kinetic Energy of the Train at First Transition Speed	$[J]$
$\dot{m}$	Evaporation Rate	$[kg/sec]$
M	Average Train Empty Mass	$[kg]$
M_{DG}	Deceleration Resistor Grid Mass	$[kg]$
M_i	Mass of Air in Subsegment i	$[kg]$
$M_{p,i}$	Mass Flow Rate Leaving Subsegment i at the Forward End	$[kg]$
$M_{n,i}$	Mass Flow Rate Leaving Subsegment i at the Backward End	$[kg]$
n	Number of Carriages per Train	$[-]$
N	Number of Trains per Hour	$[1/hr]$
N_{cars}	Total Number of Carriages per Train	$[-]$
N_{FC}	Number of Ticket Sale Boxes	$[-]$
N_{MB}	Number of Mezzanine Businesses	$[-]$
N_p	The Number of Passengers Passing Through the Station at Peak Hour	$[1/hr]$
P_c	The Power Rating of the Air Compressor	$[W]$
P_{in}	Energy Rate into the Underground System Grid	$[W]$
P_m	Maximum Useful Power	$[W]$
P_{m-g}	The Power Rating of the Motor Generator	$[W]$
Pr	Prandtl Number	$[-]$
$q_{aircomp}$	The Heat Rejection from the Air Compressor	$[W]$
q_{AC}	The Total Heat Rejection from the Air Conditioning Unit	$[W]$
q_D	The Heat Gain due to Aerodynamic Drag	$[W]$
q_i	The Rate of Heat Added into Subsegment i Excluding Environmental Control	$[W]$
q_m	The Rate of Heat Gain due to Traction Motor Losses	$[W]$
q_M	The Rate of Heat Gained due to Mechanical Resistance	$[W]$

q_{m-g}	The Heat Rejection from the Motor Generator	$[W]$
q_{Mstep1}	The Rate of Heat Gain due to Mechanical Resistance from the Train at First Transition Speed	$[W]$
q_{SR}	Starting Resistor Heat Losses	$[W]$
q_{step1}	Starting Resistor Heat Losses for First Step of Cam-Controlled Series	$[W]$
q_{step2}	Starting Resistor Heat Losses for Second Step of Cam-Controlled Series	$[W]$
q_{step2}	Total Steady State Train Carriage Heat Rejection	$[W]$
QAC_i	Rate of Heat Added into Subsegment due to Environmental Control	$[W]$
Q_{conv}	Rate of Heat Released by Convection	$[W]$
Q_{FC}	Rate of Heat Released by Ticket Sale Boxes	$[W]$
Q_{MB}	Rate of Heat Released by Mezzanine Businesses	$[W]$
Q_{out}	Rate of Heat Released by the Train's Resistor Grids	$[W]$
Q_P	Rate of Heat Released by the Passengers	$[W]$
Q_{rad}	Rate of Heat Released Radiation Heat Exchange	$[W]$
Q_{SL}	Rate of Heat Released by Station Lights	$[W]$
Q_{TL}	Rate of Heat Released by Tunnel Lights	$[W]$
$Q_{3,4R}$	Third and Fourth Rail Heat Losses During Acceleration	$[W]$
r	Radius	$[m]$
R	Resistance	$[\Omega]$
$Rate_{AC}$	Rating of the Air Conditioning Unit Based on the Amount of Heat Extracted from One Train Carriage	$[W]$
$Regen$	Regeneration Braking Efficiency	$[-]$
t	Time	$[sec]$
$\bar{t}$	Average Dwell Plus Travel Time Between Station Stops	$[sec]$
t_a	Time to Accelerate to Maximum Speed	$[sec]$
$T_{ann.avg.}$	Tunnel Annual Average Temperature	$[K]$
T_1	Temperature at Region 1 in the Tunnel Wall	$[K]$
T_2	Temperature at Region 2 in the Soil	$[K]$
T_{ds}	Deep Sink Soil Temperature	$[K]$
T_D	Design Temperature in Segment i	$[K]$

T_{DB}	Air Dry Bulb Temperature	$[K]$
T_i	Air Temperature at Segment i	$[K]$
T_g	Average Resistor Grid Temperature	$[K]$
$T_{G,E}$	Resistor Grid Temperature at Thermal Equilibrium	$[C]$
T_w	Average Tunnel Wall Temperature	$[K]$
T_{WB}	Air Wet Bulb Temperature	$[K]$
U	Maximum Train Speed	$[m/sec]$
$\bar{U}$	Average Train Speed	$[m/sec]$
V	Average Maximum Train Speed Attained Between Stops	$[m/sec]$
V_O	Third and Fourth Rail Voltage Summation	$[V]$
V_r	Free Stream Velocity of Air Relative to the Grid	$[m/sec]$
$w_{an.}$	Annual Frequency	$[-]$
w_{di}	Diurnal Frequency	$[-]$
w_i	Mass of water vapor introduced into subsection i	$[-]$
W	Mass of Train Carriage Excluding Passengers	$[kg]$
W_e	Mass of Train Carriage Including Passengers	$[kg]$
W_{FC}	Power Expended by Ticket Sale Boxes	$[W]$
W_{MB}	Power Expended by Mezzanine Businesses	$[W]$
W_{SL}	Power Expended Rate by Station Lights	$[W]$
W_{TL}	Power Expended Rate by Tunnel Lights	$[W]$
α_1	Thermal Diffusivity for Tunnel Wall	$[J/m^3\,K]$
α_2	Thermal Diffusivity for Soil	$[J/m^3\,K]$
Γ	Temperature Coefficient of Volume Expansion of Air	$[-]$
ϵ	Emissivity of Resistor Grid	$[-]$
ϵ_m	Train Motor Efficiency	$[-]$
ρ	Density	$[kg/m^3]$
σ	Stephan-Boltzmann Constant	$[W/m^2K^4]$
μ	Dynamic Viscosity	$[kg/m\,\mathrm{sec}]$
ν	Kinematic Viscosity	$[m^2/sec]$
λ	Latent Heat of Vaporization	$[J/kg]$

Train Carriage Model

Symbols

Symbol	Description	Unit
A	Area	$[m^2]$
c	Specific Heat Capacity	$[J/kg\,K]$
$c^{'}$	Heat Capacity per Unit Material Area	$[J/m^2\,K]$
C	Humidity	$[kg_{water}/kg_{air}]$
COP	Coefficient of Performance	$[-]$
d	Characteristic Length	$[m]$
f_{cl}	Clothing Area Factor	$[-]$
g	Gravitational Acceleration	$[m/sec^2]$
Gr	Grashof Number	$[-]$
h	Convection Heat Transfer Coefficient	$[W/m^2K]$
h_c	Convective Heat Transfer Coefficient	$[W/m^2K]$
h_{fg}	Latent Heat for Water Condensation	$[J/kg]$
i_{cl}	Clothing Vapor Permeation Efficiency: Ratio of Actual Evaporative Heat Flow Capability Through Clothing to Sensible Heat Flow Capability as Compared to Lewis Ratio.	$[-]$
I	Clothing Insulation Resistance	$[clo]$
I_{cl}	Clothing Insulation Resistance	$[clo]$
I_t	Clothing Insulation Resistance for the Case of Air Velocity Less Than 0.2 m/sec and Mean Radiant Temperature Equal to Air Temperature	$[clo]$
L	Length	$[m]$
Le	Lewis Number	$[-]$
MET	Body Metabolic Rate	$[W/m^2]$
N_p	Maximum Number of Persons on Train	$[-]$
Nu	Nusselt Number	$[-]$
Pr	Prandtl Number	$[-]$
Q_{Cond}	Condenser Heat to Tunnel and Platform Air	$[kW]$

Q_D	Air Flow Rate Through the Train Doors	$[m^3/sec]$
Q_{Evap}	Evaporator Heat taken from the Train Compartment	$[kW]$
Q_g	Heat Generated Inside the Train	$[W]$
Q_L	Latent Heat Transfer	$[W]$
Q_{lights}	The Heat Released by Train Lights	$[W]$
Q_P	Latent Heat Transfer	$[W]$
Q_V	Convection Heat Transfer	$[W]$
R	Infiltration Rate	$[ACH]$
R_{cl}	Thermal Resistance of Cloth	$[m^2K/W]$
S_p	Occupancy Coefficient (Schedule)	$[-]$
T	Temperature	$[C]$
T_{high}	Compartment Cooling Set-Point	$[C]$
T_{low}	Compartment Heating Set-Point	$[C]$
U_L	Air Speed at the Train Door	$[C]$
V	Speed	$[m/sec]$
W_{AC}	AC Electric Power	$[kW]$
Γ	Temperature Coefficient of Volume Expansion of Air	$[-]$
ρ	Density	$[kg/m^3]$
μ	Dynamic Viscosity	$[kg/m\,\mathrm{sec}]$
ν	Kinematic Viscosity	$[m^2/sec]$

Subscripts

Subscript	**Description**
a	air
b	Bulk Fluid
c	Train Cover
$conv$	Convection Heat Transfer
$comp$	Compartment
D	Train Door
g	Train Glazing
i	Internal Air Inside Train Carriage
$isat$	Internal Saturation Air Temperature Inside Train Carriage
$plat$	Platform
rad	Radiation Heat Transfer
sd	Solid Surface
va	Humid air
w	Train Carriage Wall

Chapter 1

Introduction

1.1 Overheating Problems in Subway Systems

Regardless of whether we refer to them as metros, tubes, or subways, underground transportation systems provide an efficient high capacity public transportation method for commuters within dense urban areas. This form of public transportation plays a significant role in reducing road congestion as well as filling the gaps in insufficient over ground public transport and road capacity. There are 160 subway rail systems around the world, distributed over 55 countries (UITP, 2014), where the London Underground is the oldest underground rail system dating back to 1863 (TfL, 2016a), while other large systems include New York, Beijing, Shanghai, Seoul, Tokyo and Moscow. In Europe, there are 71 subway networks in 20 countries. They represent more than 3000 km of tunnels and railway lines. Overall, there are more than 4000 stations distributed over more than 260 lines. Of these 71 networks, three were created before 1900 and eight after 2000. Subway systems are large energy consumers at a regional scale and the largest within a city. In large metropolitan areas such as London, the subway systems consume energy as much as 250,000 households (SEAM4US, 2014). For instance in India, the Delhi Metro Rail Corporation is the largest consumer of electricity in the state of Delhi. Typical figures regarding the consumption of electricity in the state of Delhi are approximately 300 TJ (SEAM4US, 2014). A third of the required energy goes to operating the subsystems of the subway such as lights, escalators, and ventilation, where the stations of the Barcelona metro system consume 63.1 million kWh of electricity annually (Fraunhofer, 2014).

Old subway systems particularly the deep ones, were not designed to handle the current high number of passengers and were built before the invention of modern ventilation systems and air conditioning. The combination of high ambient temperatures, rejected heat from train braking along with increased number of trains, and passenger congestion generates large amounts of rejected heat,

which results in a substantial increase in the subway environment's air temperature and the surrounding ground temperature. Consequently, these subway spaces suffer from over heating problems resulting in passenger discomfort and health issues (Gilbey et al., 2011). Overheating problems are now common among the oldest deep subway lines such as the London Underground (1863), Paris (1900), New York (1902), Berlin (1902), and Moscow Metro (1935) (BBC, 2006). During summer, some sections of the London Underground experiences temperatures reaching to 40 °C (Gilbey et al., 2011), while in the New York Subway and Berlin Subway temperatures as high as 38 °C and 33 °C have been recorded in the platforms (NA, 2014). The London Underground, particularly the deep sections have become uncomfortable during summer due to its congestion and poorly ventilated tunnels, where during the 2006 European heat wave, static air temperatures (SAT) as high as 47 °C were recorded inside the tunnels (Griffiths, 2006). Currently, during elevated summer temperatures, Transport for London (TfL) distributes bottles of water to mitigate passenger discomfort and dehydration during summer as part of the "Beat the Heat and Travel Better" campaign (TfL, 2014), and also deploys fans across the stations to increase air circulation. These measures have been insufficient, because they did not address the main issues causing the overheating in the system, which are high ambient air temperatures, train braking, and passenger congestion. TfL has published a map (Figure 1.1), that shows the daily average hot temperature spots during summer within the London Underground, which reaches 32 °C in the Central, Piccadilly, and Bakerloo lines during the peak time period between 4 pm to 6 pm.

In modern subway systems conventional air conditioning is installed in stations and aboard trains, however it remains troublesome in old deep lines because of problems in spacing the equipment and the issue of dispersing the air condition's wasted heat, that would make the tunnels even warmer (Gilbey et al., 2011). The situation can be further exacerbated by climate change in the future, where it has been scientifically established that the average SAT temperature is gradually increasing. According to temperature analysis conducted by scientists at NASA's Goddard Institute for Space Studies, the average global temperature has increased by about 0.8 °C since 1880 (NASA, 2016). Two-thirds of the warming has occurred since 1975, at a rate of roughly 0.15-0.20 °C per decade. Between 2014 and 2100 the United States Environmental Protection Agency projects that increases in average global temperatures are expected to range between 1.5 °C to 4.6 °C by 2100, depending on future greenhouse emission scenarios and the mitigation of greenhouse gas emission measures implemented by governments. This anticipated increase in temperatures has implications on these old subway systems by further worsening the overheating problems, since the outside temperature increase will result in high temperatures inside underground spaces (Arkell and Darch, 2006).

1.2 Cooling Solutions to Old and Deep Subway Systems

Modern subway stations and trains are cooled using conventional air-conditioning which aims to keep the air temperatures under control, providing acceptable levels of passenger comfort. However the big challenge remains to cool the old deep level parts of subway systems such as the London Underground, where the tunnels are so narrow that only allows enough room for trains to fit. As a consequence, there is no space for on board train air-conditioning in the deep lines.

The shallow subsurface lines in the London Underground (Circle, Hammersmith & City, Metropolitan, and District) have been equipped with new trains in 2010 that have standard train air-conditioning, since the trains are large enough to fit them and the subsurface tunnels have enough large space to displace the exhausted hot air from the air-conditioning units. There are initial studies to install air-conditioning on board the new deep line trains that are planned to be rolled out in the London Underground. This is still under question (LU, 2014), because the dissipated heat from the air conditioning in these narrow spaces could in fact further exacerbate the overheating problems in the tunnels and platforms. This effect has been demonstrated in the New York Subway,

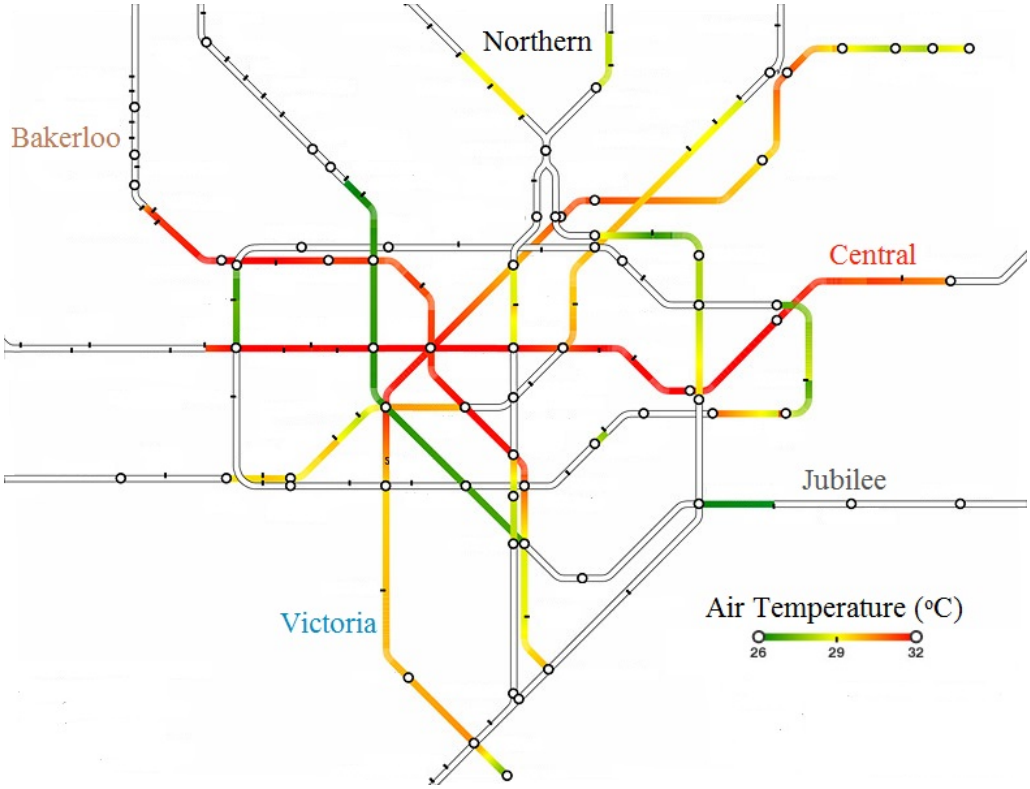

Figure 1.1: Temperature hotspots map in the London Underground during summer (Tfl, 2014).

where the first trial train air-conditioning was in 1955 (Jaffe, 2012). Currently, all the New York subway trains have been equipped with air-conditioning but that came at a price subway riders are still paying today. The energy needed to run the cooling systems emits a great deal of heat that gets trapped in the subway stations and tunnels. In other words, as subway cars have cooled down, the subway platforms have heated up (NYCTA et al., 2010). Also, Transport for London (TfL) is planning to introduce regenerative braking to the London Underground trains, which would decrease the amount of heat released, capturing some of the released heat from the train brakes and feeding the energy back as electricity into the grid which would contribute to lowering the temperature of the subway (Gilbey et al., 2011). This solution was implemented in the New York Subway, but did not result in significant reduction of the platform and tunnel temperatures (Jaffe, 2012). TfL is also investigating cooling the London Underground trains using blocks of ice inside the train, which act as a phase exchange medium in a thermal storage system. It is planned to trial having a condenser and evaporator unit under the train carriage of a Piccadilly Line train, circulating water through the phase change medium when the train is outside, building ice, then a little bit of residual cooling would go to a cooling coil then back to the condenser and evaporator unit. When the train is outside, it could be building ice, in the open section where heat rejection is not a problem, then when in the tunnels the evaporator and condenser units are turned off, then water is circulated around the phase change medium to melt the ice and cool the carriage using a closed water circuit (Westgate and Gilby, 2007).

Conventional air-conditioning for old and deep subway systems in the London Underground prove to be a daunting task because of the massive costs involved (Thompson et al., 2006). The team responsible for cooling the London Underground estimated that removing heat from the network using conventional air-conditioning would cost an average of 30 times the cost of putting the heat inside the system (IPlantE, 2007).

Cooling of the underground railway environment may also be achieved by using groundwater to directly cool the air within the tunnel (Figure 1.2). The ground water in London is located below the underground tunnels at the level of 40 m below ground level (Thompson et al., 2006). The ground water at that level has an average temperature of 12 °C. At first groundwater is pumped through heat exchangers, where hot air in the underground railway network is cooled and then circulated by fans into the platforms. Then the trains act as giant pistons, which will circulate the air around the underground railway network, where fans on top of trains suck in air to cool the train carriages.

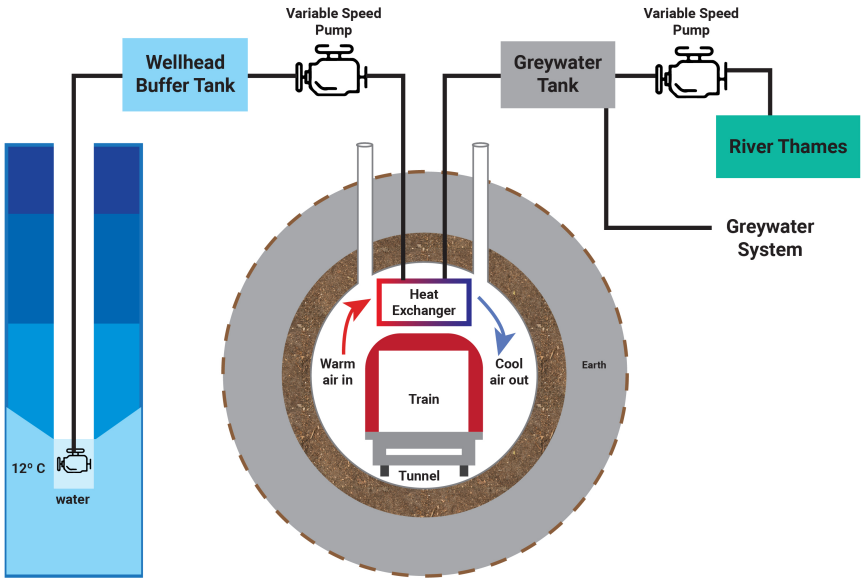

Figure 1.2: Schematic diagram of groundwater cooling. (based on (Ampofo et al., 2004c)).

The use of naturally occurring seepage water from rainfall and the river Tyburn which runs beneath the station to provide air cooling is being trialed in the middle and lower concourse of the Victoria Station. The air cooling units use fans to exchange heat with the water. The beneficial cooling effect from the existing discharge of water gave a temperature cooling of 2 degrees during the trial (Westgate and Gilby, 2007). This ground water can be potentially fed into a greywater system serving toilet cisterns, to reduce the demand for refined mains water, and then discharged in London into the river Thames (Thompson et al., 2006).

Ampofo et al. (2003) investigated in a three part paper extensively the overheating problems encountered in deep underground subway systems. In the first part of his paper Ampofo et al. (2003) reviewed published work on thermal comfort for the underground subway environment where he attempted to define a thermal comfort criteria for the underground subway environment. Ampofo et al. (2003) realized that the transient and special nature of the underground subway systems requires a distinct thermal comfort criteria.

In his second part of the paper Ampofo et al. (2004a) developed a mathematical steady state model to model the environment in a generic deep underground subway system. Ampofo et al. (2004a)

analyzed the main heat sources and sinks in the underground subway system, and has shown that the main heating source in the tunnel is train braking and in the train carriage the passengers. Ampofo et al. (2004a) has shown that additional cooling to the existing rolling stock may be provided by cooling the tunnels where the trains operate.

The third part of the paper investigated the potential methods of delivering cooling to deep underground railway environment (Ampofo et al., 2004c). The suitability of each cooling method is assessed utilizing the steady state mathematical model developed in Ampofo et al. (2004a). The model investigated several cooling methods for the London Underground: ground water cooling, air conditioning and air cycle units, ventilation fan rate increase, heat pipes to modify the thermal conductivity of the soil, regenerative braking, light weight cars, speed restrictions, train lighting reduction. Ampofo et al. (2004a) also compared these cooling method's effectiveness in cooling the tunnels and train carriages and their electricity consumption as seen in Figure 1.3. It is important to note that Ampofo et al. (2004a) model is steady state and has used constant convection heat transfer coefficients, while in reality heat and air flows in the subway system are transient in nature (Revez et al., 2015).

Recently there has been an interest in using heat pump technology to cool the tunnels in the subway systems. Heat pumps are being trialled in several subway systems and are planned to be implemented in the new Crossrail in London, where the following section discusses their uses and benefits.

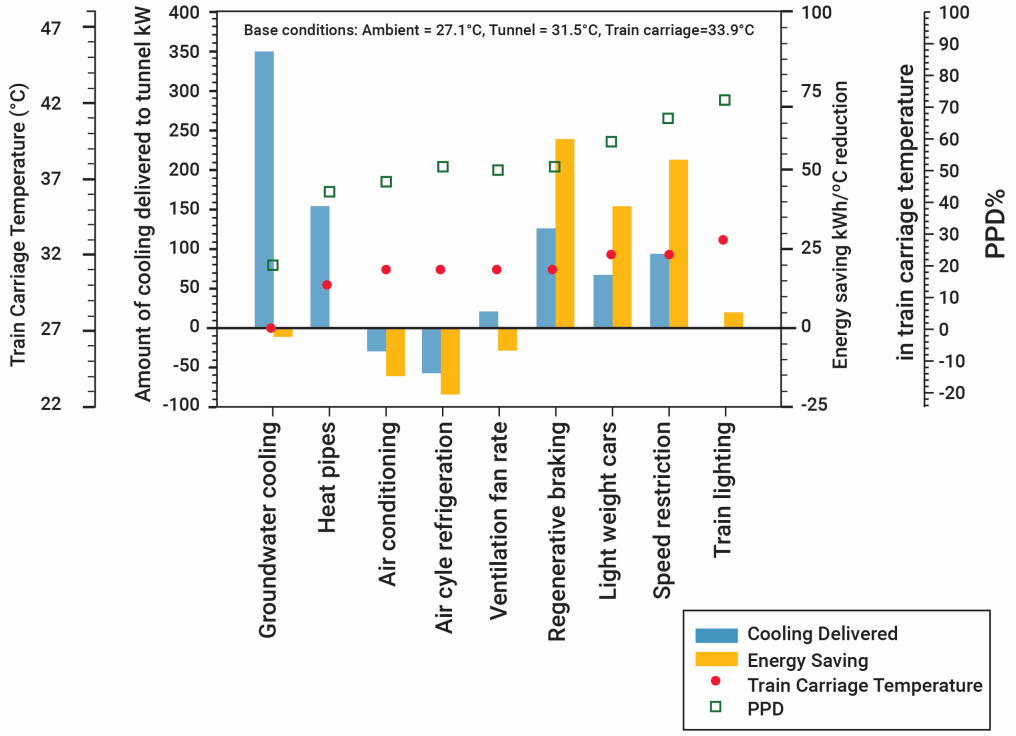

Figure 1.3: Comparison of cooling methods. (based on (Ampofo et al., 2004c)).

1.3 Geothermal Heat Pumps for Cooling Subway Systems

Existing subway systems such as the London Underground system have experienced long term increase in the temperature within tunnels and in the surrounding ground (Botelle et al., 2010). The shallow ground surrounding the subway system has a large potential of low enthalpy energy that can be used for heating and cooling purposes. Advances in ground source heat pump technology makes them increasingly feasible to capitalize on geothermal energy present in the ground (Nicholson et al., 2014). The biggest advantage of geothermal energy is that the soil temperature reaches a constant at a depth of approximately 10 to 15 m below surface. For instance, in Central London the soil temperature at 14 m below surface remains undisturbed at 14 °C (GLA, 2013).

Recent developments has seen the use of foundation piles, diaphragm walls, and base slabs as ground heat exchangers (Adam and Markiewicz, 2009), (Brandl, 2006), and (Fry, 2009). For example, thermal piles and walls involve attaching polymer absorber pipes to the reinforcement cages and this approach has been applied to Crossrail stations in London. Other application examples involving sprayed concrete linings include the tunnels at Stuttgart Metro U6 (Schneider and Moormann, 2010), Lainzer Tunnel (Franzius and Pralle, 2011) and the metro stations in the Vienna U2 subway line (Brandl et al., 2010). Heat-exchanger pipes have been placed along the lengths of the Channel Tunnel to extract heat from inside the tunnel. Franzius and Pralle (2011) discussed embedding plastic absorber pipes in the precast concrete tunnel segments of a conventional metro to collect heat from the adjacent ground. The heat is then transferred via header pipes to the ground surface, and then connected to heat pumps to supply the heat to buildings. The Crossrail project is planning to introduce thermal pile systems into its new station boxes currently under construction. These will be available for heating the overlying site developments above the stations and will help cool the station (Nicholson et al., 2014).

There has not been any attempt to retrofit existing old and deep subway systems with GSHP (Ground Source Heat Pump) systems as in the London Underground. Vertical closed loop GSHP systems are very popular in urban areas, because they do not require large spaces, and have a large system efficiency (Kavanaugh and Rafferty, 1997). Closed loop GSHP systems operate by pumping anti-freeze or refrigerant fluid through pipes or boreholes in the ground, and can be flexibly installed everywhere without considering geological conditions. On the other hand, open loop GWHP systems directly extract groundwater through a borehole, and then pump it to a heat pump, so this system requires a good underground aquifer close by, which restricts its operational area (Zhang et al., 2015b). The UK Environment Agency estimates that among the 8000 GSHP systems installed in the UK in 2009, only 300 are open loop. Closed loop GSHP's operate using conduction heat transfer, and they are not regulated. Open loop GSHP systems rely on advection heat transfer and are regulated by the UK environmental agency to achieve ground balance between heating and cooling annually (Zhang et al., 2015b). Typically GSHP systems are integrated in modern subway systems during their construction phases, because some of these systems such as embedding plastic absorber pipes in the precast concrete tunnel segments mean that old subway lines need to be reconstructed, which is uneconomical. Closed loop GSHPs would solve this dilemma, because they can be drilled close to the tunnels in old and deep subway systems without taking a lot off space, and can be positioned flexibly depending on the location of the tunnels.

The implementation of GSHP systems in urban environments could have further benefits by accessing the ground source heat generated by underground railways. Revez et al. (2015) have discussed that the literature lacks exploration of the potential for recovering heat in the ground surrounding the tunnels via nearby borehole heat exchangers (Figure 1.4). In order to examine the potential of GSHPs to recover heat from underground subway systems, an investigation of the interaction of GSHPs with the surrounding subway tunnels is required. This PhD thesis will focus on vertical GSHP boreholes as a potential cooling solution to the old and deep sections of the London Underground, while providing district heating and cooling to the buildings nearby.

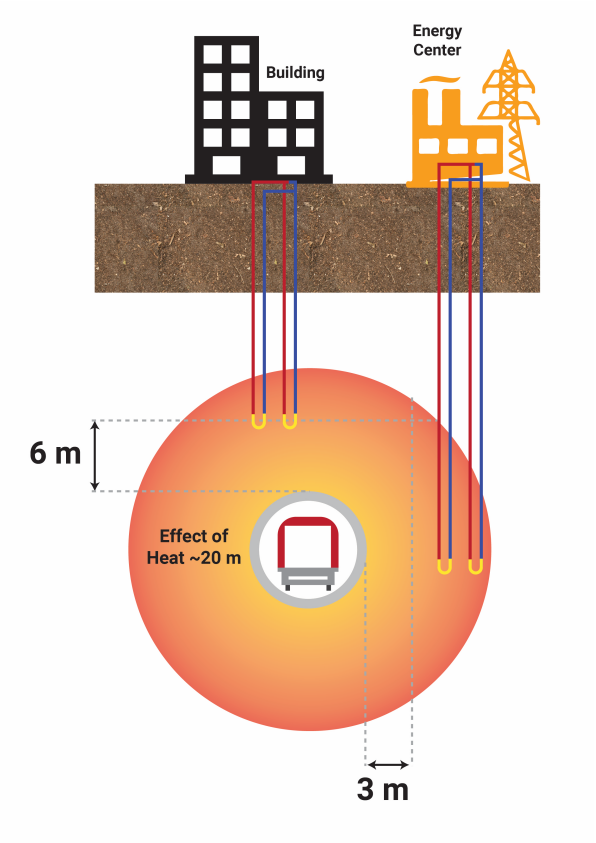

Figure 1.4: Borehole heat exchangers (BHE) for cooling subway systems. (based on (Revez et al., 2015)).

1.4 Modelling Subway Environment

The underground subway environment experiences complex thermal and fluid interactions that are transient in nature. 1D models are suitable for simulating the subway's environment on a large scale of kilometres, since they use a simplified representation of the tunnels, ventilation ducts, and the surrounding soil. Consequently, 1D models cannot provide accurate analysis of more localized optimization problems, such as redesigning ventilation shafts, or particular tunnel sections (Kim and Kim, 2009). Currently, the Subway Environment Simulation Program (SES) 1D software, enables underground tunnel designers to estimate the temperatures, airflows, humidity, as well as air conditioning requirements for subway systems (Brinckerhoff et al., 1976). The SES was developed by Parsons Brinkerhoff under the supervision of the United States Department of Transportation in 1976 (Brinckerhoff et al., 1976). The SES has been constantly updated and improved, where the latest release was in the year of 2000. The updates included modelling of platform screen doors and train skin friction heating (Kennedy et al., 2000). The SES does not provide calculation of the thermal capacitance in the tunnels and trains which causes errors in calculating the heat sink effect of the ground that might reach as high as 50 % (Brinckerhoff et al., 1976). This makes the SES unable to make credible predictions for thermal storage and geothermal-based cooling systems.

IDA tunnel is the most recent 1D tunnel simulation software, that simulates the tunnel heat and airflows. It was developed by EQUA in 1995 (IDA, 2006), and based its fundamental equations and concepts on the SES. IDA tunnel resolves many of the SES's drawbacks and has post-processing capabilities, better visualization of the subway system, and additional features such as pollutant dispersal simulations for particulates, CO, CO_2, NO_x concentrations (IDA, 2006).

IDA tunnel is employed in this thesis to model sections of the London Underground. This is because IDA Tunnel is the latest subway environmental software and has been used in designing various tunnel and subway rail systems.

1.5 3D Finite Element Model of Vertical Ground Heat Exchangers

Several numeric and analytic models exist to model a single or an array of vertical boreholes. These models can be 1D, 2D or 3D, and are either transient or steady state (Connolly et al., 2010). The Kelvens line source model, and the cylindrical heat source model are widely used 1D heat transfer models, which utilize the Fourier law of heat conduction. The line source theory assumes the ground to be an infinite medium with an initial uniform temperature, while the vertical borehole heat exchanger (BHE) is shaped as an infinite line source. The cylindrical heat model assumes a cylindrical borehole with infinite length buried in the ground. This model's equations can be solved analytically through either a constant BHE outer surface temperature or a constant heat transfer rate across the borehole surface (Carslaw and Jeager, 1959) & (Ingresoll and Plass, 1948) . Hellstrom (1991), Kavanaugh (1995),Bernier et al. (2004), and Hikari et al. (2004) have focused on making the 1D analytic BHE models more accurate and comparable to numerical ones (Fayegh and Rosen, 2012). Molina-Giraldo et al. (2011) has developed a new analytical approach in which both axial heat transfer and ground water flow are considered in the thermal analysis of GSHP systems, while previous analytical models used to neglect one of them.

A 2D finite line source model was established by (Zeng et al., 2002). Cui et al. (2006) and Yi et al. (2010) developed a finite 3D vertical BHE analytic models (Yi et al., 2012). However, significant simplifications in the analytical borehole models render them unsuitable for complex geometries and short-time step transient simulations of boreholes (Yi et al., 2012). Numerical models of boreholes are attractive to conduct parametric analysis at small time-steps and when high resolution solutions are required. Consequently, to model the transient thermal interactions of complex geometries such as between multiple vertical boreholes and subway tunnels, a 3D finite element model is required. Stauffer et al. (2013) reviewed and developed series of mathematical tools and simulation models based on analytical and numerical solutions for GWHPs and GSHPs. Stauffer et al. (2013) also based his models on case studies in Austria, Germany, and Switzerland, where Stauffer et al. (2013) focused on urban thermal energy use as well as heat storage and cooling. Stauffer et al. (2013) also developed MATLAB computer codes ready for immediate application or design for GWHP and GSHP systems.

Qi (2015) developed a COMSOL model that models the amount of heat that can be extracted from the Crossrail tunnel and surrounding ground by thermal piles in the proposed Crossrail Dean Street Station, however he introduced fixed temperatures in the tunnel's outer walls as boundary layers, while the tunnel heat and air flow were not modelled.

There has not been any model developed that combines transient simulations in both the subway systems and BHEs, in which the thermal effects of the boreholes on the subway tunnel environment are modelled transiently. This PhD will focus on using 'Comsol', which is a general purpose multi-physics simulation software, to develop a 3D model of vertical close loop BHE and co-simulate it with a 1D subway model.

1.6 Thesis Aims

The main aim of this thesis is to examine the vertical geothermal borehole heat exchangers (BHE) potential in cooling old & deep subway lines to mitigate the subway's overheating problems and enhance passenger thermal comfort, while using the tunnel's wasted heat in the surrounding soil to provide district heating and cooling to the buildings above the tunnels.

In order to do so the following main contributions in the fields of subway environmental modelling and geothermal vertical borehole simulation are explored, developed, and detailed:

- Model a representative section of a deep and old subway line which has overheating problems and validate the model based on measured data. In this case the London Underground's Central Line is chosen as a representative case study.
- Conduct a parametric analysis on the Central Line model, inorder to quantify the extent to which the system's heat sources and sinks can impact the air temperatures in the tunnels and stations.
- Examine several future scenarios, where the Central Line's environment is simulated taking into consideration the future infrastructure & train upgrades in the system, and the passenger & train traffic projections till the year of 2050. Also, the effects of climate change on the London Underground's environment is assessed to determine whether the upgrades in the London Underground's infrastructure will mitigate the overheating problems or at least preserve the status quo.
- The 1D Central Line model is modified to simulate the environmental conditions on other deep lines in the London Underground. The aim is to study the different factors that effect the climate conditions on these deep lines in the London Underground.
- A 3D Finite Element Model (FEM) that includes geothermal vertical boreholes on the tunnel sides is developed using Comsol to asses their potential in cooling the London Underground tunnels and platforms. A methodology for co-simulating The 1D subway model and the 3D FEM borehole model is developed through exchanging boundary outer tunnel wall temperature information in order to model the transient interactions between the boreholes and the tunnel and platform environment.
- The vertical borehole's arrangement and distance with respect to the tunnels is optimized to achieve the optimum heat extraction and tunnel and station cooling. Also, a new concept consisting of partially insulated boreholes is explored. These specialized boreholes alternate between

extracting and injecting heat into the soil simultaneously. These boreholes are modelled using Comsol to assess their potential in coping with building heating and cooling demand simultaneously and improve the overall borehole performance.

- Retrofitting sections of an old and deep line in the London Underground with vertical closed loop boreholes is examined. An ArcGIS-based simulation model for the building heating and cooling demand for Central London is used to investigative the potential for the tunnel retrofitted boreholes to provide district heating and cooling for the buildings above. The Central Line is also chosen as an exemplary case for this study.

- The environmental conditions within the train carriages in the subway system are modelled taking occupants, internal heating sources and ventilation to the surrounding tunnel into account. The cooling requirements of the carriage are also computed. The cooling benefits of the vertical boreholes on the passengers thermal comfort is assessed in the platforms and train carriages. Also, the electrical consumption of air-conditioning on board trains is simulated, where the implementation of vertical boreholes can come as an energy efficient solution to either reduce the electrical consumption of on-board air conditioners or negate the need to install air conditioners in the first place.

The overall structure of this Thesis and a description of each chapter is presented below and summarized in Figure 1.5:

- Chapter 2 describes the history behind modelling the subway climates, and the different simulation techniques that are used for that purpose. This chapter highlights the challenges encountered in the early days of subway builders, in terms of design and air quality. The development of several subway environment simulation software is discussed in this chapter. The chapter also, describes in details IDA Tunnel Software, which is used in this thesis to model the London Underground Environment, and explains the fluid and thermal equations used.

- Chapter 3 describes the methodology used to model a representative section of the London Underground's Central Line, which is used as a case study in this thesis, using IDA Tunnel Software. In this chapter the 1D Central Line model is validated and parametric analysis are conducted on the model. The effects of future infrastructure upgrades, future passenger and train traffic predictions, and climate change are investigated. Other deep and old lines within the London Underground are modelled, taking into consideration the distinct characteristics of each line.

- Chapter 4 Describes the methodology used to co-simulate the 1D Central Line Model and the 3D FEM model of geothermal borehole heat exchangers (BHE) through exchanging boundary outer tunnel wall temperature information. This chapter also, analyses the cooling effect of the geothermal boreholes on the Central Line tunnels and stations. The optimization of the boreholes arrangement and distance with respect to the tunnels is described. The concept of retrofitting the tunnels with partially insulated BHE, that alternate between extracting and injecting heat into the soil, is explored in this chapter.

- Chapter 5 Describes the application of retrofitting the Central Line with vertical closed loop boreholes in the City of London as a case study. The chapter also examines the potential of using the heat extracted from the Central Line system to provide part of the heating and cooling demand in the surrounding buildings above the tunnels. The benefits of using the BHE to enhance the passenger thermal comfort is investigated. In this chapter, the electrical consumption of on-board train air conditioning is simulated along with the impact of the air-conditioning on the Central Line climate.

- Chapter 6 draws out conclusions and outlines possible avenues for future improvements in modeling subway systems and mitigating the overheating problems in old and deep subway lines.

The content of Chapter 3 was published in the proceedings of the International Building Physics Conference (IBPC2015). The Content of Chapter 4 and Chapter 5 was published as a 2 part paper in the Journal of Building Performance Simulation Journal (JBPS). The content of Chapter 4 was published in the proceedings of The International Building Performance Association Conference (IBPSA2015), where it won the best paper prize.

CHAPTER 2:

Literature review of:
- The subway environment models and software.
- BHE analytical and numerical models
- Subway passenger thermal comfort methodologies

CHAPTER 3

- 1D IDA Central Line model description and validation.
- Parametric analysis on the Central Line model.
- Simulating the effect of climate change on the Central Line air temperatures.
- Modelling other lines in the London Underground based on the Central Line model.

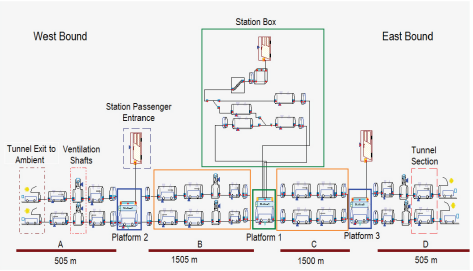

CHAPTER 4

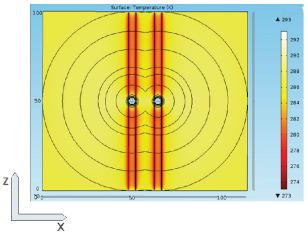

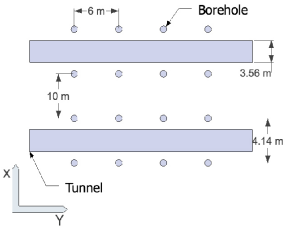

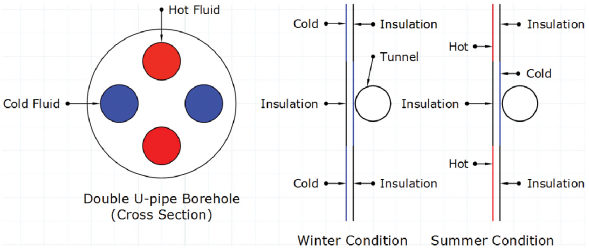

- Coupling 1D IDA Central Line model with a 3D COMSOL BHE model.

- Optimizing the BHE distribution around the tunnels.

- Analyzing the cooling effect of the BHE system on the tunnels and platforms.

- Describing partially insulated boreholes and simulating their thermal interactions with the tunnel.

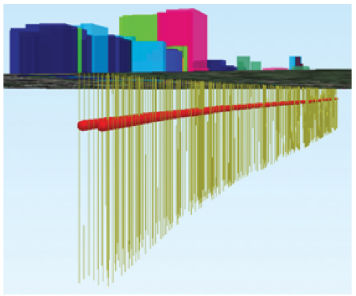

CHAPTER 5

- Integrating the BHE around the tunnels with a section of the Central Line to assess the heating and cooling delivered to the surrounding building blocks in London.

- Modelling the train carriage climate and analyzing the effect of utilizing BHE and onboard air-conditioning on the air temperatures.

- Assessing the thermal comfort of passengers in the platforms and tunnels.

Figure 1.5: Overall structure of the thesis and a summary of each chapter.

Chapter 2

Literature Review and Description of Subway Environmental Models

2.1 Survey of Subway Environmental Models

Past practices in predicting the subway environment depended on trial and error, where it encompassed determining all the phenomena, which affected the comfort and the well being of the passengers and operating personal. This includes thermal, aerodynamic, air quality, and noise conditions such as subway tunnel and station temperature, air movement, noise, dust and odors (Brinckerhoff et al., 1976). The Boston and New York subway builders in 1897 and 1901 learned from the overheating problems that the London Underground experienced due to heat released from the train brakes, and proposed a tunnel design that incorporated grating side walk ventilation openings in New York (Figure 2.1), and ventilation by duct in the crown of the tunnel in Boston as seen in Figure 2.2 (Walker, 1970). Though these ventilation designs did not significantly solve the overheating problems in the tunnels, it was one of the first attempts where environmental considerations were given in the design of the system (SES, 2001).

In these early days of underground design, little research was done on underground environment prediction and design, where the first significant research from which data was gathered and analyzed, was conducted by Davies (1912), who studied the piston effect and its contribution to tunnel and station ventilation. Eventually all the metro systems at that time began retrofitting their tunnels with mechanical ventilation systems and adding more naturally ventilated shafts to improve passenger comfort and air quality (Brinckerhoff et al., 1976). Unfortunately, engineers at that time were not able to accurately predict heat transfer and airflow in the subway system using closed form analytical solutions, due to the complex geometry and the dynamics of the variables. The

emergence of high-speed digital computers in the late 1960's meant that models could be developed to evaluate the environmental conditions in the subway system (Brinckerhoff et al., 1976).

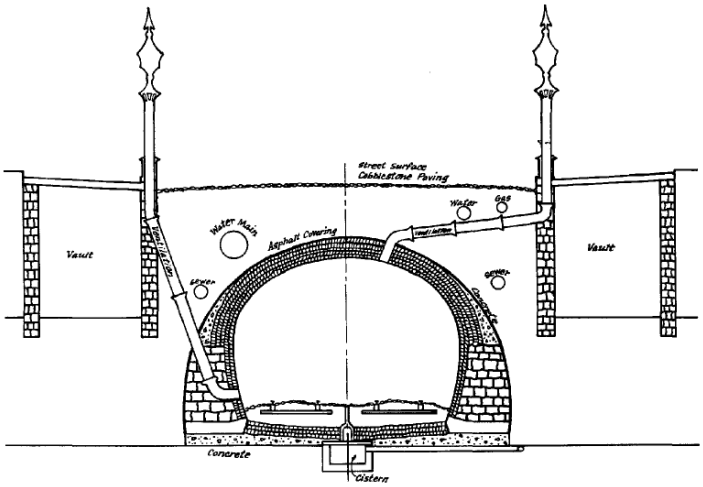

Figure 2.1: Section of Underground Tunnel Showing Subsurface Structures and Ventilation as conceived by A. P. Robinson in 1864 (Brinckerhoff et al., 1976).

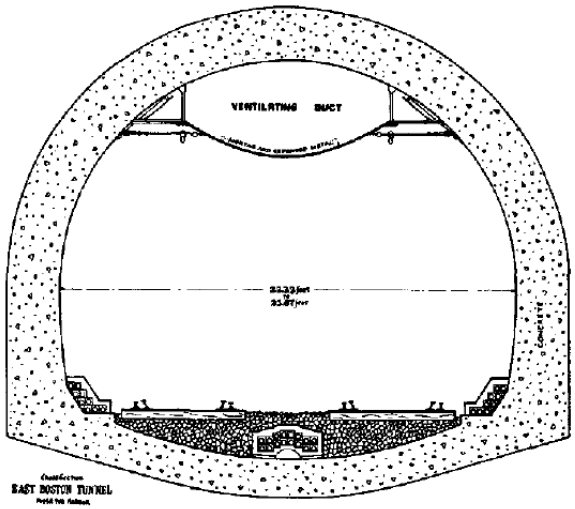

Figure 2.2: East Boston Tunnel Ventilation System (Brinckerhoff et al., 1976).

There are a number of mathematical models that have been developed since the early 1970's which model the airflow and heat transfers of both large and small sections of the subway railways (EQUA, 2013). At first 1D models that are capable of modeling the environmental conditions of the subway rail systems on a large scale are introduced followed by 3D/2D models.

2.1.1 1D Environmental Underground Models

- **Subway Environment Simulation Program (SES)**:

  Parsons Brinkerhoff developed the Subway Environment Simulation Program (SES) under the supervision of the United States Department of Transportation in 1976 (Brinckerhoff et al., 1976). The SES enables subway designers to estimate the temperatures, airflows, humidity as well as air conditioning requirements for both currently existing and future planned multi track subway systems. The SES is a 1D based program that is capable of predicting the subway environment through simulating the various movements of trains including their propulsion and braking system, the environmental controls systems including natural and forced ventilation and air conditioning, and airflows in the tunnels and stations. The SES also incorporates steady state and transient heat sources in its modelling. Also, an additional feature was added that can simulate the long term impact caused by reduction in the tunnel wall heat absorbing capacity after many years of operation (SES, 2001). The SES program is composed of four interdependent subprograms: a train performance subprogram, an aerodynamic subprogram, a temperature/humidity subprogram, and a heat sink/environmental control subprogram. Moreover, it includes a special option that simulates the aerodynamic and thermodynamic effects in case of a fire incident (Thompson et al., 2006). These subprograms get their inputs from a mutually shared set of the subway parameters and operate together to provide a dynamic simulation of the subway environment.

  The SES has been experimentally validated in several metro systems across the globe by comparing measured sensor data to the SES simulation results. Thus, the SES credibility has made it an essential design tool in most of the subway rail systems, and even rail tunnels such as the English Channel. The SES was always updated with new version releases to be compatible with the latest computer systems and added several features, where the latest version is the SES 2000 (Thompson et al., 2006). A drawback for the SES is that it does not provide thorough calculation of the heat storage capacitance provided by the trains and tunnels

which may lead to inaccuracies in calculating the heat sink effect from the ground (Brinckerhoff et al., 1976). The SES heat sink module compensates by relying on approximations and empirical relations derived from experiments.

- **Thermotun**:

  This model is an ongoing project that has its origins in the 1970's, and is similar to the SES program in many aspects (Thompson et al., 2006). However, its main purpose is to simulate airflow in the subway environment, where it models pressures, velocities and temperatures induced by fans and the movements of trains in the tunnels and stations. Simulated tunnel systems can be composed of simple or complex elements as seen in Figure 2.3. Thermotun can handle complex systems with hundreds of tunnel elements with each exhibiting variations in cross section diameter, elevation and wall temperature. Trains are either modeled as simple cylindrical blockages or as a line of wagons depending on their geometry, where they can be assigned more than 20 properties such as their geometry, resistance, motor, and braking system (DTR, 2009). Thermotun analysis is based on the method of characteristics, which makes it suitable for simulating rapid events such as pressure fluctuations induced by train crossings (Thompson et al., 2006). Thermotun is also used as a pre-preprocessing step for thermal computations, where it computes the airflows. Then, the results are imported to a another software that calculates thermal properties such as heat transfer, temperature, and moisture content (IDA, 2006).

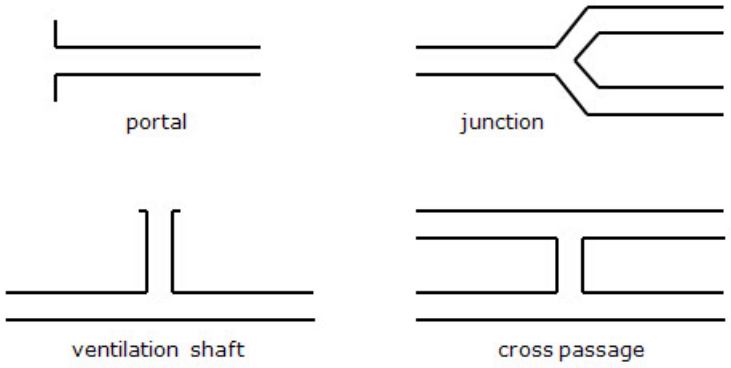

Figure 2.3: Sample of subway rail system elements modeling by Thermotun (DTR, 2009).

- **Ampofo Train Carriage Thermal Comfort Model**:

  A steady state model was developed to simulate the heat loads in a generic deep subway railway network (Ampofo et al., 2004b), particularly the tunnel and carriage. The model is written in EES engineering equation solving language that contains built in psychometric functions which enables the prediction of temperature and humidity in the subway system. The tunnel and its content are considered to be a control volume. The heat loads that are included in the analysis are shown in Figure 2.4 and Figure 2.5. The model also predicts the passengers' thermal comfort based on the Predicted mean Vote (PMV) and predicted percentage of dissatisfied (PPD) scale (Fanger, 1970b) and could incorporate various methods for cooling and their subsequent effect on thermal comfort. However, this model does not simulate pressure effects and airflows in the tunnels (Thompson et al., 2006).

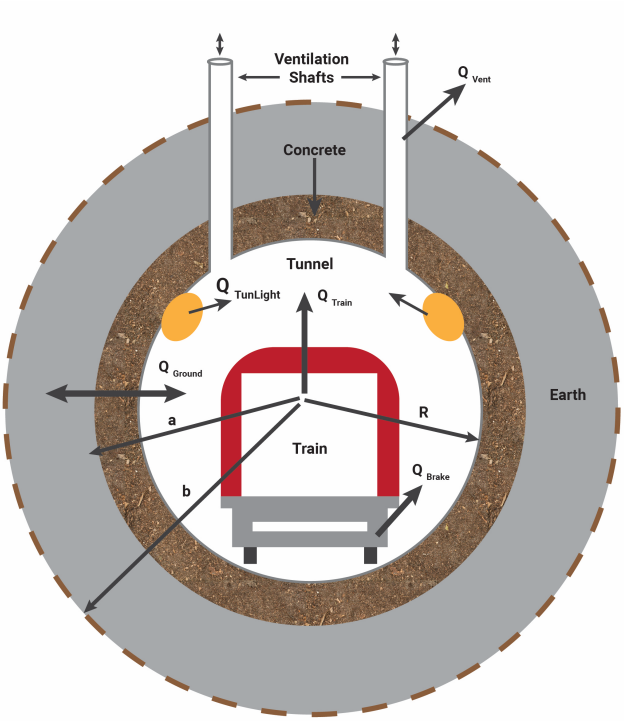

Figure 2.4: Heat loads in a subway railway tunnel. (based on (Ampofo et al., 2004b)).

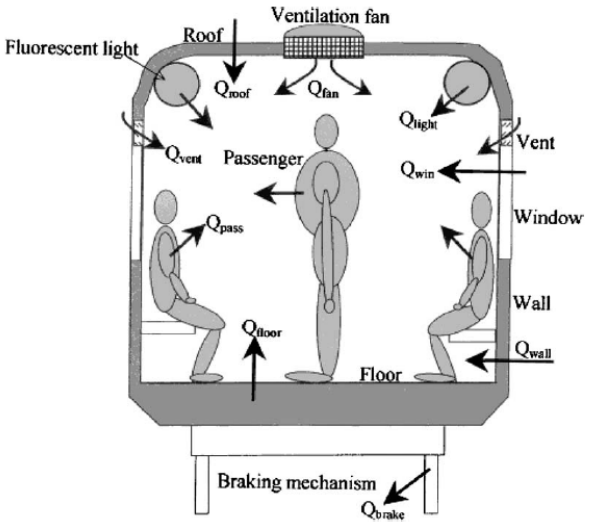

Figure 2.5: Heat loads in a subway railway carriage (Ampofo et al., 2004b).

- **IDA Tunnel Rail**:

  It is a tunnel environment simulation program that was developed by EQUA in 1995. At first it was intended for road tunnel ventilation simulation to address the engineering challenges posed in designing "Sdralnken", which was a new tunnel system in Sweden. The program was rewritten in Modelica modeling language in 2004, and modified to incorporate underground train environmental analysis (EQUA, 2013). IDA Tunnel addresses the various climatic and safety issues within the subway train systems. Multiple geometrical, systematic, and thermal parameters are entered into the model to simulate the environmental conditions and airflows including pollutant dispersal. A graphical user interface is provided to set up the model (Figure 2.6) and the simulation results are post processed, where the stations, tunnels, and trains can be animated in 3D view if integrated with 3D schematics from design software such as Solid Works and Autocad.

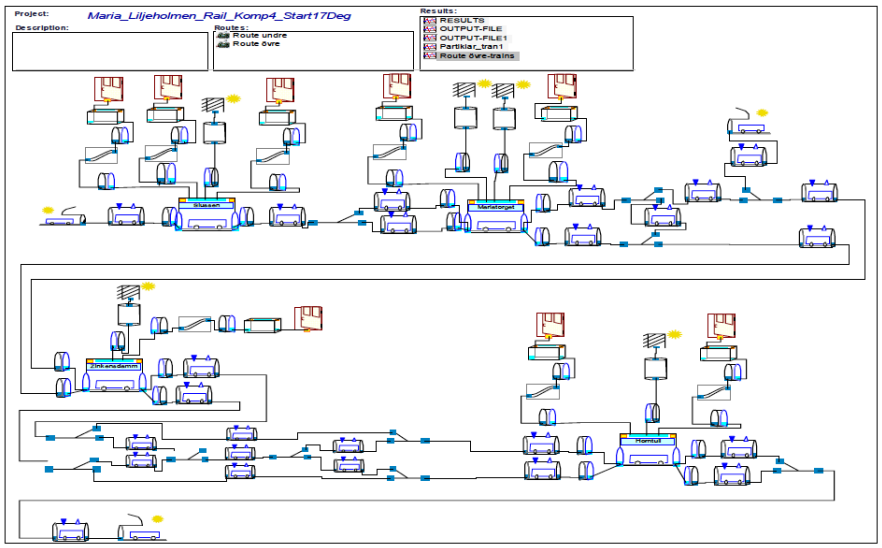

Figure 2.6: IDA Tunnel schematic representation of tunnels, platforms, shafts, and openings (IDA, 2006).

Hourly measured climate data can be used as well as user supplied acceleration, braking and speed of the trains, which allow day by day and long term modeling of the subway system. The model assumes the air to be weakly compressible when modeling 1D airflows of the train's piston effect, buoyancy, and wind pressure. However, it is unable to deal with pressure waves compared to the compressible air model of Thermotun, but the overall bulk air flows correlate

well (IDA, 2006). The airflow models used in IDA tunnel are similar to those of the SES, where the train aerodynamic parameters are identical. In contrast to the SES, this model is able to simulate the radial temperature of the ground encompassing the tunnel segments and can be superimposed with the surface above the ground and other near by tunnels, taking into consideration the surrounding soil's thermal capacitance (EQUA, 2013). Also, ground water flow due to water seepage in the tunnels is simulated along with its effect on the temperature distribution within the ground surrounding the tunnels, and their corresponding heat transfer interactions (IDA, 2006). IDA tunnel was validated through several full scale modeling projects with Stokholm transport and the Swedish Rail Authority. The model was also compared with other 1D subway environmental models such as the SES and Thermuton and also with analytical solutions of different aspects of the underground rail system (IDA, 2006).

2.1.2 2D/3D Underground Modeling Techniques

2D and 3D subway modelling techniques solve fundamental heat, fluid and mass transfer equations using established numerical solving techniques, and are particularly useful when the equations are coupled or if the geometry is complex as in subway train systems. Numerical methods are commonly used for 2D and 3D subway modelling (Colella et al., 2009) and they can be categorized into finite difference and finite element methods. Finite difference methods solve the system across discrete points while finite element methods solve it across a number of sub domains (Lapidus and Pinder, 1982), which makes the latter more complex to set up and more computationally expensive (Thompson et al., 2006). Finite difference methods provide faster results, but finite element systems provide a solution at every point within the domain, enabling them to handle much more complex boundary conditions (Lapidus and Pinder, 1982).

While 1D models are suitable for simulating the underground's environment on a large scale, they do not provide detailed and precise analysis of small scale optimization problems, such as redesigning ventilation shafts, jet fans, or a particular section of a tunnel (Kim and Kim, 2009); this is because these 1 D methods use a simplified representation of the tunnel and ventilation ducts. Consequently, when detailed analysis is needed 2D and 3D numerical methods are used, but their scale of application remains relatively small because of their high computational cost, compared to mono dimensional models (Colella et al., 2009).

Computational Fluid Dynamics (CFD) is typically used to model flows and heat exchanges in 2D and 3D in complex geometries such as the subway system domain, where the Navier Stokes equations are solved along with the energy equation. A large family of commercial CFD software is available that can effectively model the subway environment, which includes PHOENICS, CFX, and Fluent.Yuan and You (2007) used AIRPACK, that is derived from fluent, to simulate the velocity and temperature fields of air in a side platform station in order to optimize the ventilation system. Guan et al. (2007) developed a 3D model for a subway station in Harbin using fluent, while Kim and Kim (2009) conducted CFD analysis of the performance of vent shafts with the purpose of improving their performance by determining the optimal vent shaft positions with respect to the subway station using CFX as seen in Figure 2.7.Yuandong and GAO (2010) coupled Fluent with an experimental setup based on Kim and Kim (2009) to investigate unsteady air flows in subway train systems with natural ventilation ducts, where this methodology was implemented in the tunnels of the Seoul Subway (Huang et al., 2011). Ryu et al. (2012) used CFX to examine the effect of introducing Platform Screen Doors (PSD) on the air quality inside subway station and tunnel.

This study was followed up by Ke et al. (2002) and Juraeva et al. (2013) which discussed the introduction of air curtains to the tunnels, its contribution towards reducing the pollution levels, and their influence on the airflow in subway systems (Figure 2.8).

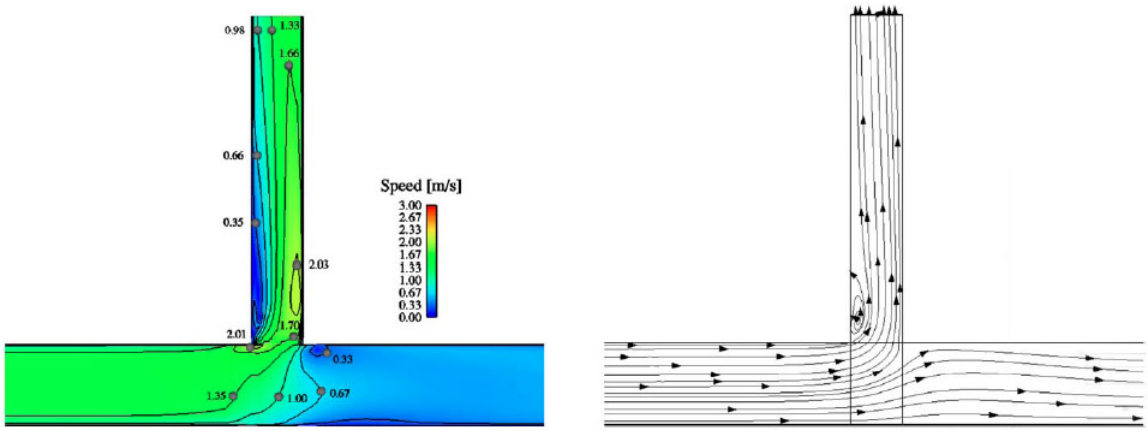

Figure 2.7: Air velocity (left) and streamlines (right) around the vent shaft before the train approach from the left. The scale of the tunnel and shaft shown is Length = 1.4 m, and height = 0.25 m, which is 1/20th of a real subway tunnel (Kim and Kim, 2009).

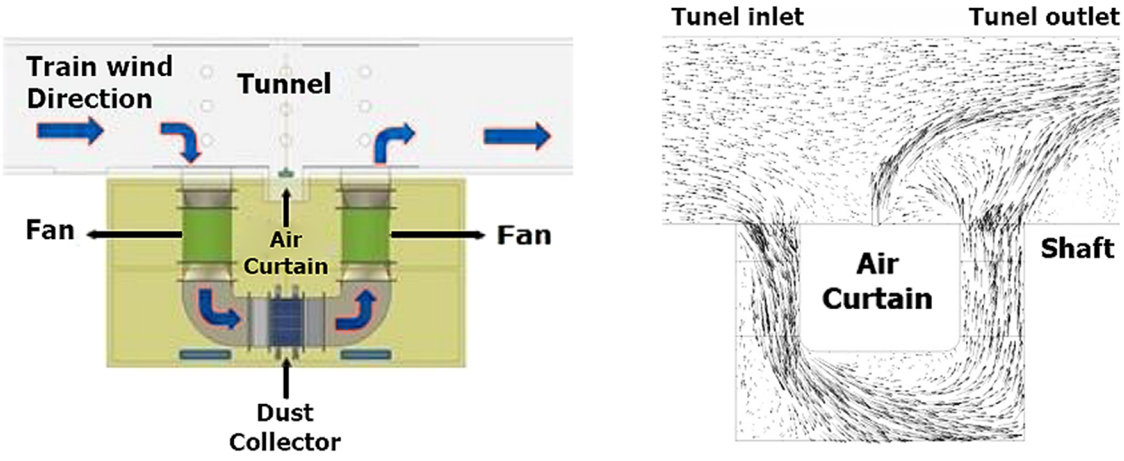

Figure 2.8: Schematic of an air curtain,ventilation shaft,and tunnel (left) and the corresponding velocity distribution (right) (Juraeva et al., 2013).

On the other hand, modelling heat transfer through the tunnel walls and surrounding grounds requires the use of conduction and convection heat equations through finite element methods. These can be coded or modelled using one of the computing languages such as matlab, fortran, C++ and commercial software's like NEi Nastran, ThermoAnalystics, HEAT 3, Fluent, or CFX (Juraeva et al., 2013).

An effective way for modeling the environment in subway train systems is the multi-scale approach (Colella et al., 2009). In this method both 1D and 3D models are coupled, where large portions of the subway system is modeled using the simpler 1D approach, while the regions of interest can be simulated in more detailed 3D and 2D models. Consequently, this method achieves acceptable accuracy in describing the heat and air flows in the system at a reduced computational cost. This method was first demonstrated by Ke et al. (2002), where the SES was used to analyze the subway ventilation system, and the results were inputted as boundary equations in the 3D CFD software PHONIECS, in order to model selected sections of the Taipei Subway system, particularly the under platform exhaust. This methodology was further explored by Colella et al. (2009) who examined several coupling techniques and compared the numerical results with experimental data. Colella et al. (2009) concluded that this methodology is valid and capable of modeling the complex behaviors of airflow in subway train systems with significant reduction in overall computational time.

2.2 IDA Tunnel Fluid and Heat Transfer Equations

Modelling the environmental conditions in the subway requires the combination of heat transfer and fluid equations that are transient in nature, since the conditions in the system are constantly varying. For this reason, developing a new subway environmental model would be cumbersome and would require field and experimental testing, gathering a large data base for train and station properties and comparing with existing software to validate the model, which is beyond this thesis's time scale. IDA Tunnel is going to be used as a platform to model representative sections of the London Underground's tunnels and stations. This is because IDA Tunnel is the latest subway environmental software and has been used in designing various tunnel and subway rail systems (EQUA, 2013). In the following sections the equations that describe the air and heat flows in typical subway systems are described as well as how they are solved in IDA Tunnel.

2.2.1 Subway Model Geometrical Distribution

The actual subway system should be simplified and converted into a schematic representation, which facilitates the input of geometrical data into the program. The system is divided into four basic geometrical categories: Segments, Sections, Nodes, and Subsegments. A sample for how these subway elements are connected is shown in Figure 2.9 and an extended schematic of a subway station along with its adjacent tunnels is found in Appendix A.1.

- **Segment:** A line segment is a continuous length of the station or tunnel that has uniform material and geometric properties in terms of parameter, cross sectional area and construction material. Consequently, a segment would have uniform air velocity in the absence of a passing trains. A ventilation shaft is a special type of segment that is used to model the movement of air between the tunnel or station and the ambient air outside, where they cannot contain train tracks but may include a fan. It can represent actual ventilation shafts, escalators, stairways, and walkways. Unlike line segments, ventilation shafts don't contain steady or unsteady heat sources and the viscous friction between the air and the walls is considered negligible compared to the minor head losses. However, parts of the station, containing heat sources such as lights, escalators, and passengers could be modelled as line segments.

- **Section and Node:** A section is a length of tunnel which has uniform flow rate. Hence, it could contain multiple segments with different cross sectional area. A section is bounded from

both sides by a node, that functions as a reference point where two or more sections are joined, and can be also composed from either line or ventilation shaft segments. The aerodynamic sub-program of IDA Tunnel calculates the airflow for each segment in a section where the train's piston effect, fans, buoyancy, viscous damping, minor head losses, and inertial effects are taken into consideration. Sections can be connected to other sections or the atmosphere through nodes, but can not terminate at dead ends. Also, the air flows at each node must satisfy the conservation of mass and energy laws.

- **Subsegments:** The temperature and humidity might vary within a segment, so it is necessary to divide the segments into smaller sub segments (Figure 2.9), where the humidity and temperature are independently computed. This will enable the software to calculate small-scale variations in sensible and latent heat in the subway system.

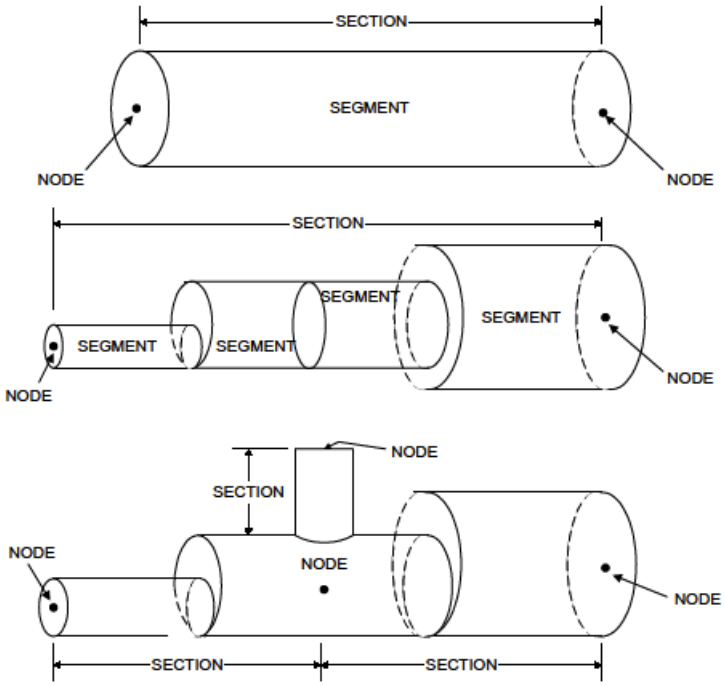

Figure 2.9: Sample schematic of a subway system consisting of sections divided into segments which are connected by nodes (SES, 2001).

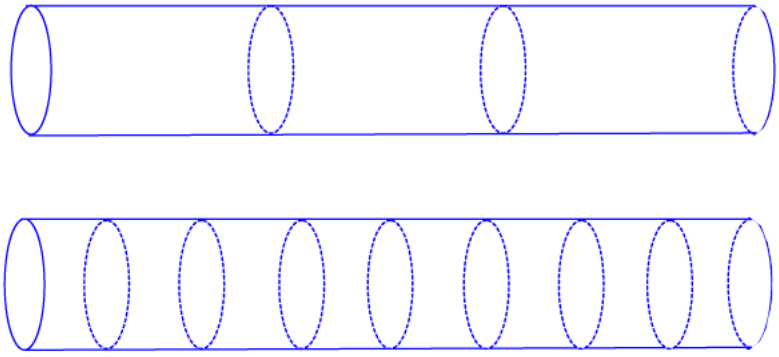

Figure 2.10: Division of segments into three subsegments (above) and eight subsegments (below) (SES, 2001).

2.2.2 Airflow Equations

The main influences on the airflow in subway rail systems are the structure's geometry and material, forced ventilation, trains piston effect, soil and outside air conditions, and heat sources. These factors drive forced and buoyancy flows and influence aerodynamic drag and shear forces, flow rates, as well as air velocities (Figure 2.11). The airflows that are generated by the trains, ventilation, and temperature difference within an irregular subway system geometry in addition to the complex interactions of these flows, renders them unsteady. Thus, the airflows in the subway system are transient in nature and cannot be modeled as steady state systems. Airflows in the system can be approximated to be incompressible due to the relatively low speeds of the trains reaching a maximum of 100 km/hr (bombardier, 2013). The effects of air compressibility becomes significant in the case of high speed trains in combination with high blockage tunnel ratios and long length of tunnel (SES, 2001). The equations for the various airflow phenomena and assumptions in the subway system are described briefly in the upcoming section and in detail in Appendix B.

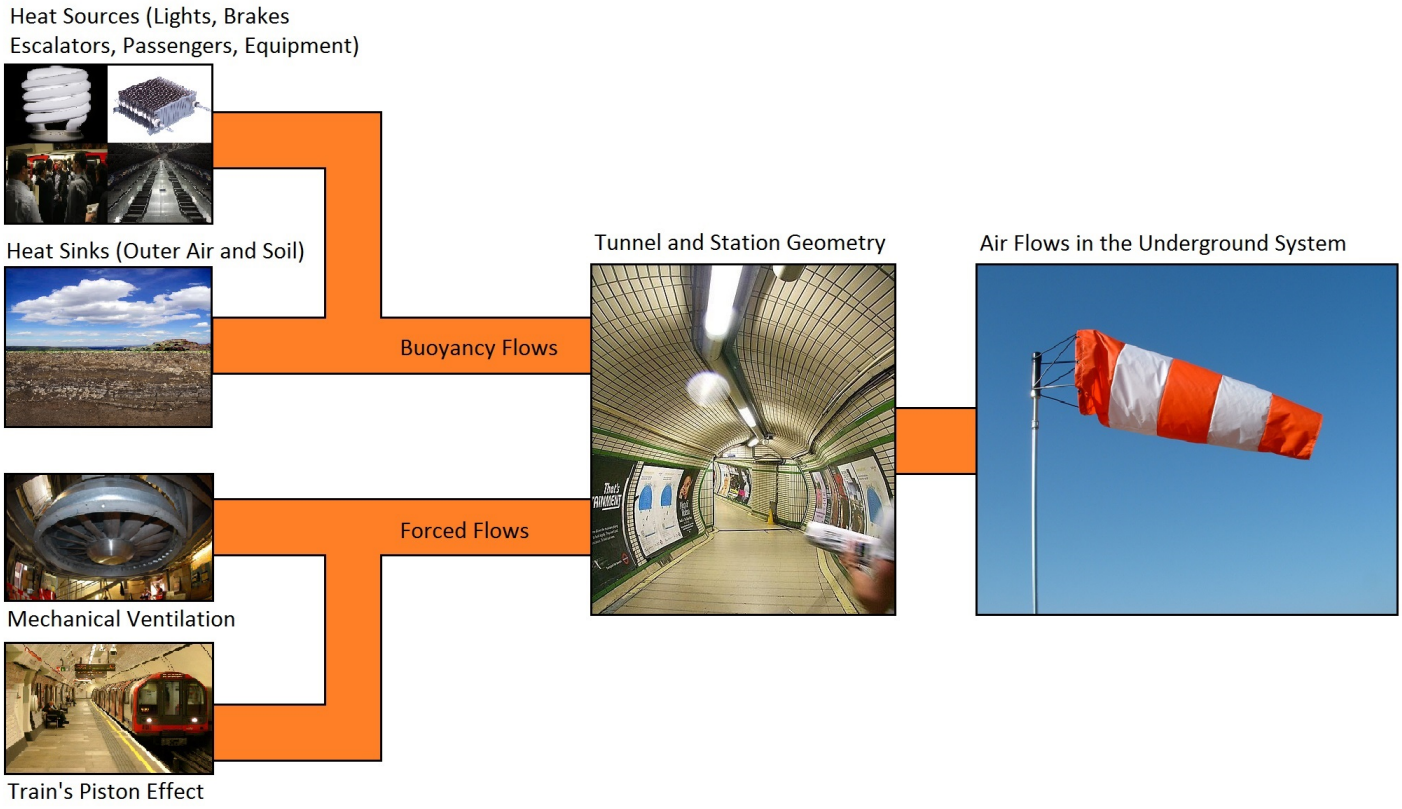

Figure 2.11: Factors that drive and influence the airflow in a subway rail system.

For a given control volume the mass continuity equation states that the mass of the system should remain constant, that is the mass of the flow entering the system is equal to the mass exiting it:

$$\frac{\partial}{\partial t}\int_{CV}\rho dV = -\frac{d}{dt}\int_{CS}\rho\vec{V}.d\vec{A} \tag{2.1}$$

In the case of incompressible fluid, the density remains constant, so equation (2.1) is simplified to:

$$\frac{\partial}{\partial t}\int_{CV} dV = -\frac{d}{dt}\int_{CS}\vec{V}.d\vec{A} \tag{2.2}$$

The momentum equation for inertial control volume states that the sum of all forces acting on a non accelerating control volume is equivalent to the summation of the net rate flux of momentum

throughout the control surface and the sum of the rate of change of momentum inside the control volume (Fox et al., 2004) which is given as:

$$\vec{F}_S + \vec{F}_B = \frac{\partial}{\partial t}\int_{CV} \vec{V}\rho dV + \frac{d}{dt}\int_{CS} \vec{V}\rho\vec{V}.d\vec{A} \tag{2.3}$$

The energy equation is used to calculate the mechanical energy balance within a control volume, where the conservation of energy principle applies. This mechanical energy balance for a pipe flow, which is analogous to the case of the subway system is written between two points 1 and 2 (Figure 2.12) along the same streamline as:

$$\left(\frac{P_1}{\rho} + \alpha_1\frac{{V_1}^2}{2} + gz_1\right) + \left(\frac{P_2}{\rho} + \alpha_2\frac{{V_2}^2}{2} + gz_2\right) = \sum h_T = \sum h_l + \sum h_l m \tag{2.4}$$

details about calculating h_T, h_l and $h_l m$ is found in Appendix B.2. For the case of the subway system $\alpha = 1$ because of the turbulent nature of the flows. In IDA Tunnel equation (2.4) (EQUA, 2013) is rearranged into:

$$P_2 - P_1 + \frac{\rho{V_1}^2}{2} - \frac{\rho{V_2}^2}{2} + \frac{\rho C_1{V_1}^2}{2} + \frac{\rho C_2{V_2}^2}{2} + \rho G_{12} = 0 \tag{2.5}$$

In equation (2.5) the friction losses h_l and $h_l m$ are grouped in C and the change in head due to height difference is grouped in G_{12}.

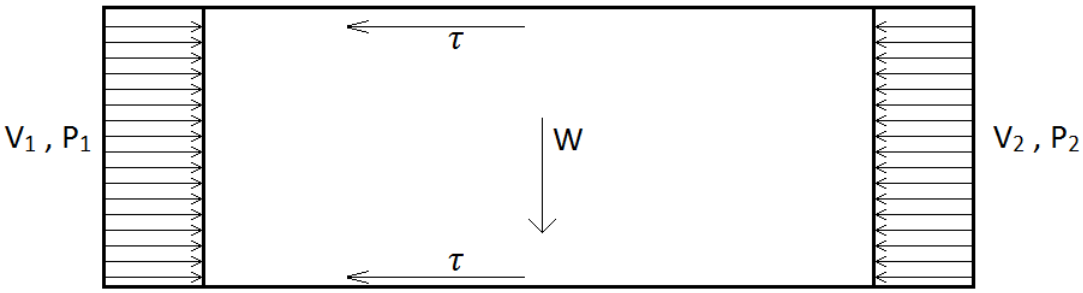

Figure 2.12: Momentum balance for a pipe control volume between sections 1 and 2, which includes surface forces (P, τ) and body forces (W).

As explained earlier in the geometry section, IDA tunnel calculates the airflows by dividing the subway system into sections which are further divided into segments, where the geometry, material properties, and head loses should be inputted for each. The geometrical, performance, and schedule data for the trains should be provided to accurately model the train induced flows in the system, which behave like pistons in an open ended tube filled with air (SES, 2001). The performance characteristics for the ventilation fans should be also provided, for calculating the flows from forced mechanical ventilation, which can exceed that of the trains piston effect in some cases (Brinckerhoff et al., 1976). The subway system experiences rapid changes in air flow which is attributed to the passage of trains whether they are pushing or sucking air through vent shafts or the station or in the case of two trains passing in opposite direction. In order to accurately model these rapid flow changes, the time interval between each airflow calculation should be reduced to a range of seconds. There is also a velocity stability criterion for the aerodynamic program, which states that the maximum velocity in the system should not exceed the ratio of the subsegment length over the calculation time interval. This criterion helps with specifying the dimensions of segments along with the numbers of its subsegments in a subway system. The equations that calculate the air flow and pressures in each of the subway sections taking into effect the various components of drag, fans, buoyancy and piston effect are described.

2.2.3 Heat Transfer Model

Temperature and humidity throughout the subway system are influenced by the airflows carrying sensible and latent heat through the tunnels and stations, as well as the heat added by heat sources and sinks. Also, the surrounding boundary conditions which are the outside air and deep soil temperatures affect the thermal conditions in the system.

In order to calculate the thermal conditions in the subway, the system is assumed to be one dimensional as in the case of the airflow model. Consequently, air temperature and humidity are assumed to be uniform across any cross section. Also, axial conduction as well as radiation heat transfers are assumed to be negligibly small compared to heat transferred by convection via airflow. Though, the heat dissipated to viscous air friction with the wall and trains is relatively small, IDA Tunnel can optionally take it into account in the calculations. Similar to the air flow calculations, the subway system is also partitioned into sections and segments that are connected by nodes as a basis for the thermal computations. However, since temperature and humidity can vary along the length of a segment, the segments are partitioned into smaller subsegments (Figure 2.2) as explained earlier where temperature and humidity are calculated in each. Thus, the accuracy of the model is improved, because small-scale variations in the system's sensible and latent heat are taken into account. The calculated airflows are used in each subsegment to determine the heat content net difference between the air entering and exiting the subsegment. Then, the amount of sensible and latent heat added or removed in each subsegment is computed taking into consideration the heat rejected from the trains. The heat transfer across the wall is determined using the wall temperature and the tunnel's air heat convective coefficient. The heat sources in the subway along with their heat transfer equations are described below, while the temperature, humidity, heat sink equations, and additional heat transfer equations are explained in details in Appendix B and are based on EQUA (2013).

1. **Steady State Heat Sources**

- **Station and Tunnel Lighting:** A portion of the energy that powers the lights is wasted as heat, where the total amount of heat released is dependent on the type of the lights and the density of lights in the station. For typical neon lights, which are commonly used in tube stations and tunnels. The heat released by the tunnels and stations lights is respectively given as:

$$Q_{TL} = W_{TL}L \tag{2.6}$$

$$Q_{SL} = W_{SL}A_s \tag{2.7}$$

From equation (2.6) Q_{TL} depends on the tunnel length whereas in (2.7) Q_{SL} depends on the station area. Also W_{TL} and W_{SL} depend on the efficiency of the lights.

- **Ticket Sale Boxes and Mezzanine Businesses:** The equipment found in these places can generate a noticeable amount of heat that can be estimated as:

$$Q_{FC} = W_{FC}N_{FC} \tag{2.8}$$

$$Q_{MB} = W_{MB}N_{MB} \tag{2.9}$$

- **escalators and lifts:** Heat is generated from both the escalators and lifts. The heat released from lifts is dependent on the power rating and efficiency of the motor and is taken as an average heat source over the period of its operation. Whereas the escalators are continuously operating during the subway's opening times and the heat released is calculated as:

$$Q_E = W_E L_F \tag{2.10}$$

- **Passengers:** The passengers also contribute to the heat released in the stations, since the human body's chemical energy is transformed to heat and mechanical work by the metabolic activities within the body. In thermal comfort standards, the metabolic rate is expressed in MET units, where every $1MET = 58.2\,W/m^2$, and the surface area of an average person is $1.8m^2$ (ASHRAE, 2010). Typical metabolic rates for the passengers in the station can be assumed the same as people walking, which is $2MET = 115\,W/m^2$. The Passenger sensible and latent heat can be lumped into one heat rate Q_{SP} (ASHRAE, 2010) and is given as:

$$Q_P = N_P Q_{SP} \tag{2.11}$$

- **Third and Fourth Rail Losses:** Most metros are operated with dc power voltage ranging between 600 V and 1500 V with third rail or overhead contact line (Yadav, 2012). The London Underground is one of the few systems that use a fourth rail powering line (Figure 2.13), where the third rail is beside the track providing +420 V DC, and a fourth one is located midway between the rails carrying -210 V DC, summing the total power provided to 630 V DC (Tfl, 2007). These additional power lines would incur losses when the train accelerates to maximum speed, and when the train maintains or increases speed, which are calculated as:

$$Q_{3,4R} = \frac{201(KE + Q_D + Q_M + Q_m + Q_{SR})^2 R}{N t_a V_O^2} \tag{2.12}$$

  Details for calculating the components of equation (2.12) are found in Appendix B.5.

- **Train Steady State Heat Sources:**

  The steady state heat rejection from the subway trains consist of the auxiliary equipment such as the lights, the braking air compressors, and environment control units if the train is air conditioned. The equations for these sources are described in appendix B.6.

Figure 2.13: London Underground tracks showing the third and fourth power rails.

2. **Transient State Heat Sources**

A significant amount of heat is released due to train braking in the subway, where it contributes to a large portion of the total heat released in the system reaching around half in the Tehran metro system (Aidbi et al., 2011). Modern subway systems including the London Underground utilize rheostatic braking (Figure 2.14) in combination with regenerative braking (Tfl, 2007). In a rheostatic braking system the electrical energy from the motors is dissipated by onboard resistors, which are cooled by large fans to prevent the resistors from high temperature damage.

IDA tunnel models the unsteady heat release from the brakes resistor grids and computes the heat rejection values and their consecutive locations along the tunnels and stations. The parameters that characterize the resistor grids are its mass, effective radiant and convective surface area, and characteristic diameter. A representation diagram of the resistor grids is presented in (Figure 2.15). A simplified approach is adopted to estimate the resistor grid thermal behavior, because detailed analysis would involve taking into account unstable turbulent flows and complex heat transfer along the grids. This approach is fundamentally based on the assumption that the temperature for all the resistor grids on a train can be represented by an average temperature. Though the resistor grids experience temperature variations among its elements during operation, it has been experimentally proven that taking the average temper-

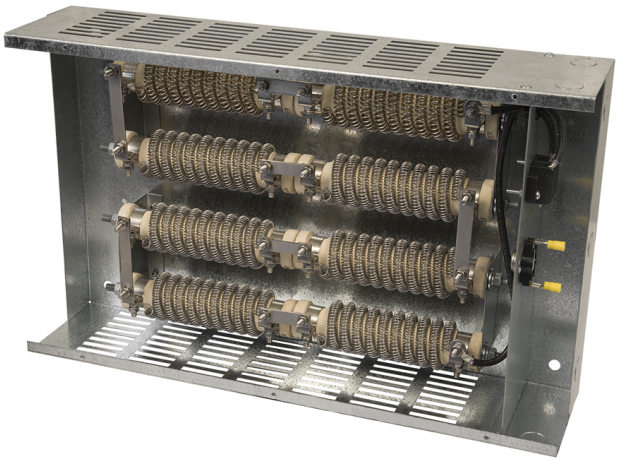

Figure 2.14: Rheostatic dynamic resistor grid braking used in trains (postglover, 2016).

ature is sufficient for estimating the heat transfer rates (SES, 2001). By applying conservation of energy on a resistor grid and assuming all the grid elements as one lumped mass the average grid temperature equation is given as :

$$MC_p \frac{dT_g}{dt} = P_{in} - Q_{out} \tag{2.13}$$

The heat released from the resistor grid Q_{out} is transferred in the form of convection and radiation, while conduction is assumed negligible due to poor heat path flow to the train's underbody (Brinckerhoff et al., 1976). The resistor grid brakes convection Q_{conv} and radiation Q_{rad} and their respective heat transfer coefficients equations are discussed in details in Appendix A.8.

$$Q_{out} = Q_{conv} + Q_{rad} \tag{2.14}$$

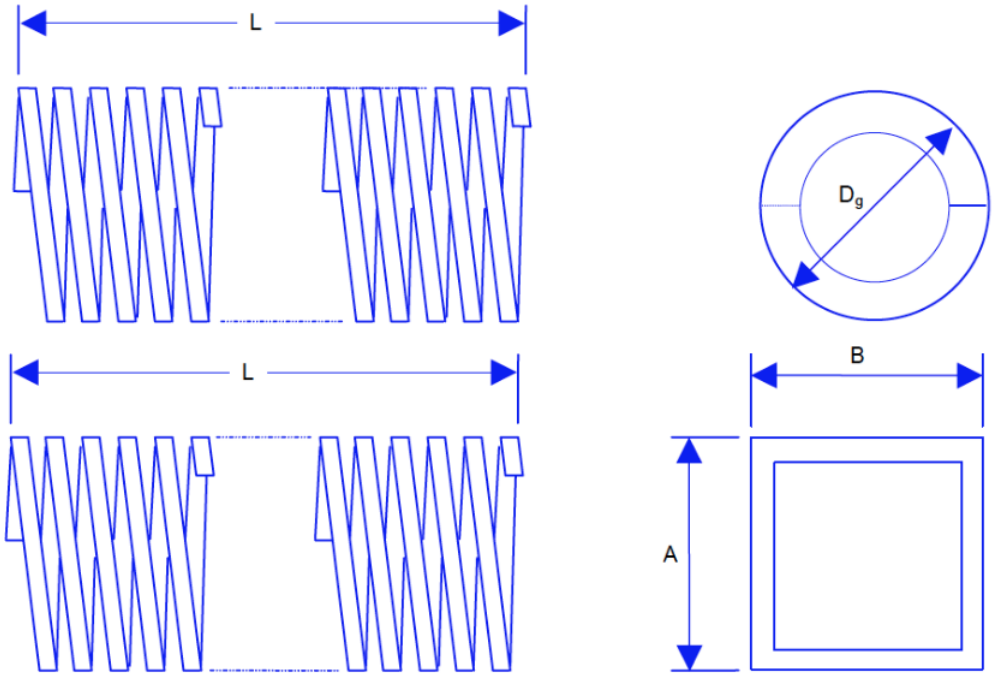

Figure 2.15: Schematic and effective convective area and diameter of the resistor grid for circular elements (above) and rectangular (below).

3. **Soil Heat Conduction Model**

For IDA tunnel heat conduction across the tunnel walls and surrounding earth is modelled as a two material region area (Figure 2.16) (EQUA, 2013). Region I extends from the inner wall surface to the tunnel wall-earth interface, while region II extends from the tunnel wall-earth interface to the surrounding earth. The model assumes that the initial earth temperature is at the background soil temperature, where the tunnel is assumed to be deep enough such that outside temperature fluctuations has a negligible effect on the temperature of the material surrounding the tunnel. Each region is assumed to have uniform material where the thermal conductivity and diffusivity of each is constant. The inner wall convective heat transfer coefficient $\overline{h_w}$ is taken as the 24 hour daily average computed by the air flow model. The fluctuations of the annual air temperature at the wall's surface, range of diurnal temperature as well as diurnal temperature variations are modeled as simple harmonic functions. Through onsite experiments it was found that a simple harmonic function is adequate to calculate heat conduction across the tunnel walls and earth (EQUA, 2013). The diurnal surface temperature vary with an amplitude equal to the difference between the diurnal maximum and

diurnal minimum temperatures that are computed in the thermodynamic model. Axial heat conduction parallel to the tunnel is considered to be negligible and cylindrical coordinates are used in the heat transfer calculations. In the case of rectangular shaped tunnels, the hydraulic diameter is taken. Taking these assumptions into consideration, the air temperature at the wall surface is given as:

$$T_{air} = T_{ann.avg.} + A_{ann.} sin(\omega_{an.} t) + A_{di} sin(\omega_{di} t) \tag{2.15}$$

The partial differential transient equations describing the heat transfer across the two regions are described in details in Appendix A.12.

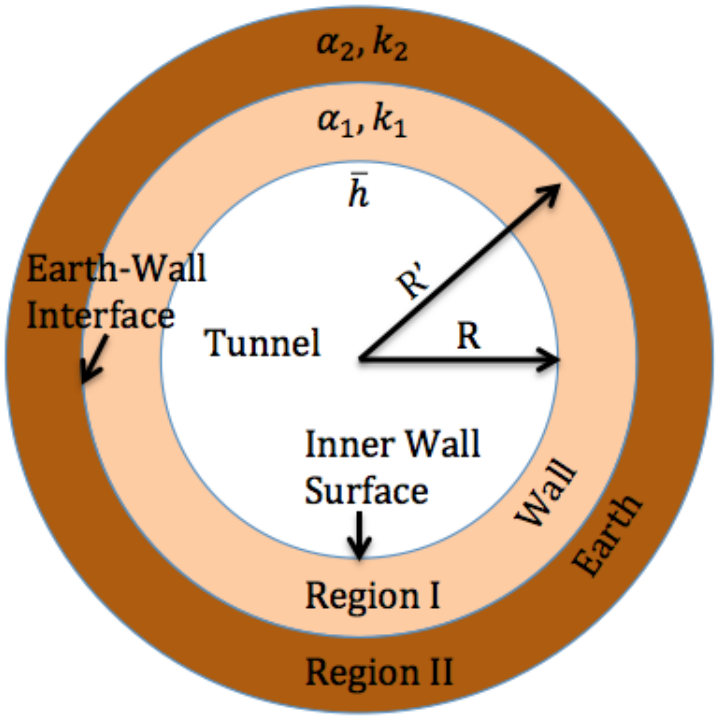

Figure 2.16: Tunnel heat conduction model.

2.3 Train Carriage Model

The passengers spend a significant amount of time in the train carriage as they travel from one station to another. Thus, it is essential to model the train carriage's environment to asses the thermal passenger's comfort during their journey. IDA tunnel has a one dimensional transient model that models the heat and mass transfers in the train carriage in order to simulate the carriage's environmental conditions (Figure 2.17). The model was coded in Modelica and allows for customizing properties and formulas of IDA objects using scripting. The model consists primarily of two layers which are the carriage's material wall and the air within, while there is one boundary layer which is the varying tunnel temperature. The model assumes that the train carriage layers are homogeneous and their temperature and humidity is independent of the position within the layer. Also, radiation heat transfer is assumed negligible except for radiation exchange with passengers, since the temperature gradient is relatively small and the edge heat transfer effect is neglected since the carriage is sufficiently large. For each of the layers the heat losses and gains by conduction, convection, ventilation, phase change and mass transfer is simulated. The model can be mathematically described as a system of three heat balance and one vapor balance equations:

$$\frac{dT_w}{dt} = \frac{1}{{c_w}' A_w}(Q_{V(i,w)} - Q_{V(w,e)} + Q_{L(i,c)}) \tag{2.16}$$

$$\frac{dT_g}{dt} = \frac{1}{{c_g}' A_g}(Q_{V(i,g)} - Q_{V(g,e)} + Q_{L(i,c)}) \tag{2.17}$$

$$\frac{dT_i}{dt} = \frac{1}{\rho_a c_a V_c}(-Q_{V(i,w)} - Q_{V(i,g)} - Q_{V(i,e)} + Q_g) \tag{2.18}$$

$$\frac{dC_i}{dt} = \frac{1}{h_{fg} V_c}(-Q_{L(i,e)} - Q_{L(p,i)}) \tag{2.19}$$

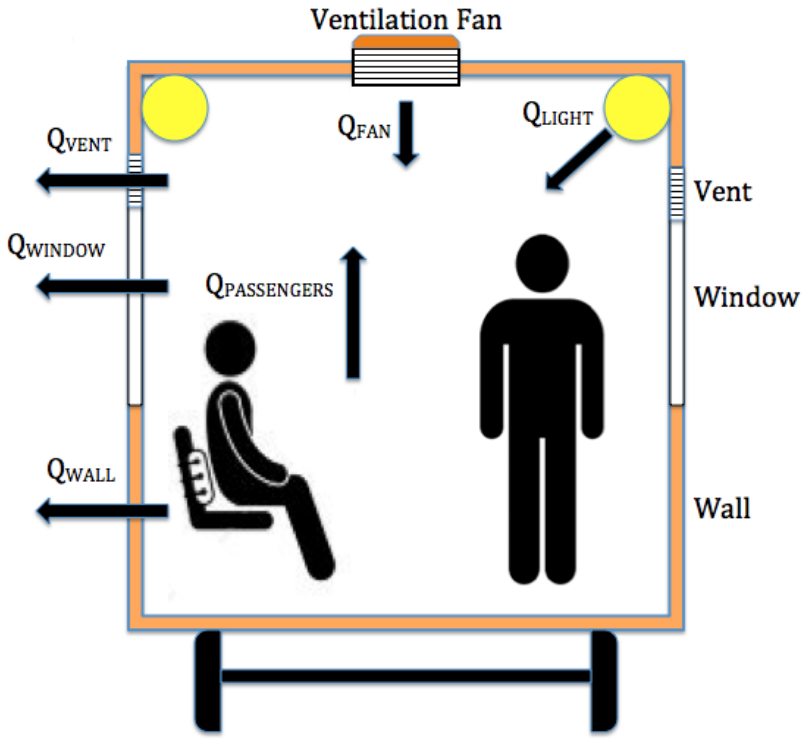

Figure 2.17: Heat and Mass transfer in the train carriage.

- **Train Carriage Cover:** The cover forms the barrier between the inner train carriage climate and the outer tunnel temperature. The cover can be split into the carriage's wall which is typically made of layers of aluminum and fire resistant insulation and the glazing which forms the carriage's windows. Both sides of the wall and glazing is assumed to have the same temperature T_w and T_g for each respectively, where they exchange convective heat transfer with the inside air $Q_{V(i,w)}$ & $Q_{V(i,g)}$ and the external air $Q_{V(w,e)}$ & $Q_{V(g,e)}$, where the formulas used to determine the internal and external convective heat coefficients are given in Appendix C.1. Also, the velocity of the train varies as it traverses the subway from the operational speed to zero when it stops and this is taken into consideration when calculating the external convective heat transfer coefficient, which effects the convective heat exchange between the train carriage cover with the external tunnel air. In rare cases condensation might occur, especially if the train is packed with passengers, which would consequently raise the water vapor content of the inner air. $Q_{L(i,c)}$ and $Q_{L(i,c)}$ takes into consideration the latent heat transfer in the case of condensation.

- **Train Carriage Air Heat Exchange and Internal Heat Sources:** The internal air exchanges heat through convection with the carriage cover and air mixing with the external tunnel air, and takes into consideration the various internal heat sources. The heat sources inside the carriages compromise mainly of the heat released by the passengers, lights, and any other auxiliary equipment, which are summed up in Q_g. The internal air mixes with the outer tunnel air through ventilation ceiling fans, infiltration and the periodic opening and closing of the carriage's doors upon making a stop at a station, where the corresponding heat and mass exchange is represented by $Q_{V(i,e)}$. The internal air humidity C_i is influenced by the air exchange with the external tunnel air $Q_{L(i,e)}$ and the moist generated by the passengers inside the carriage $Q_{L(p,i)}$.

  The heat and mass transfer due to the mixing of the inner train and outer tunnel air depends on the air change rate in the carriage R_a (EQUA, 2013). R_a is a summation of the train infiltration rate, the ventilation rate by ceiling fans and ventilation panes installed, and the periodic rate of air change due to the opening and closing of the carriages' doors as the train stops at the station. The train's infiltration and ventilation rate varies depending on the train's geometry and the fan type. The air exchange rate through the train's doors R_d is approximated as a case of single side ventilation through open windows, in which the flow rate is explained in Warren and Parkins (1985). The heat and mass transfer between the train compartment and the tunnel equations are discussed in details in Appendix A.13.

- **Train Carriage Air Conditioning:**

  IDA tunnel also simulate on-board train carriage air-conditioning and heating, where set point temperatures for heating (T_{low}) and cooling (T_{high}) are assigned, and also the coefficient of performance (COP) of the heating or cooling devices. The train compartment's cooling load Q_{cool}, air condition's electrical consumption (W_{AC}), heat removed from the train compartments through the evaporator (Q_{Evap}), and rejected heat to the tunnels through the condenser (Q_{Cond}) are calculated as follows:

$$Q_{Evap} = Q_g - U_{tot}(T_{high} - T_{air}) \tag{2.20}$$

$$COP = \frac{Q_{Evap}}{W_{AC}} \tag{2.21}$$

$$Q_{Cond} = (1 + COP)Q_{Evap} \tag{2.22}$$

$$Q_{Cond} = Q_{Evap} + W_{AC} \tag{2.23}$$

- **Boundary Conditions:** The tunnel air temperature T_e acts as a boundary condition that varies with respect to time and location of the train in the subway. The output of the tunnel and station temperature from the model is going to be used as the boundary condition for the train carriage model.

2.4 Modeling Borehole Heat Exchanger (BHE)

A range of GSHP models have been developed depending on the modeling objectives. Some GSHP models focus on the internal process within the system, while others focus on the surrounding soil around the ground heat exchangers, and some models integrate the GSHP system with building simulations to study the overall system performance (Revesz et al., 2016). The level of complexity and details of these models depends on the objectives of the model and the required times scales. There are two main categories for modeling GSHP systems: analytical and numerical methodologies. Stauffer et al. (2013) reviewed extensively a series of analytical and numerical models. Stauffer et al. (2013) used case studies in Germany, Austria and Switzerland, focusing on urban thermal energy use as well as heat storage and cooling.

Numerical methods utilize established numerical differential equation solving techniques such as finite volume, finite element and finite difference. Numerical methods are very useful when modeling borehole heat exchanger (BHE) because they might have complex geometries with three dimensional transport phenomena that are transient in nature, such as in this thesis where we model BHE's next to subway tunnels. Numerical methods can couple systems

with different time scales, and can incorporate transient boundary conditions into the system (Revesz et al., 2016). One of the main disadvantages of using 3D numerical models is that its computationally expensive, which can results in long computational times. Al-Khoury et al. (2005) presented simplifications on the numerical methods for the analysis of BHEs that result in reducing computational simulation times. Al-Khoury et al. (2005) also simplified analysis for heat transfer in BHEs so that the model uses large elements, which saves computational time and the need for extremely fine meshes. The simplification methods include having a specialized model for the BHEs which include thermal interactions among different components of the BHE (Revesz et al., 2016). Sequential numerical algorithms can be used to solve non-linear equations which reduces computational times, by decreasing the number of elements in the model.

Other approaches to decrease computation times is by using symmetry. For example, a BHE can be 3D discretized while the surrounding soil is described as a 2D axis symmetric mesh. In this approach heat conduction in the horizontal cross section is solely considered, and the BHE wall is assumed to have a uniform temperature across its circumference, where the simulation results have marginal errors as shown in (Hellstrom, 1991).

Analytical methods are used to validate numerical models for BHE's, and their advantage is that they can be solved readily, but have limitations when it comes to complex geometries and time steps. Also, it is sometimes difficult to obtain sufficient data in deep ground so an analytical model is preferred to validate the numerical model.

2.4.1 Analytical BHE Models

The kelvin line source (Ingresoll and Plass, 1948) and the infinite cylindrical source (Carslaw and Jeager, 1959), are the earliest and simplest analytical approaches for modelling the thermal interactions of BHEs. These models assume a purely conductive and radial heat transport while neglecting convective heat transfer. However, the main disadvantage for these models is that they don't account for vertical heat transfer, and neglect the advective heat transfer in the aquifer systems (Casasso and Sethi, 2013). Analytical BHE models are still widely used for thermal response tests (TRT) for BHEs, because of the short time of BHE operation such that vertical heat transfer is minimal. Witte (2013) has shown that seasonal ground water

level changes can change the TRT results, where Wagner et al. (2013) has developed a method to adjust the TRT results to account for groundwater flow.

Eskilson (1987) has developed a semi analytical method with a finite BHE length and several layout distribution of BHE fields, where he neglected convection and advection heat transfer due to ground water. Eskilson (1987) method is applied in two popular BHE modeling software: GLHEPRO (Spitler, 2000a) and Earth Energy Design (Hellstrom and Sanner, 2000). Recently, Bandos et al. (2009) have developed an analytical finite length model of BHE, and Diao et al. (2004) model included the effects of ground water, while Molina-Giraldo et al. (2011) combined both these features in his model.

2.4.2 Numerical BHE Models

Hellstrom (1991) developed one of the earliest numerical BHE models which he called the duct storage model, which followed a 2 D finite difference method. Thornton et al. (1997) continued development of the duct storage model, which was programmed in TRNSYS. Lei (1993) and Muraya et al. (1996) analyzed the thermal interference between arrays of BHEs. Early numerical models were known for low computational efficiency. Al-Khoury et al. (2005) improved the BHE numerical models computational efficiency by developing a 3D finite element steady state flow model. Al-Khoury and Bonnier (2006) modified the model to include transient heat transfer. (Stauffer et al., 2013; Di-Donna and Laloui, 2014) have also worked on developing transient numerical models from BHE for GSHP and GWHP systems.

Hecht-Mendez et al. (2010) coupled MODFLOW with the solute transportation package MT3DMS by applying analogies between heat transfer and solute transport or with the specific heat transport package (Langevin et al., 2008). The FEFLOW code for advection and groundwater flow have been modified to incorporate modeling BHEs (Diersch et al., 2011; Dierch et al., 2011). Rees and He (2013) and Al-Khoury and Bonnier (2006) have recently developed 3D models to simulate dynamic heat transfer and ground water flow for BHE.

2.4.3 Ground Thermal Energy Storage

Among the thermal energy storage technologies available (Lanahan and Tabares-Velasco, 2017), underground thermal storage meets the requirements for large scale applications where

the costs and space required needs to be minimized, yet high storage capacity is desired. The most common methods for utilizing the ground for thermal storage are Aquifer Thermal Energy Storage (ATES), and Borehole Thermal Energy Storage (BTES) (Lanahan and Tabares-Velasco, 2017).

ATES utilizes the open loop geothermal method which relies on seasonal storage of cold or warm ground water in an aquifer. ATES usually involve storage and recovery of cold water and less frequently warm water if excess heat is available during summer (AHGI, 2018). During winter, ground water is pumped through a heat exchanger and stored in a designated cold section of an aquifer. During summer, this cold water is recovered from the cold section of the aquifer and used for cooling purposes, which will warm this water. Afterwards, the warm water is injected into a warm section of the aquifer to be used during winter, where this cycle is repeated seasonally (Lanahan and Tabares-Velasco, 2017). ATES systems can be coupled with renewable energy, such as the use of solar hot water panels to create hot water for storage in summer, and with solar or wind electricity to power the ATES mechanical components (AHGI, 2018).

ATES systems require a suitable aquifer with at least two thermal wells. Also, ATES requires fluids, such as water, that minimize the risk of aquifer contamination with hazardous chemicals (Sanner, 1999), which have a negative impact on the surrounding environment and species. ATES also have strict environmental permit conditions, thermal pollution can also have a negative impact on the surrounding environment (Arnfield, 2003). In the US, ATES systems are regulated by the Underground Injection Control (UIC) registration (AHGI, 2018), while in the UK by the UK environmental agency (Zhang et al., 2015b). Since ATES requires an aquifer to function, requires large areas, and is regulated, BTES are considered to be more flexible and practical among the thermal energy storage technologies (Lee, 2013).

BTES systems use the surrounding rock and soil as a medium to store thermal energy via BHEs (Sibbet, 2012; McClenahan et al., 2006). BTES is among the most used methods of ground thermal storage because of the flexibility in applying it, in contrast to ATES for example which require specific ground formations (Rad and Fung, 2016) . BTES is an improvement on the conventional GSHP systems, in which an array of BHEs is operated to store or dissipate heat seasonally using the earth as a thermal battery, while conventional GSHP systems dissipate or absorb heat into the soil acting like a radiator. BTES systems can achieve coefficient of

performance between 4 - 8, which is higher than conventional GSHP systems with an average of COP of 3.5. This is because BTES has a larger heat storage volume (Mangold et al., 2004; Zhang et al., 2015a). When coupled with BTES arrangement, GSHP systems can utilize the ground as a heat sink during summer, by combining cooling and heating, where cooling will result in heat injection into the soil, which also acts as storing heat in the soil to be used in the winter season (Rad et al., 2013) as seen in Figure 2.18 and Figure 2.19. He and Lam (2017) simulated BTES heating and cooling in TRNSYS with enerypiles in place of BHEs.

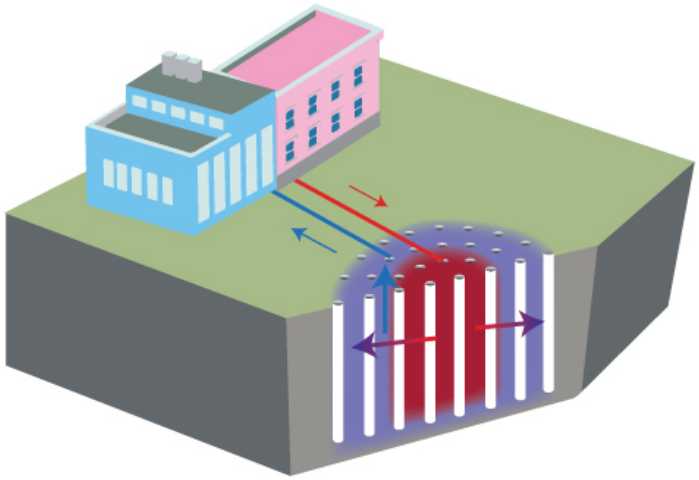

Figure 2.18: BTES summer operation schematic when cooling the buildings (based on (AHGI, 2018)).

BTES can be coupled with solar energy in which excess solar energy is input into the ground (Lundh and Dalenback, 2008), where this system is implemented at the Drake Landing Solar Community (Sibbet, 2012). Nam et al. (2015) found that coupling GSHP systems with solar thermal energy does maintain better thermal balance in the soil and achieve high COP and less electrical consumption. Raising the temperature of the ground using solar energy does increase the efficiency of the BTES system in colder climates as demonstrated in (Wang et al., 2010) and (Reuss et al., 2015). Sliwa and Rosen (2015) has also investigated a number of heat regeneration methods to couple with BTES as an alternative to solar thermal coupling. The

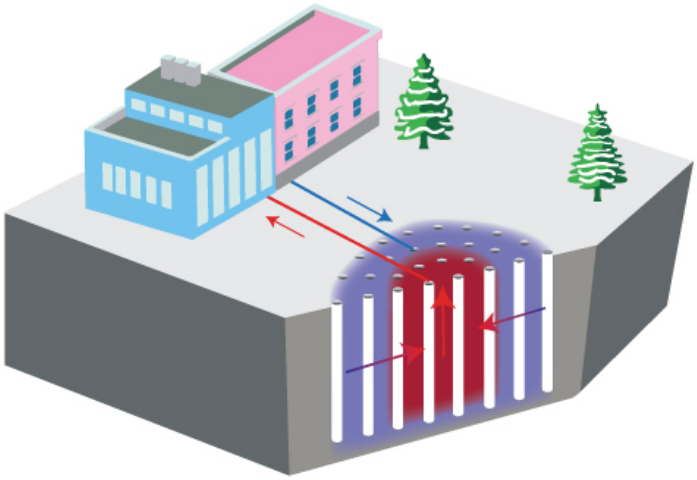

Figure 2.19: BTES winter operation schematic when cooling the buildings (based on (AHGI, 2018)).

functionality of BTES systems has been well demonstrated in several Scandinavian countries, Germany, Netherlands, Austria, Canada and the United States, where these systems were both large and small scale for residential, commercial, and industrial sectors (Lanahan and Tabares-Velasco, 2017). Large BTES systems require significant capital cost as a large number of BHEs need to be drilled, compared to few thermal wells required for ATES systems (AHGI, 2018). However, the installation costs of BTES systems is similar to that of conventional GSHP systems, while having higher COP. For example, the cost of the BTES system at Drake Landing is $2.6/kWh thermal energy stored (Sibbet, 2012). The International Energy Agency (IEA) solar heating and cooling program (SHC), worked on standerdizing and documenting guidelines for the design of seasonal BTES systems (Sibbitt and McClenahan, 2015). The SHC program reported that there is limited literature on the cost of BTES systems, and provided some costs for existing installed BTES systems, and other conceptual costs as well, where the price was reported to drop significantly as the system size increased (Sibbitt and McClenahan, 2015). Another constraint for the BTES system is the available land area needed to install the borehole field, while it is relatively easy to obtain permits for constructing BTES systems as they are are a closed looop technology, where in the UK GSHP systems are not regulated (Zhang et al., 2015b).

2.5 Passenger Thermal Comfort Models Review

There has been little research on defining thermal comfort criteria for underground subway systems (Ampofo et al., 2004a). Fanger has developed the thermal comfort PMV index (Fanger, 1970b), where the PMV scale is a seven-point thermal sensation scale ranging from -3 (cold) to +3 (hot), where 0 represents the thermally neutral sensation. Fanger PMV index was originally developed for use in buildings and office spaces.

It rests on steady state heat transfer theory and was calibrated chiefly against (Nevins et al., 1966) and (McNall et al., 1967) data for the thermal sensations of a large number of American students, obtained during a series of studies in a climatic chamber. Some of these studies have given support to PMV, while others have found discrepancies, and it has become apparent that no individual field study can adequately validate PMV for everyday use in buildings (Humphreys and Nicol, 2002). Validation, therefore, requires the results of many field studies, covering the ranges of indoor conditions encountered in occupied buildings in a variety of climates. Despite its limited validation over the years, the PMV-index (Fanger, 1970b) is probably the index of thermal comfort most widely used for assessing moderate indoor thermal environments.

There has been limited literature related to subway passenger thermal comfort. The major publications that dealt with the topic are (Parker, 1972), (Bell and Watts, 1971), (Booth and Galliers, 2001), and (OIIS, 2002), while in the US only the Transportation Air Conditioning Committee of ASHRAE has done research about the topic (ASHRAE, 2002). Parker (1972) presented the following chart for passenger thermal comfort in Figure 2.20, which was based on American passenger volunteers in US conditions only (OIIS, 2002).

The UK Department of the Environment, Transport and the Regions (DETR) conducted a project about the quality of environment in public transport buildings with the aim of developing methods to increase the use of public transport, which was called the BSRIA report (Booth and Galliers, 2001). The report covered 6 public transport buildings across the UK, which included two railway stations, one airport, one harbor, and two London Underground stations. The two London Underground stations studied are one modern underground tube station and one deep line underground tube station during the summer months of the year

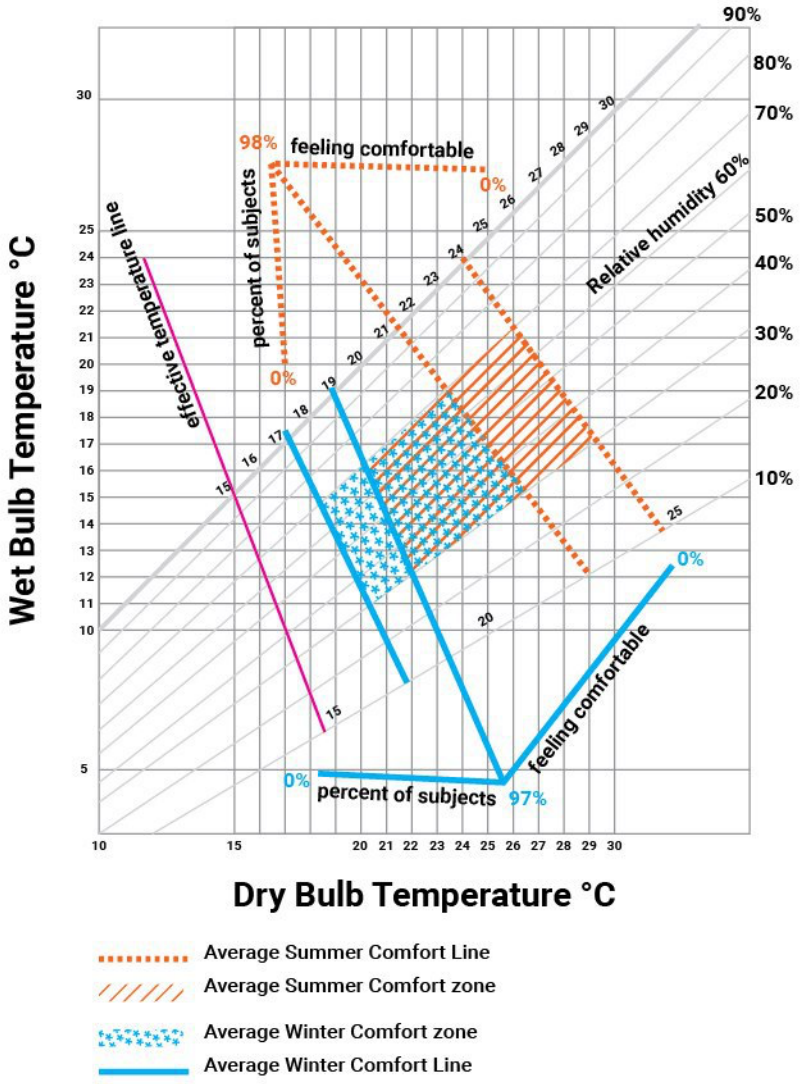

Figure 2.20: Passenger thermal comfort chart range. (based on (OIIS, 2002))

of 2000. The study in the London Underground focused on the ticket office area and the platform. The relative humidity was assumed to be 50 % for the purpose of calculating the PMV and PPD (Ampofo et al., 2003).

Transport for London (TfL) commissioned an extensive survey in 2004, and monitored conditions aboard train carriages, to determine passenger thermal comfort ranges in the London Underground (BRE, 2004a). The survey work found that passenger comfort in the London Underground depended on air temperature. The average temperature range for passenger

thermal comfort in the train was between 21 °C and 26 °C, and in the stations between 17 °C and 25 °C (BRE, 2004a). (BRE, 2004a) also observed average temperatures of 28 °C in the trains and 26 °C in the stations over the period the survey was conducted, where the maximum recorded temperatures in the trains and stations were 41.5 °C and 36.2 °C respectively.

Chapter 3

1D Tunnel London Underground Model and Parametric Analysis

3.1 Introduction

A representative section of an old subway system – the tunnels and the platform – is modeled using IDA tunnel. A 1D model is developed to simulate the environment conditions in the Central Line's Tunnels and Platforms, where air temperature measured data provided by the London Underground are used to validate the model. Transport for London monitors the air temperature across the stations and tunnels. Station building maps, rolling stock schematics, ventilation rates, and passenger traffic information are used to achieve a near realistic model of the London Undergrounds Central Line, where the system's heat sources and sinks are identified and quantified. A parametric analysis is performed on the system's heat sources and sinks to identify the key factors that influence the subway station's climate. This chapter examines several future scenarios, simulating the Central Line's environment taking into consideration the future infrastructure & train upgrades in the system, and the passenger & train traffic projections till the year of 2050. Also, the effects of climate change on the London Underground's environment are assessed to determine whether the upgrades in the London Underground's infrastructure will mitigate the overheating problems or at least preserve the status quo. The 1D Central Line model is modified to simulate the environmental conditions on other deep lines in the London Underground.

The aim is to study the different factors that affect the climate conditions on these deep lines in the London Underground by modifying the existing Central Line model parameters: soil temperature, passenger traffic, train models, and tunnel diameter.

3.2 Methodology

3.2.1 Central Line Model

3.2.1.1 Underground Model Representation

Modelling an entire subway line using IDA tunnel would be cumbersome and computationally penalizing. The Central Line consists of 16 stations underground and simulating the environment of each tunnel and station would take hours of simulation for a single day. Simulations were performed on a 2.7 GHz quad core CPU computer. Super computers can not be used to speed the process, because IDA tunnel does not have parallel processing capability, so a cluster super computer will not speed the simulations since the computational speed is limited to the performance of single CPUs in the cluster. Therefore, a representative section of the Central Line is modeled to emulate the characteristics of this London Underground Line as a whole. The representative model, shown in Figure 3.1, constitutes of 4015 m of bi-directional tunnels (westbound and eastbound) and 3 platforms of 140 m in length each. In this model, tunnel sections A & D (which are open to ambient) and platforms 2 & 3 are close to the exits of the tunnels to the ambient air, and their purpose in the model is to homogenize the underground climate conditions and therefore provide feasible boundary conditions for tunnel sections B & C and platform 1. The tunnel lengths between platforms 1, 2 & 3 are typical for Central Line stations in Central London. The middle station box at platform 1 is modelled in detail based on the old Tottenham Court Road Central Line station schematics (Figure 3.2), since the rest of the Central Line stations follow similar design patterns in terms of passenger entrance, ticketing hall, escalators and passages. The model assumes no interference from other lines in the station. Cross service tunnels are tunnels between the inbound and outbound tunnels of the London Underground, they are used for servicing, maintenance and emergency purposes. Transport for London refused to provide information on them for security purposes. The cross service tunnels between the eastward and westward bound tunnels are neglected in the model, since their effects are localized.

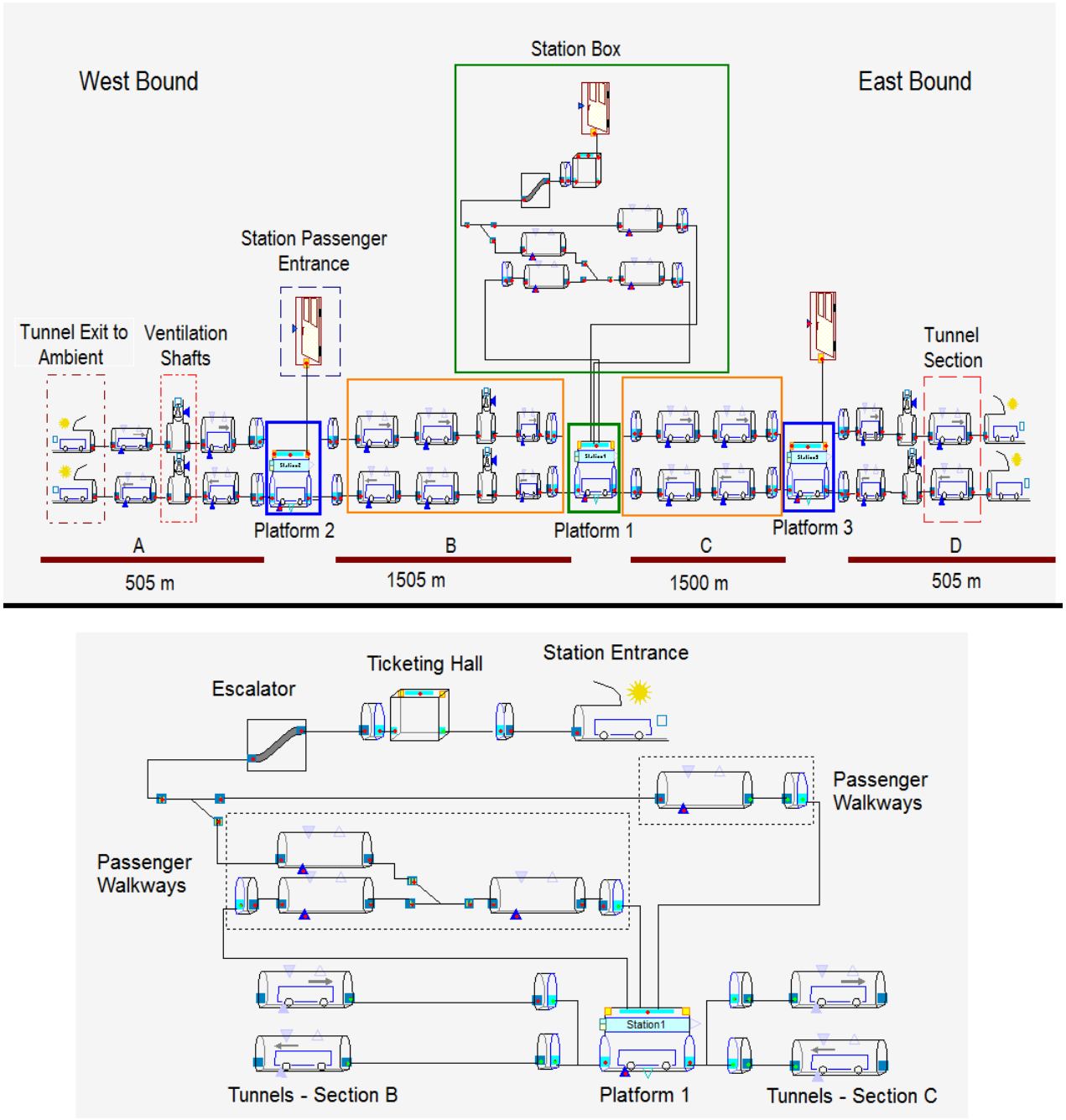

Figure 3.1: Schematic for the Central Line Model (Above), Schematic for the Station Model (below). Both images are generated using IDA tunnel software.

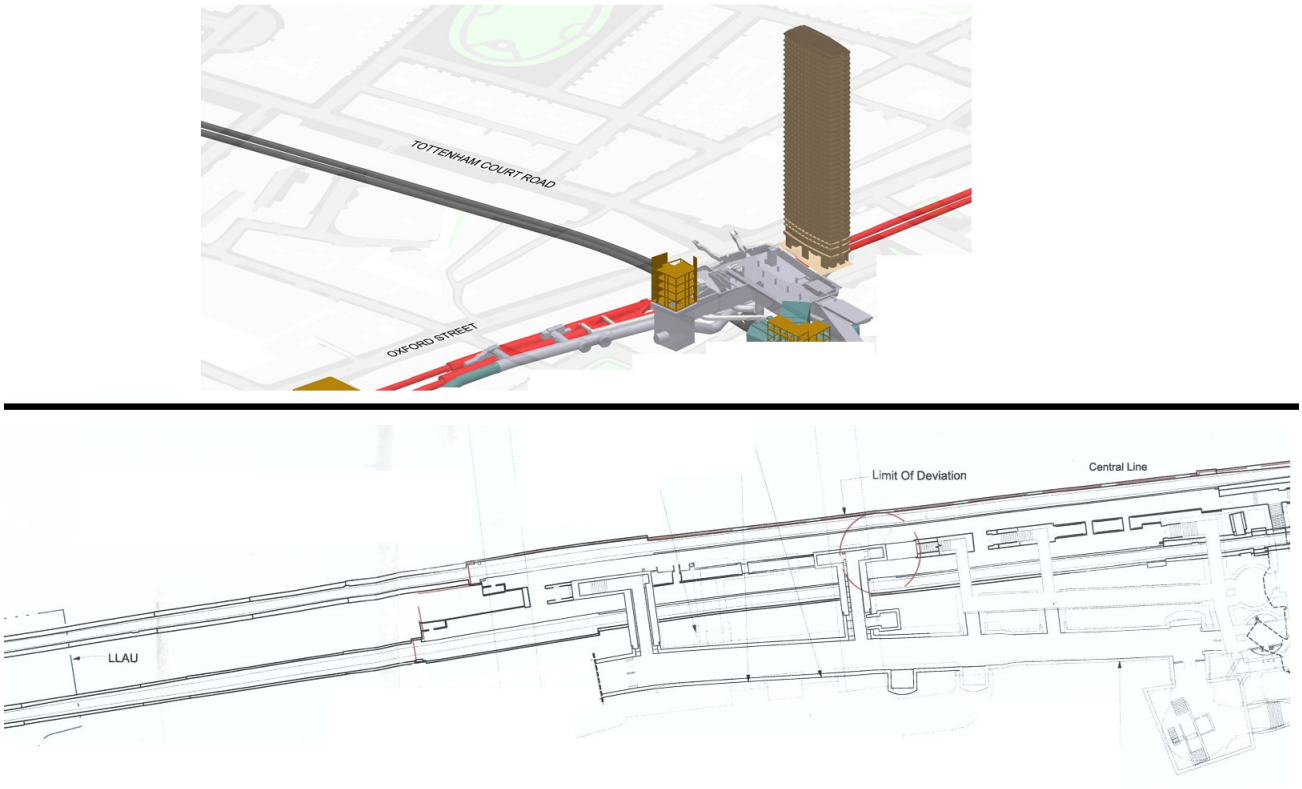

Figure 3.2: 3D model for the Tottenham Court Road station (Above). Map for the Tottenham court road station (Below).(provided by London Underground).

3.2.1.2 Boundary Conditions

The underground system boundary conditions consist of the outside ambient climate conditions and the surrounding soil temperature. London's climate profile for the year of 2013 (Figure 3.3) was generated using "Meteonorm", which is a software that generates a weather profile based on recorded data between 1996-2010. The weather profile input into IDA Tunnel includes: Dry Bulb Temperature, Relative Humidity, Wind Speed, Wind Direction, Direct Normal Irradiance, and Diffuse Horizontal Irradiance. The outer ambient conditions act on the rail tunnel Entry/Exit (Westbound and Eastbound), the entrances of station boxes, and the ventilation shafts (Figure 3.1).

The background soil temperature in London is set to 14 °C, based on recorded temperature measurements (Webb et al., 2009). The tunnel wall is composed of a 2 cm cast iron layer having an inner diameter of 3.56 m, followed by a 5 cm grout layer, while the surrounding

soil is composed of London Clay. The soil properties are taken to be that of London Clay having thermal conductivity = 1.6 W/m.K, density = 1800 Kg/m^3, and thermal capacity = 1200 J/kg.K (Webb et al., 2009). The thermal conductivity of London clay takes into consideration seasonal water saturation by averaging the value over the year (Webb et al., 2009). The thermal conductivity, density, and thermal capacity of cast iron, London clay, grout (concrete), brick and glass are listed in Table 3.1. The soil is assumed to be infinitely thick because the Central Line stations are typically at a depth of 30 m, where the background soil temperatures are fairly stable between 10 m - 100 m soil depth (Webb et al., 2009). The upper first floor of the station is made of a composition of brick walls and glazing (Webb et al., 2009).

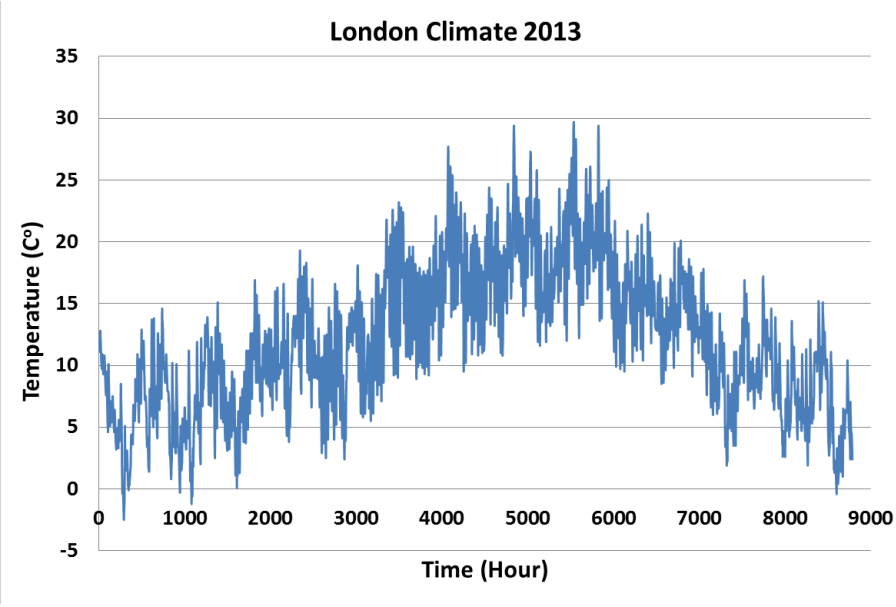

Figure 3.3: The ambient air temperature (°C) for the City of London in the year of 2013, which is simulated using Meteonorm software.

3.2.1.3 Model Heat Sources and Heat Sinks

The heat sources in the model are split mainly between the train braking, passengers, lighting, and equipment. All sections of the station contain lights, signs, and advertisements in which they are mainly composed of fluorescent lights that have an average power consumption of 11 W/m^2. The electric power of fluorescent is converted into 40% radiation and 60% convective heat, where these two forms of heat are included in the model (ASHRAE, 2010). The ticketing

Material	K [W/m.K]	C_p [kJ/kg.K]	ρ [kg/m^3]	Thickness [cm]
Cast Iron	55	0.456	7920	2
grout (Concrete)	1.1	0.88	2400	5
Clay Soil	1.52	1.8	1800	-
Brick Wall	0.595	0.9	1601	30
Window Glass	0.96	0.84	2600	0.3

Table 3.1: Material Properties of the Walls and Soil in the Tunnels and Stations.(Toolbox, 2014) and (Webb et al., 2009).

hall also includes ticketing machines, monitors, and other auxiliary equipment, where their power consumption is provided in Table 3.2. The heat released by the escalators in the station box are computed by calculating the power required to carry the passengers while including a 90% motor efficiency (RAE, 2007), where the wasted energy is converted into heat.

$$P_e = \frac{mass * g * height}{time} \tag{3.1}$$

The escalators in the London Underground travel at a speed of 0.75 m/sec and each foot step is 1 m wide and 0.4 m long (RAE, 2007).

The heat released from the station lifts is calculated by computing the electrical consumption of the lifts where 10% of this energy is converted into heat; the computations were done using a software specialized in estimating the lift's electrical consumption (KONE, 2014). The lights, ticketing machines, escalators, and lifts operate during the opening times of the London Underground. The London Underground typically operates from 5:50 am till 12:30 am. The heat released by the escalators and lifts varies depending on the station's occupancy, which is discussed in the next paragraph.

The occupancy in the station is approximated based on statistical information published by (LUL, 2013). Tottenham Court Road is a busy Central Line station, where an average of 110000 passengers enter/exit daily. A report released by TfL has described the typical patterns of passengers, in which there are daily peaks spanning 1hr between 8:30-9:30 AM, and 17:00-18:00 PM, and 15% of the total daily passengers enter/exit (TfL, 2011) in each

Appliance	**Power Rating**
Fluorescent Lighting	11 W/m^2
Monitor	150 W
Computer Case	120 W
Flat Screen	120 W
Ticket Machine	270 W

Table 3.2: Power rating of appliances in the station.

of the times. The passenger travel patterns are plotted in Figure 3.4, in which unity in the y-axis represents the proportion of passengers during peak times. The Passengers are assumed to be walking on their way from the station entrance to the platform, and remain standing in the platform, where their metabolic rate is taken to be 207 W and 126 W respectively. The passengers are assumed to be distributed equally among the station sections, in which a third are in the upper ticket hall, a third in the escalators and passages, and a third in the platforms. This assumption is used because we have no data on the passenger traffic patterns inside specific sections of the station, but we do have attendance for the station as a whole using the entry and exit gates .

The ventilation in the Central Line is composed of high capacity ventilation fans connected to the outside through ventilation shafts (marked on Figure 3.1). The ventilation fans are operated at full capacity 24 hours a day in exhaust mode at approximately 30 m^3/s all around the year (Gilbey et al., 2011). The outer ambient boundary conditions act on the station entrances, the tunnel's entry & exit points, and the ventilation shafts (Figure 3.5).

3.2.1.4 Train Properties and Schedule

The 1992 Stock is currently used in the Central Line. The 1992 Stock trains are 163 m long, 2.6 m wide, and with a height of 2.8 m, while the train consists of 8 carriages in total. The train has 272 seats and a maximum full load capacity of 930 passengers, so the maximum capacity of the train is 1202 passengers (Tfl, 2007). The 1992 stock is equipped with rheostatic and electro-pneumatic main braking systems and an air released parking brake. The electric traction motors are frame mounted with a fixed gear ratio. The main lightning consists of fluorescent tubes powered by the train's 50V DC inverters, where each carriage contains 26

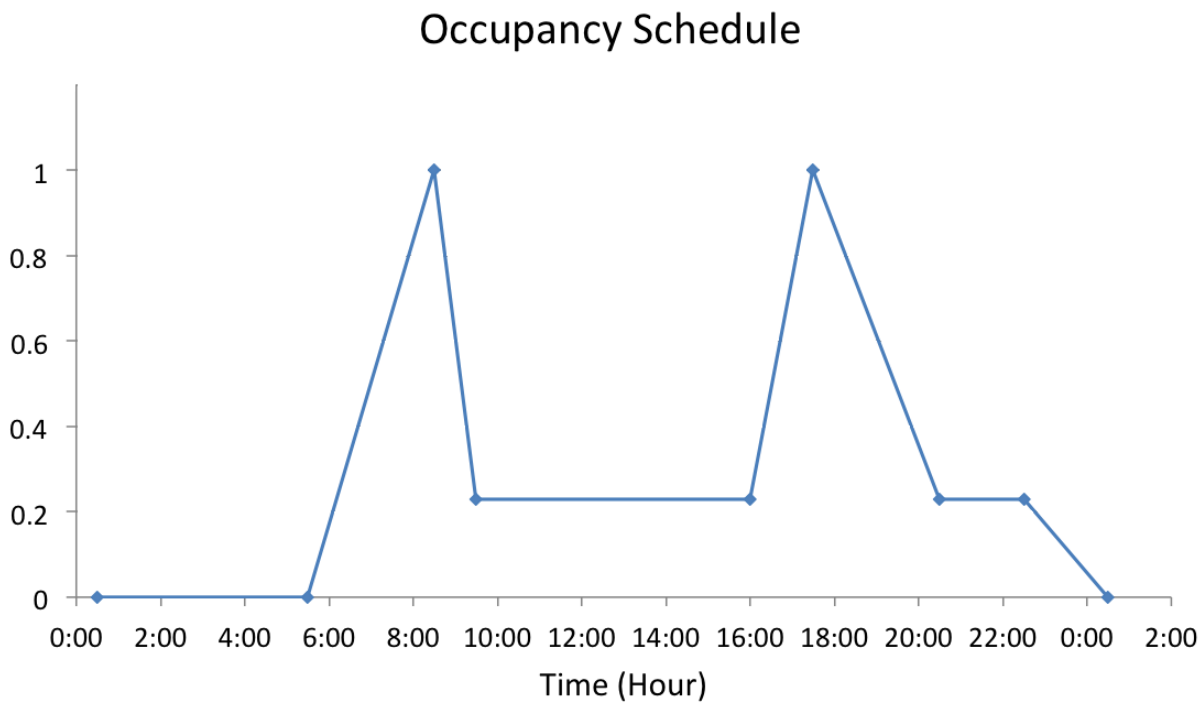

Figure 3.4: Occupancy schedule for the Tottenham Court Road Station.

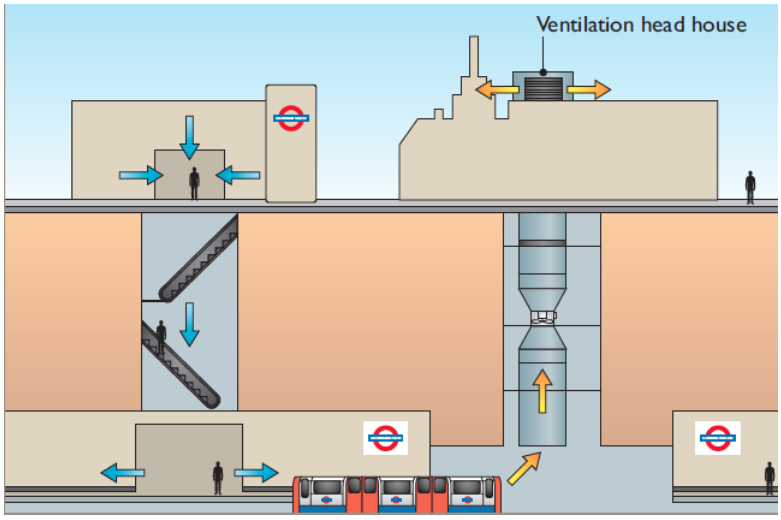

Figure 3.5: Schematic of the ventilation system in London Underground (TfL, 2016a).

tubes (Tfl, 2007). The 1992 rolling stock is not equipped with regenerative breaking. The 1992 Stock train properties used in the simulation are shown in Table 3.3, based on information provided by TfL rolling stock technical manual (Tfl, 2007), and in depth details about the

Central Line trains are found in Figure B.5 and Figure B.6 in Appendix B. The train schedules are provided by London Underground and tabulated in Figure 3.6 : there are 462 trains/day and 30 trains/hour at peak times (8-9 am & 5-6 pm). There are two Routes in the model, EastBound and WestBound.

Properties	**Quantity**	**Properties**	**Quantity**
Front Area (a_t)	10.5 m^2	Kinetic Energy Coefficient (K_m)	1.09
Front Drag Coefficient (C_D)	0.45	Brake Regeneration	0
Vehicle Parameter (P_v)	11 m	Brake Heat Capacity (C_{Brake})	200 KJ/K
Train Length (l_v)	163 m	Train Heat Capacity (C_{Train})	117000 KJ/K
Train Mass (M)	235000 Kg	Brake Area (A_{Brake})	39.6 m^2
Maximum Useful Power (P_m)	1*10^9 W	Passengers Capacity	1202

Table 3.3: Properties of the 1992 Stock Trains. (Tfl, 2007)

The train carriages are manufactured by combining an aluminium body on a steel frame (Transit, 2014). The train walls are generally made from a composition of aluminium walls and mineral/rock wall insulation slabs along with fire resisting layers. The carriage glazing is made from laminated glass, based on a composite of PVB plastics and glass layers, which gives the glazing strength and geometric integrity in case of breakage (Solutions, 2014). The properties of the train carriage material are provided in Table 3.4.

Material	K [W/m.K]	C_p [KJ/Kg.K]	ρ [Kg/m^3]	Thickness [m]
Aluminum	205	0.91	2700	0.005
Carbon Steel	43	0.49	7850	-
Mineral Wool	0.04	0.84	45	0.05
Laminated Glass	0.207	1.96	2500	0.01

Table 3.4: Train Carriage Material Properties (Toolbox, 2014).

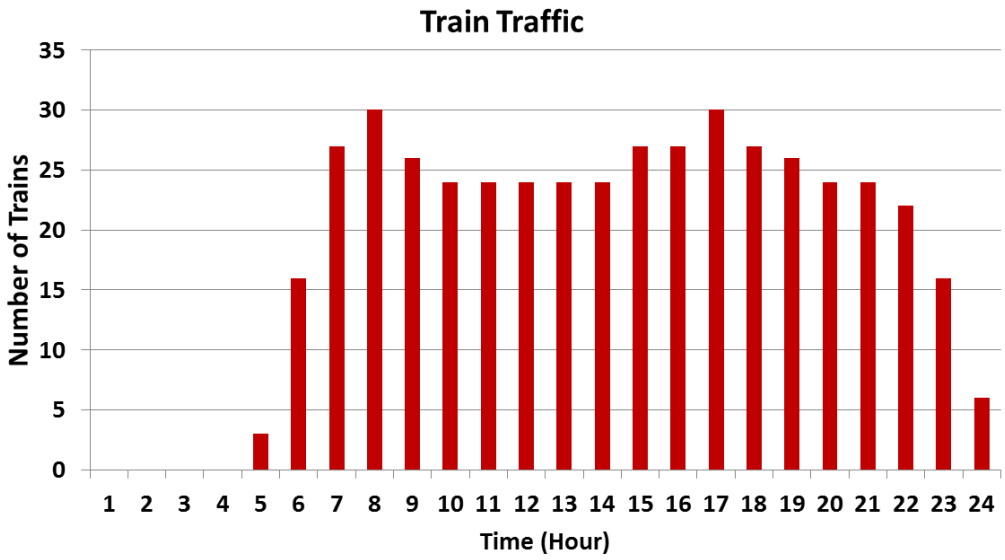

Figure 3.6: Train schedule for the Tottenham Court Road Station.

3.2.1.5 1D Model Simulation Setup, and Model Verification

The Central Line opened in 1890, so its surrounding ground was exposed to heat dissipation from the line that have raised its temperature over the last 114 years. The ground temperature profile for the beginning of 2013 has to be determined in order to accurately simulate the Central Line station and tunnel environmental conditions for that year. This can be achieved by performing a simulation covering several years. However, large and complex systems will in general yield completely unrealistic execution times in IDA Tunnel. In order to reduce execution times to realistic levels while preserving the accuracy within an acceptable tolerance. IDA Tunnel has a procedure called 'long-term model where the time scale for the heat transport in the surrounding bedrock is rescaled to yield a faster transport. Thus, temperature developments which in reality cover years, will in simulations be shortened to hours or days. In 'long-term mode the material properties of the rock are adjusted, such that a long term temperature field is established with only a small fraction of the amount of energy that normally would be required. Simultaneously, the climate data are adapted to the artificial time scale (IDA, 2013).

The model is run in long-term mode for 114 years and then simulated in detail, at a time scale of minutes, for the year of 2013. To validate the model, the resulting simulated tunnel and platform temperatures are compared with actual temperatures in the Central Line for the same year, obtained from Transport for London.

3.2.2 Central Line Model Parametric Variations

A parametric analysis is conducted on the 1D Central Line model in order to quantify the extent to which the system's heat sources and sinks can impact the air temperatures in the tunnels and stations. The study consists of varying the main heat sinks: background ground temperatures & ventilation rates and two main heat sources: train brakes & train traffic. While we acknowledge that Monte Carlo simulations would allow for more scenarios and parameters to be explored, IDA tunnel does not allow for Monte Carlo simulations, so each scenario or parameter change has to be simulated individually. The parametric study will vary the background soil temperature, ventilation rates, brake regeneration rate, and train traffic according to Table 3.5. In case A the background temperatures is changed to 8°C and 18°C, which is far from the tunnels. Also, in case A a radial temperature of 8°C is placed at 0.4 m far from the tunnels, to compare with the previous 8°C background temperature, and to emulate the effect of placing ground heat exchangers such as geothermal vertical boreholes close to tunnels on the tunnel and stations environment. For scenario B the ventilation rate is varied to study the effectiveness of increasing ventilation rates in the system in cooling the Central Line. In Scenario C the brake regeneration rates are varied by varying the train properties in IDA tunnel, where the aim to assess the effectiveness of implementing train regenerative braking in cooling the system, knowing that the current Central Line trains are not equipped with regenerative braking. In scenario D the train traffic is varied such that the Central Line model Train Schedule is increased uniformly by +50% and decreased uniformly by -50 %. Also in Case D the increase in traffic by +50% is combined with equipping the trains with 40% regenerative braking, to assess how regenerative braking can mitigate the predicted air temperature rise in the system due to traffic increase.

Cases	Description
Scenario A : Soil Temperature	8 °C & 18 °C back ground soil temperature and 8 °C soil temperature at 0.4 m distance from outer wall (sections B & C only, platforms excluded).
Scenario B : Ventilation Rate	No ventilation, and quadrupling ventilation rate to 120 m^3/sec per shaft.
Scenario C : Brake Regeneration	Regenerative braking rates (Regen) of 20% & 40%
Scenario D : Train Traffic	+50% & -50% in train traffic, and combined +50% Traffic & 40% regenerative braking.

Table 3.5: Case descriptions of the parameters to be studied using the Central Line model.

3.2.3 Central Line Modernization and Climate Change Scenarios

3.2.3.1 Central Line Modernization

In order to accommodate the rapid population growth of the city of London, which would reflect as an increase in train traffic and passenger numbers in the London Underground, TfL will embark on projects to modernize the existing London Underground Lines in order to increase capacity, reduce journey times, and enhance the passengers comfort (LU, 2014). Several upgrades are planned for these deep lines, which include the introduction of new trains with regeneration braking, new signaling system, and the operation of more trains per hour.

The Central Line passenger traffic is expected to increase by 25% in 2032 and by 65% in 2050, while the train traffic is predicted to increase by 20 % in 2032 and a further 20 % by 2050 (Mayor, 2015). Also, the number of trains during peak times will increase from 28 trains/hour to 36 trains/hour in 2032 and to 40 trains/hour in 2050 (for London, 2013).

Year	**2032**	**2050**
Passengers	+20 %	+65 %
Train Traffic	+20 %	+40 %
Peak Time Trains/hour	36	40

Table 3.6: Changes in the Central Line for the Year 2032 & 2050 compared to current situation.

New trains for the Central Line are planned to be introduced in 2032, where they will be equipped with regenerative breaking, have lower weight, and higher acceleration, however the installation of on-board air-conditioning it is still uncertain (LU, 2014). Since the new trains are still in the design process, a large portion of its specifications has not been determined yet, so it is assumed in the model that the train is a hybrid between the existing Central Line's 1992 train and known specifications of the new trains, such as 40 % regenerative braking.

3.2.3.2 Climate Change Scenarios

Not only the Central Line is changing in terms of passenger numbers and train traffic, but also the climate surrounding the London Underground, which forms one of the main boundary conditions besides the surrounding soil. Indeed, climate change is taking effect across the globe, and it is having adverse effects on our lives and the planet's eco-system as well. Thus, in order to properly asses the future changes in the London Underground's environment, climate change has to be taken into consideration.

The UK Climate Projections (UKCP09) are used to simulate the future environment of the Central Line. UKCP09 was produced and funded by The Department for Environment, Food & Rural Affairs (DEFRA) based on scientific methods used by the Met Office, where they are used to help organizations and governments explore adaptation measures, based on future climate projections (DEFRA, 2009). The UKCP09 provides predictions between the years of 2020 till 2080, within a downscale of a 25 km resolution, which is considered a regional scale. The climate future projection assumes three future emission scenarios: low, medium, and high. The UKCP09 projects a number of climate variables for both land and marine areas. These variables include: Air Temperatures, Precipitations, Humidity, Cloud Coverage, Sea Level Air Pressure, and Sea Wave Heights. The emission scenarios from the IPCC Special Report on Emissions Scenarios (SRES) are based on human activity projections over this century, taking into consideration socio-economic factors, such as population growth, technology, economy, energy, and agricultural activity (DEFRA, 2009). The UKCP09 projections for the climate variables are provided for the probability levels of 10%, 33%, 50%, 67% and 90%. The probabilities provided in the UKCP09 are not the same as a number for chance games, rather they follow a bell curve where 50% is the central estimate, median, or most probable. For this reason, the 50 % is adopted to simulate the future environment of the Central Line.

The 1D Central Line model is simulated using the UKCP09 climate projections for the years of 2032 and 2050, considering a 50 % probability and two scenarios for each year: medium emissions (ME) and high emissions (HE). These years were chosen, because in 2032 the new trains are expected to start operation in the Central Line, and in 2050 the European Union set its low carbon targets for that year (EC, 2016) and the Mayor of London Office has set this year as paramount for their future transport infrastructure vision (Mayor, 2015). The median static air temperature (SAT) for 2013, 2032 ME, 2032 HE, 2050 ME, 2050 HE are 12.2 °C, 13 °C, 13.1 °C, 13.7 °C, and 13.9 °C respectively. As an illustration, the air temperatures for the years of 2013 and the UKCP09 projected temperatures for 2032 & 2050 for medium & high emissions are plotted in Figure 3.7 for 4 days in the month of August. The 2050 HE air temperatures are the highest, while the 2013 are the lowest but sometimes overlap with the 2032 ME temperatures. This is because the future climate model is probabilistic and temperature extremes within one day may vary between different years, but there is a general trend of having higher air temperatures as we move into the future and for the case of HE scenarios within the same year.

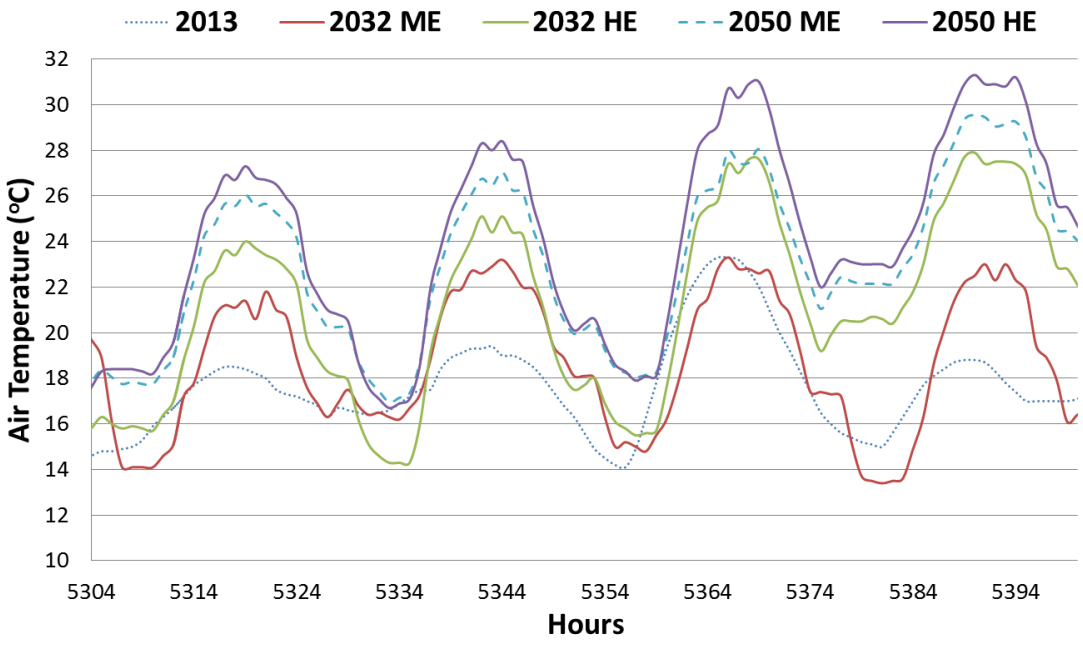

Figure 3.7: The air temperatures for 4 days in the month of August for the years of 2013 and the UKCP09 projected temperatures for 2032 & 2050 for medium (ME) & high emission (HE) scenarios (DEFRA, 2009).

Long term simulations, are needed to determine the ground temperature profile between the years of 2013 & 2032 , and 2033 & 2050, in order to simulate the climates in detail for the years of 2032 and 2050. The methodology is similar to what has been explained in section 3.2.1.5. The increase in passenger and train traffic is assumed to be linear between the years of 2013 & 2032 , and 2033 & 2050, so linear interpolation is used to calculate these values and input them in the Central Line model between these years. The long term simulations are done over time steps such that between the years of 2013 & 2032 they are divided 6-6-7 year intervals (2013 - 2019, 2019 - 2025, 2025 - 2032) , and between 2033 & 2050 they are divided by three 6 equivalent year intervals (2033 - 2039, 2039 - 2045, 2045 - 2050). For example between the years of 2013 - 2019, the soil temperature profile of the 2013 is input in the model, and a long term simulation is conducted up till 2019. For the year of 2019, the SAT temperature profile, train and passenger traffic is modified based on climate change and linear interpolation for future passenger and train traffic trends then a long term simulation is conducted for 6 years until the year 2025. This process is repeated until we get to the year of 2050. In total 6 long term simulations are conducted between 2013 and 2050.

3.3 Results and Discussion

3.3.1 Model Validation

After the long term simulations, the obtained ground temperature radial profile is used to simulate the model for the entire year of 2013 at a time step of 1 min. The temperatures of tunnel sections B and C (Figure 3.1) are similar so the tunnel section C is used to display the simulated tunnel temperatures, whereas the simulated platform temperatures are shown for platform 1. Measured air temperature sensor data was obtained from Transport for London over 5 years between 2007 - 2012 for the operational times of the Central Line (6 am to midnight) in the form of a linearised relationship between the outer ambient temperature and the temperature measured in the tunnels and platforms. The linearised data show that platform temperatures tend to be around 2 °C warmer in average than the tunnels, because of localized train braking in the platform. The linearised measured data for platform and tunnel air temperature in winter conditions are 20 °C to 15 °C higher than the outer SAT temperature of 1 °C (Figure 3.8). Also during summer conditions they are higher by 3 °C and 1 °C respectively at an outer SAT temperature of 30 °C (Figure 3.8).

The simulated temperatures for the tunnel and platform during operational hours are plotted in Figure 3.8 and Figure 3.9 against the linearised measured data. The simulated air temperatures for both the tunnel and platform are close to the measured data, when fitted linearly. The linear fit for the simulated platform temperatures indicates that the model predicts a slightly cooler platform temperature at low ambient temperatures (winter conditions). This difference can be attributed to air-heated train cabins during winter conditions which is not included in the model nor are additional heat sources such as spot/localised heating in areas of the subway stations (eg information and ticketing offices). The simulated tunnel temperatures (Figure 3.9) match the measured data, except for a slight 0.5 °C higher temperature prediction at 30 °C ambient temperature. This small difference can be attributed to the simplification of the tunnel system in the model. Indeed, cross tunnels between eastbound and westbound tunnels were neglected in the current model. Thus, the model has slightly less tunnel volume than the actual tunnel, but similar amount of heat dissipation.

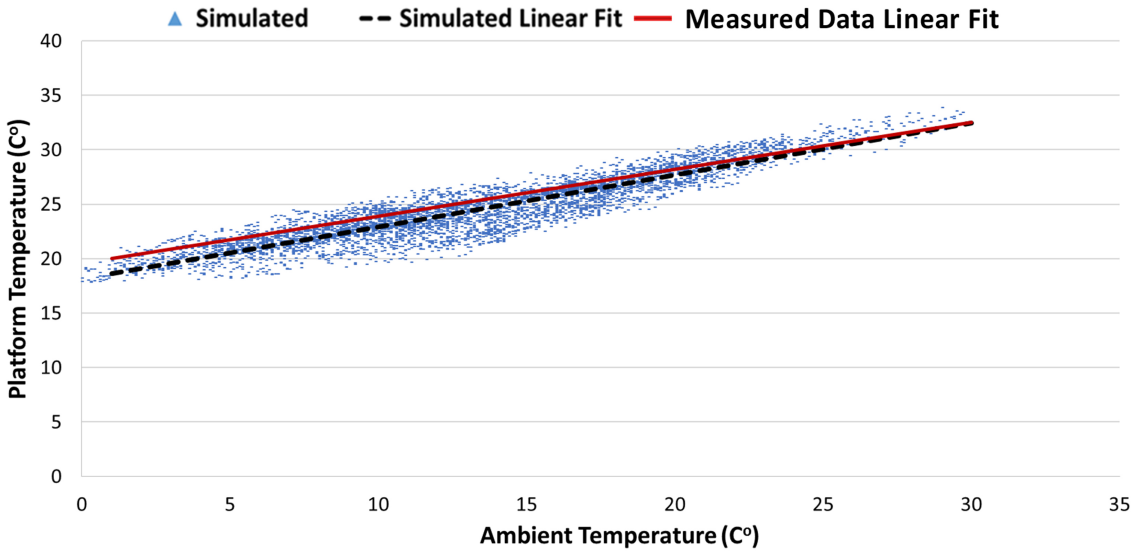

Figure 3.8: Central Line model simulated platform air temperatures compared with measured data.

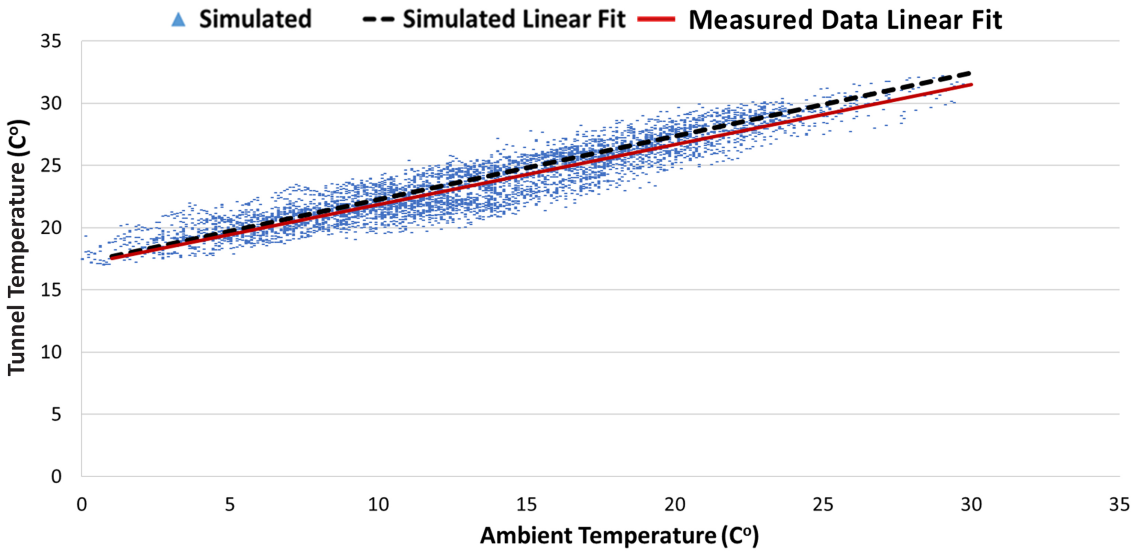

Figure 3.9: Central Line model simulated tunnel air temperatures compared with measured data.

The contribution percentages of the different heat sources during peak times in the system which includes section B, section C, platform 1, and the station box are shown in Figure 3.10. At peak times, braking contributes to approximately 61% of heat dissipation in the subway system (Figure 3.10), as the 1992 stock has no brake regeneration. Passenger traffic in the station and trains combined contribute approximately to 34% of the total heat dissipation in the system. The lights and equipment in the tunnels and station only contribute to a

combined 5% of the total heat dissipation in the system combined.

The results are compared with (Ampofo et al., 2004a). In his model Ampofo et al. (2004a) evaluates operation under peak load conditions.Ampofo et al. (2004a) assumed in his model that the trains are operating fully loaded at midday in August with ambient conditions of 27.1 C, 60% RH and 101 kPa barometric pressure. The model broke down the heat loads for the tunnels and trains under these environmental conditions. (Ampofo et al., 2004a) results show that 85 % of the heat load is due to train braking, while 13 % is due to train equipment and train carriage passengers, and 2 % for tunnel lighting. Ampofo et al. (2004a) did not account for the heat loads in the station equipment, and also the passengers in the platform and station.

To compare (Ampofo et al., 2004a) with Figure 3.10, we do not need to account for the station equipment and passengers, and only include heat sources from the trains and tunnels. If only train and tunnels are considered in the IDA Central Line model, train brakes will account for 78% of the total heat released, while 21 % is for train equipment and train carriage passengers. The IDA tunnel results are close to (Ampofo et al., 2004a) model, where the difference in numbers can be attributed to several factors. (Ampofo et al., 2004a) is a steady state model, which highlighted the heat break down of the loads occurred at specific environmental conditions stated in the previous paragraph. The IDA Central Line model is transient, and the heat break down at peak loads is the average for peak times all around the year. Ampofo et al. (2004a) used the train rolling stock of the Victoria line, while the IDA Central Line model used the rolling stock of the Central line.

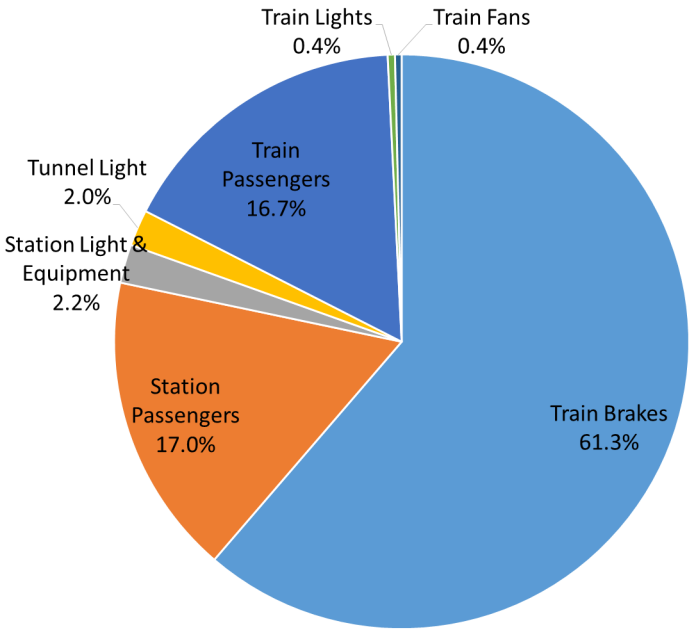

Figure 3.10: Peak Time Heat Source Distribution in the Central Line Model.

3.3.2 Central Line Model Parametric Variations

A parametric analysis was conducted on the verified Central Line model to quantify the extent to which existing heat sources and sinks can influence the Central Line's environment and how can they be utilized to lower the subway system temperatures during overheated periods. The two main heat sinks (case A) background ground temperatures and (case B) ventilation rates and two main heat sources (case C) train brakes and (case D) train traffic are selected for the analysis.

The results of scenario A (Figure 3.11) show that varying the background soil temperature to 18 °C and 8 °C has a slight effect on the Central Line's climate in both the platform and tunnel. This is because the background soil temperatures are around 50 meters far from the tunnel, where the tunnels thermal interference with the background soil temperatures is minimal, this has been also shown in (Soga et al., 2014), which modeled heat dissipated from the Cross Rail tunnels using COMSOL, while Hu et al. (2008) has shown that the thermal effect from the wall of an Underground Rail tunnel built in silty clay can reach up to 20 m. On the other hand having 8 °C soil temperature at 0.4 m distance from the outer wall of

the tunnel has a significant effect on the subways climate where temperatures have dropped by 5 °C and 6 °C in the platform and tunnels respectively from 32 °C and 31 °C to 27 °C and 25 °C respectively during summer conditions, as a result of the close proximity to the tunnel compared to background soil temperatures. To achieve these low temperatures in the proximity of the tunnel wall, a cooling effect is needed such as either a ground source heat pump or groundwater cooling. Ampofo et al. (2004c) has investigated the cooling effect due to ground water cooling in the tunnels in the London Underground where his model fixed the ambient conditions at °C. The results of (Ampofo et al., 2004c) are compared to scenario A at ambient conditions of 27.1 °C. At ambient conditions of 27.1 °C the background soil temperature of 8 °C would result in cooling the tunnels by 0.75 °C (Figure 3.11), which is equivalent to water ground cooling load of 44 kW/km (Ampofo et al., 2004c). At ambient conditions of 27.1 °C, having 8 °C soil temperature at 0.4 m distance from the outer wall of the tunnel would result in cooling the tunnels by 5.9 °C (Figure 3.11), which is equivalent to water ground cooling load of 270 kW/km (Ampofo et al., 2004c).

In scenario B (Figure 3.11), the platform and tunnel air temperatures increase 3 °C and 2 °C respectively when the mechanical ventilation is turned off, as fresh air intake is only through the trains piston effect and natural ventilation through openings in the station and tunnel exits. Increasing the ventilation rates by 4 times would only lower the temperatures by around 1 °C during summer conditions, because increasing the ventilation rates would bring the London Underground temperatures closer to the ambient conditions which are already high during summer. However, during winter there is a significant decrease in the tunnel and platform temperatures, and the effect is more prominent in the platforms because the ventilation shafts are situated close to the platforms. The slope for this plot is steeper for increasing the ventilation rates by 4 times, which indicates that the London Underground climate is made closer to the ambient conditions as a result of increased air exchange rate. Ampofo et al. (2004c) also examined the effect of ventilation fan capacity rates on tunnel and train carriage temperatures at different ambient conditions. Ampofo et al. (2004c) varied the ventilation fan rates while fixing the ambient air temperatures at 27 °C and 20 °C from the current rate of 30 m^3/sec until 300 m^3/sec which is ten times the current ventilation fan rate. The results of (Ampofo et al., 2004c) are compared to scenario B at ambient conditions 27 °C and 20 °C in Figure 3.11, where the ventilation is increased by 4 times to 120 m^3/sec. Based on Figure 3.11 at ambient conditions 27 °C and 20 °C increasing the ventilation rate by

4 folds decreases the temperatures in the tunnels by 2 °C and 2.4 °C respectively compared to (Ampofo et al., 2004c) which gave a result of 2.75 °C and 3.5 °C. The difference between (Ampofo et al., 2004c) and the IDA Central Line model is because (Ampofo et al., 2004c) model is steady state while the Central Line model is transient. Also, Ampofo et al. (2004c) modeled a generic section of a deep line in the London Underground, while Scenario B models in particular the Central Line. Although increasing the ventilation rate would lower the air temperature in the London Underground, achieving this change in ventilation rate may be a formidable civil engineering task in older deep underground railways where it is much easier to implement such changes near the surface (Ampofo et al., 2004c).

Results of scenario C (Figure 3.11) show that equipping trains with 20% and 40% regenerative braking will decrease the temperature in both the subway platform and tunnel by 2 °C and 1 °C respectively. The current Central Line 1992 rolling stock has no regenerative braking, while the new S7 and S8 Stock servicing the shallow Metropolitan, Hammersmith & City, Circle, and District Underground Lines in London have 20% regenerative braking (Tfl, 2007). Ampofo et al. (2004c) examined the effect of regenerative braking on tunnel and train carriage temperatures at fixed ambient conditions 27 °C, by varying the regenerative breaking percentage between 0% and 90 %. The results of (Ampofo et al., 2004c) are compared to scenario C at ambient conditions 27 °C in Figure 3.11, where the regenerative braking percentage is varied to 20 % and 40 %. Based on Figure 3.11 at ambient conditions 27 °C, equipping the train brakes with 20 % and 40 % regenerative braking decreases the temperatures in the tunnels by 1.2 °C and 1.8 °C respectively compared to (Ampofo et al., 2004c), which gave a result of 1 °C and 1.8 °C respectively. The major effect of brake regeneration, is to electrically carry the kinetic energy away from the train braking without converting it to heat inside the underground rail environment (Ampofo et al., 2004c).

The simulations for scenario D (Figure 3.11) show that increasing the train traffic by 50% significantly increases the temperatures in the tunnels and platform by 2 °C. Decreasing the traffic by 50% will decrease the temperatures in the tunnels and platform by 1 °C during summer conditions, while there is a significant decrease in temperatures by around 5 °C during winter conditions. As the train traffic decreases, the Central Line climate tends to get closer to the outer ambient conditions. This is clearly shown in the platform temperature slope, because the station interacts more than the tunnels with the outer ambient conditions. Combining +50% traffic with 40% regenerative braking results in similar temperatures to the

original Central Line simulation during summer conditions because the increase in released brake heating due to +50% traffic is balanced by brake heat reduction due to 40% regenerative braking. However, during winter conditions air temperatures are reduced in the platform and tunnels by 2 °C, since less heat is released by each train even though there are +50% trains running in the system.

By examining scenarios A,B,C and D (Figure 3.11), having a soil boundary temperature of 8 °C (Figure 3.11), would result in the most effective cooling in the Central Line, followed by regenerative braking, while increasing ventilation rates is the least effectiveness among the three mentioned. These results agree with (Ampofo et al., 2004c), who compared several cooling methods in the London Underground and found out that ground water cooling would result in the most effective cooling in the system, followed by applying regenerative braking, then increasing ventilation rates which had the least effect on cooling the London Underground tunnels among those three. Ampofo et al. (2004c) also concluded that increasing ventilation rates would result in increased electricity consumption to power these fans, while ground water cooling requires much less electricity.

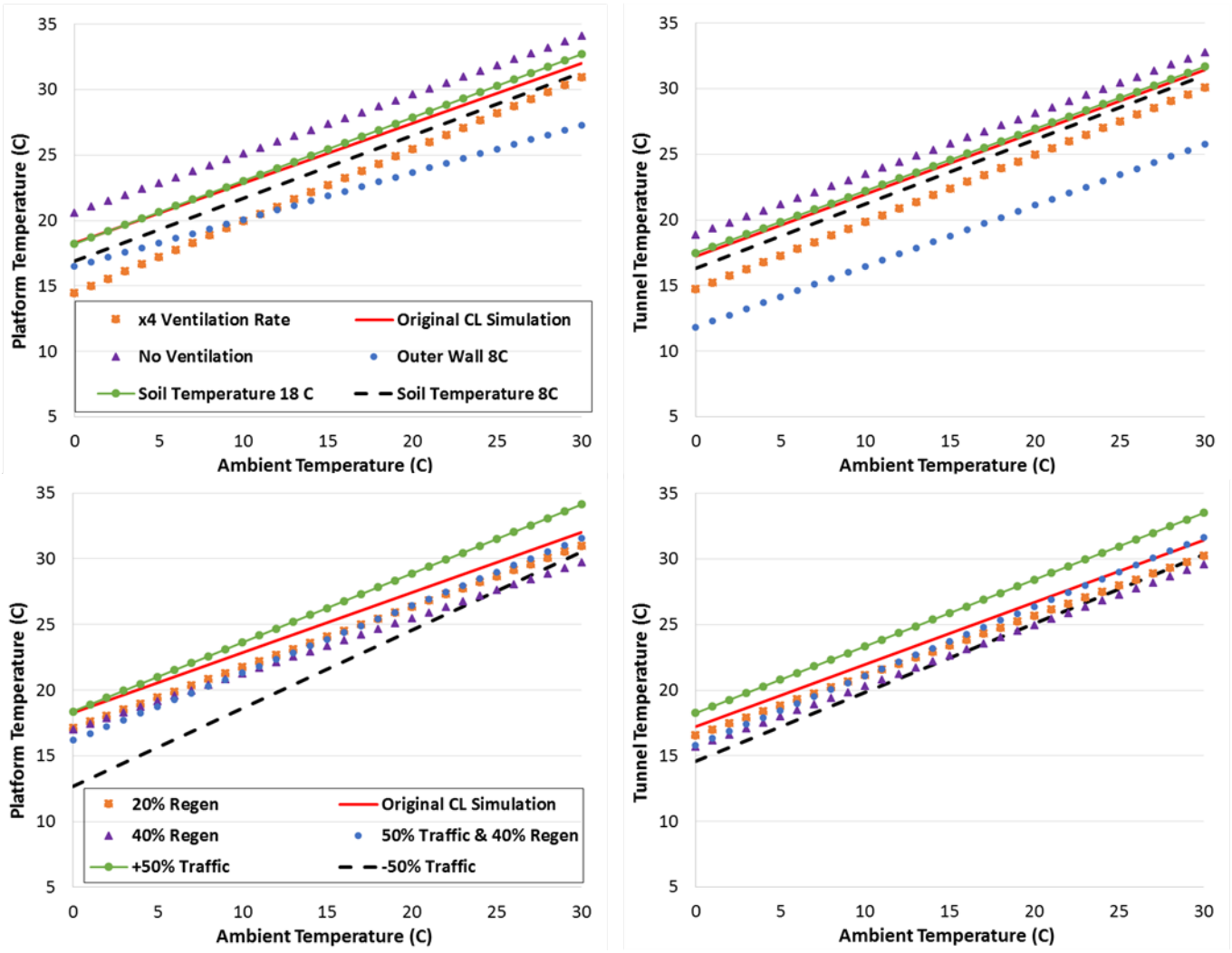

Figure 3.11: Comparing the original simulated Central Line linear fitted platform and tunnel temperatures with (a) Cases A & B and (b) Cases C & D.

3.3.3 Climate Change Scenarios

The 1D Central Line model is first simulated for the year of 2013, varying the climate conditions so it resembles the climate projections of 2032 and 2050 for medium emissions (ME) and high emissions (HE) scenarios, while keeping the passenger numbers, train traffic, and train type the same as 2013. The aim is to assess the effect of solely climate variations on the Central Line environment if nothing changes in the operation of the line. The resulting platform and tunnel temperatures for 2032 ME & 2032 HE and 2050 ME & 2050 HE are equivalent with negligible differences between them, so only ME scenarios are shown through

the rest of this paper. The simulation results (Figure 3.12) have shown that the tunnel and platform temperatures gradually increase as we go to 2032 ME climate and 2050 ME climate. The platform temperatures increase by 1.5 °C between 2013 and 2050 ME climates, while for the tunnels, the air temperatures increase by 1.2 °C between 2013 and 2050 ME climate. Thus, climate change will result in exacerbating the overheating problems in the Central Line, because the increase in ambient temperature would inevitably result in an increase in tunnel and platform air temperatures, since the outer ambient conditions interact directly with the underground section of the Central Line.

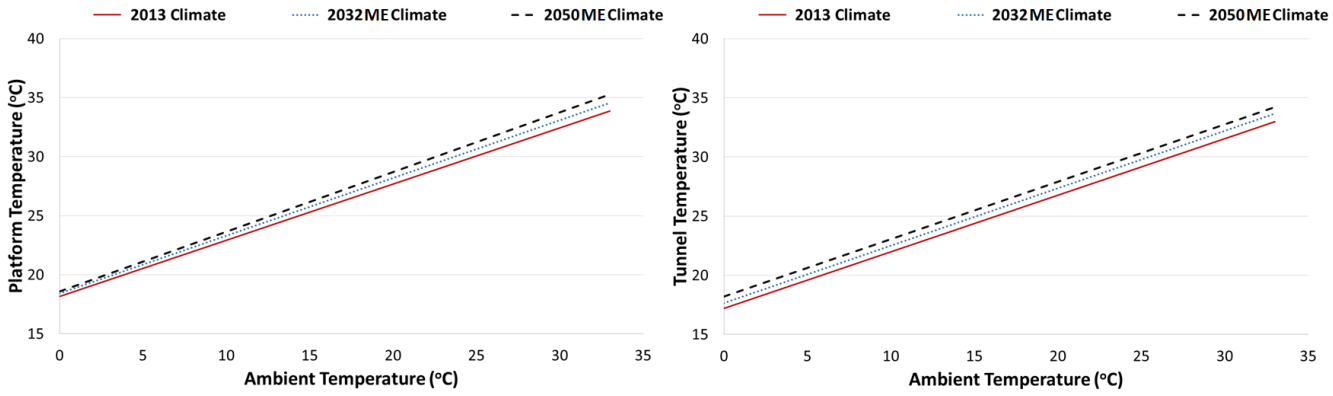

Figure 3.12: Central Line model simulated platform and tunnel air temperatures for the climate profiles of 2013, 2032 ME, and 2050 ME.

The "Long Term" simulation soil temperature results between the years of 2014 & 2050 are provided in Figure 3.13 for the radial distances of 0.1 m , 0.4 m, 1 m, 8 m, 20 m, and 30 m away from the tunnel walls. Figure 3.13 shows that the initial ground temperatures for 1st January tended to increase by 1.2 °C between the years of 2014 & 2050.

Next, the Central Line model was simulated for the years of 2032 and 2050 taking into consideration the future train traffic, passenger numbers projections, climate change, and the introduction of new trains as shown in Table 3.6. The results are compared with the original case (2013) and shown in Figure 3.14. The addition of brake regeneration in 2032 cools the platforms by 1 °C and the tunnels by 0.5 °C during summer conditions. This small benefit

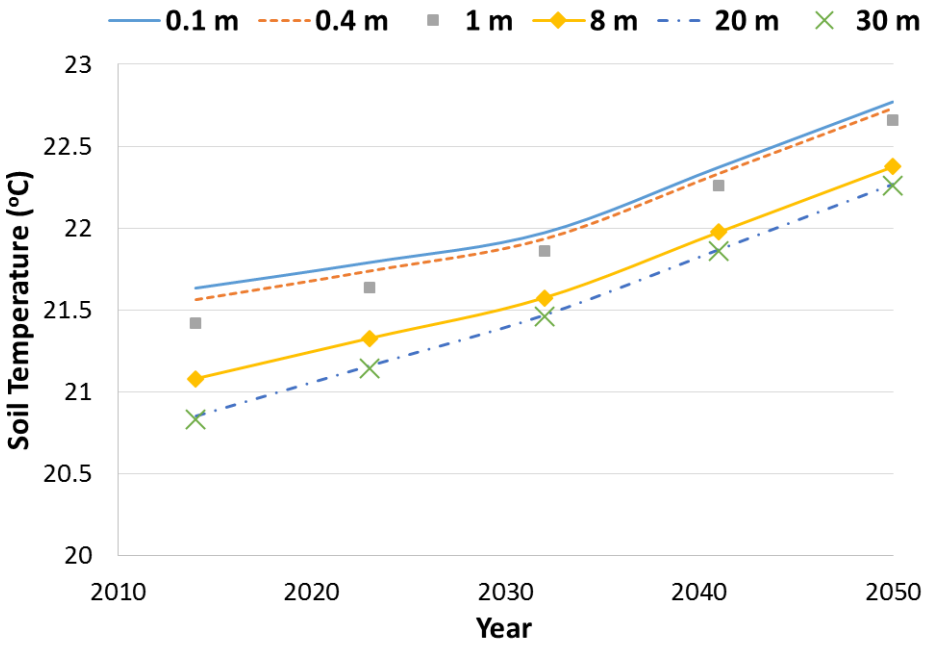

Figure 3.13: Central Line Model ground soil temperature profile between the years of 2013 - 2050 for January 1st.

is temporary since by 2050 the combination of warmer ambient temperature and increase in passenger and train traffic would lead to higher platform and tunnel temperatures compared to the original case (2013) by 1.2 °C & 1.5 °C respectively. As for winter conditions, the platforms and stations air temperatures cool by 2.5 °C and 1.5 °C for the years of 2032 ME and 2050 ME respectively, which is due to the use of regenerative braking, which has also been observed in the parametric variation analysis in section 3.3.2 Figure 3.8.

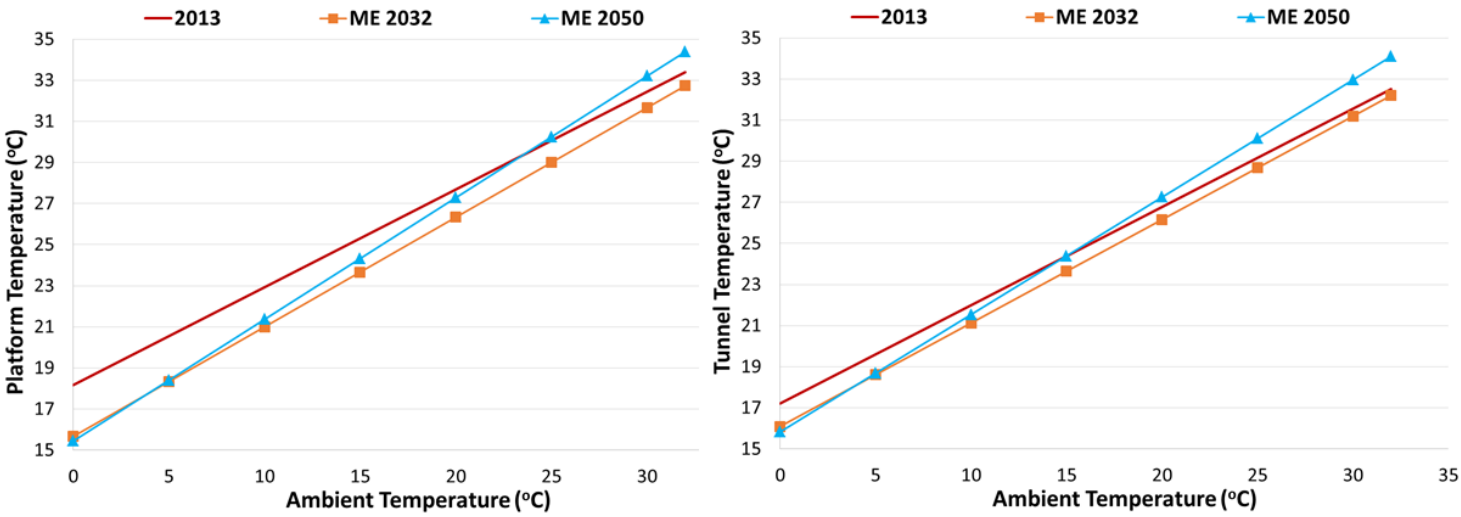

Figure 3.14: Central Line model simulated platform and tunnel air temperatures for the projected climate, traffic, passenger, and new train scenarios for 2013, 2032 ME, and 2050 ME.

3.3.4 Modelling Other London Underground Lines

The Central Line model is modified to simulate the environment conditions on other deep lines in the London Underground. The aim is also to assess how these deep line's distinct parameters influence their climate conditions. London Underground has installed data loggers to monitor the air temperature at the end of the platforms and tunnels across several stations. This data was provided in a form of variation between the averaged temperatures in both platforms and tunnels and the outside ambient temperature across several lines as shown in Figure 3.15, which will be used to verify the subway model's simulation results.

The Northern Line, Bakerloo Line, and Jubilee Line will be modelled using a modified version of the Central Line model. The properties of these lines are displayed in Table 3.7. The Northern Line dates back to 1890 (TfL, 2016b), where it has ferried 253 million passengers in 2013. What makes this line different from the Central line is that its trains operate at speeds 25 km/hr lower than the Central Line, because some of its sections have smaller diameters forcing the trains to travel at lower speeds and the daily train traffic is 70 trains less. Also, the Northern Line's 1995 Rolling Stock trains have 20% brake regeneration capability (Tfl, 2007). The Bakerloo Line opened in 1906 and currently carries 112 million passengers annually, the line operates the 1972 Rolling Stock, which is the oldest train stock in the London Underground

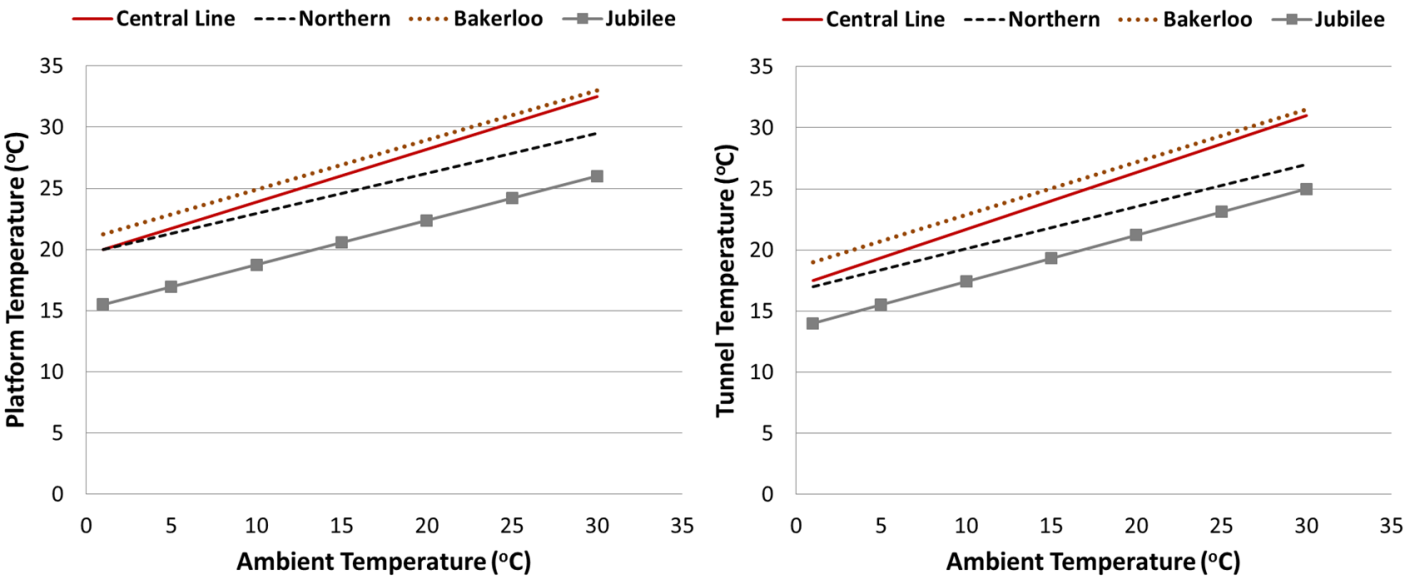

Figure 3.15: Variation of platform temperature (°C) with respect to outside ambient temperature (°C) for London Underground's Central, Bakerloo, Northern, and Jubilee Deep Lines.

(Tfl, 2007). These trains do not have brake regeneration, and are less efficient than their 1990's counterparts. Also, the ground soil temperature in the area where the Bakerloo Line passes is higher by 2 °C than the Central Line reaching 16 °C. The ground temperature profile below London for the London Clay deposit was compiled by (Headon et al., 2009) and represented in a map (Figure 3.16), which has found that the soil temperatures increase from east to south west reaching highs of 16 °C, where the majority of the Bakerloo Line is located. The Jubilee Line is the newest line in the London Underground (1979) and currently services 214 million passengers (TfL, 2016b), utilizing the 1996 Rolling Stock trains which also has 20% brake regeneration. The tunnel diameter in most of the Jubilee Line is wider than the Central Line having a diameter of 4.4 m (Water, 2013). High capacity ventilation shafts are provided at stations and at 1000 m intervals between stations along the Jubilee Line (Ritchie, 2016), since its modern design and construction allowed the designers to take into consideration current passenger numbers and train traffic unlike the older deep lines in the London Underground. The parametric variation study described previously in section 3.2.3 is essential to characterise how the the different London Underground climate conditions in the deep lines will vary depending on their characteristics.

Line	Central	Northern	Bakerloo	Jubilee
Brake Regeneration	0%	20%	0%	20%
Opening Date	1900	1890	1906	1979
Daily Train Traffic	440	370	357	467
Train Model	1992	1890	1972 MKII	1996
Peak Time Trains/Hour	30	23	22	30
Annual Ridership (millions)	262	252	111	213
Soil Temperature (°C)	14	14	16	14
Tunnel Diameter (m)	3.56	3.56	3.56	4.4

Table 3.7: Characteristics of the London Underground Central, Northern, Bakerloo, & Jubilee Deep Lines.

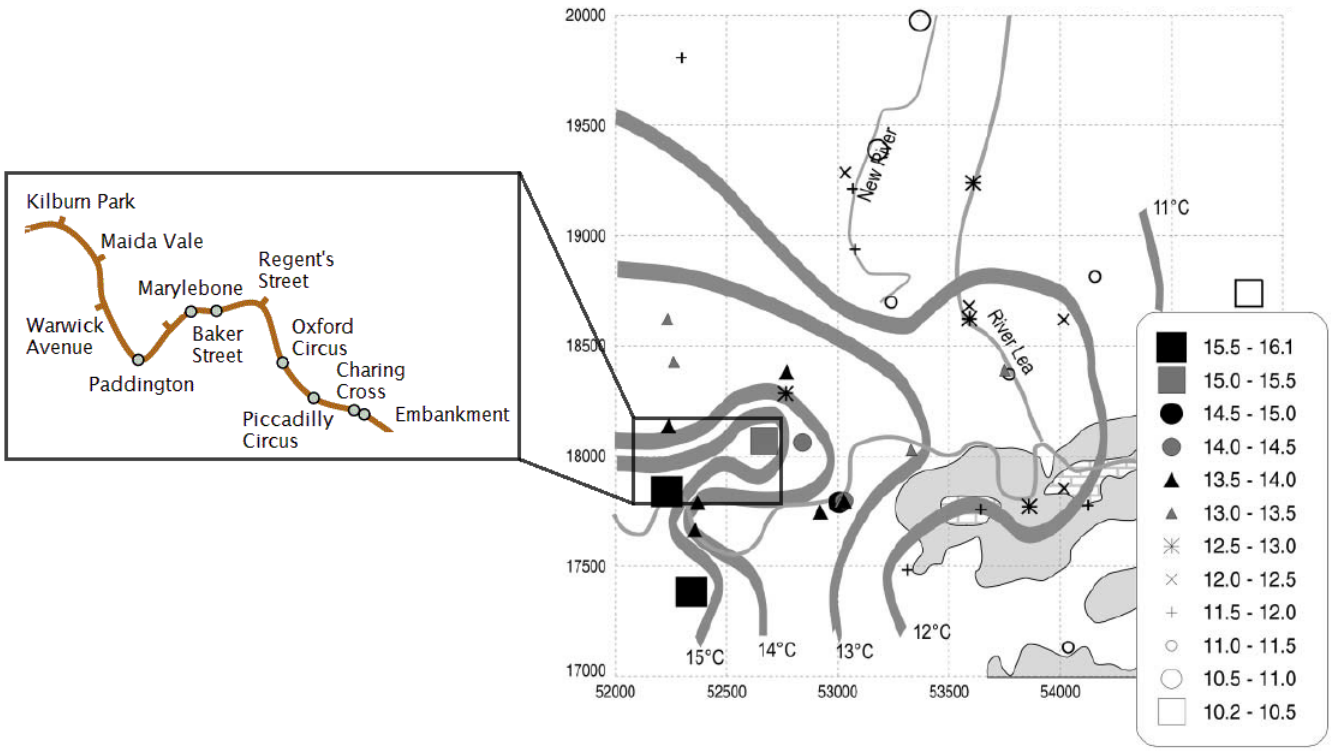

Figure 3.16: Soil Temperatures measured at the depth of 20 m for the London Clay Layer in the London Basin (Headon et al., 2009) and (for London, 2013)

The 1D simulation models for the Northern, Bakerloo, and Jubilee Lines are also run in "Long Term Mode" from their opening years. The ground temperatures obtained are used as initial soil temperatures for simulating the year of 2013.

The Northern Line model simulation results fit well with the measured data for both the platforms and the stations as seen in Figure 3.17. Since the Northern Line's trains operate 25 km/hr slower than the Central Line and have 20% brake regeneration, there is less heat released in the system compared to the Central Line which results in lower temperatures in both the platforms and the stations. Also, the Northern Line has 70 less trains passing through its tunnels daily and 7 trains/hour less during peak times when compared to the Central Line (Table 3.7).

A parametric analysis is conducted on the Northern Line model inorder to quantify the extent to which increasing the train speed, or increasing the brake regeneration rate can impact the air temperatures in the tunnels and stations. The study consists of varying two parameters: The velocity of the trains is increased by 25 km/hr to match that of the Central Line, and the brake regeneration rate is increased from 20 % to 40 % which is the same for the new trains that are planned to be introduced in 2032 in the deep lines. The results are plotted in Figure 3.18. Increasing the train speeds to 100 km/hr would result in increasing the platform and tunnel temperatures by 2 °C and 1 °C respectively during summer conditions. This is because higher speeds would result in an increase in heat released as a result of train braking. This increase in train speed is possible if Transport for London is looking into decreasing journey times. However, the platform and tunnel temperatures would still be below that of the Central Line, because the Northern Line experiences less train traffic, and its trains are equipped with 20 % brake regeneration. Equipping the trains with 40 % brake regeneration would result in cooling the platforms and tunnels by 1 °C and 0.25 °C respectively. Brake regeneration does not significantly impact the Northern Line air temperature in the tunnels during summer, because the line's temperatures are already lower than outer ambient conditions by 3 °C. Combining 100 km/hr train speed with 40 % brake regeneration would result in mitigating the over heating caused by the increase in train speed, where the temperatures in the platforms and tunnels decrease by 1 °C and 0.5 °C respectively. Overall, tunnel temperatures in the Northern Line would remain cooler than the outer ambient temperatures in the summer even if the train speeds are increased to 100 km/hr, while the platform temperatures would rise above ambient temperatures reaching 31.5 °C during summer.

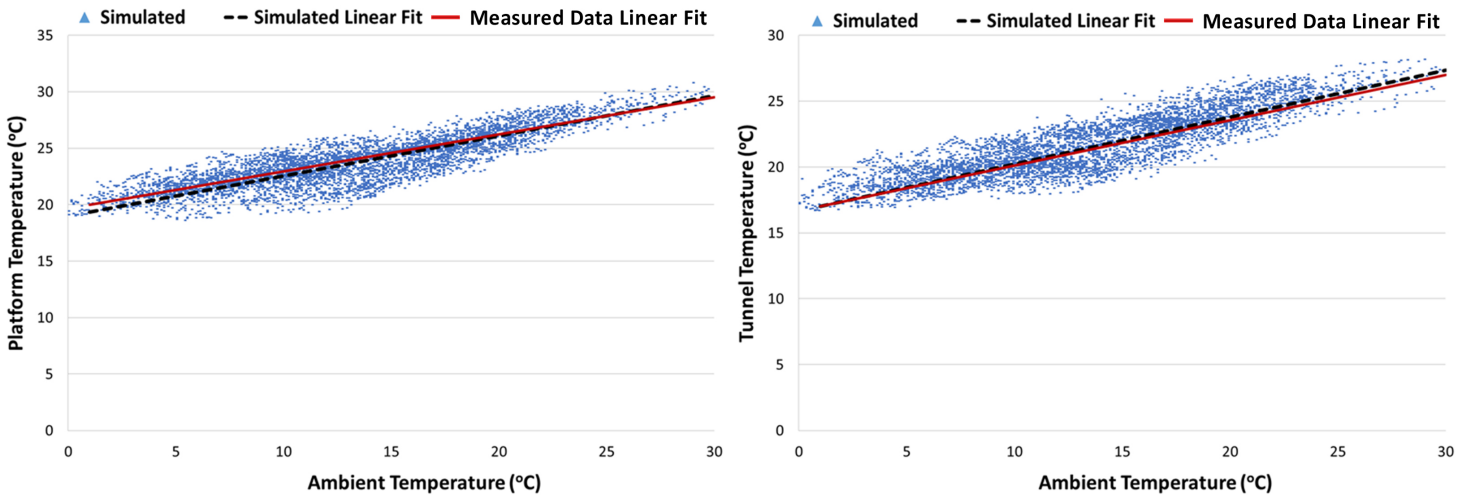

Figure 3.17: Northern Line model simulated platform and tunnel air temperatures compared with measured data.

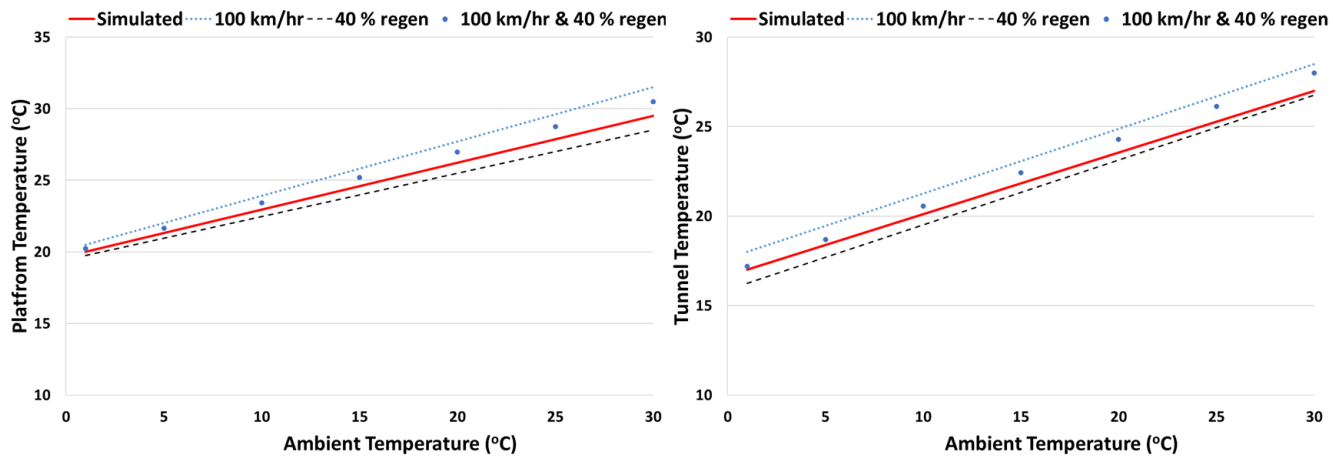

Figure 3.18: Northern Line Model parametric variation results (Regenerative Braking (regen), Train Speed, and a Combination of both) Compared to the original simulated Northern Line linear fitted platform and tunnel temperatures.

The simulation results for the Bakerloo Line model was close to the measured data as seen in Figure 3.19. Although the Bakerloo line has less train traffic compared to the Central Line, the higher background soil temperature of 16 °C raises its tunnel and platform temperatures slightly higher during summer conditions by 0.5 °C.

The Bakerloo Line is the warmest line in the London Underground both during summer and winter as seen in Figure 3.15. Inorder to address the overheating problems, the cooling effect of lowering the surrounding soil temperatures next to the tunnels, and equipping the trains with brake regeneration are investigated in the Bakerloo Line. The study consists of varying two parameters: A radial temperature of 8 °C is placed at 0.4 m far from the tunnels, and the brake regeneration rate is set to 40 % which is the same for the new trains that are planned to be introduced in 2032 in the deep lines. The results are plotted in Figure 3.20. Having 8 °C soil temperature at 0.4 m distance from the outer wall of the tunnel has a significant effect on the Bakerloo's climate, where temperatures have dropped by 4.9 °C and 5.9 °C in the platform and tunnels respectively from 33 °C and 31.5 °C to 27 °C and 26 °C respectively during summer conditions. To achieve these low temperatures in the proximity of the tunnel wall, a cooling effect is needed such as either a ground source heat pump or ground water cooling. Equipping the trains with 40 % brake regeneration would result in cooling the platforms and tunnels by 2 °C and 1.8 °C respectively during summer. Brake regeneration does not significantly impact the Bakerloo Line air temperature when combined with the 8 C soil temperature in the platforms and tunnels during summer, because the line temperatures are already significantly lower than outer ambient conditions by 5 °C and 6 °C respectively. Thus, a combination of geothermal cooling and heat brake regeneration would successfully mitigate the overheating problems in the Bakerloo Line.

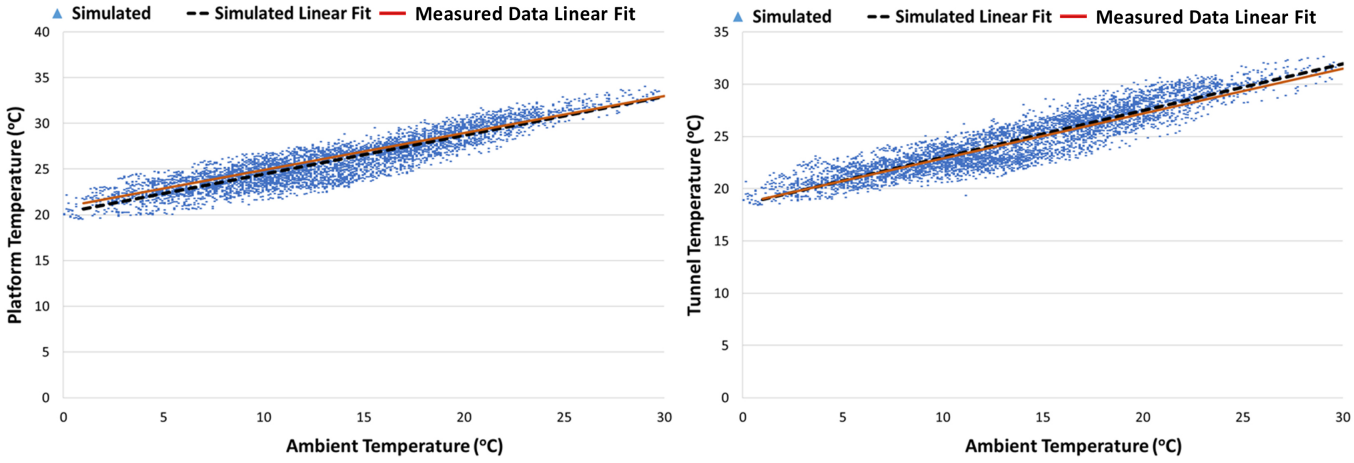

Figure 3.19: Bakerloo Line model simulated platform and tunnel air temperatures compared with measured data.

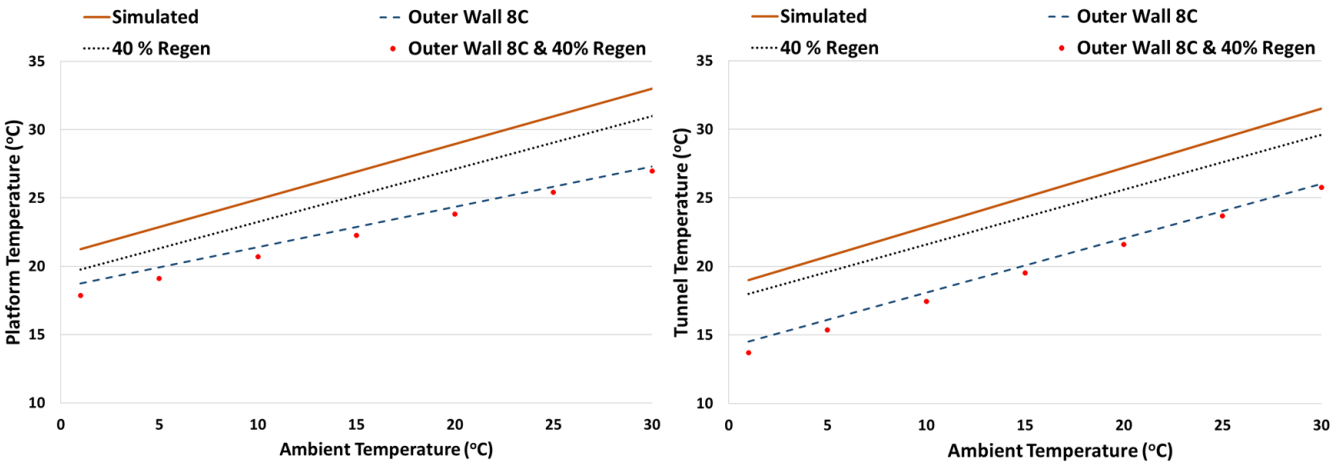

Figure 3.20: Bakerloo Line Model parametric variation results (Regenerative Braking (Regen), 8 °C soil boundary temperature , and a Combination of both) Compared to the original simulated Bakerloo Line linear fitted platform and tunnel temperatures.

Before conducting the Jubilee Line model simulations, the effect of changing the tunnel diameter on the London Underground's environment is investigated, since the Jubilee Line has a larger diameter of 4.4 m, and it would be beneficial to conduct a sensitivity analysis on varying the diameter. The Central Line model's tunnel diameter is changed to 4.4 m and 6.2 m, which resembles the large Crossrail tunnels (Crossrail, 2016), and re-simulated for the year of 2013 and compared to the original results in Figure 3.21. Increasing the diameter would result in an overall decrease in temperatures in the tunnels and stations as seen in Figure 3.21. Expanding the tunnel diameter to 6.2 m leads to a decrease in platform and tunnel temperatures by 4 °C and 4.5 °C respectively during summer conditions. Having a tunnel diameter of 4.4 m, similar to the Jubilee line, leads to a decrease in platform and tunnel temperatures by around 2 °C and 2.7 °C respectively during summer conditions. This is attributed to the increase in the volume of air in the subway system, while having the same amount of heat released in the system. Thus, the air temperature increase in the system will be less compared to smaller tunnel diameters, since the system has more heat capacity as a whole. We realize that expanding the diameter of the tunnels is economically unfeasible, but these simulations are useful to help gain further understanding about heat dissipation inside the tunnels and why the Jubilee line is cooler than all the other London Underground Lines (Figure 3.15).

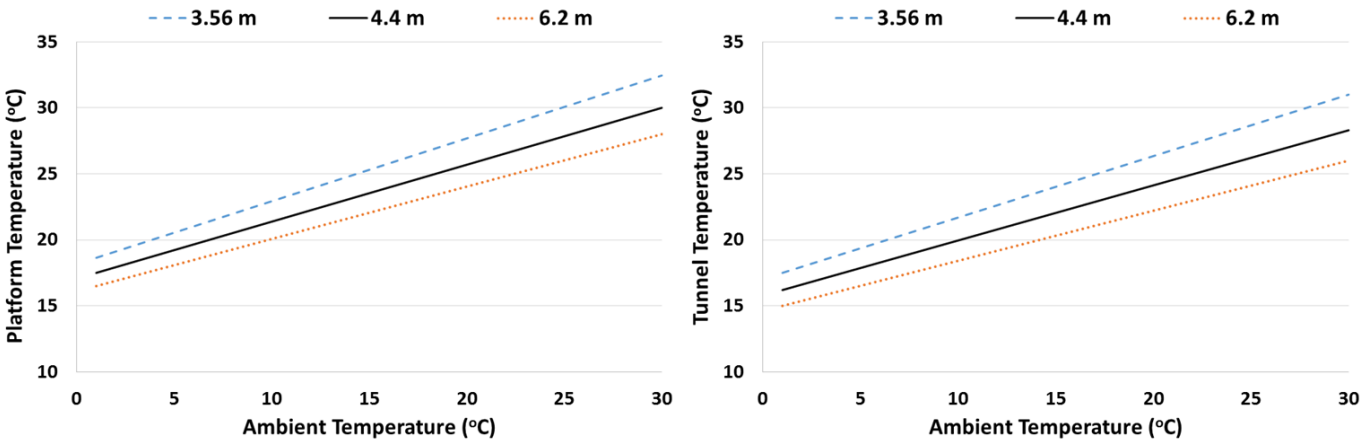

Figure 3.21: Central Line model simulated platform and tunnel air temperatures for tunnel diameters of 3.56 m, 4.4 m and 6.2 m.

The ventilation rates in the Jubilee Line model had to be varied in order to get the results displayed on Figure 3.22. At first the ventilation rate was doubled then quadrupled, since the Jubilee Line is known to have ventilation shafts at every 1000 m, so it has higher ventilation rates compared to the Central Line (Ritchie, 2016). Although, the Jubilee Line has similar train traffic to the Central Line in terms of number of trains per day and at peak time, the Jubilee Line's higher ventilation rate, 20% brake regeneration, and larger tunnel diameter (4.4 m) makes its platform and tunnel environment significantly cooler than the Central Line by 4.5 °C and 5.5 °C respectively during summer conditions.

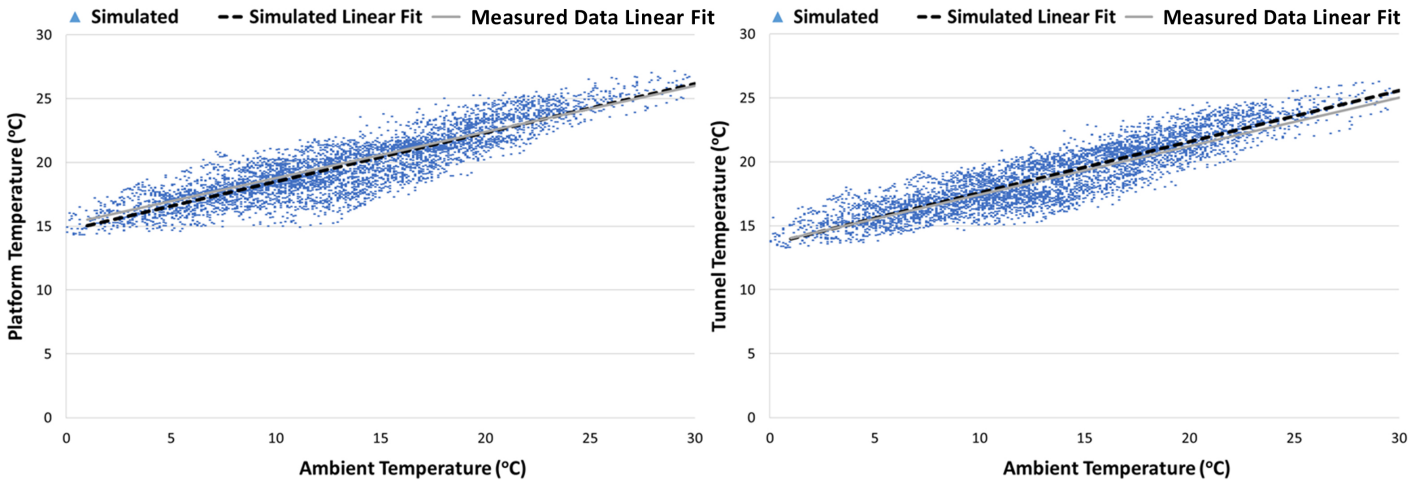

Figure 3.22: Jubilee Line model simulated platform and tunnel air temperatures compared with measured data.

3.4 Conclusion

A representative section of the London Underground's Central Line is modelled using IDA tunnel. The 1D Central Line model was validated using measured air temperature data for the tunnels and platforms obtained from Transport for London. A parametric analysis was conducted on four major heat sources and sinks in the model to assess their influence on the Central Line climate, particularly during summer conditions, where passengers experience discomfort due to elevated air temperatures. The most prominent cooling of the subway during summer conditions occurs when soil temperatures close to the outer tunnel wall (0.4m) are lowered to 8 °C, where the air temperatures of the platform and tunnels decrease by 5 °C and 6 °C respectively. Increasing the ventilation rates does lower the temperatures of the system slightly during summer, however it is constrained by outer ambient conditions, where high outside ambient conditions would result in high air temperatures within the London Underground system. The model has also shown that regenerative braking rates of 20% and 40% have a slight effect in lowering the Central Line temperatures by 1 °C and 2 °C respectively. However, the cooling effects of 40% regenerative braking are negated by a +50 % increase in train traffic. Whilst the parametric analysis considered several options to lower the temperature in the London Underground such as decreasing the soil temperature, increasing ventilation, and brake regeneration the best solution may be to apply a combination of these

cooling methods.

The model was simulated between the years of 2013 - 2050, taking into consideration projected passenger numbers, train traffic, infrastructure upgrades, and climate change. Results have shown that introducing new trains equipped with regenerative braking will manage to to slightly cool the Central Line by around 0.5 °C during summer conditions in the Year of 2032, preserving the status qou as the year of 2013. However, by 2050 the projected increase in train traffic, passenger numbers, and outer ambient temperatures associated with climate change will overcome the benefits of the new trains making the Central Line warmer than it originally was in 2013 by 1.5 °C during summer, which will further exasperate the overheating problem. The Central Line model simulations showed no noticeable differences within the same year of 2032 and 2050 between the medium emission and high emission scenarios, because their climate profiles and annual median temperatures differed slightly.

The Central Line model was modified to model several Deep London Underground Lines: Northern, Bakerloo, and Jubilee. The modification were based on each of the Line's distinct characteristics such as train type, train traffic, passenger numbers, and tunnel diameters. The modified subway model results were close to the measured data for the three deep lines. However, for the 3 lines the model tended to estimate slightly cooler temperatures compared to measured data for winter conditions because train & local station heating was neglected, and slightly higher temperatures for the tunnels because cross tunnels were neglected in the model. The results have confirmed that higher surrounding soil temperatures make the Bakerloo Line slightly warmer than the Central Line and a combination of brake regeneration & less train traffic & lower train speeds makes the Northern Line cooler than the Central Line. Overall, tunnel temperatures in the Northern Line would remain cooler than the outer ambient temperatures in the summer even if the train speeds are increased to 100 km/hr, while the platform temperatures would rise above ambient temperatures. Also, it was shown that a combination of lowering the soil boundary condition around the tunnels which emulates geothermal cooling and heat brake regeneration would successfully mitigate the overheating problems in the Bakerloo Line. As for the Jubilee Line, a combination of brake regeneration, larger tunnel diameters and higher ventilation rates makes this line the coolest between all the modelled four lines. This approach proves that the methodology used in modelling the Central Line can be expanded flexibly to model other deep lines across different cities and understand the fundamentals behind their climate conditions.

The following chapters will asses the feasibility of using ground source heat pumps in the vicinity of the tunnels in order to lower the tunnel wall temperatures, where a 3D finite element model (FEM) was developed to model thermal transient interactions between the subway tunnels and vertical boreholes.

Chapter 4

3D Vertical Borehole Model and Optimization

4.1 Introduction

Geothermal systems could serve as one of the potential energy efficient solutions to cool underground subway systems, while providing heating to residential and commercial blocks above the tunnels. In the UK, such systems can also take advantage of subsidiaries and benefits under the UK Government's Renewable Heat Incentive Scheme (DECC, 2014a). To do so, one must be able to quantify the net gains: How much useful heat can be feasibly extracted from underground subway spaces over a time period ? What is the optimal geothermal vertical borehole set-up that could maximize heat extraction ? and What are the resulting temperature drops in the subway tunnels and platforms ?

The London Underground's Central line is selected as a representative case of an old subway system that suffers from overheating and ventilation problems. The Central Line is the busiest line in the London Underground, and suffers from over heating problems particularly during summer conditions, where temperatures above 35 °C have been recorded in some areas (Gilbey et al., 2011). In 2015, TfL started distributing bottles of water to manage passenger discomfort and dehydration during summer as part of "Beat the Heat and Travel Better" campaign (TfL, 2014). Efforts to alleviate the overheating problems in the London Underground have been so far limited to expanding the ventilation shafts and installing fans with higher air exchange rates. These strategies - though helpful - have been insufficient. A key problem is that

many subway systems (including the Central Line) were built when there was no concept of air-conditioning (TfL, 2014). Installing air-conditioning in the trains of the deep and old lines is particularly challenging because current sizes of air-conditioning units are difficult to fit in the trains, and furthermore the exhausted heat from these units would exacerbate the overheating problems in the tunnels and platforms. The Central Line's current rolling stock is the 1992 model which is not equipped with regenerative breaking (Tfl, 2007). New trains for the Central Line are planned to be introduced in 2032, where they will be equipped with regenerative breaking. The installation of on-board air-conditioning is, however, still uncertain (LU, 2014). Given these challenges as well as the potentially favourable context for geothermal vertical borehole systems, the Central Line of the London Underground is a good candidate to investigate if waste heat from subway systems can be usefully extracted through vertical borehole ground source heat pumps (GSHP) systems.

Environmental simulation of subway transit systems is typically 1D (SES, IDA) (SES, 2001) & (IDA, 2006). On the other hand, the behaviour of underground heat exchangers (geothermal systems) is better quantified via 3D finite element models (FEMs). This chapter couples a 1D model of a representative section of an old subway system of London - the Central Line - with a 3D FEM model of vertical borehole heat exchangers. The 1D tunnel model is used to model the transient heat and air flows in the Central Line, while the FEM model simulates vertical close-loop boreholes heat exchangers (BHE) next to the tunnels. The two models are co-simulated such that information is passed back and forth through a common temperature boundary layer at the outer tunnel walls, until both models converge. Using this approach, the cooling effect of vertical BHEs on the subway climate is examined, and the heat extraction rates of the BHEs next to the train tunnels are compared with standard stand-alone vertical BHE. Different arrangements and distances of the vertical boreholes with respect to the tunnels are examined to achieve the best heat extraction and cooling in the tunnels and platforms simultaneously. The concept of using partially insulated BHEs is also investigated to optimize the system as per variations of building heating and cooling demand and the need to cool the London Underground throughout the year.

4.2 Modelling Methodology

4.2.1 3D Finite Element Model of Ground Heat Exchangers

Several 1D, 2D and 3D simulation models, both numeric and analytic, have been developed to model a single or an array of underground geothermal systems, in both transient and steady state conditions (Connolly et al., 2010; Stauffer et al., 2013). The analytical and numerical methodologies for modeling borehole heat exchangers are extensively reviewed in chapter 2, where this section touches briefly on them. Widely used classical 1D heat transfer models are the Kelvens line source model, and the cylindrical heat source model, which use the Fourier law of heat conduction. The line source theory assumes the vertical geothermal borehole as an infinite line source of heat in the ground, and the ground is assumed to be an infinite medium with an initial uniform temperature. The cylindrical heat model assumes a cylindrical borehole with infinite length buried in the ground, where the model's governing equation can be analytically solved through either a constant heat transfer rate across the borehole surface or a constant borehole surface temperature (Carslaw and Jeager, 1959) & (Ingresoll and Plass, 1948). Hellstrom (1991), Kavanaugh (1995),Bernier et al. (2004), and Hikari et al. (2004) have focused on making the 1D analytic borehole models more accurate and comparable to numerical ones (Fayegh and Rosen, 2012). A 2D finite line source model was established by Zeng et al. (2002), while Cui et al. (2006) and Yi et al. (2010) developed finite 3D vertical borehole analytic models (Yi et al., 2012).

The long-time step g-function model was developed by Eskilson (1987) to model Boreholes for thermal storage applications. The g-function is essentially a normalised step-response function that describes the relationship between the average borehole temperature and a step in the extraction-rejection for a defined configuration of Boreholes. In this approach, the complex geometry of a borehole is simplified as a cylinder with a finite length and diameter. A single temperature is used to represent the borehole wall temperature. The thermal conductivity and capacity of all the different materials inside a borehole, including fluid, pipes and grout, are neglected. The long-time step g-function models provide an efficient solution to simulate borehole fields with defined configurations over long timescales, ranging from one month to several years. In order to expand the application of the long-time step g-function model, Yavuzturk (1999) developed a two-dimensional numerical model on a polar grid to compute

the so-called short time step g-function. The model that combines the short time step g-function and the long-time step g-function was implemented in GLHEPro (Spitler, 2000b), a design software for vertical borehole ground loop heat exchangers. However the borehole geometries modelled by g-functions remained simple, where Eskilson (1987) calculated over 200 g-functions for multiple boreholes arranged in different shapes, such as in a line, in a rectangle, and in a square, with different distance between two boreholes.

Significant simplifications in the analytical borehole models render them unsuitable for complex geometries and short-time step transient simulations of boreholes (Yi et al., 2012). Numerical borehole models are attractive when the aim is to obtain high-resolution solutions or conduct parametric analysis at small time-steps. However, numerical models have to be setup efficiently in terms of symmetry, boundary conditions and mesh distribution, since they can be computationally time penalizing. Al-Khoury et al. (2005) worked on improving BHE numerical models computational efficiency by developing a 3D finite element steady state flow model and then Al-Khoury and Bonnier (2006) modified this model to include transient heat flows. Hecht-Mendez et al. (2010) modified the multi-species transport model MT3DMS to simulate heat transport for BHEs, since the effects of buoyancy and changes in viscosity are small. The FEFLOW code for groundwater flow and transport has been modified for modeling BHEs (FEFLOW, 2014). Holzbecher and Ruschel (2014) described how 1D model components for flow and heat transport inside a BHE can be coupled with a 2D or 3D component for the ground in COMSOL. Holzbecher and Ruschel (2014) set up the BHE conductance so that the coupled model is capable to cope with laminar, turbulent and transitory flows in the BHE pipes. Nora et al. (2016) used symmetry to model arrays of boreholes to asses their thermal energy storage in the soil in combination with solar thermal energy harvesting using finite element methods. Therefore, to model the transient thermal interactions between multiple vertical boreholes and subway tunnels, a 3D finite element model is developed using 'Comsol', which is a general purpose multi-physics simulation software.

4.2.2 3D Model Geometry, Setup and Boundary Conditions

A typical vertical close-loop borehole design that adheres to DECC's Microgeneration Certification Scheme standards is used (DECC, 2011). As seen in Figure 4.1 and Figure 4.2, the model consists of two tunnels, 10 m apart, representing the eastbound and westbound tunnels

of the London Central Line. The boreholes are 13 cm in diameter, and 100 m deep. They are located 20 cm from the tunnel outer walls: the primary aim of the boreholes is to cool the tunnels, and the optimum way to achieve this is by placing them as close as possible to the tunnel walls. As the boreholes get closer in proximity to the tunnels the potential for heat recovery will become greater, but there is a limit to how close structures can be constructed to the tunnels, the minimum distance London Underground (LU) allows for non-LU owned property is about 3 m in horizontal and 6 m in vertical directions (TfL, 2013). LU owned structures distance is flexible depending on the practicality of constructing the structure (TfL, 2013), where LU officials didn't mind having the LU owned boreholes at 20 cm distance from the tunnels. Boreholes are placed on both sides of the two tunnels, such that they are 6 m apart in the direction of the tunnel and 4.16 m apart across a tunnel (Figure 4.1). For this particular analysis, the boreholes are exclusively placed on the sides of the entire tunnel sections B & C and not the station platforms. The soil properties are taken to be that of London clay and are assumed uniform (variation of the soil thermal properties due to local moisture content and ground flow are neglected).

The London clay properties facilitated the construction of the London Underground, unlike the cases of the hard metamorphic assemblages of New York city and the soft Quaternary sands of Berlin (Paul, 2016, 2009). London clay is easily excavated, largely impermeable and has high loadbearing characteristics, where most of the London Underground has been excavated in London Clay (Ellison et al., 2004; Standing and Burland, 2006; Newman, 2009). Fissures close to the surface are the chief factor contributing to the observed permeability in the ground through the London Clay layer (Mott, 2010). Since London Clay has a vertical hydraulic conductivity of 5 x $10^{-11} m/d$ and an observed permeability of around $10^{-11} m/sec$ (Mott, 2010), the Peclet number of the London Clay is in the order of 10^{-3} (Busby et al., 2009). Molina-Giraldo et al. (2011) has shown that the influence of groundwater flow is negligible for Peclet numbers lower than 1.2, so neglecting the ground flow for the case of the Comsol model developed for the London Underground is valid.

The background soil temperature is 14 °C (Webb et al., 2009) at 50 m distance from the tunnel center in all directions, except for the upper ground surface temperature which assumed to follow the London ambient air temperatures used in the IDA tunnel simulations. The initial temperature of the borehole surfaces is assumed to be constant at 0 °C. This assumption is commonly used in modelling soil temperatures surrounding the boreholes (Fayegh and Rosen,

2012; Revesz et al., 2016), where 0 °C temperature is a typical average borehole refrigerant fluid temperature (DECC, 2011). For this initial modeling study, the geothermal system (boreholes) are assumed to be always operating to assess the maximum achievable tunnel cooling. However, geothermal systems usually operate based on heating/cooling demand.

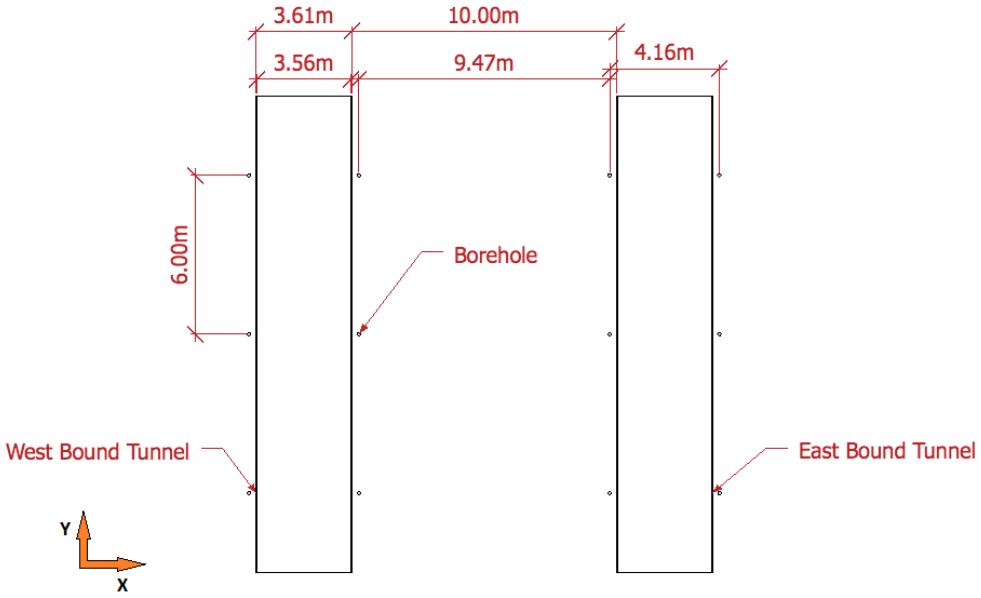

Figure 4.1: Schematic of the vertical borehole and Central Line tunnels.

Figure 4.2 shows the cross section view of the model, where the two tunnels are in the centre, and each tunnel has a set of vertical 100 m deep boreholes 20 cm from the tunnel outer wall. The circular sections that surround the tunnels in Figure 4.2 are for specifying initial soil temperatures at specific distances. These are obtained from IDA long term simulation soil temperature profile (the soil temperatures for the Central Line after 114 years of operation, as explained in section 3.2.2.5). The meshing of the 3D ground model is tetrahedral and is set to very fine between the tunnel walls up to a radius of 19 m from the tunnel center, which has a minimum element size of 0.02 m and a maximum element size of 2 m. Beyond the radius of 19 m, the mesh is set to be fine, which is coarser having a minimum element size of 0.15 m and a maximum element size of 3.5 m. In order to reduce computation time, symmetry is used along the x-axis through the tunnel center. Also, symmetry is applied along the zx planes in both the positive and negative direction, to model a continuous array of boreholes on the sides of the two tunnels. Hence, the Comsol model contains 4 boreholes in total, and

Soil	• The initial ground temperature within the soil domain was set based on the background soil temperature in London, which is 14 °C. • A time dependent temperature boundary was applied on the surface of the soil domain based on London climate data. • The soil properties are taken to be that of London clay and are assumed uniform. Variation of the soil thermal properties due to local moisture content and ground flow are neglected.
BHE	• The temperature of the BHE surface is fixed at 0 °C
Tunnel	• A time dependent temperature boundary was applied to the wall of the tunnel based on the output from the 1D IDA Central Line model.

Table 4.1: Initial, boundary and operating conditions of the Comsol

the remaining ones are modelled using symmetry (Figure 4.2). Simulation for 1 year iteration in Comsol for a 2.7 GHz quad core computer takes 31 hours.

4.2.3 1D Subway and 3D Borehole Model Co-simulation

After the 1D Central Line model, which is described in detail in chapter 3, is simulated for 114 years on the so-called long-term mode, the radial soil temperature profile thus obtained from the 1D model tunnel sections B & C is used as initial soil temperatures in the 3D FEM model. The outer tunnel wall temperatures of sections B & C output by 1D one year simulations are used as boundary temperatures in the 3D FEM model. The 3D FEM model of the boreholes is simulated over the same time period and time-steps of 1 min as that of the 1D subway model. The average radial soil temperature output by the 3D FEM model at 20 cm from the outer tunnel walls are then used as boundary temperatures in the 1D subway model sections B & C. The 1D subway model is re-simulated with the same time interval, but with the

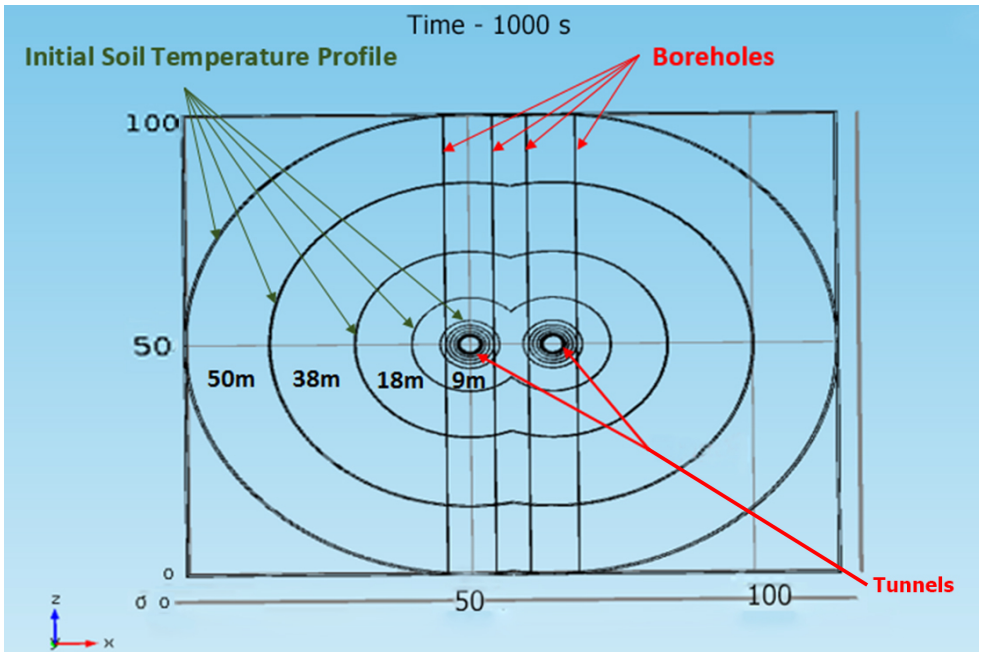

Figure 4.2: Cross section of the Comsol vertical borehole model (scale in m).

updated radial soil temperature boundary from the 3D FEM model of the boreholes. The newly obtained outer wall temperature is re-input in the 3D FEM model of the boreholes. This process is repeated until the change in the outer tunnel wall temperature in the 1D model of the subway line becomes negligible after a number of iterations, indicating that both the 1D and 3D models have converged. This co-simulation process is illustrated in (Figure 4.3).

Figure 4.4 shows the outer tunnel wall temperatures for the month of January as a result of consecutive iterations using the coupled co-simulation. In the first iteration (IT1) the outer tunnel wall temperatures drops significantly. Over subsequent iterations, the temperature decrease is less, until it is negligible (IT11), indicating that the transient co-simulations have converged. Since the 3D FEM model of the boreholes is setup such that that the vertical boreholes start operation at the beginning of January, the outer wall temperatures are identical at the beginning of January. The difference, at subsequent time-steps, between the outer wall temperatures of the original model (without boreholes) and the converged co-simulation (shown as IT11 in Figure 4.4) is indicative of the cooling effect (or heat extraction) due to the boreholes. Indeed, Figure 4.4 shows, by mid-January, a 2 °C difference in the outer wall temperatures due to the vertical boreholes. This cooling effect will be much significant during summer months.

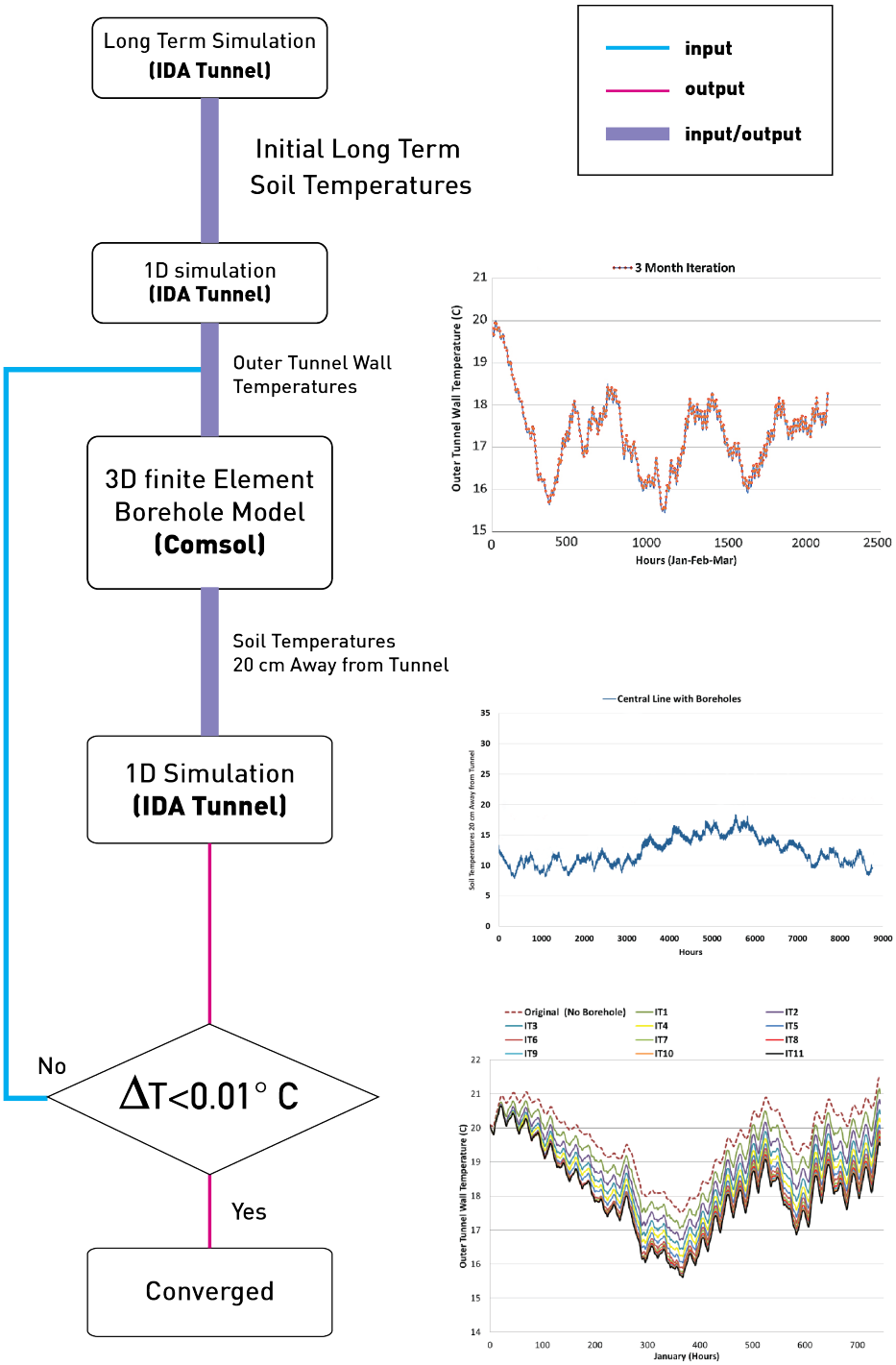

Figure 4.3: 1D IDA and 3D comsol co-simulation process.

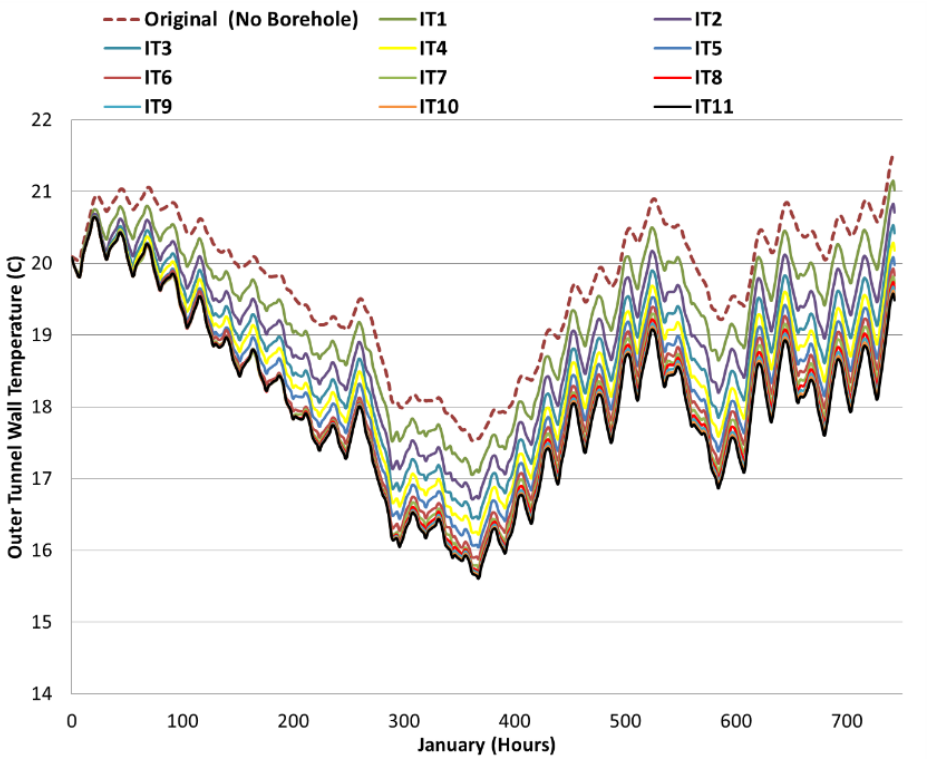

Figure 4.4: Variation of the outer tunnel wall temperature for the month of January with every Comsol-IDA iteration (IT). IT 1 to IT 11 includes tunnels with BHE, while Original has no BHE.

The temperatures shown in Figure 4.4 are obtained by co-simulating the 1D subway line model and the 3D FEM model of the boreholes over a time period of a month, starting January. As the two models converge, the co-simulation is moved to the following months, until the entire year is covered. However, simulating an entire year using monthly time periods is time-consuming, and it would be more efficient to simulate them over longer time periods. Consequently, the two models are also co-simulated with time periods of 3 months for an entire year, and the results are compared to the single month simulations. The converged outer tunnel wall temperatures for 1 month and 3 month time period iterations are compared in Figure 4.5. The outer tunnel temperatures were almost identical for both iteration intervals over the periods of January, February, and March. Thus, the two models can be co-simulated over longer time period without affecting the accuracy of the solution. A 4 month time period was used to co-simulate the results shown in the following section. Consequently, the total number of co-simulations for the entire year was 33 iterations, since every four month required 11 iterations to converge.

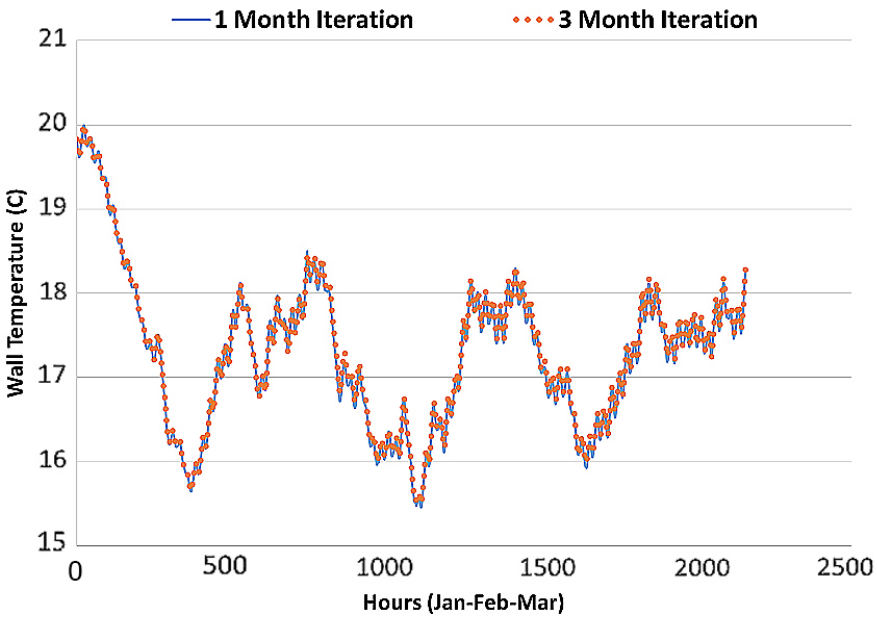

Figure 4.5: Comparison of IDA-Comsol outer tunnel wall temperature results for the months of January, February, and March, using 1 month iterations, and 3 month iterations.

4.3 Simulation Results and Discussion

4.3.1 Borehole Cooling Effect

In order to assess the cooling effect of the vertical boreholes on the platform and tunnel temperatures, a radial boundary soil temperature is introduced around tunnel sections B and C in the 1D subway line model (Figure 3.1). A 10 °C constant temperature is applied at a distance of 20 cm from the tunnel walls, the temperature is applied in the soil surrounding the tunnels. The distance 20 cm is selected so that the boreholes are as a close as possible to the tunnel walls while allowing a soil clearance distance between the walls and the boreholes. This boundary layer emulates the soil temperatures that would result from heat extracted by the geothermal system. Note that the 10 °C boundary is not used in the co-simulation model. It is used only in the 1D subway line model to emulate approximately the cooling effect of the boreholes close to the tunnels. This setup, similar to the one used in chapter 3, serves to roughly assess overall effect when temperature boundary lower than the background soil temperature is applied across proportion of the subway tunnel length (1%, 25% 50%, 100%).

The 1D subway line model is simulated for an entire year with a time step of 1 min for the scenarios having the 10 °C temperature boundary applied on 1% (15m), 25% (375m), 50% (750m) and 100% (1500m) of tunnel sections B and C, both westbound and eastbound.

Figure 4.7 compares the resulting tunnel and platform air temperatures with original temperatures (Central Line without ground heat exchangers). In Figure 4.6 and Figure 4.7, 'WB%' means 'without boundary' and plots the temperature of those parts of the subway tunnel where the 10 °C boundary temperature is not applied (for example, the 10 °C boundary is not directly applied to parts of the tunnel that contain the platform). For example, for the case of Tunnel B-50%, the 10 °C soil boundary is applied to 750 m of tunnel section B and section C in (Figure 3.1), while 750 m in tunnel section C and B are simulated normally with the surrounding ground (Figure 4.6). As expected, the influence of the 10 °C soil boundary temperature on these parts of the tunnel depends on the overall proportion of the tunnel to which it is applied. When it is only applied to 1% (15m) of the tunnel, it has negligible effect on the tunnel and platform air temperatures. However, as this proportion is increased to 25% (375m), 50% (750m) and 100% (1500m) the cooling effect is clearly noticed even in those parts of the tunnel where the 10 °C soil boundary temperature is not applied ('WB').

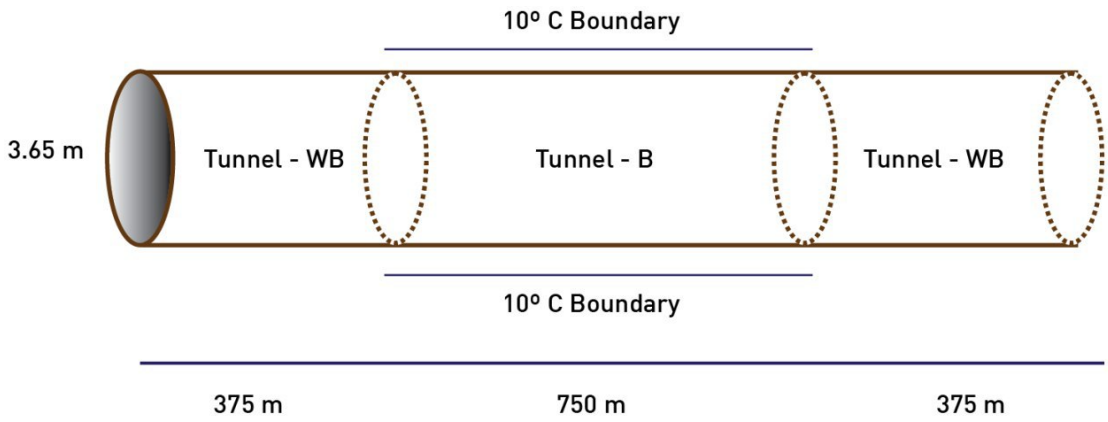

Figure 4.6: Schematic of tunnel section with 10 °C boundary temperature (B-50%) and without the boundary temperature (WB-50%).

Naturally, the parts of the tunnel containing the 10 °C boundary will be even cooler since it will experience the highest heat transfer due the high temperature gradient created by the 10 °C temperature in the soil. This is shown when comparing temperatures of those parts of

the tunnel to which the 10 °C soil boundary temperature is applied ('B%'): The right-hand plot of (Figure 4.7) compares Tunnel WB-25% with Tunnel B-25%, and Tunnel WB-50% with Tunnel B-50%. The main point of these comparisons is that the 1D-3D co-simulations are necessary, as the cooling effect of the boreholes can be quite localized.

Figure 4.8 further demonstrates this by comparing the cooling effect (temperature decrease) of applying a 10 °C boundary soil temperature on 100% of the tunnels in the 1D model against the outputs of the co-simulation. It shows that the tunnel and platform temperatures drop by 8 °C and 9 °C respectively when the 1D model is simulated using the 10 °C boundary soil temperature across 100% of the tunnel length. However, as per the co-simulation results, the annual average soil temperature at 20 cm from the tunnel walls is 17 °C, which is 7 °C higher than 10 °C. This shows that the assumption of using the 10 °C temperature boundary results in an exaggerated temperature drop in the tunnel and platform. The co-simulation outputs plotted in (Figure 4.8) also show that the borehole configuration described in Figure 4.2 results in decreasing the platform and tunnel air temperatures by 4.5 °C and 5 °C respectively during summer conditions. The decrease in outer tunnel wall temperatures for the third year as a result of borehole cooling is shown in Figure 4.9, where there is an average decrease of 7.5 °C across the entire year.

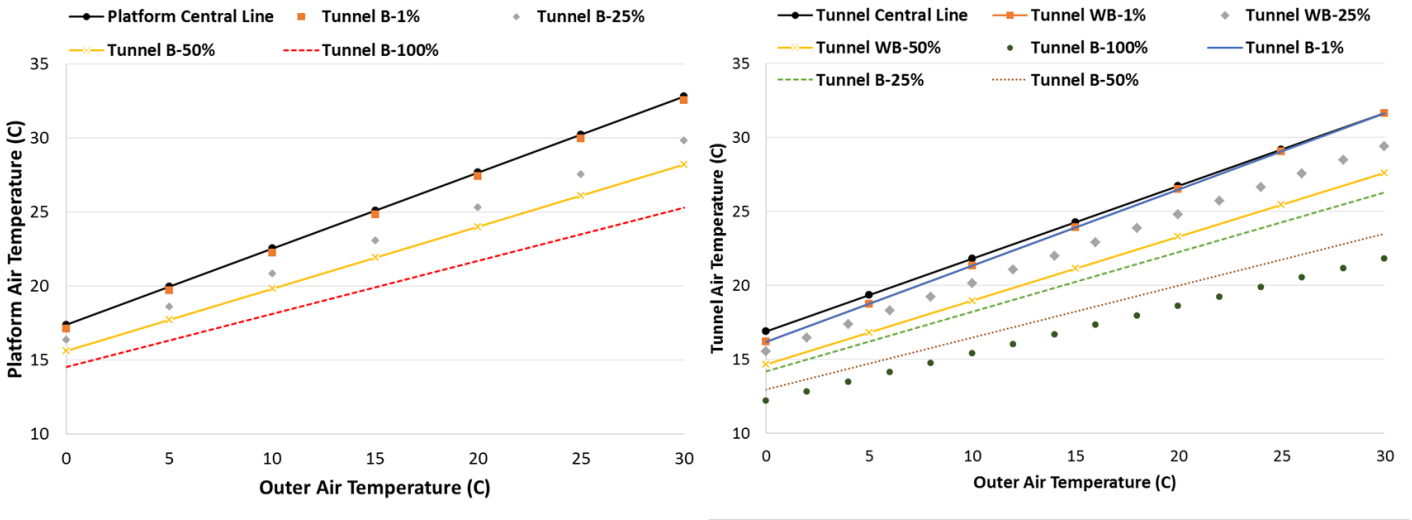

Figure 4.7: Comparing the original simulated Central Line linear fitted platform (left) and tunnel (right) temperatures, and 10 °C tunnel soil boundary temperature case studies.

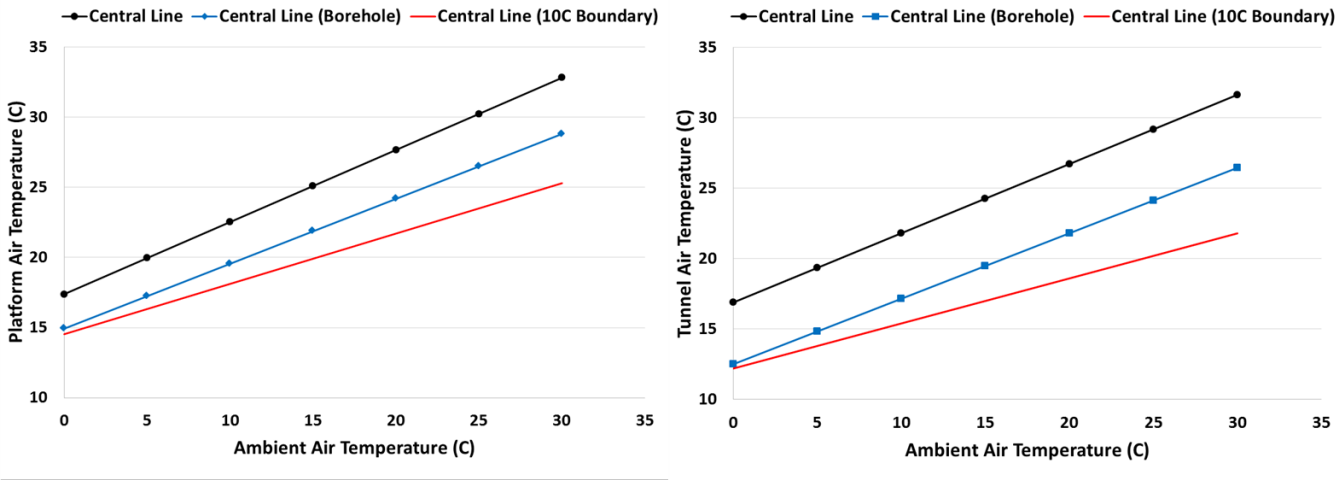

Figure 4.8: Comparing the original simulated Central Line linear fitted platform (left) and tunnel (right) temperatures, with the Comsol borehole fitted tunnels (Tunnel Borehole), and a 100% 10 °C tunnel soil boundary temperature case study.

4.3.2 Borehole Heat Fluxes and Annual Extracted Heat

This section discusses the heat extracted by the boreholes adjacent to the subway tunnels, as output by the co-simulation, and compares it against simulation outputs of a standard stand-alone borehole.

In ground heat transfer problems it is standard to neglect the simulation outputs of first two years, as steady-periodic conditions take a number of years before being established. Figure 4.10 therefore shows the heat flux at the surface of the boreholes adjacent to the subway tunnel against the stand-alone borehole for 3 simulation simulation years. Figure 4.10 plots the transient surface heat flux developing at different sections of a borehole adjacent to the tunnel. Negative heat flux indicates that the direction of heat transfer is inward the borehole surface. In Figure 4.10, heat flux at 'borehole (0 m-9 m)' represents the borehole section from the height of the tunnel center to 9 m above and below the tunnels, 'borehole (9 m-19 m)' is the borehole section between 9 m to 19 m above and below the tunnel center, and the same applies to 'borehole (19 m to 50 m)'. The three sections together constitute the entire borehole of 100 m length, and the average heat flux over the entire borehole is also plotted in Figure 4.10. Also included in the figure is the average heat flux at the surface of a similar standard stand-alone borehole (100 m long vertical closed loop heat exchanger).

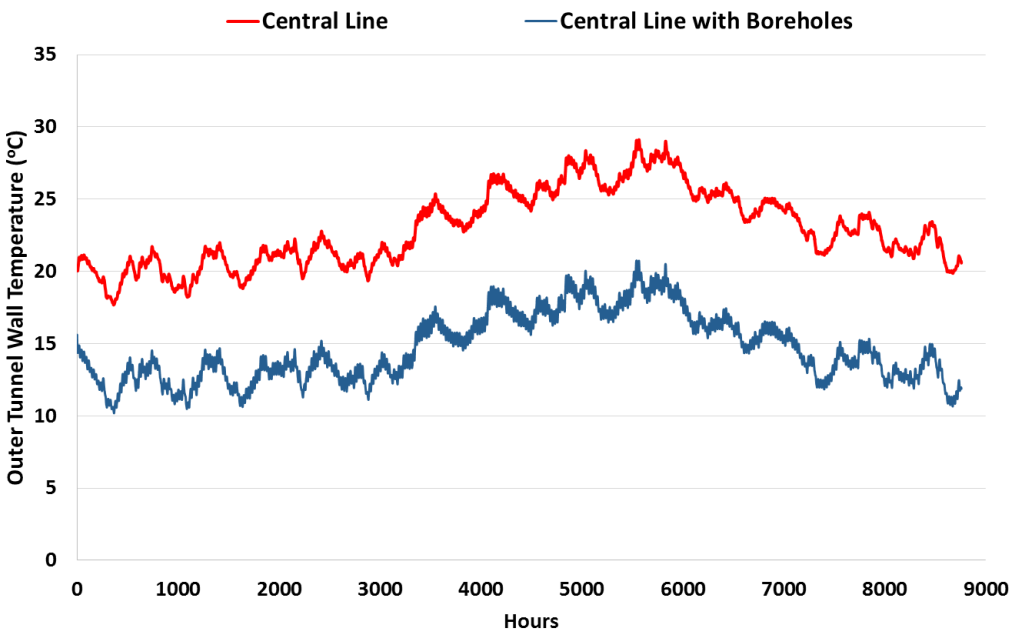

Figure 4.9: Outer tunnel wall temperatures for the Central Line model after three years of simulation for two cases: Tunnels Without Boreholes and Tunnels with Boreholes.

Plotting heat fluxes at different sections of the stand-alone borehole is not necessary, since the heat transfer is uniform over its entire length, except at the tips.

Figure 4.10 shows that for the stand-alone borehole the heat flux is relatively high at the beginning, but as the surrounding soil cools, the heat flux decreases gradually until steady state is reached after 3500 hours (146 days) of continuous operation. On the other hand, the average heat flux of the borehole adjacent to the subway tunnel continues to fluctuate slightly due to the transient temperature profile of the tunnel walls. This is more explicit when the heat fluxes in different sections of the borehole are examined, where transient effects are most dominant near the tunnels at 'borehole (0 m-9 m)'. Figure 4.10 also shows that the heat transfer from the tunnels to the boreholes indeed occurs mostly within the first large circle which is 18 m in diameter. The borehole section near the tunnels (0 m-9 m) has the highest heat flux, which is almost 50% (19 W/m^2) more than the stand-alone borehole, because of the relatively high temperatures of the tunnels.

The average heat flux of the borehole adjacent to the subway tunnel is slightly less than that of the stand-alone borehole. This is due to thermal inference between the boreholes in

the direction across the width of the tunnels (Figure 4.12). Indeed, the thermal interference between the boreholes is also noticeable when observing that the transient heat extraction between 19-50 m of the borehole length is 13 W/m^2 less than that of the stand-alone borehole (Figure 4.10): One would expect that, if the boreholes were spaced so as to not allow thermal interference, the heat extraction between 19-50 m of the borehole length would be almost identical to the stand-alone borehole, as the influence of the elevated subway tunnel temperatures is negligible at that distance. This compromise is necessary though, since to better cool the subway tunnels, the boreholes have to be placed as close as possible to them. At steady state, the average heat flux of the borehole adjacent to the tunnel is 8 W/m^2 less than that of the stand-alone borehole. The annual average heat flux of the borehole adjacent to the tunnel is 30 W/m^2, which is equivalent to 17.64 W/m for every meter of the borehole. This value is close to the tabulated value of 20 W/m in the Microgeneration Installation Standard for vertical boreholes (DECC, 2011) with 0 °C average fluid temperature, a diameter of 13 cm, and surrounding background soil temperature of 14 °C, whilst operating for 7200 hours compared to our simulation (recall that we assume the boreholes to operate at all hours in the year).

In sum, the annual heat extracted by a single borehole adjacent to the tunnel is 9336 kWh, and in the stand-alone borehole it slightly increases by 9% to 10177 kWh. The heat from the tunnel per meter is 3100 kWh/m. The average annual domestic heating demand of one house in 2013 was 9300 kWh (Palmer and Cooper, 2013), so a single borehole could potentially supply an equivalent of one UK house (note though that we do not yet account for 'timing of demand versus supply' within this study).

4.4 Simulation Scenarios

4.4.1 Borehole Model Optimization

The locations of the boreholes are varied in order to assess whether there is a better arrangement that can compromise between heat extraction from the tunnels and the surrounding ground while minimizing thermal interference between the boreholes (Table 4.2). Case A represents the base case simulated previously, where the distance between the boreholes across

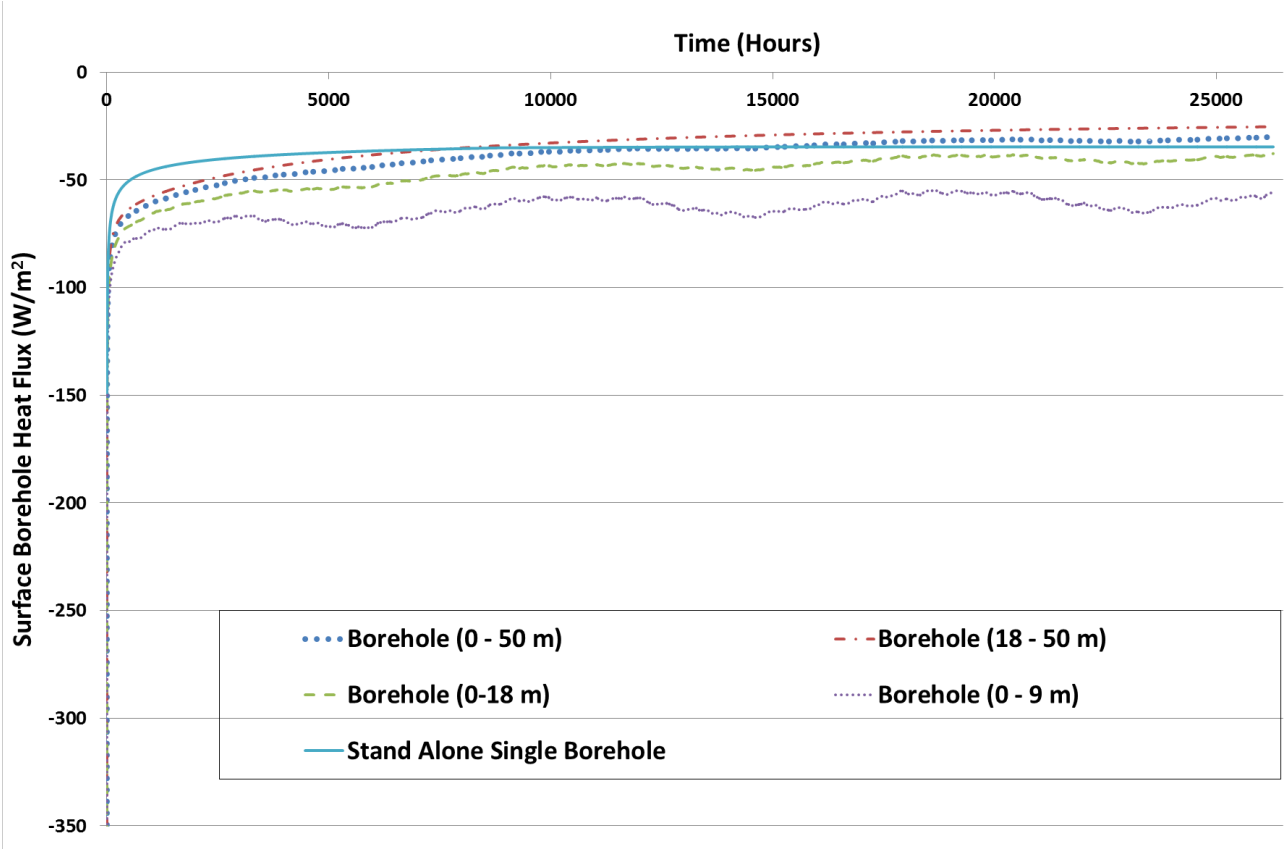

Figure 4.10: Comparison between the Comsol tunnel borehole and single stand-alone borehole annual heat flux variations.

the tunnel sections is 4.16 m , which is the closest possible to the tunnels (Figure 4.13. In Case B, the distance between the boreholes is increased to 6 m , which is recommended by the Microgeneration Certification Scheme Standards (DECC, 2011) to minimize thermal interference between the boreholes. Cases C and D have the same geometry of A and B respectively, except that they are not adjacent to a subway tunnel, making it possible to study the thermal interference of the boreholes without the influence of the subway tunnel acting as a heat source. In Case E the distance between the two line arrays of boreholes across is kept at 4.16 m, but their arrangement is scattered such that the boreholes in one line are shifted by 3 m , which is half the distance between two boreholes in the same line as seen in Figure 4.13, and there is no subway tunnel. The purpose of Case E is to test if this scattered arrangement would decrease thermal interference between the boreholes compared to case C.

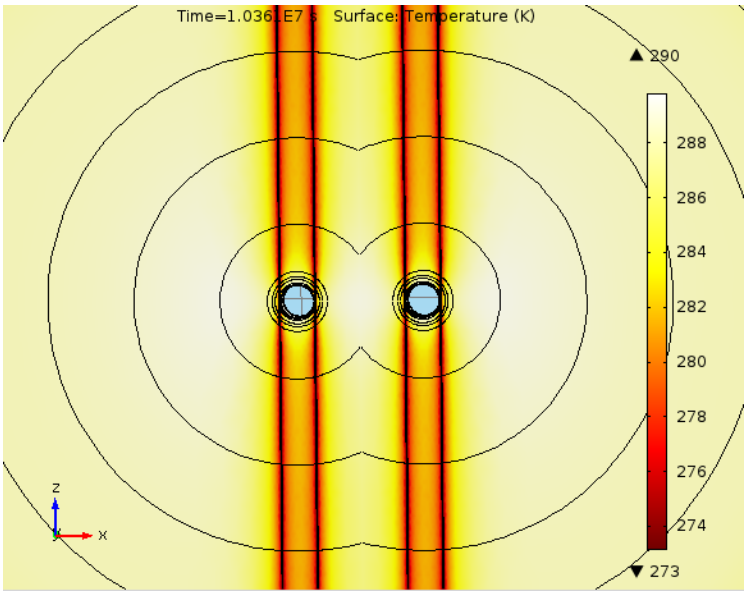

Figure 4.11: Cross sectional 3D borehole Comsol model temperature distribution at the end of April (temperature in Kelvin).

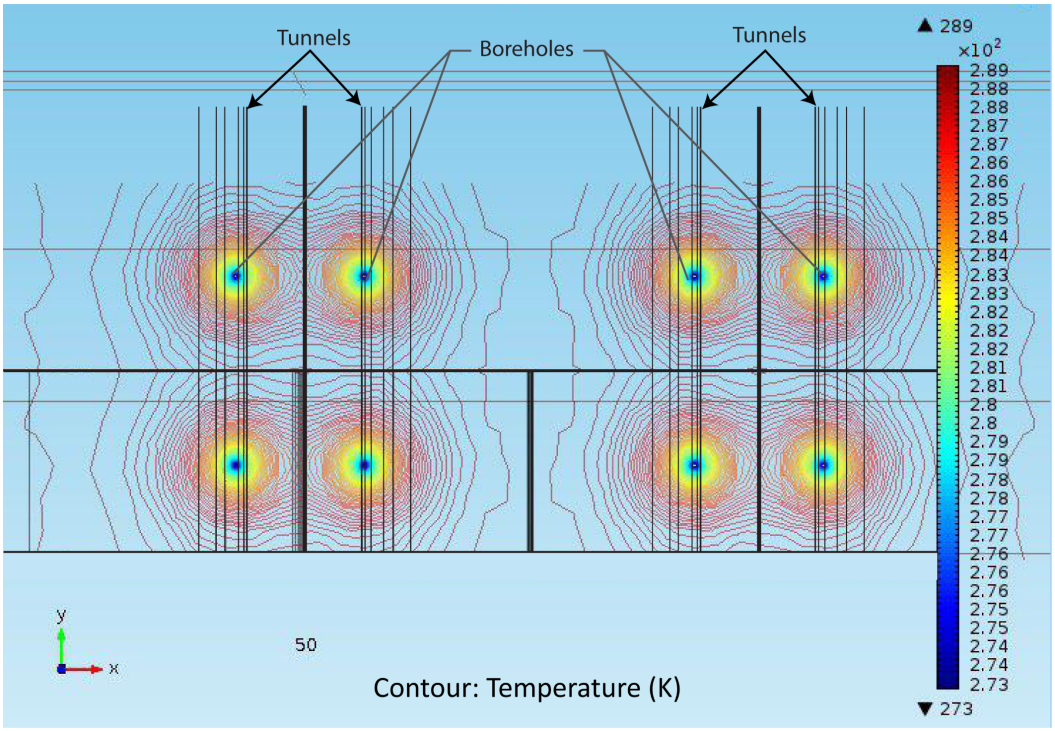

Figure 4.12: Top view section (19 m above tunnel centres) of the Comsol borehole model, temperature (in Kelvin) contour distribution at the end of April simulation.

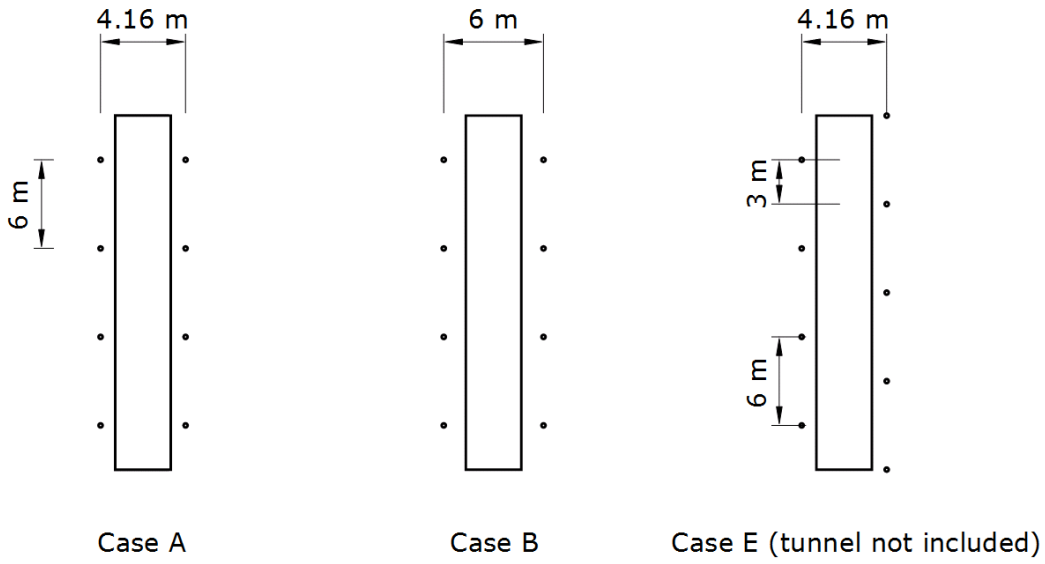

Figure 4.13: Schematic of cases A, B and E

Case	Borehole Distance (m)	Description
Case A	4.16	tunnel
Case B	6	tunnel
Case C	4.16	no tunnel
Case D	6	no tunnel
Case E	4.16	no tunnel - stratified borehole distribution

Table 4.2: Description of the cases used to optimize the borehole design.

The heat fluxes at the entire borehole surfaces for the 5 cases and the stand-alone borehole are compared over a 3 years in Figure 4.14. Also the borehole heat fluxes for cases A & B at borehole sections (0 m-9 m) next to the tunnel are compared in (Figure 4.14), to asses the effect of distance on the amount of heat extraction from the Underground Tunnels. By examining Cases A & B, the boreholes in case A experience more thermal interference initially, because they are closer in distance (4.16 m) across the tunnels, however after 5500 hours, the boreholes in case B will start thermally interfering and the ground will cool down such that the borehole heat flux becomes 5 W/m^2 less than case B at the end of the year (8760 hours). Also, the amount of heat extracted from the tunnel surface for case A exceeds that of case B (Figure 4.15) by 11 W/m^2 or 25%, so the borehole distribution in case A is more effective

at cooling the Tunnels than case B. The thermal interference between the boreholes is shown when comparing cases C & D, where the heat flux in case D is 2.5 W/m^2 more than case C at the end of year 3.

Staggered borehole distribution produces no benefits, as seen when comparing cases C & E, where their heat fluxes are almost identical. The single borehole's heat flux performs better than all the cases, where its heat flux is 5 W/m^2 or 15% more than case A. However, the single borehole is an ideal scenario, because it is not feasible in a restrained land size or urban environment to have boreholes that are separated by large distances, which will decrease the overall amount of heat extracted, since the number of boreholes will decrease in total. Case A is the most optimal arrangement for the boreholes around the tunnel, resulting in the highest heat extraction from the tunnel surfaces and consequently the most effective cooling effect in the Underground's Tunnels. However, case A does suffer from slight thermal interference between its boreholes leading to a decrease in borehole heat flux, which is compensated by the heat extracted from the tunnels.

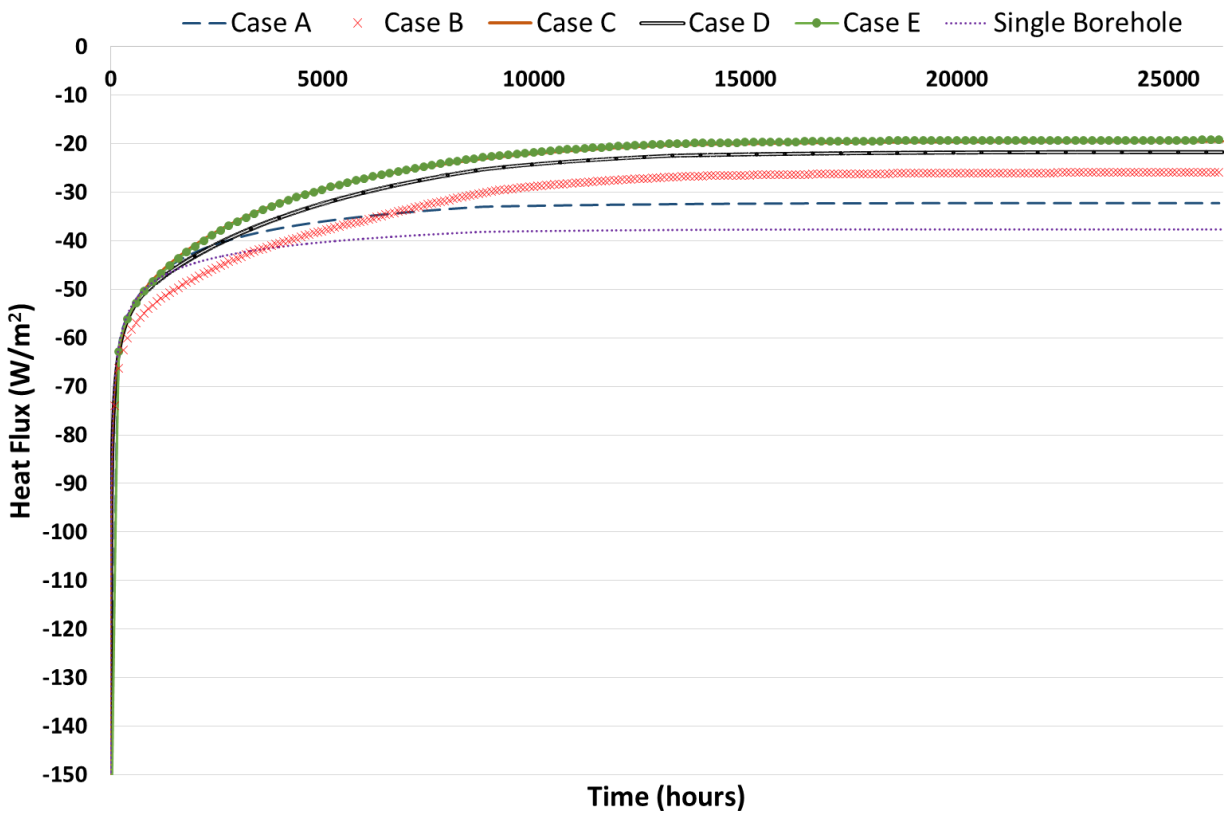

Figure 4.14: Comparison between Case A, Case B, Case C, Case D, Case E and single stand-alone borehole heat flux variations for 3 years of simulation.

4.4.2 Partially Insulated Boreholes

The heat demand of buildings is typically high in winter conditions and low in summer conditions. However, the London Underground requires cooling during summer conditions. This creates a paradox, because at a time when heat demand is low in the buildings above, the borehole heat extraction should be at its maximum. Also, it is not feasible to have the boreholes extract heat all around the year, as that would lead to the cooling of the surrounding soil, and consequently a decrease in borehole performance. To tackle these two problems simultaneously, a double U borehole arrangement is used (Figure 4.16). Each of the two U tubes inside the borehole is insulated using refrigerant pipe insulation in the arrangement seen in Figure 4.16. This arrangement allows the borehole to operate in two modes across the year. For winter conditions (including spring and autumn) the two U pipes will be extracting heat

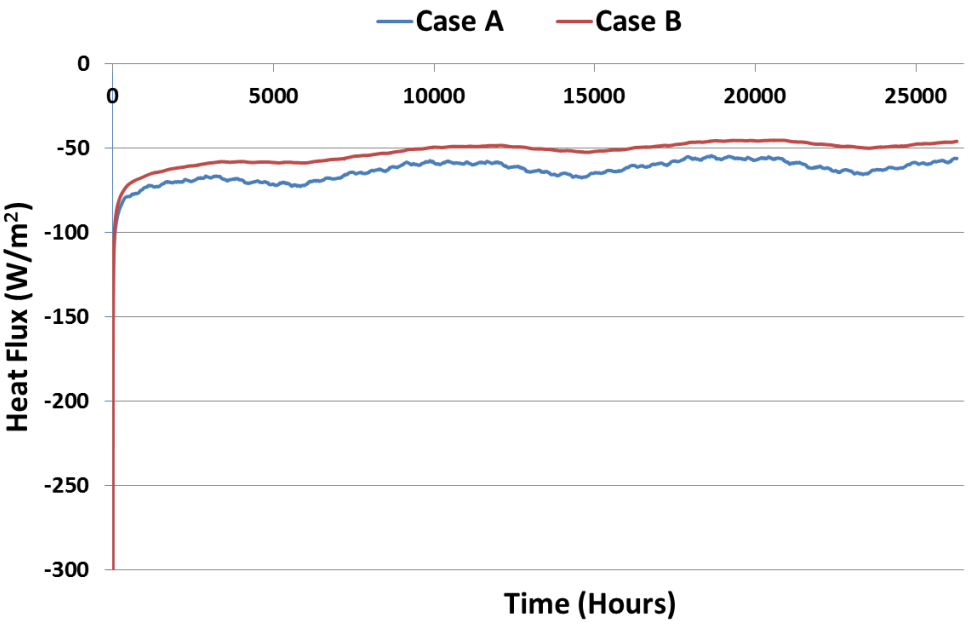

Figure 4.15: Comparison between Case A and Case B borehole section (0m-9m) annual heat flux variations.

from the ground. During summer conditions the U pipe that is exposed to the tunnel, will keep extracting heat, while hot refrigerant is pumped in the second U pipe that is insulated next to the tunnel section, such that it will inject heat in the soil far away from the tunnel. Hence, the boreholes can provide heating to the buildings during winter conditions, and both cooling and heating to the buildings during summer depending on their demand. Also, by iterating operation modes between heating and cooling, we can ensure a heat balance between the heat extracted and injected in the soil, which would maintain borehole and heat pump thermal performance.

The partially insulated boreholes concept is similar to borehole thermal energy storage (BTES), which is explained in details in chapter 2. Both BTES and partially insulated boreholes use the ground a medium for storing heat seasonally through BHEs (Lanahan and Tabares-Velasco, 2017), to provide the heating and cooling demand for buildings. For example, the "cold" of the winter is captured and stored in the ground, and used in the summer for cooling a building, while the "heat" in the summer is captured and stored in the ground and used for heating a building in the winter (Hammock and Hammock, 2015). The BTES system will result in increasing the COP of the GSHP system compared to conventional closed loop systems

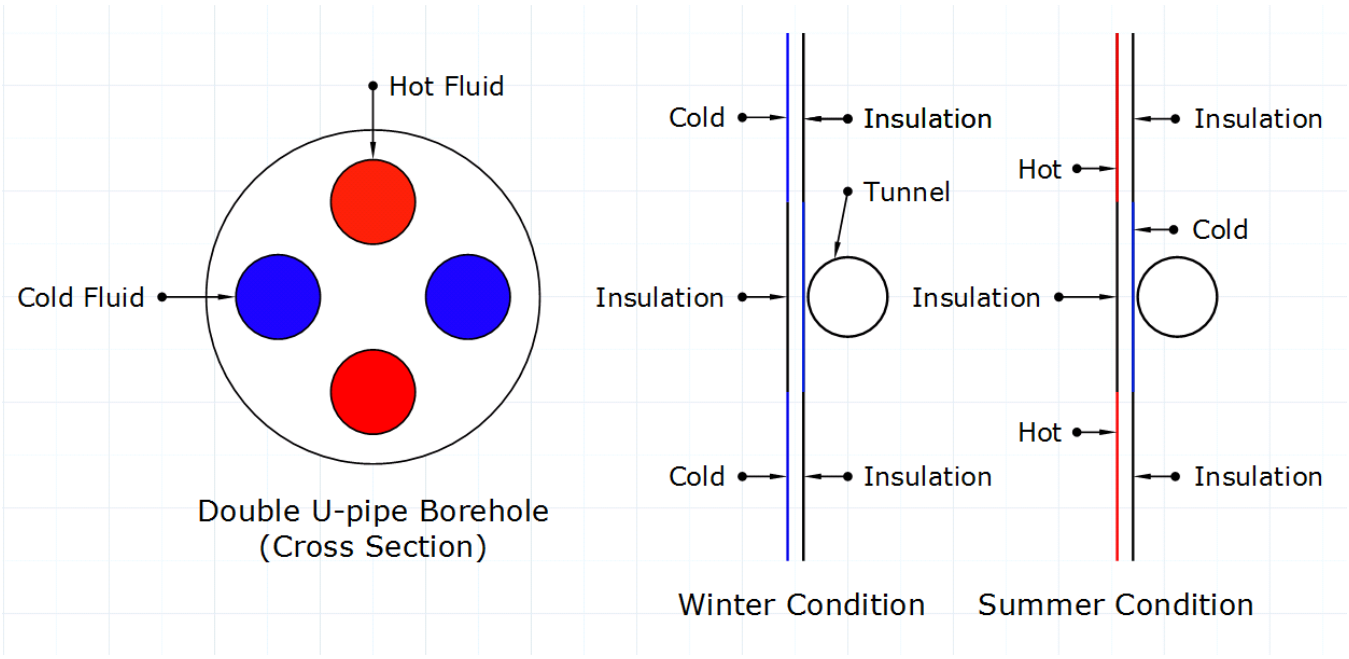

Figure 4.16: Partially Insulated Borehole Cross-section design (left) , and the variation of the insulated and non insulated sections operation modes between winter and summer conditions (right).

(Lanahan and Tabares-Velasco, 2017). However, BTES systems have two main constraints: The array of BHEs required to drill the BHE will require available area above the ground which is difficult to find in urban areas like London. The drilling cost of BHE is significant compared to aquifer based ATES systems since several BHEs need to be drilled within an array (Mielke et al., 2014). Since the space in the London Underground is restricted, particularly that London is heavily built, and the Central Line passes under the roads which are restricted in spacing, a BTES borehole array is difficult to implement unless drilling under the buildings is allowed. Partially insulated boreholes need less spacing since the same borehole operates in cooling and heating modes extracting and injecting heat in each of its U pipes, rather than each borehole operating in a single mode as in the case of the BTES system. The BTES system will store and extract the heat from the ground radially from the borehole, while the partially insulated borehole applies the same principle but stores and extracts the heat based on depths within the same borehole. For example, the BTES array constructed in 2008 in Crailsheim, Germany consists of 80 double U-tube BHEs drilled at the depth of 55 m, and separated by 3 m to each BHE center takes an area of 706 m^2 (Mielke et al., 2014).

As a basic case the partially insulated boreholes are assumed to run on 2 modes during the year, from January to April the boreholes are ran in winter mode, only extracting heat, and on summer mode from May to September, where the boreholes are both extracting heat near the tunnel and injecting heat far from the tunnel, from October to December the boreholes are ran in winter mode again, only extracting heat. Similar to before, the 1D Central Line and 3D borehole models are co-simulated over a time period of an entire year, where the same borehole arrangement as that of Case A is used, and the temperature of the borehole is 0 °C when extracting heat and 30 °C when injecting heat. Thus, during summer one U-tube is extracting heat and the other is injecting heat simultaneously. It is also imperative to determine the dimension of the non-insulated U pipe sections that extracts heat from the tunnel over the entire year. This is achieved by varying the dimension of the non-insulated U pipe facing the tunnel, during the simulations, such that the temperature of the soil, 20 cm away from the tunnel wall, output by comsol is equivalent to the temperature output by the base cooling case before (100 m non-insulated borehole). Thus, the cooling of the tunnel would not be effected by the switching of the U pipe between heating and cooling modes during summer conditions, because the U pipe section operating constantly in cooling mode creates a cooling bubble around the tunnel that shields it from the heat injected in the soil by the other U pipe section.

The 1D Central Line and 3D borehole models are co-simulated for 1 iteration over the period of 3 years for the original case before, where the boreholes operate in cooling mode (extracting heat from the ground) all around the year , and the partially insulated boreholes where the non-insulated U pipe facing the tunnel dimensions are 7 m , 18 m , and 30 m, and also operate in cooling mode all around the year. Results show that the partially insulated boreholes with a dimension of 30 m will have a similar cooling effect to the original case, because they both yield the same outer tunnel wall temperatures, as seen in Figure 4.17 & Figure 4.18. On the other hand, for the case of 7 m and 18 m, the outer tunnel wall temperatures are influenced by the uninsulated sections of the boreholes far from the tunnel that alternate between cooling and heating (injecting heat in the ground) modes, such that the outer tunnel wall temperatures are higher particularly for 10 m compared to the original case. These temperatures are equivalent for all the cases at the beginning of the first year till the month of May (Month 4), where the temperatures start diverging from the original case. The temperature divergence increases for 10 m and 18 m as the upper and lower borehole sections switch from cooling to heating

mode (injecting heat in the ground) between the months of May (Month 4) and September (Month 9), and then decreases as the entire borehole switches back to operating in heating mode only, where the maximum temperature difference between 10 m and 18 m is around 0.35 °C during the month of September. Therefore, the cooling of the tunnel would not be effected by the switching of the U pipe between Heating and Cooling modes during summer conditions, because the U pipe section operating constantly in Cooling mode creates a cooling bubble around the tunnel that shields it from the heat injected in the soil by the other U pipe section as seen in Figure 4.18.

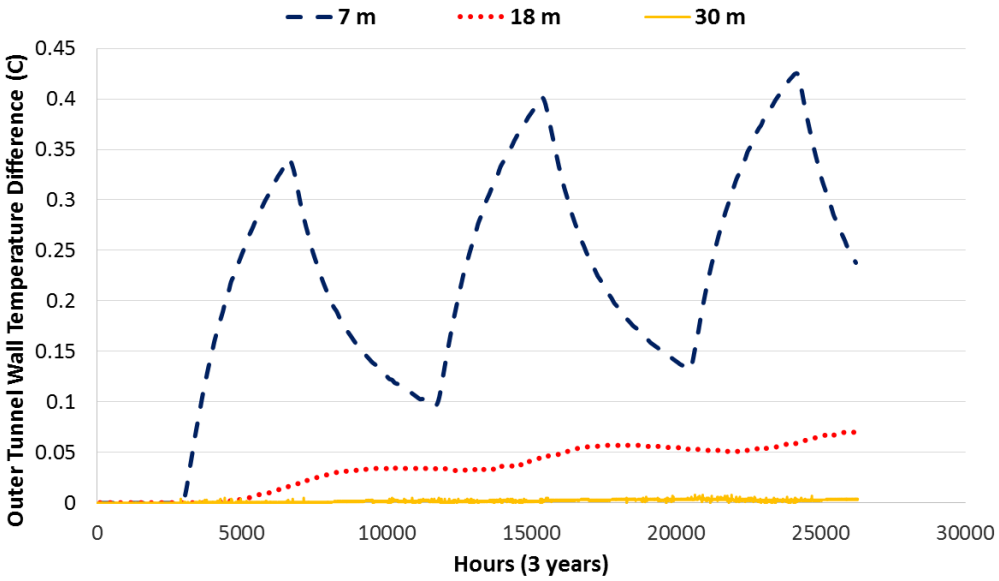

Figure 4.17: Outer tunnel wall temperature difference between the completely non insulated borehole, and partially insulated borehole having non-insulated sections facing the tunnels 7 m, 18 m & 30 m lengths for a simulation period of 3 years.

The comsol partially insulated boreholes model with 30 m non-insulated section next to the tunnel is co-simulated with the 1D Central Line model over a period of 3 years until the two models converge. The borehole surface heat fluxes over the period of 3 years are shown in Figure 4.19, where 0 m-15 m represents the 30 m non-insulated section next to the tunnels, and the 15 m-50 m the borehole section that switches between heating and cooling modes far away from the tunnel. Figure 4.19 shows that the heat fluxes in both the 0 m-15 m , and 15

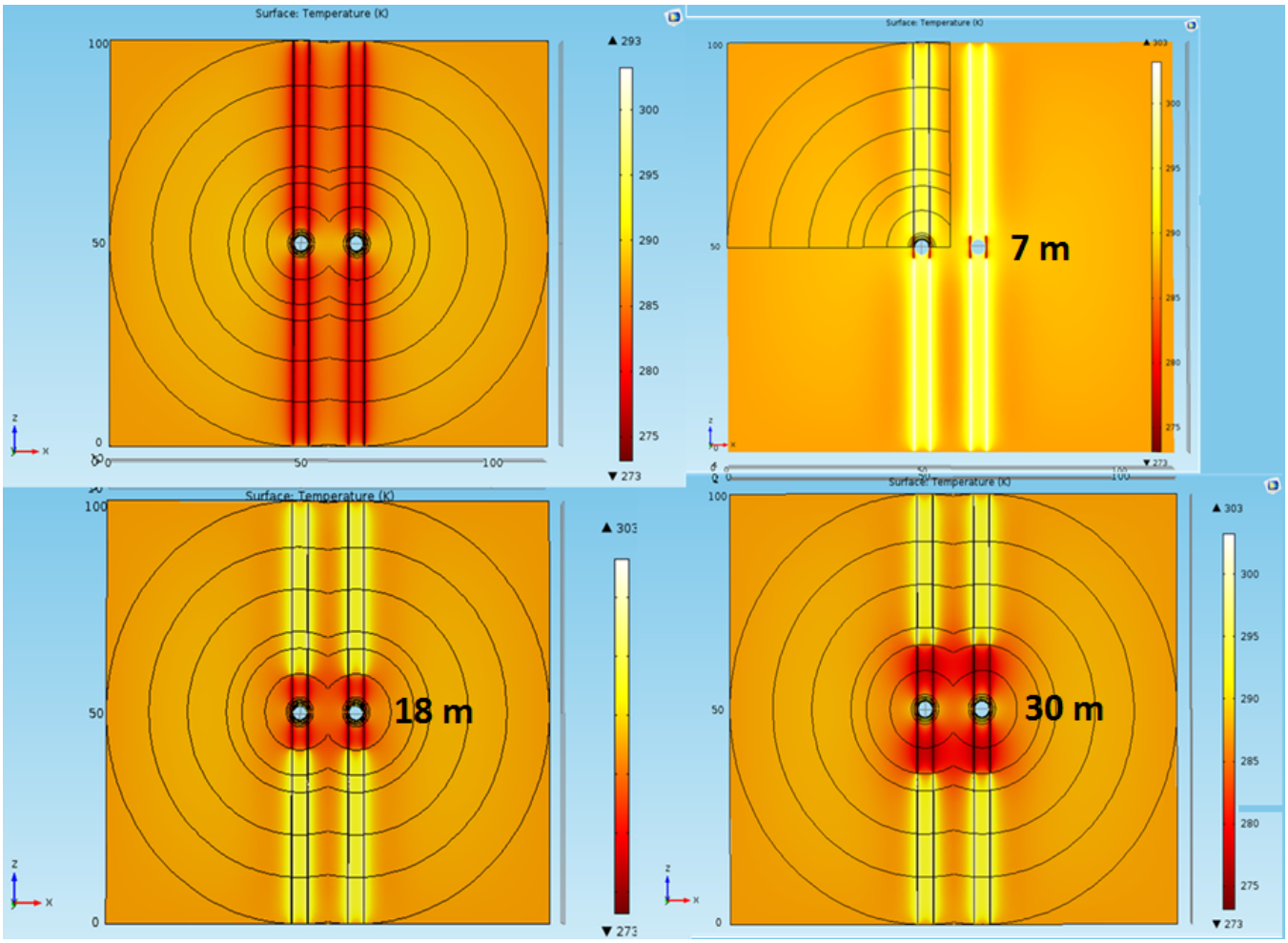

Figure 4.18: Cross sectional Comsol borehole model temperature distribution at the end of September in the third year for a completely non insulated borehole (top left), and partially insulated borehole having non-insulated sections facing the tunnels 7 m, 18 m & 30 m lengths

m-50 m become consistent in performance over the last 2 years, where the variation in the heat fluxes in 0 m-15 m section is dependent on the outer tunnel wall temperatures. In Table 4.3 the total amount of heat extracted in each section of the partially insulated boreholes for the third year is listed, and compared to the original case where the boreholes are operated in heating mode all around the year.

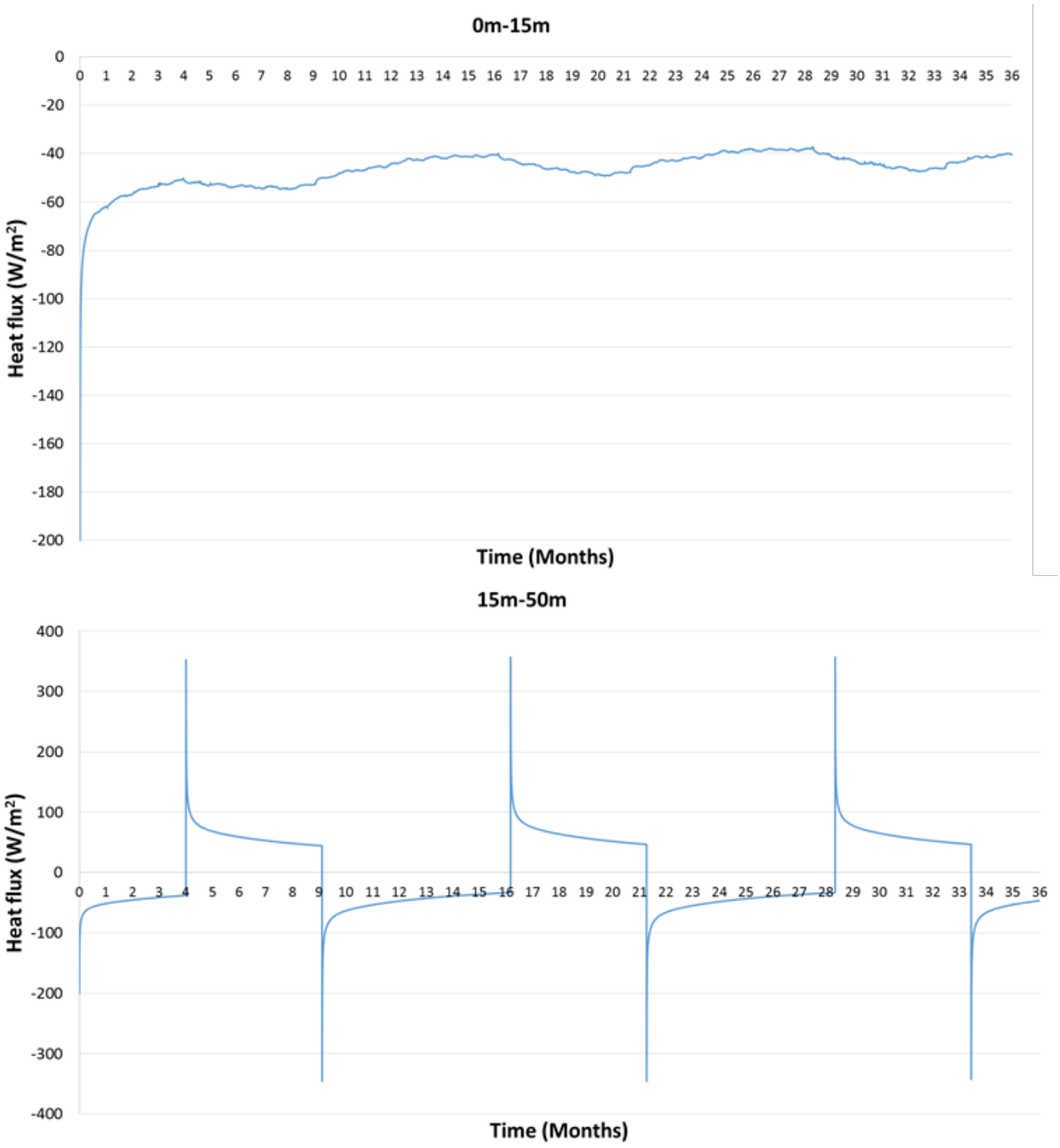

Figure 4.19: partially insulated borehole surface heat flux for section (0m-15m) (upper figure) near the tunnel and (15m-50m) far away from the tunnel for a period of 3 year simulations.

Borehole	Total Heat Extracted All Year (kWh) (0m-15m)	Total Heat Extracted Jan-Apr (kWh) (15m-50m)	Total Heat Extracted Oct-Dec (kWh) (15m-50m)	Total Cooling May-Sept (kWh) (15m-50m)	Total Heat Extracted All Year (kWh)
Partially Insulated Borehole	-2271	-1570	-1861	3350	-5702
Non Insulated Borehole	-	-	-	-	-4668

Table 4.3: Annual heat extracted and cooling potential for a non-insulated and partially insulated borehole.

Using comsol surface heat flux integration over the borehole surfaces the amount of heat extracted and injected in the soil is calculated for both the non-insulated borehole and the partially insulated borehole for the third year of operation Table 4.3. The value calculated is for half of the borehole (0 m-50 m), because of the symmetry used in the 3D FEM model. Over the third year the non-insulated borehole extracts 4668 kWh of heat, which is 9336 kWh for the entire borehole. The partially insulated borehole extracts 2271 kWh for the entire year for its (0 m-15 m) section next to the tunnel, and for the 15 m-50 m section it extracts 1570 kWh from January to April, and 1861 kWh from October to December. In total the partially insulated borehole extracts 5702 kWh over the entire year, which is 11404 kWh for the entire borehole. The partially insulated borehole (15 m-50 m) section injects 3253 kWh into the soil from May to September, which is 6506 kWh for the entire borehole which could be used to cool the buildings above the tunnels. Since the annual average UK house heating and water heating demand is 9300 kWh, a single non-insulated borehole can provide heating for 1 UK house hold, while the partially insulated borehole can provide heating for 1.25 UK households and an addition of 6700 kWh of cooling during summer conditions. It is worth to note that the total amount of heat extracted from the ground by the the partially insulated borehole (15 m-50 m) sections is approximately equal to the amount of heat injected back when operating in cooling mode, which indicates that the ground achieves a thermal balance throughout the year.

4.4.3 Boreholes Performance in 2032 & 2050

The 1D Central Line Model and the 3D comsol borehole model are co-simulated for the years of 2032 & 2050 to asses the cooling effect of the boreholes in the future, along with the influence of climate change, passenger & train traffic increase, and modernization of the trains. The HE and ME scenarios are combined because their differences are negligible as has been shown previously in section 3.3.3.

The boreholes will result in significant cooling for the tunnels and platforms in the years of 2032 and 2050 as seen in Figure 4.20 and Figure 4.21. The boreholes manage to lower the air temperatures of the platforms and tunnels by around 3.9 °C & 4.3 °C respectively for the year of 2032, and by 4.1 °C & 4.7 °C respectively for the year of 2050. Thus, the boreholes will help in mitigating the overheating problems in the Central Line by significantly cooling the system for the years to come in the future scenarios, which are described in detail in section 3.2.4.1.

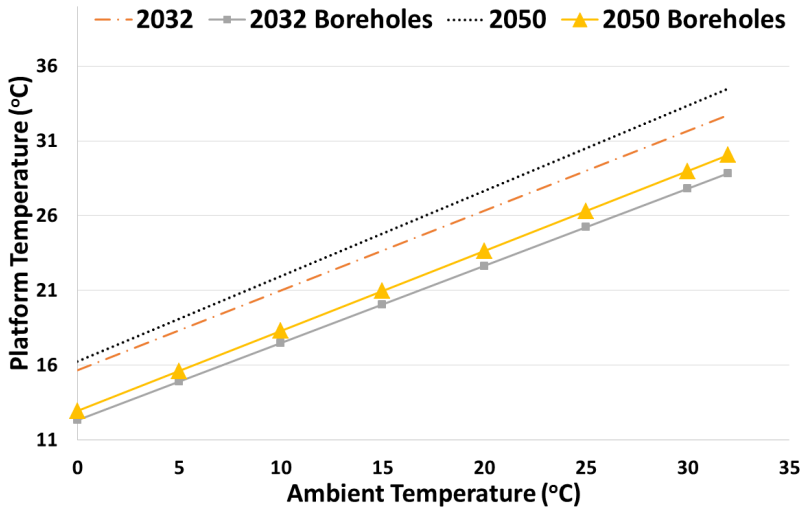

Figure 4.20: Comparing the Central Line linear fitted platform temperatures (°C) for the years of 2032 and 2050 for two cases: The current tunnels, and tunnels equipped with vertical boreholes.

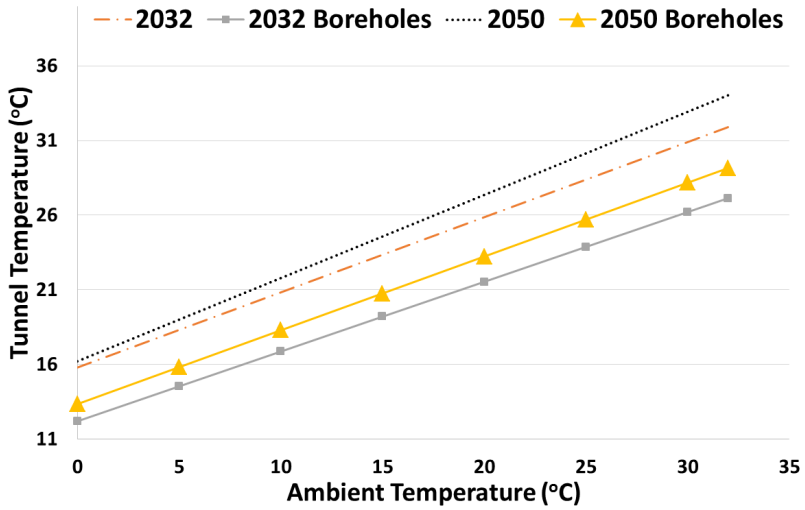

Figure 4.21: Comparing the Central Line linear fitted tunnel temperatures (°C) for the years of 2032 and 2050 for two cases: The current tunnels, and tunnels equipped with vertical boreholes.

4.5 Conclusion

A 1D model was developed using IDA Tunnel to model the climate conditions in the London Underground's (LU) Central Line station and tunnel, which is considered the busiest in the LU system. The simulation results are validated with measured temperature data in both the platforms and the tunnels. A 3D Comsol finite element model was developed to model thermal transient interactions between the subway tunnels and vertical boreholes, to assess their effectiveness in cooling the Central Line tunnels and platforms. The 1D Central Line and the 3D borehole models are co-simulated, through exchanging outer tunnel wall and soil temperature profiles, until both models yield a similar outer tunnel wall temperature, which indicates that both models have converged to a single solution. The 1D - 3D co-simulations converged in 11 iterations, where varying the iteration time interval between 1 month and 3 month yielded equivalent results, which allows for conducting annual simulations with fewer numbers of total iterations. The boreholes next to the tunnels manage to cool the tunnel and platform temperatures in the Central Line model by 5 °C and 4.5 °C respectively during summer conditions. A single borehole's third of year operation heat extraction (9336 kWh) was 9% slightly below a stand-alone borehole (10177 kWh), because the boreholes thermally interfered along the sides of the tunnel, which slightly reduced their performance. This was a

necessary compromise, since to better cool the tunnels, the boreholes were placed as close as possible to the tunnel outer walls. Nevertheless, a single boreholes's annual heat extraction was found to be equivalent to the annual heat demand of 1 UK households. Ground thermal storage using BTES would enhance the efficiency of the borehole storage seasonally, and enhance the quantity of heating delivered to the buildings, however it would require alot of surface area above the ground which is not available in the case of the London Underground, where it is located within the heavily built Central London. Variations on the borehole arrangement and distance from the tunnel have shown that the optimum arrangement is having the parallel boreholes at a distance of 20 cm from the outer tunnel walls at each side, since the further the distance the less heat will be extracted from the tunnels, which will consequently result in less cooling in the tunnels and stations. The vertical boreholes were able to lower the air temperatures of the platforms and tunnels by around 3.9 °C & 4.3 °C respectively for the year of 2032, and by 4.1 °C & 4.7 °C respectively for the year of 2050. This future scenario takes climate change, passenger & train traffic increase, and modernization of the trains into consideration. Consequently, the boreholes will help in mitigating the overheating problems in the Central Line by significantly cooling the system for the years to come in the future.

A new concept of partially insulated boreholes is introduced to address the issue of having low heat demand in the buildings during summer conditions, while the underground tunnels and stations require cooling. The partially insulated boreholes are able to provide district building heating during winter conditions, and both building cooling and heating simultaneously during summer conditions while cooling the LU. The partially insulated boreholes do follow the same principle as BTES, but they use the same borehole to inject and extract heat seasonally simultaneously using the same borehole. The optimum dimensions of the partially insulated borehole was found to be 30 m for the non-insulated section next to the tunnel which extracts heat all around the year (building heating), while the other 70 m section alternates between extracting heat during winter conditions between January - April and October - December, and injecting heat into the soil (building cooling) during summer conditions between May - September. One partially insulated borehole can annually provide heating for 1.25 UK households and an additional 6700 kWh of building cooling, while the non-insulated borehole provides less building heating annually equivalent to 1 UK household. These results provide a starting point to examine the potential of using vertical boreholes to cool the older lines

of the LU while providing district heating and cooling to the surrounding buildings above. Another aspect to take into consideration in the following chapter is the variation of building heat demand across the year, which dictates the borehole's operation schedule, and the optimum length of the boreholes. The internal section of the partially insulated borehole wasn't modeled in this thesis, where the focus was on the outer sections and the interaction of the partially insulated borehole with the soil. Thus, future work would require modeling the partially insulated boreholes internally using COMSOL, while making sure that the simulation process is computationally efficient. Furthermore, the technical aspect of constructing the inner section of the partially insulated boreholes, and identifying the proper material of insulation needs to be investigated as well.

Chapter 5

Multiple Benefits of Vertical Boreholes Overground & Underground

5.1 Introduction

In 2009 the EU created a wide action that aims to increase the use of renewable energy, where the UK committed to achieve a 15 % renewable energy by the year of 2020 (DECC, 2014b). Approximately half of the energy consumed in the UK is used to produce heat. Consequently, the UK plans to have 12% of building heating demand energy generated from renewable energy by the year of 2020 (DECC, 2013). Large scale renewable energy networks for heating can contribute significantly to meeting the renewable targets and contribute to net-zero energy districts. Ground source heat pumps (GSHP) is an established technology, that transfers the heat to or from the ground to provide heating or cooling to the buildings.

A 3D FEM model of vertical ground boreholes was coupled with the 1D Central Line model in chapter 4, to study the cooling effects of the boreholes on the London Underground's Environment. Chapter 4 showed that the vertical boreholes manage to cool the tunnel and platform air temperatures in the Central Line by 4.5 °C and 4 °C respectively during summer conditions, which helps mitigate the overheating problems in the line. The resulting outer tunnel wall temperature output by the 1D - 3D co-simulation is used for the simulations in this chapter.

The application of retrofitting the Central Line with vertical geothermal closed loop boreholes in the City of London is investigated. The heat extracted from the Central Line system is used to provide part of the heating and cooling demand in the surrounding buildings above the tunnels. The 1D - 3D co-simulation methodology developed in chapter 4 is used to estimate the amount of heat extracted and injected by the boreholes across a tunnel section of the Central Line that spans 6 stations in Central London. The boreholes length are adjusted such that priority is given to cooling the London Underground, while maximizing the amount of heat extracted and reducing capital cost. The boreholes are co-simulated for each of the borehole lengths for the 6 station section. The amount of heating and cooling provided by the vertical GSHP's in this Central Line section is compared to the heating demand and cooling demand of the buildings in the proximity of the tunnels.

The cooling of the Central Line tunnels would influence the passengers thermal comfort in both the platforms and the train carriages. Since the vertical boreholes would lower the air temperatures of the tunnels and platforms, the passenger thermal comfort is enhanced in both the platforms and the train carriages where the passengers spend most of their time in the subway system. A train carriage model in IDA tunnel is setup to model the environment of these train carriages inside the subway system. The Train Carriage model and the 1D Central Line model are run to quantify the air temperature decrease in the train carriages and the platforms, where the outer tunnel wall temperature profile from the 1D - 3D co-simulation results is used. The platform air temperatures were obtained from previous simulations in chapter 3 and chapter 4. To quantify the improvements of passenger thermal comfort this chapter based its thermal comfort standard on survey work commissioned by London Underground in the summer of 2003 (BRE, 2004a).

The electrical consumption of the on-board train carriage air conditioning is simulated in the 6 station Central Line section. The 1D Central Line model is expanded to include the 6 Central Line stations. The aim is to study the effect of using traditional air-conditioning in the Central Line if the technical difficulties of installing air-conditioning in restricted tunnel spaces is solved. The on-board air conditioning is combined with vertical boreholes in the tunnels to the asses the borehole's effect in reducing the air-conditioning electrical consumption in the Central Line train carriages. To achieve that the outer tunnel wall temperature profile from the 1D Central Line model and 3D borehole model co-simulation results is used for the expanded 1D Central Line Model, while modifying the train carriage model to include air

conditioning. The impact of the air-conditioning on the Central Line climate in the platforms and tunnels is also assessed, since the rejected heat from the carriages would result in an increase in air temperatures in the system.

The main objective of this chapter is to examine the overall thermal benefits of retrofitting a deep and old subway line suffering from overheating problems by using vertical closed loop GSHP systems, while providing heating and cooling to the buildings above the tunnels by utilizing ground source heat pumps: (a) The useful heat extracted from the GSHP is quantified and compared against the heating and cooling demand of buildings above ground, (b) The influence of resulting lower tunnel and platform temperatures on passenger's thermal comfort is examined, and (c) the energy cost of conventionally air-conditioning the train carriages is compared against the GSHP system. We use the outer tunnel temperatures derived from the coupled 3D FEM and 1D simulation from Chapter 4 for these analyses. a schematic of the different simulation processes is shown in Figure 5.1.

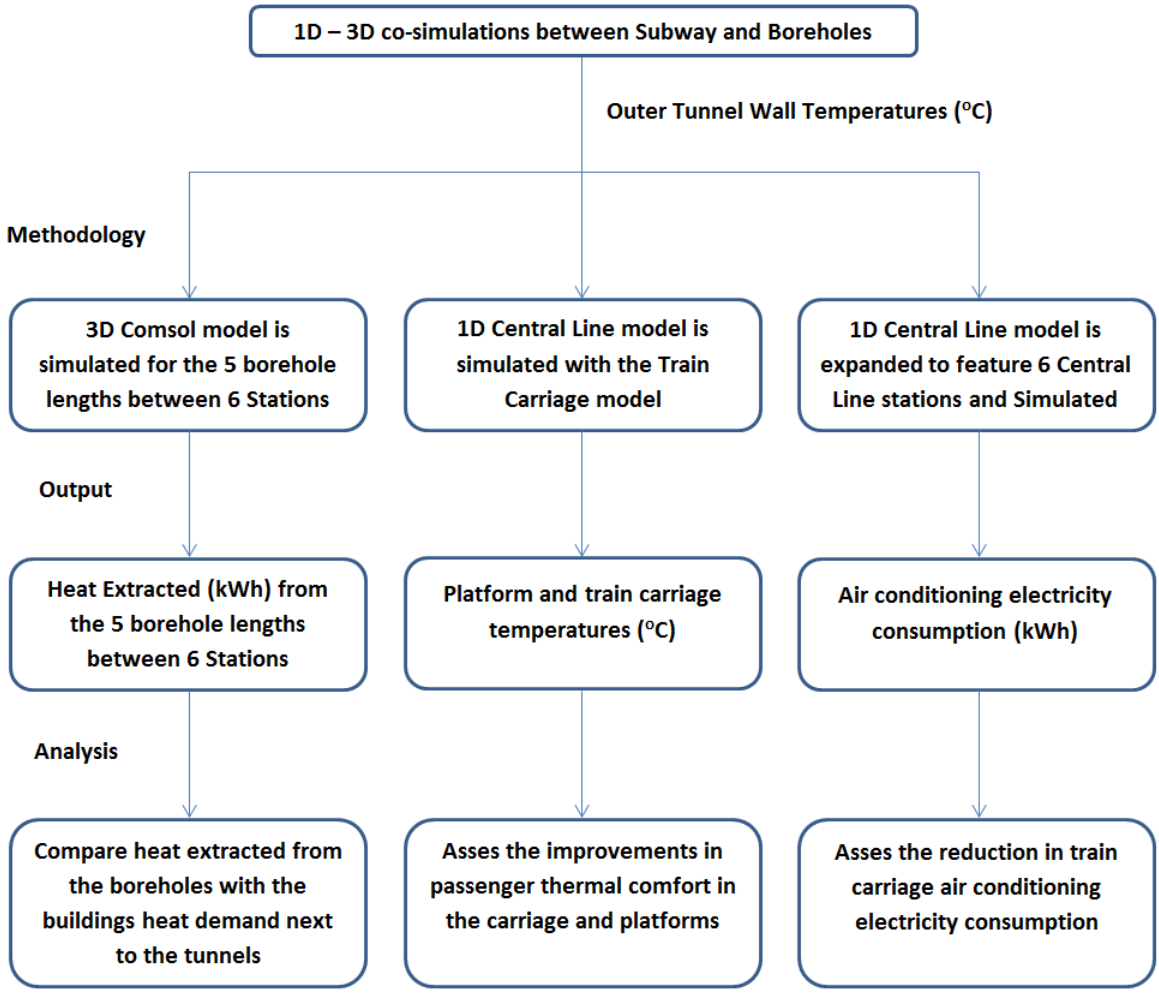

Figure 5.1: Flow chart for the simulation processes used in this chapter.

5.2 Integrating the Central Line Vertical Boreholes with Central London Building Heat Demand

5.2.1 Model Description and Parameters

The boreholes that are placed between the tunnels of the 6 stations were shown in chapter 4 to decrease the temperature of the Central Line's tunnels and platforms. The extracted heat from the tunnel and its surrounding soil via the boreholes can be utilized to provide part of the heat demand for the buildings in the tunnel proximity overground. One constraint in this application is the availability of space above the London Underground's tunnels. Vertical

boreholes can be bored when the tunnels are under open public spaces such as roads and parks, while it is impractical to apply this when there are buildings and other infrastructure above the tunnels. Some of the London Underground Lines were bored under the roads to avoid the need for agreement with owners of property above the surface (Green, 1987). Among the deep level London Underground lines, a large portion of the Central Line approximately 9.5 Km of length, was constructed under existing roads, spanning 13 stations from Shepherd's Bush Station continuously to Bank (Green, 1987).

The city of London is used as a case study to identify and map areas where the vertical boreholes can be constructed under roads, sideways and parks along the sides of the West Bound and East Bound tunnels of the Central Line to provide part of the heating demand for the buildings above. A GIS data base, obtained from the UK Geo-information Group, provides the floor area, height and usage of every building. The building heating and cooling demands were obtained from the results of (Zhang et al., 2015b).

A section of the Central Line containing 6 stations is used for this study: Queensway, Lancaster Gate, Marble Arch, Bond Street, Oxford Circus, and Tottenham Court Road. The Central Line passes under Bayswater Road next to Hyde Park, and Oxford Street, covering 4.8 Km of tunnels as seen in Figure 5.3. The borehole arrangement shown in Figure 5.2 is considered for this section of the Central Line. It is composed of a typical vertical close-loop borehole design that adheres to DECC's Microgeneration Certification Scheme Standards (DECC, 2011). The arrangement of the boreholes is described previously in chapter 4, section 4.2.2 and Figure 5.2. The boreholes are placed on the sides of the tunnels and not the platforms. Since the platforms are 140 m long, and the total length of the tunnels between the 6 stations is 4.8 Km. The length of the tunnels, platforms excluded, is 3910 m, which can accommodate 2600 borehole heat exchangers (BHE) if we consider there are 4 BHE's every 6 m, 2 for the westbound and 2 for the east bound tunnels. The depth of the stations vary between 25.2 m and 30.1 m (Figure 5.5) based on data provided by Transport for London.

The vertical boreholes are assumed to be linked to the GSHP system in the building blocks next to them on both sides of the road. Thus we define a group of buildings next to the Central Line by a block of buildings delimited by streets as shown in Figure 5.3. There is a

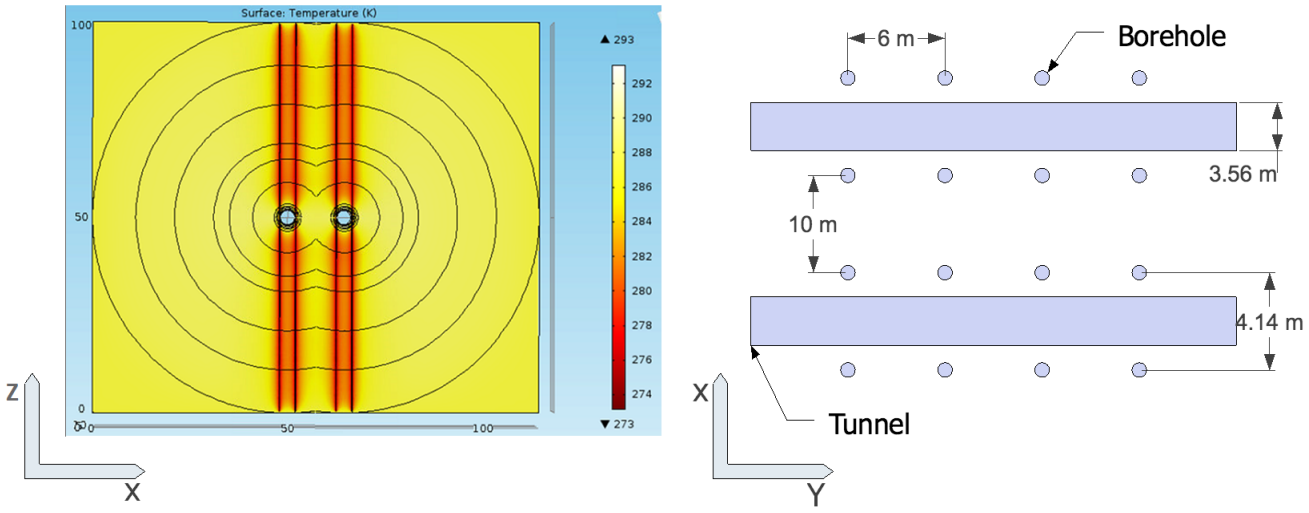

Figure 5.2: Front view vertical borehole and Central Line tunnels Comsol model (Left).Top view schematic of the vertical borehole and Central Line tunnels (Right).

total of 62 blocks of buildings on both sides of the road within this area. The building blocks are grouped into 31 building clusters , where the clusters are the building blocks on the right and left sides of the road, under which the Central Line tunnels are located, and are numbered from 1 to 31 from the left side of the map to the right side of the map. The building type composition of each of the clusters by area is shown in Figure 5.4. The 31 clusters contain a total of 5335 buildings.

In order to reduce capital costs, have the most thermally efficient heat extraction, and optimally cool the London Underground tunnel environment, it is more efficient to bore the vertical boreholes up to a certain level under the tunnels, particularly 15 m below the depth of the tunnels, as has been discussed in Chapter 4, section 4.4.2. This would result in the most thermally and cost efficient arrangement of boreholes, rather than to spend large capital boring 100 m or deeper boreholes next to the tunnels. This is because the primary purpose of these BHE's is to cool the tunnel, while providing cooling and heating to the upper building is secondary. A schematic of the depth of the station platforms, the vertical borehole depth, and the tunnel distance between the stations is shown in Figure 5.5. It has to be noted that all depth of the stations and tunnels are true vertical depths (TVD). The depth of the boreholes

between the stations is determined by having them 15 m below the depth of the tunnels, where the tunnel depth is assumed to vary linearly between two platforms. For example in Figure 5.5 : Queensway is 30.1 m deep and Lancaster Gate is 27.5 m deep. The tunnels between these two stations will vary between the depth of 30.1 m and 27.5 m. Since Queensway is deeper than Lancaster Gate, the depth of the boreholes in the tunnels between them is calculated as the depth of Queensway (30.1 m) plus 15 m which equals to 45.1 m. This method is applied between all the stations so that the tunnels between every two stations will have at least 15 m of borehole depth beneath the tunnels, and the vertical borehole depth is fixed between two stations.

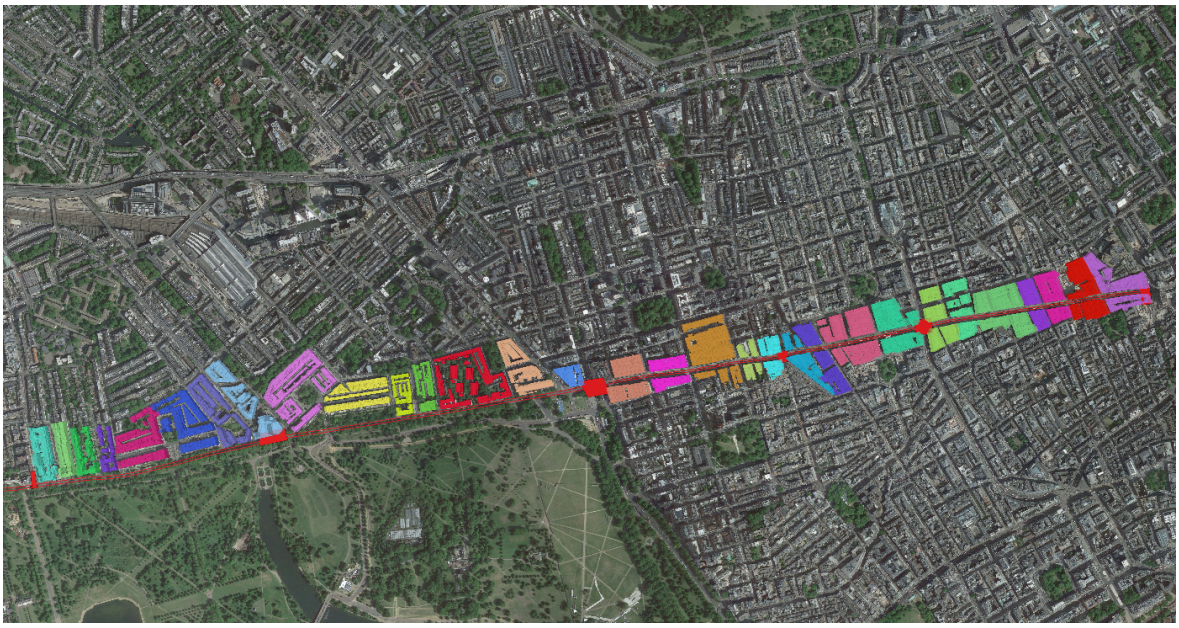

Figure 5.3: Map showing the Central Line in the City of London, and the 31 building clusters surrounding the tunnels, where each cluster is marked by a distinct color, and they are numbered from 1 to 31 from the left to the right side of the map.

Since the temperature drop in the tunnels is similar if the boreholes are 15 m or longer below and above the tunnel as discussed in Chapter 4, section 4.4.2. The outer tunnel wall temperatures for having a borehole length of 100 m can be used in the simulations as shown in Figure 4.9 in Chapter 4. These outer tunnel wall temperatures are used for the 5 borehole length. The results for third year are used, where the amount of heat extraction balances with

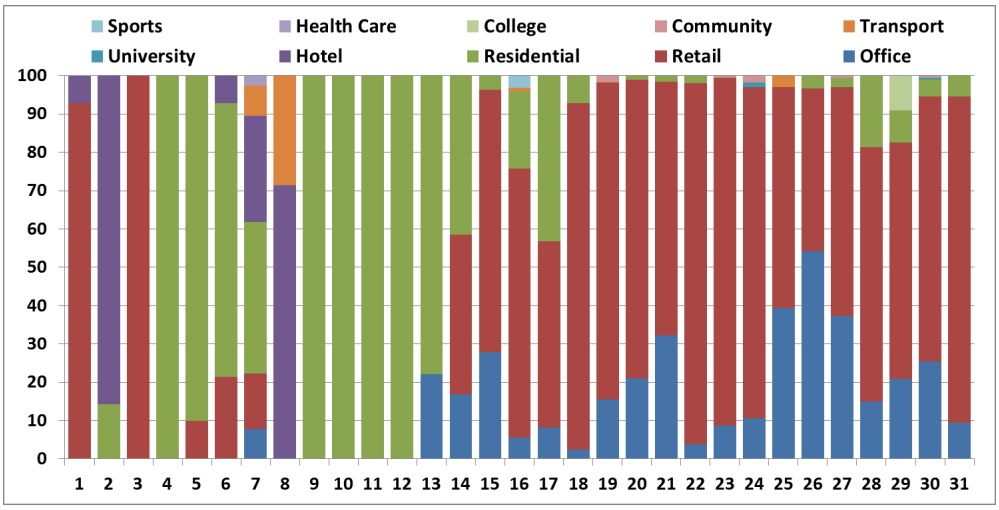

Figure 5.4: Building type percentage distribution by area of each of the 31 building clusters, obtained from the UK Geo-information Group.

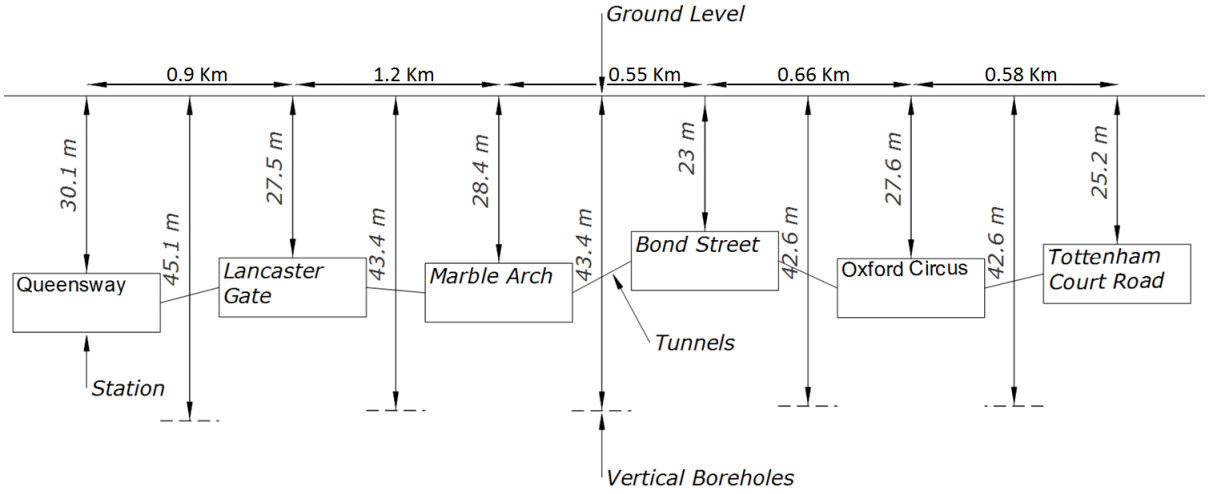

Figure 5.5: Station, tunnel, and vertical borehole depths & tunnel distances between Queensway and Tottenham Court Road stations along the Central Line.

the ground and the borehole reaches a thermal steady state with the surrounding ground. The 5 distinctive borehole depths are simulated, to determine the amount of heat extracted by each of the borehole length. The heat extracted from the vertical boreholes are summed along the tunnels bordering each of the building clusters. This is done by multiplying the annual amount of heat extracted by each of the boreholes length with the number of boreholes present between each of the 6 stations. The average GSHP COP is taken to be 3.3, which is a

common typical design value for vertical closed loop GSHP systems (Kavanaugh and Rafferty, 1997), where this value was obtained as an average of COP's over the entire season, so this is equivalent to the Seasonal Performance Factor (SPF) of the GSHP.

The concept of using partially insulated vertical boreholes, which was studied in chapter 4, is also applied at the scale of the City of Westminster, to provide both cooling and heating to the building clusters. The partially insulated boreholes will use a double U borehole arrangement, which is explained and illustrated in details in section 4.4.2 to allow the borehole to operate in two modes across the year. Consequently, the partially insulated boreholes provide heating to the buildings during winter, and both cooling and heating to the buildings during summer depending on their demand. The boreholes are assumed to run on 2 modes during the year, from January to April the boreholes are ran in winter mode, only extracting heat, and on summer mode from May to September, where the boreholes are both extracting heat near the tunnel and injecting heat far from the tunnel, from October to December the boreholes are ran in winter mode again, only extracting heat. The depth of the boreholes in this case will still be 15 m below the depth of the tunnels similar to the boreholes described in the previous paragraph and in Figure 5.5, but there will be a section on the upper side of the boreholes which will alternate between heat extraction and injection, when alternating between heating and cooling modes. The depth of the partially insulated boreholes and length of the section that alternates between cooling and heating modes and the section that operates in heating mode only is shown in Table 5.1. For example in Figure 5.5 : Queensway is 30.1 m deep and Lancaster Gate is 27.5 m deep. The total depth of the boreholes in the tunnels between them is calculated to be 45.1 m as shown in the previous paragraph. Lancaster Gate is 27.5 m deep, the length of the borehole that alternates between heating/cooling between Queensway and Lancaster Gate is calculated as 27.5 m - 15 m = 12.5 m, since at least 15 m of boreholes above the tunnels are needed to operate on extracting heat only to ensure optimum cooling of the tunnel. This method is applied between all the stations so that the tunnels and the length of the sections in the boreholes is provided in Table 5.1.

Station	Queensway	Lancaster Gate	Marble Arch	Bond Street	Oxford Circus	Tottenham Court Road
Heat Extraction and Injection Section (m)	12.5	12.5	8	8	10.2	10.2
Heat Extraction Only Section (m)	32.6	30.9	30.9	34.6	30	30
Total Borehole Length (m)	45.1	43.4	43.4	42.6	42.6	42.6

Table 5.1: Vertical partially insulated boreholes depths and section lengths between Queensway and Tottenham Court Road Stations along the Central Line.

The amount of heat and cooling provided by the vertical GSHP's is compared with the annual, monthly and hourly heat demand of these clusters for two cases: The tunnels equipped with heat extracting boreholes only, and partially insulated boreholes that can provide both heating and cooling.

5.2.2 Results and Analysis

The total simulated heat demand for the 31 clusters is 162 x 10^6 kWh, and the total area of the 31 clusters is 1.37 x 10^6 m^2. Dividing the total annual heat demand for the 31 clusters by their total building area gives 118 kWh/m^2. The heat demand of each of the dominant building types in the 31 clusters is summed and divided over their consecutive area, which are shown in Table 5.2. The building types listed in Table 5.2 constitute 97 % of the area, and 95 % of the total annual heat demand of the entire buildings in the 31 clusters. These values were found to be within the ranges of the heating consumption benchmarks found in (CIBSE, 2012), where the ranges used from the CIBSE Guide F are taken for typical performance of these building types.

The annual amount of heat that can be potentially extracted from the vertical boreholes is calculated for each borehole length and the entire boreholes spanning 6 Central Line stations

Building Type	Retail	Offices	Residential	University	Hotels
Total Annual Heat Demand per Building Type (MWh)	30199	48222	38937	7128	29240
Total Building Type Area (m^2 1000's)	407	315	649	31	79.9
Annual Heat Demand per Area (kWh/m^2)	113	165	70	390	382
CIBSE Guide F Range (kWh/m^2)	0-249	151-210	45-200	120-600	360-460

Table 5.2: The Building clusters total annual heat demand by building type per m^2 compared to their typical energy consumption bechmark from from the CIBSE Guide F Range (CIBSE, 2012).

from Queensway to Tottenham Court Road over a distance of 4.8 Km of tunnels as seen in Table 5.3. The total monthly heat extracted from the boreholes is compared to the total monthly heat demand of the 31 building clusters combined on the sides of the Central Line in Figure 5.7 & Table 5.5.

During the winter months (January, February and December) the vertical boreholes are able to cover 4.5% of the total building clusters heat demand. During summer months (June, July and August) the boreholes can meet a higher percentage of the building heat demand as in June (33.4%), July (74%) and August (49.2%). The building heat demand in the month of July is attributed to hot water heat demand where dividing the building heat demand in the month of July by the total building area gives an annual equivalent of 13 kWh/m^2, which is close to the annual average water heat demand of 11 kWh/m^2 for buildings of mixed use according to (Palmer and Cooper, 2013). The heat demand per unit area for the residential building types for the month of July is 17 kWh/m^2, which is within the range of residential water heat demand which ranges between 13 kWh/m^2- 25 kWh/m^2 (Burzynski et al., 2011). The amount of heat extracted by the boreholes varies throughout the year, where it is minimum during the month of January 1050 MWh and maximum in the month of July 1295 MWh as a result of variations in the Central Line tunnel temperatures as has been shown in Figure 4.9 in chapter 4, since the temperatures of the tunnels rise during summer conditions. The Central

Borehole Length (m)	Annual Heat Extracted per Borehole (kWh)	Clusters	Number of Boreholes	Annual Heat Extracted Between Stations (MWh)
45.1	5454	1-9	708	4.2
43.4	5352	10-15	632	3.4
43.4	5352	16-20	460	2.5
42.6	5304	21-24	320	1.7
42.6	5304	25-31	492	2.6

Table 5.3: The annual heat (kWh) extracted from each borehole length (m), and the total amount of heat extracted (kWh) between each of the tunnel sections between the 6 stations in the Central Line.

Line tunnels act as heat sources for the vertical boreholes, which provide a consistency with the amount of heat extracted throughout the year. The vertical boreholes manage to cover a portion of the 31 clusters heat demand annually, where it covers the most for cluster 10 (29%) and least for cluster 16 (3.2%) as seen in Figure 5.8 and Figure 5.9 .

The total annual amount of heat the boreholes, which have an averaged length of 43.6 m, can provide between the 6 stations is 14.3×10^6 kWh compared to 24.2×10^6 kWh if the boreholes were 100 m long. Thus, adjusting the borehole length to 15 m below the tunnels results in a more efficient heat extraction compared to the 100 m boreholes since a larger portion of the boreholes is closer to the tunnels. Since the COP of the heat pumps is 3.3, the heat pumps would consume 4.33×10^6 kWh of electricity. This would emit the equivalent of 1705 tons of CO_2, since the carbon emission foot print of UK electricity production is 0.394 Kg CO_2/kWh (DECC, 2015). Currently these buildings utilize gas boilers for their heating which have a median efficiency of 96 % (Garber et al., 2013), so it would take 14.9×10^6 kWh worth of gas combustion to provide an equivalent amount of heating to the vertical boreholes. This would emit the equivalent of 2772 tons of CO_2, since the carbon foot print of gas combustion in boilers is 0.194 kg CO_2/kWh (Garber et al., 2013). Consequently, retrofitting the tunnels with verticals boreholes would result in reducing building heating carbon emissions by 1067 tons of CO_2 annually.

The results can be compared to (Blum et al., 2010), which has studied the savings of CO_2 emissions due to the use of ground source heat pump (GSHP) systems in comparison to conventional heating systems. Based on (Blum et al., 2010), the average GSHP with a BHE depth of 150 m and COP of 4 in Germany can save 1.8 tons CO_2 annually compared to conventional gas boilers with a standard deviation of 0.5 tons CO_2. Blum et al. (2010) conducted the analysis based on Germany's electricity production carbon emission foot print of 0.594 Kg CO_2/kWh in 2010. The average savings for the GSHP system in the Central Line is calculated as 1067 tons CO_2/2600 = 0.41 tons CO_2 annually for an average depth of 43 m as shown in Figure 5.5. If the parameters of the GSHP system in (Blum et al., 2010) is adjusted to that for the Central Line BHE's, we can get a rough comparison between exiting GSHP systems and the one proposed for the Central Line. The ratio between the COP, Depth, and electricity carbon foot print between the proposed Central Line System and the GSHP system in (Blum et al., 2010) is 0.8, 0.27, and 0.7 respectively. If we divide the average savings for the GSHP system in the Central Line by the COP and depth difference ratio we get 0.41 / (0.8)(0.2) = 1.9 tons CO_2, then multiply by the electricity production carbon emission foot print ratio 1.9 * 0.7 = 1.33 tons CO_2, which is 1.8 - 1.33 = 0.47 tons CO_2 lower than the average value of (Blum et al., 2010), but within the standard deviation of 0.5 tons CO_2 in (Blum et al., 2010). This comparison did not consider difference in soil temperatures and also the difference in soil thermal conductivity, but it is a good benchmark to compare and to validate the numbers simulated in the Central Line GSHP system with existing systems in (Blum et al., 2010).

The analysis in the previous paragraph focused on the GSHP CO_2 saving based on the net energy consumption due to the operation of GSHP compared to gas boiler heating. To get a more precise quantification of the CO_2 emissions, we having to incorporate the life cycle analysis of the GSHP to our analysis in the previous paragraph. Saner et al. (2010) has shown that on average the electricity consumption accounts for (87%) of the life cycle emissions of GSHP systems, while the remaining 13% is distributed among constructing the GHSP systems, transporting the material, and the GSHP refrigerant. On the other hand, the majority of gas boilers CO_2 emissions 98% is due to operations as shown by (Zheng et al., 2016). Applying this to the suggested BHEs in the Central Line the total GSHP life cycle emissions are calculated as 1705 tons of CO_2 / 0.87 = 1960 CO_2 tons / year, while for equivalent gas boiler emissions are calculated as 2772 CO_2 tons / 0.98 = 2829 CO_2 tons / year. Thus, considering life cycle of

the GSHP, the BHEs in the Central Line will reduce CO_2 emissions by 869 CO_2 tons annually which is equivalent to 31% decrease.

The Domestic Renewable Heat Incentive (RHI) is a Government financial incentive to encourage homeowners and landlords to switch from conventional fossil fuel heating to renewable heating (OFGEM, 2018). The Domestic RHI scheme main aim was to support homeowners and landlords who have chosen to invest in renewable heating technologies like biomass boilers and stoves, heat pumps or solar thermal panels (OFGEM, 2018). Currently GSHP system owners are paid as of April 2018 20.46 p GBP / kWh for 7 years. Thus, based on the annual heat provided by the proposed BHE system in the Central Line, the London Underground can potentially receive 14.3x10^6 kWh x 20.46 p GBP / kWh = 2.93 Million GBP per year for 7 years, which is a total of 20.51 Million GBP.

A limited amount of data is available for the implementation of borehole thermal energy storage (Sibbitt and McClenahan, 2015). For instance, the cost of the BTES system at Drake Landing is $2.6/kWh thermal energy stored (Sibbet, 2012). Lanahan and Tabares-Velasco (2017) has shown some of the more prominent examples across the world that utilize BTES combined with solar energy storage in communities as seen in Table 5.6. Sibbitt and McClenahan (2015) has shown the specific cost for installed BTES that have been implemented as well as some that are only conceptual as seen in Figure 5.6. According to (Sibbitt and McClenahan, 2015), the cost of the BTES system drops significantly as the size increases (Figure 5.6). Table 5.4 and Figure 5.6 are used to estimate the cost of each of the systems per kWh. For example, the University of Ontario has a storage volume of 1400 x 10^3 m^3 which based on Figure 5.6 has an approximate cost of $\$5/m^3$ storage volume, which is 7 Million USD in total, and is divided by the total thermal storage capacity of 9700 MWh to get $0.72/kWh. Since, the total annual amount of heat the boreholes, which have an averaged length of 43.6 m, can provide between the 6 stations in the Central line is 14.3 x 10^6 kWh, we multiply this number by $0.72/kWh to get 10.5 Million USD. We do this for each of the projects listed in Table 5.4 to get a rough costing range for the proposed GSHP system in the Central Line. This will give a cost range between 10.5 - 37.2 Million USD if we include the Drake Landing system cost of $2.6/kWh (Sibbet, 2012), which is the highest among the cases examined. This range is a rough cost approximation of the GSHP system proposed for the 6 Central Line stations. This range varies significantly because of the different nature of the land, the building type, the particular specifications of the system, and the system size

for the projects listed in Table 5.4. For the Central Line case, several additional factors has to be taken into consideration such as, the dense urban area of London and the disruption to the roads above the tunnels which should also be factored into the cost. Thus, the range of cost stated above is only a rough estimate and precisely estimating the cost of the system will need further work.

Location	Building	Year Built	Energy Source	Number of Boreholes	Storage Volume [1000 m^3]	Estimated Thermal Storage Capacity [MWh]	Cost per m^3	$/kWh	Central Line Model Cost [Million USD]
DLSC in Olbotoks, Canada	52 Residential Homes	2007	Solar - GSHP	144	34	780	27.5	1.20	17.5
Neckarsulm, Germany	300 Homes & Shopping Center	1997	Solar - GSHP	528	63	1000	22.5	1.42	20.7
Brdstrup District Heating, Denmark	1500 households	2013	Solar - GHSP	48	19	616	33	1.02	14.9
Crailshem, Germany	School & Gymnasium	2007	Solar - GSHP	80	39	1135	25	0.86	12.5
Anneberg, Stockholm	50 homes	2001	Solar - GSHP	99	60	1467	22	0.90	13.1
University of Ontario, Canada	Four University Buildings	2004	Heating and Cooling GSHP	370	1400	9700	5	0.72	10.5

Table 5.4: Community sized BTES constructions, with their system size and cost approximation based on (Sibbitt and McClenahan, 2015; Lanahan and Tabares-Velasco, 2017)

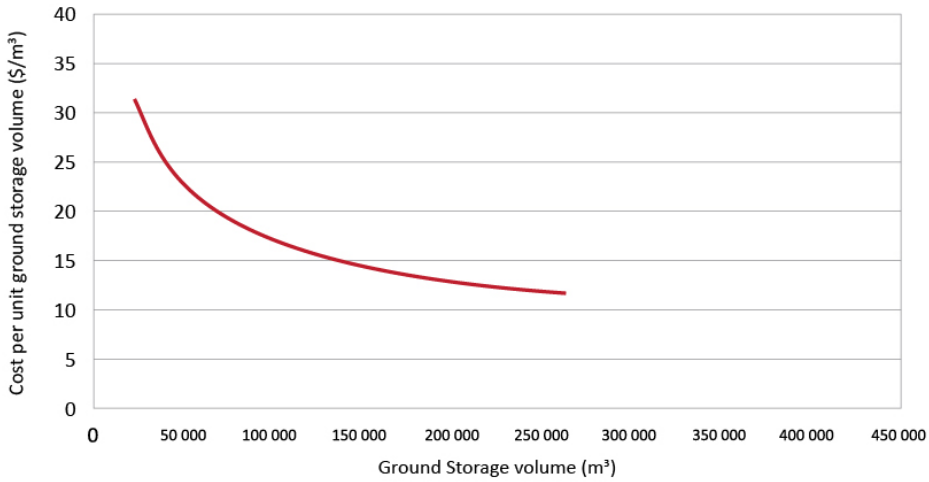

Figure 5.6: Specific installation cost for several borehole thermal energy storage. (based on (Sibbitt and McClenahan, 2015)).

Month	Jan	Feb	Mar	Apr	May	Jun	Jul	Aug	Sep	Oct	Nov	Dec
Head Demand (%)	4.5	4.1	6	9	20	33.4	74	49.2	24.5	10.3	6.1	4.4

Table 5.5: Building clusters total monthly heat demand compared to the heat extracted from the vertical boreholes in the Central Line in percentage.

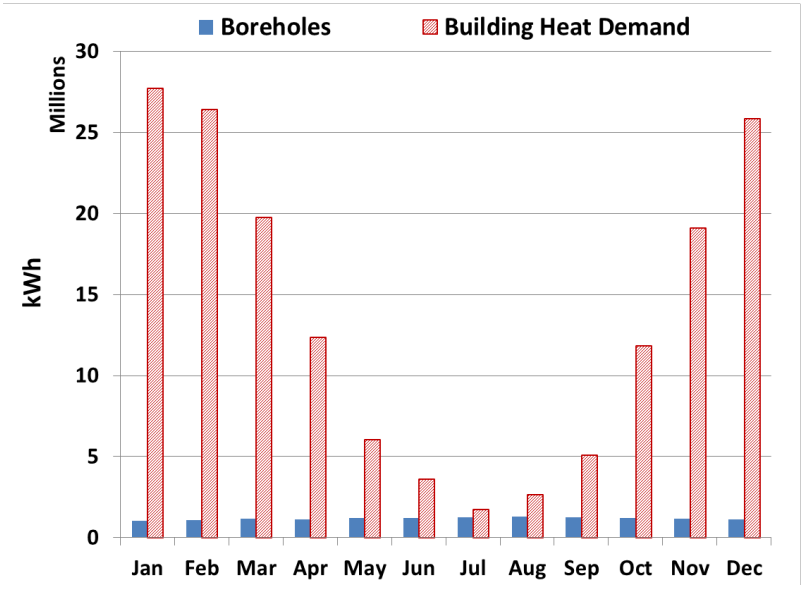

Figure 5.7: Building clusters total monthly heat demand (kWh) in millions compared to the heat extracted from the vertical boreholes in the Central Line.

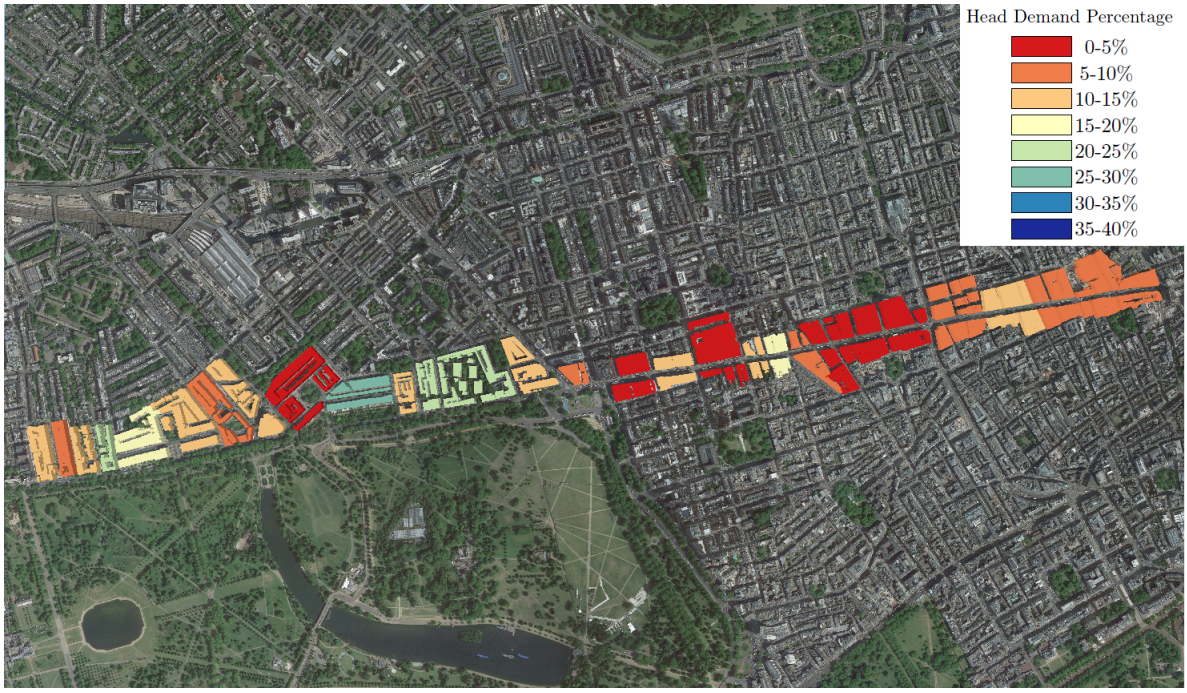

Figure 5.9: Map of the building cluster's annual heat demand compared to the heat extracted from the vertical boreholes in the Central Line in percentage.

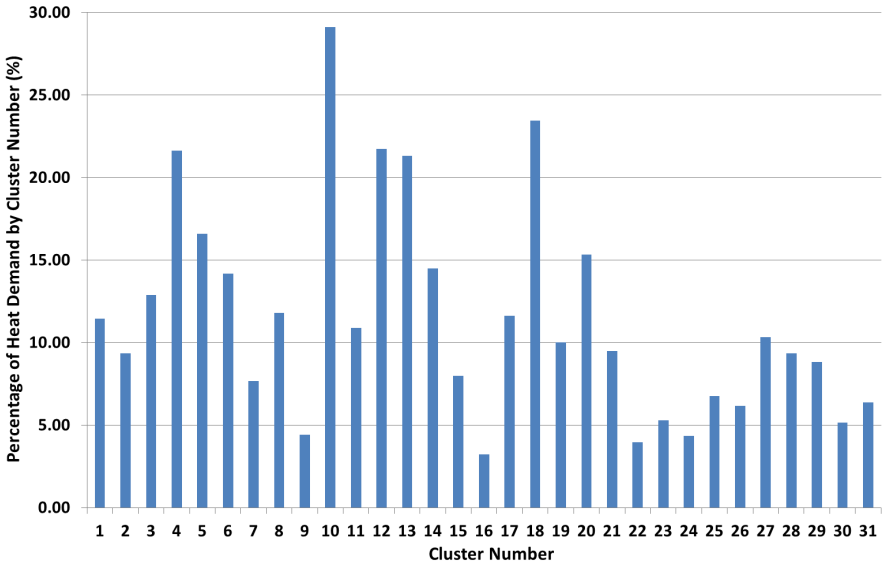

Figure 5.8: Building clusters annual heat demand compared to the heat extracted from the vertical boreholes in the Central Line in percentage.

The hourly heat demand for the clusters varies depending on the month, where it is lowest during the month of July and highest during the month of January, since it is dependent on the climate conditions. The minimum and maximum hourly heat demand for a typical day in July is compared to the amount of heat the boreholes can provide in Figure 5.10. The amount of heat provided by the boreholes is less or equivalent to the minimum hourly heat demand for the month of July for each of the 31 building clusters. Thus, the boreholes can be run all days annually at full capacity, since the amount of heat extracted remains under the hourly heat demand all around the year, which would not lead to over supply from the vertical boreholes GSHPs.

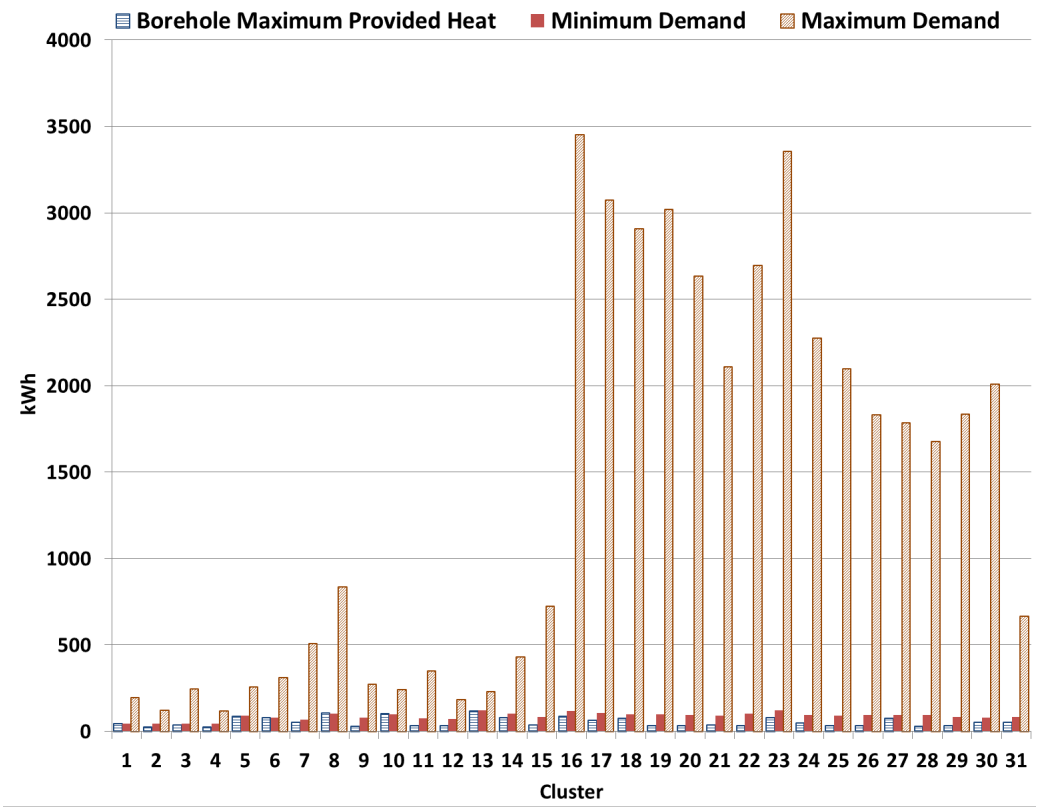

Figure 5.10: Minimum and Maximum hourly heat demand for the 31 building clusters in the month of July compared to the hourly heat extracted from the vertical geothermal boreholes.

Similarly annual amount of heating and cooling provided by the partially insulated boreholes is calculated for the entire boreholes spanning 6 Central Line stations. The total monthly heating from the partially insulated boreholes is compared to the total monthly annual heat demand of the 31 building clusters combined on the sides of the Central Line in Figure 5.11 & Table 5.6. The percentage of building heat demand provided by the boreholes is close to the values of the heat only extracting boreholes described in the paragraph before. This is because the dimension of the boreholes section operating in heating only mode in the partially insulated boreholes is slightly smaller than the total length of the boreholes. Thus, the analysis of the heat provided by the partially simulated boreholes is similar to the analysis for the boreholes that operate in heat extraction in terms of building clusters hourly demand.

As for the cooling building cluster demand the partially insulated boreholes are able to cover part of the total building monthly demand, where the percentage varies from 21.3% to 6.2%

depending on the month as seen in Figure 5.12 & Table 5.7. The partially insulated boreholes provide cooling only between the months of May and September. During July, the building cooling demand is maximum, where the boreholes provide 6.2 % of the building cooling demand, compared to 21.3 % in May. The boreholes are able to provide the largest amount of cooling during May, because at this month a section of the boreholes switches from heating to cooling mode. The ground at this time is cool due to heat extraction, so this will produce a high value of heat injected compared to the other month, as has been shown in section 4.4.2. The partially insulated vertical boreholes manage to cover a portion of the 31 clusters heat demand annually, where it covers the least for cluster 10 (2.7%) and most for cluster 2 (26.3%) as seen in Figure 5.13 and Figure 5.14 .

The hourly cooling demand for the clusters varies depending on the month, where it is highest during the month of July, since it is dependent on the climate conditions. The section of the partially insulated boreholes that alternates between cooling and heating modes can be switched on and off depending on cooling building demand. This is done without affecting the heat extraction in the tunnel since the section extracting heat next to the tunnels operates independently, using a second U pipe as explained in section 4.4.2. The number of hours per day, where the cooling demand of the clusters exceeds the amount supplied by the boreholes during the month of July varies between 9 hours and 23 hours depending on the cluster number (Figure 5.15), where at these hours the borehole section injecting heat and providing cooling can be operated at full capacity.

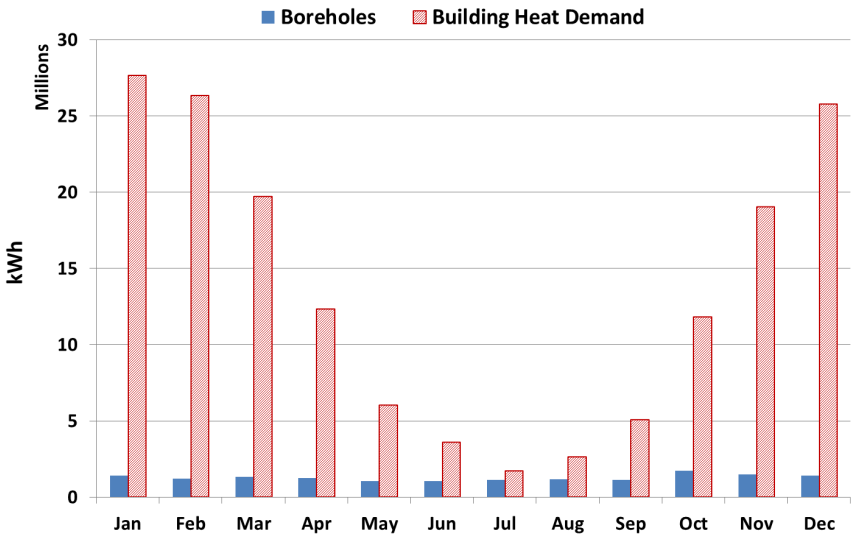

Figure 5.11: Building clusters total monthly heat demand (kWh) in millions compared to the heat extracted from the partially insulated vertical boreholes in the Central Line.

Month	Jan	Feb	Mar	Apr	May	Jun	Jul	Aug	Sep	Oct	Nov	Dec
Head Demand (%)	5.1	4.7	6.7	10.1	17.2	29.4	65.8	43.9	22	14.7	7.8	5.5

Table 5.6: Building clusters total monthly heat demand compared to the heat extracted from the partially insulated vertical boreholes in the Central Line in percentage.

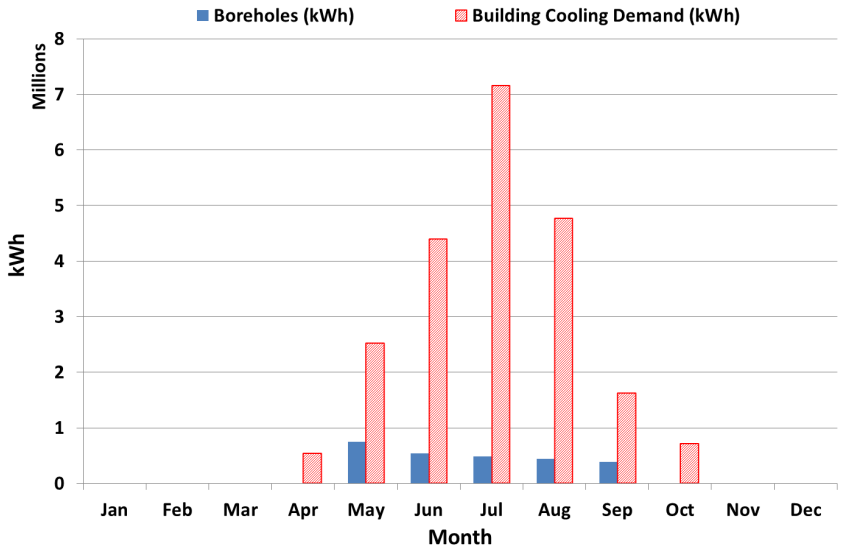

Figure 5.12: Building clusters total monthly cooling demand (kWh) in millions compared to the cooling provided by the partially insulated vertical boreholes in the Central Line.

Month	Jan	Feb	Mar	Apr	May	Jun	Jul	Aug	Sep	Oct	Nov	Dec
Head Demand (%)	0	0	0	0	21.3	11.2	6.2	8.2	0	0	0	0

Table 5.7: Building clusters total monthly cooling demand compared to the cooling provided from the vertical boreholes in the Central Line in percentage.

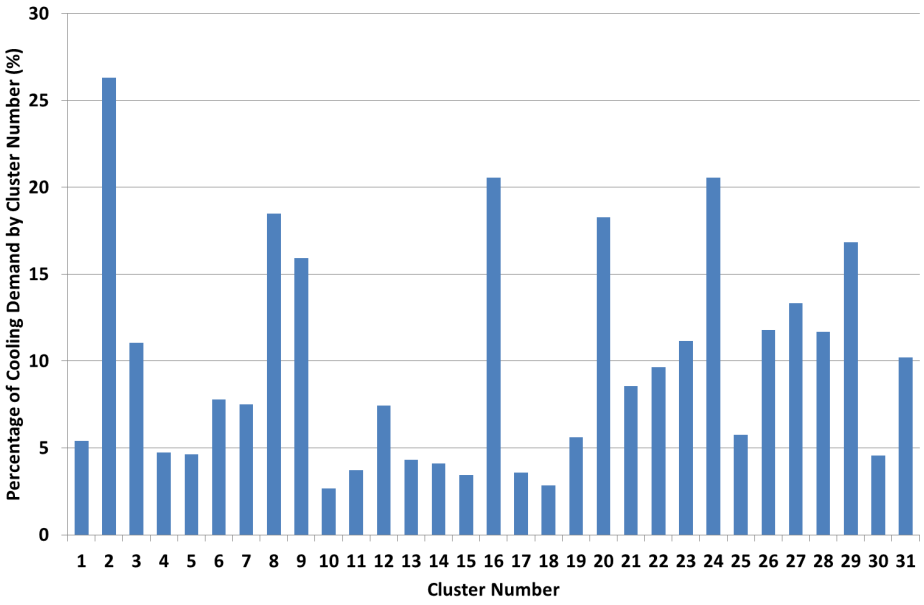

Figure 5.13: Building clusters annual cooling demand (kWh) compared to the cooling provided by the vertical boreholes in the Central Line in percentage.

Figure 5.14: Map of the building cluster's annual cooling demand compared to the heat extracted from the vertical boreholes in the Central Line in percentage.

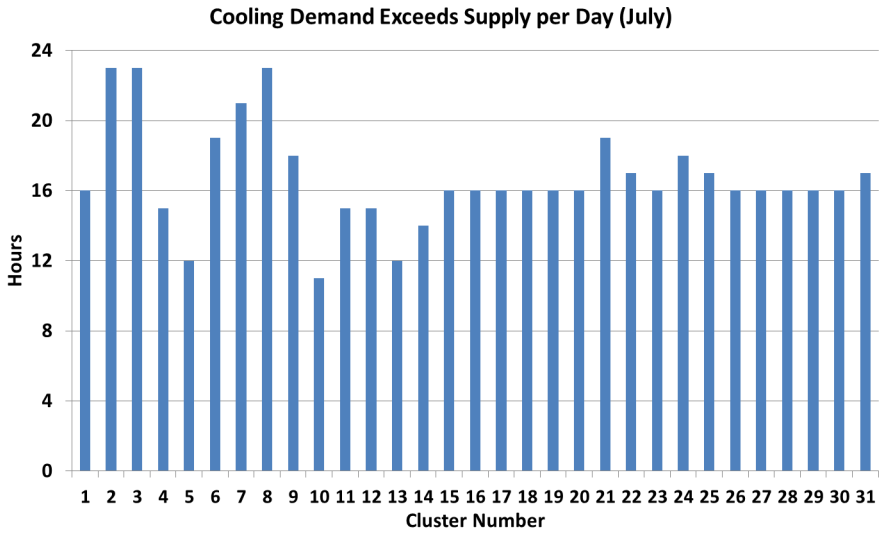

Figure 5.15: The number of hours per day, where the cooling demand of the clusters exceeds the amount supplied by the boreholes during the month of July.

5.3 1D Train Compartment Model

5.3.1 Train Materials and Properties

Train materials and properties are previously discussed in detail in Chapter 3 section 3.2.1.4.

5.3.2 Heat Sources

Heat is released primarily from the passengers and lights within the train. The fluorescent lights cover the roofs of the train carriage with a power rating of 11 W/m^2 (Tfl, 2007). The passengers metabolic rate varies depending on if they are seated 105 W or standing 126 W (ASHRAE, 2010), where the model assumes that the passengers must first occupy all the seats in the carriage and any additional passengers will be standing. The occupancy numbers of the trains is modelled based on the number of passengers entering the Tottenham Court Road station, where at peak times the trains are assumed to be at full capacity (8-9 am & 5-6 pm).

5.3.3 Ventilation

The main ventilation in the train carriage is provided by ceiling extractor fans. Based on rolling stock specifications provided in (Tfl, 2007). According to ANSI/ASHRAE Standard 62-2001 the average value to maintain an acceptable level of air quality in a train carriage is 8 liter/passenger/second. The designers of the 1992 trains adhered to that standard. The train carriages is separated environmentally from one another.

5.4 Vertical Boreholes Effect on Passenger Thermal Comfort and Air Conditioning Electrical Consumption

5.4.1 Train Compartment Temperature and Passenger Thermal Comfort

The benefits the boreholes will have on the passengers comfort are assessed, in which their cooling effect on the train carriages are examined. Survey work in summer 2003 commissioned by London Underground identified the average temperature range for passenger thermal comfort between 21 °C and 26 °C in trains and between 17 °C and 25 °C in platforms (BRE, 2004a). These temperature ranges are used to asses the thermal comfort of passengers on board the train compartments & platforms, and examine the potential of the vertical boreholes to enhance the passenger thermal comfort.

The 1D Central Line tunnel model is co-simulated with the 3D borehole model for the year of 2013, using a similar methodology to the one described previously in chapter 4, section 4.2.2. Two scenarios are taken: The current tunnels, and tunnels equipped with vertical boreholes. A sample of the results is plotted in Figure 5.16 and 5.17 for 5 warm summer days during August. In Figure 5.16 the train compartment temperatures T_{comp} is plotted for the duration the train is operating. The tunnel air temperatures experience two sharp rises, the minor one for the morning peak, and the major one for the afternoon peak, where the underground experiences both high train and passenger traffic, but during the afternoon the ambient outer air temperatures are much higher than the morning. The compartment temperatures are typically higher than the tunnel temperatures by 0.5 - 2 °C, where this difference depends on the passenger traffic inside the train. During peak times in the morning and afternoon, this temperature difference is maximum, because there are more passengers inside the train generating more heat within the compartment.

The boreholes manage to cool the tunnel by around 4 °C during the Central Line's opening times (6 am till 12 pm). The borehole cooling effect inside the tunnel also cools the compartments by 3-4 °C (Figure 5.16), since the train compartment temperatures are influenced by their surrounding tunnel temperature through direct air exchange. It is important to point

that the train compartments interact with the platforms when the trains stop and their doors open, but most of the train time is spent travelling in the tunnels.

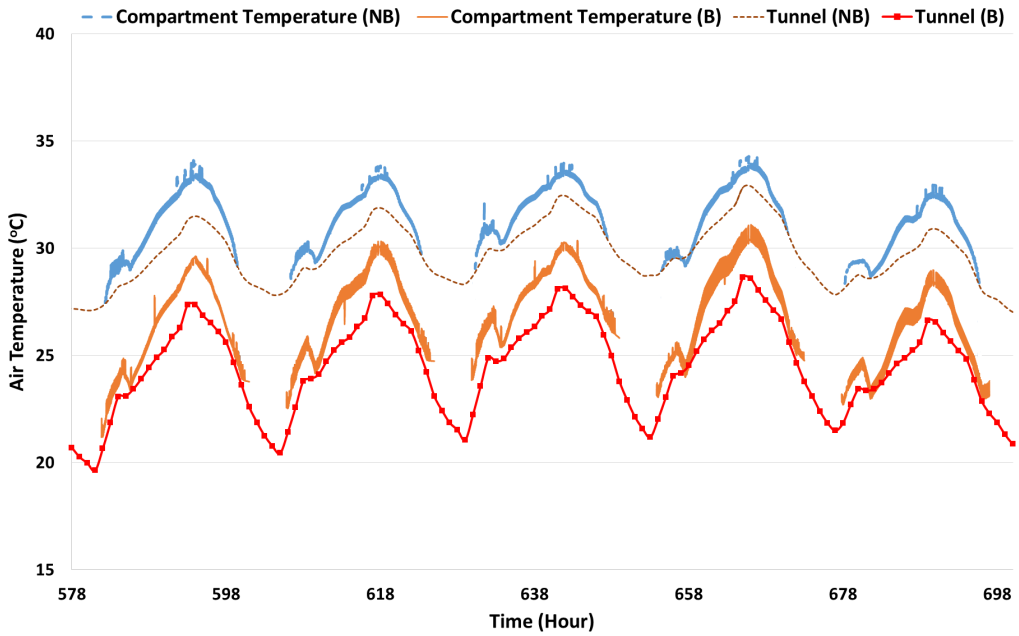

Figure 5.16: Central Line model simulated train compartment and tunnel air temperatures (°C) for the year of 2013 for two scenarios: The current tunnels (NB), and tunnels equipped with vertical boreholes (B).

The hourly frequency for the year of 2013, in which the temperature of T_{comp} and platform temperature T_{plat} exceeds 26 °C & 30 °C and 25 °C & 30 °C respectively is plotted in Figure 5.18 & Figure 5.19 & Table 5.8. The platform air temperatures are taken from simulation results in chapter 3 and 4. The passengers will experience discomfort in the train compartments and platforms between the months of April and November, where the warmest temperatures are recorded in August. T_{comp} & T_{plat} above 30 °C occur between June and September. The vertical boreholes significantly reduces the hours T_{comp} and T_{plat} exceed the recommended temperatures for passenger comfort. The number of hours T_{comp} exceeds 26 °C decreases by 4.5 times from 1553 hours to 341 hours annually when the tunnels are equipped with boreholes. The number of hours T_{comp} exceeds 30 °C is reduced from 158 to 31, and the months annually where passengers experience discomfort between the months June to August. Also, the number of hours T_{plat} exceeds 30 °C is reduced from 280 to 0 annually.

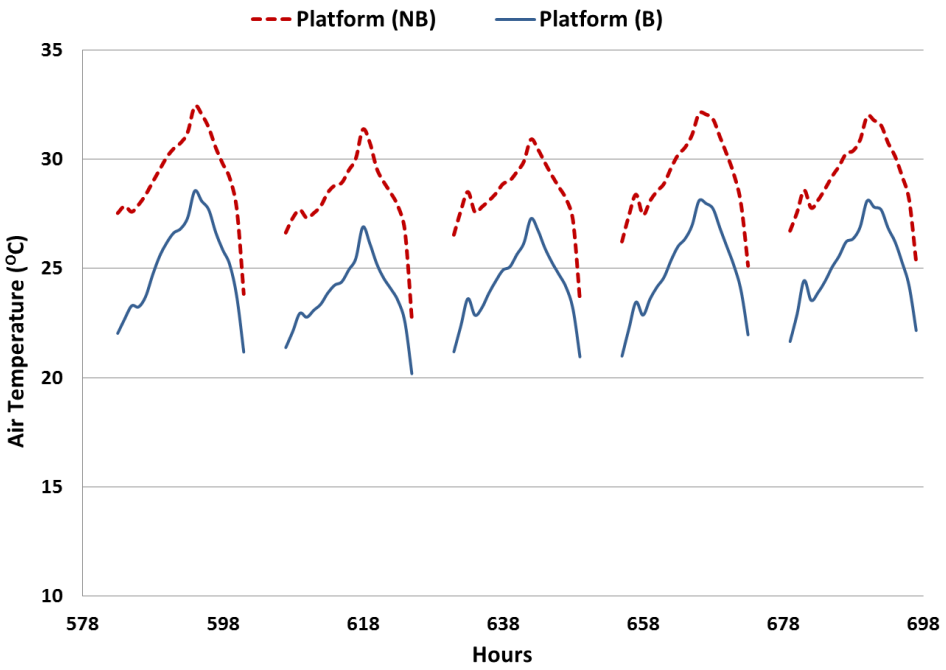

Figure 5.17: Central Line model simulated platform air temperatures (°C) for the year of 2013 for two scenarios: The current tunnels (NB), and tunnels equipped with vertical boreholes (B).

Consequently, the vertical boreholes manage to significantly mitigate over heating in the platforms and train compartments, by maintaining the platform temperatures below 30 °C, and reducing the annual hours T_{comp} & T_{plat} exceeds 26 °C and 25 °C respectively. This would enhance passenger comfort across their journey in the Central Line, where most of the time is spent in the platforms and train carriages.

Case	Jan	Feb	Mar	Apr	May	Jun	Jul	Aug	Sep	Oct	Nov	Dec	Total
Plat > 25	0	0	0	14	147	336	499	532	454	190	80	0	2252
Plat(B) > 25	0	0	0	9	10	105	203	159	67	14	0	0	567
Plat(A) > 25	0	0	0	16	178	388	515	537	472	221	147	0	2474
Plat > 30	0	0	0	0	0	40	82	144	14	0	0	0	280
Plat(B) > 30	0	0	0	0	0	0	0	0	0	0	0	0	0
Plat(A) > 30	0	0	0	0	0	45	123	188	23	0	0	0	379
Comp > 26	0	0	0	1	41	249	375	398	350	94	45	0	1553
Comp(B) > 26	0	0	0	0	7	86	120	96	26	6	0	0	341
Comp > 30	0	0	0	0	0	36	52	63	7	0	0	0	158
Comp(B) > 30	0	0	0	0	0	8	16	7	0	0	0	0	31

Table 5.8: Hourly frequency where the platform temperature Tplat (°C) exceeds 25 °C and 30 °C, and train compartment temperature Tcomp (°C) exceeds 26 °C and 30 °C, for the year of 2013 for three scenarios: The current tunnels, and tunnels equipped with vertical boreholes (B), and trains equipped with air conditioning (A).

5.4.2 Train Compartment Air Conditioning Electrical Consumption

The air conditioning systems are assumed to be conventional split unit systems that are compressed to fit in the already compact Central Line 1992 rolling stock. The cooling set point temperature is set at 24 °C, which is recommended by the ASHREA standard and adopted by the London Underground in its existing sub-surface air conditioned trains and National Rail Companies (ATOC, 2014). The COP (Coefficient of Performance) of the air-conditioning is taken to have an average value of 2.5 (Elsayed and Hariri, 2011). IDA tunnel output the train air conditioning electrical consumption (W_{AC}), heat removed from the train compartments through the evaporator (Q_{evap}), and rejected heat to the tunnels through the condenser (Q_{Cond}). Where the following equations relate these outputs:

$$COP = \frac{Q_{Evap}}{W_{AC}} \tag{5.1}$$

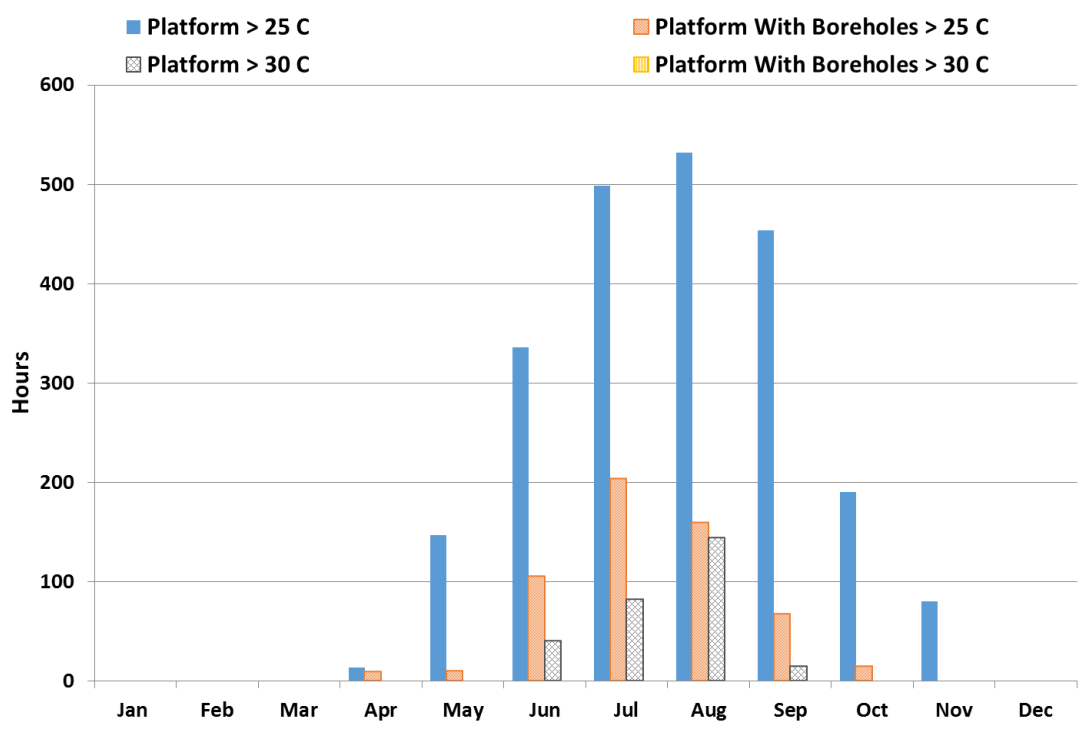

Figure 5.18: Number of hours per month the platform air temperatures (°C) exceeds 25 °C and 30 °C, for the year of 2013 for two scenarios: The current tunnels, and tunnels equipped with vertical boreholes.

$$Q_{Cond} = Q_{Evap} + W_{AC} \tag{5.2}$$

The Central Line section spanning between Queensway Station and Tottenham Court Road is taken for this study, which encompasses 6 underground Central Line stations and spans a distance of 4.8 km of tunnels. The 1D Central Line Model is modified and expanded to feature the 6 Central Line stations as seen in Figure 5.20. The stations in the model are identical to the design of the representative Central Line model summarized in chapter 3, section 3.2.1. The Model is simulated for the year of 2013 and the W_{AC}, Q_{evap}, and Q_{Cond} for the trains are calculated. A single train will pass briefly in the 6 stations, and afterwards another train will pass within a time gap of few minutes depending on the train's schedule. Also, in the tunnels and platforms there are several trains traversing these sections simultaneously. Consequently, looking into the air conditioning electrical consumption W_{AC} of one train is limited in terms

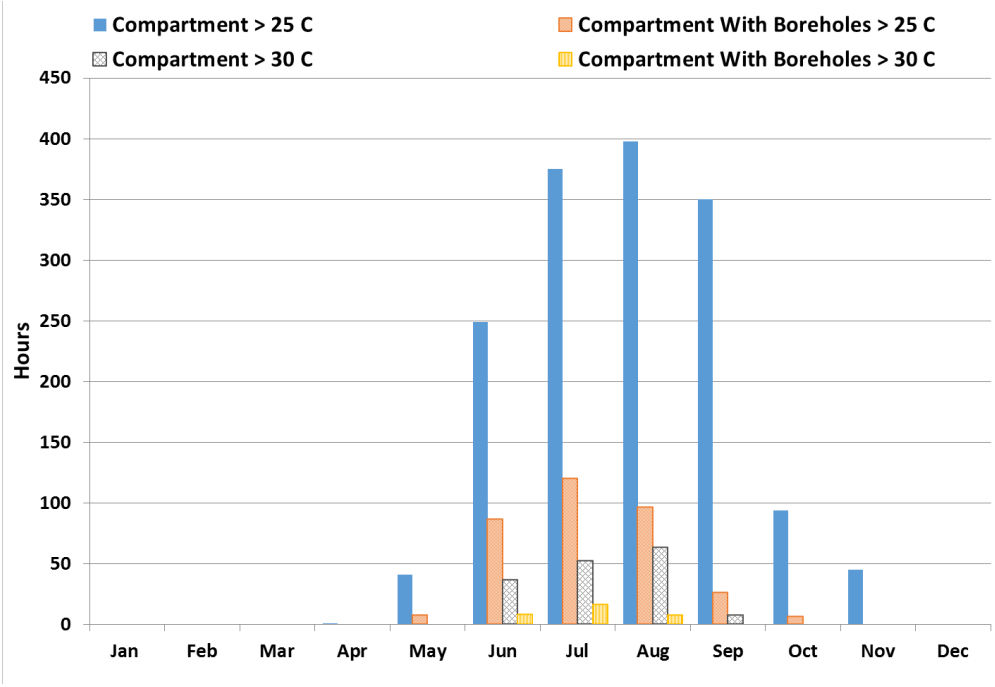

Figure 5.19: Number of hours per month the train compartment air temperatures (°C) exceeds 25 °C and 30 °C, for the year of 2013 for two scenarios: The current tunnels, and tunnels equipped with vertical boreholes.

of time because the train only covers the sections of the Central Line Model in a few minutes. An effective method to track electrical consumption is to examine the train's air conditioning system in the model as a whole through the time that the trains are travelling in the subway system and sum them through out the day to get an aggregated W_{AC} for the trains that have passed. The Central Line train's working schedule was acquired from TfL (LU, 2015), where it displays the number of trains operating between stations at a given interval of time within the day, and also the approximate time intervals between the trains in the tunnels as well. The number of trains operating at a given time between Queensway Station and Tottenham Court Road Station over the day is plotted in Figure 5.21. The W_{AC} for the train air-conditioning at a given time between the 6 stations is obtained as a product between the W_{AC} for a single train passing in the Central Line Model and the number of trains present between the 6 stations at the same given time.

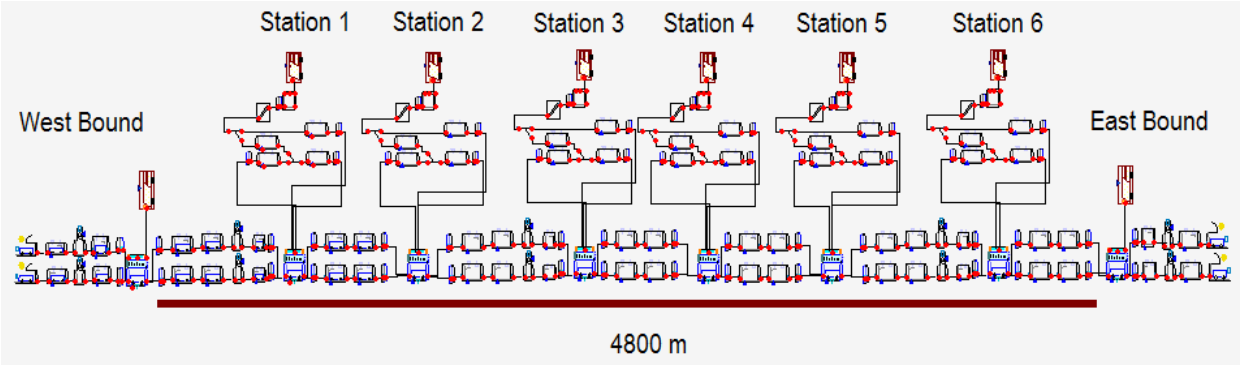

Figure 5.20: Schematic of the 1D Central Line model for 6 stations.

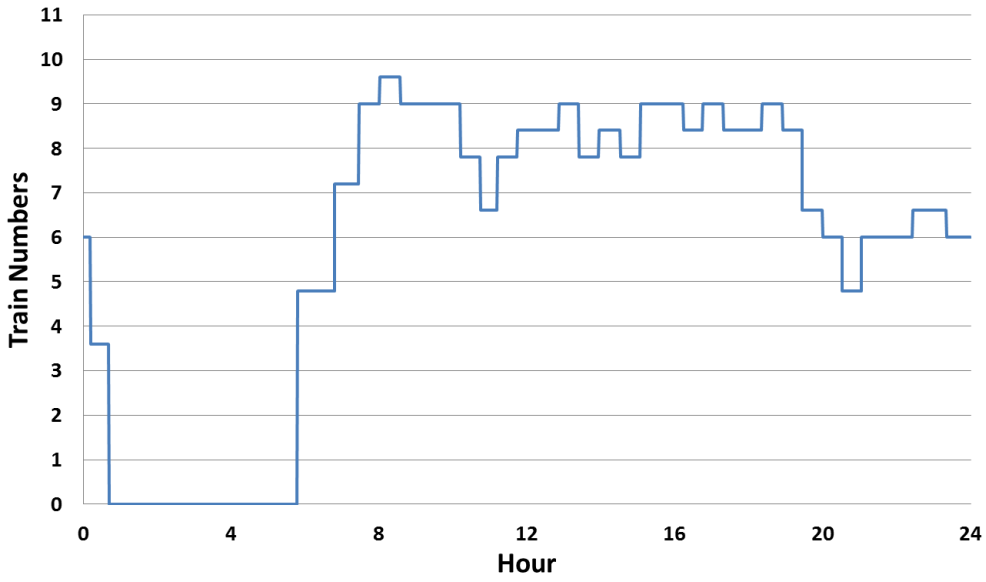

Figure 5.21: The number of trains operating at a given time between Queensway Station and Tottenham Court Road Station throughout the day.

The model is simulated for the year of 2013 for two scenarios: The current tunnels, and tunnels equipped with vertical boreholes. In order to simulate the vertical boreholes in the 6 stations Central Line Model, the outer tunnel wall temperatures obtained from the 1D - 3D co-simulations summarized in section in chapter 4, section 4.2.2 are used Figure 3.9. The simulations for a period of one year took 42 days for each of the cases, because as the Central Line Model is expanded the simulation time increases. A sample of one train on-board air-conditioning W_{AC}, Q_{evap}, and Q_{Cond}, along with the temperature variation is plotted in (Figure 5.22) for the 5 days in the month of August. The air-conditioning turns on when

T_{comp} exceeds 24 °C, and as seen before when examining compartment temperatures in the previous section 5.4.1, there are two consumption peaks, a minor one during the morning peak and a major one during the afternoon peak passenger time.

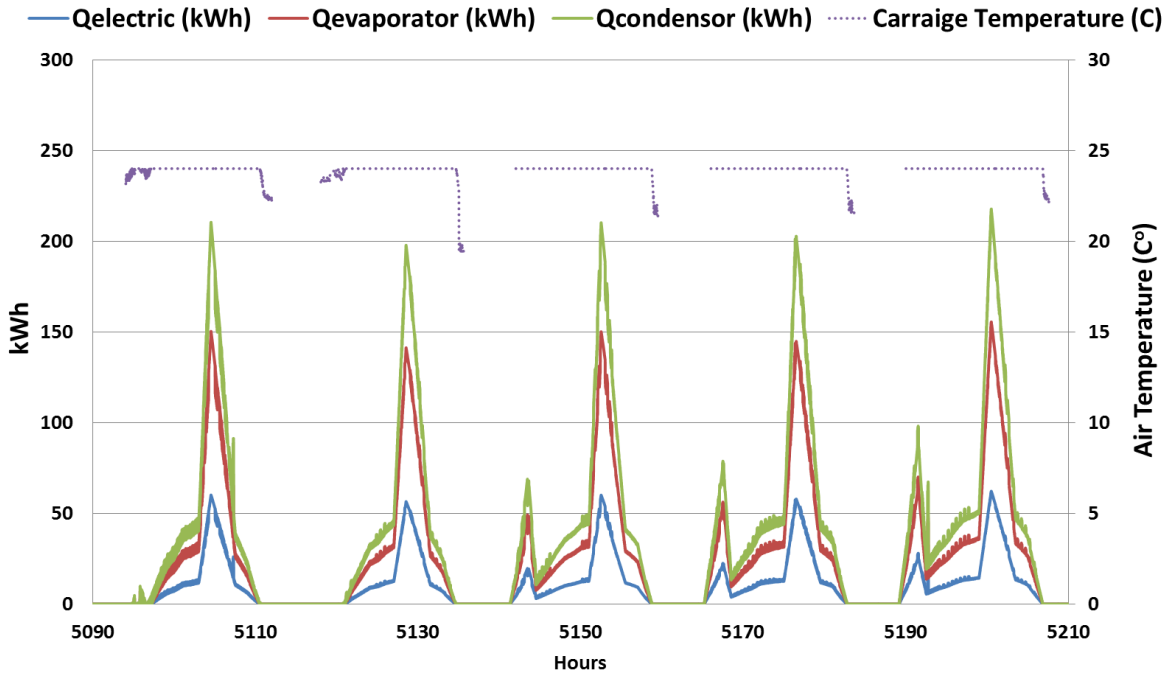

Figure 5.22: Electrical consumption (W_{AC}), Evaporator Heat Removed (Qevap), Condenser Rejected Heat (Q_{Cond}), and Train Carriage Temperature for 5 days in the month of August and year of 2013.

The same interval is plotted in Figure 5.23, where W_{AC} and T_{comp} for the two scenarios are compared. The borehole cooling effect in the tunnels, will result in the cooling of the train compartment temperatures as has been shown in the previous section 5.4.1. When boreholes are applied T_{comp} decreases, and the temperature will less often exceed 24 °C compared to the current situation by 72 % from 1553 hours to 435 hours around the year. Thus, the train air-conditioning operating time is reduced and also the cooling load inside the carriage when the air-conditioning is operating which leads to reductions in W_{AC}. This is shown in Figure 5.23, where W_{AC} is reduced when the tunnels are equipped with boreholes, particularly during the morning peak, where the air-conditioning isn't required due to indirect borehole compartment cooling.

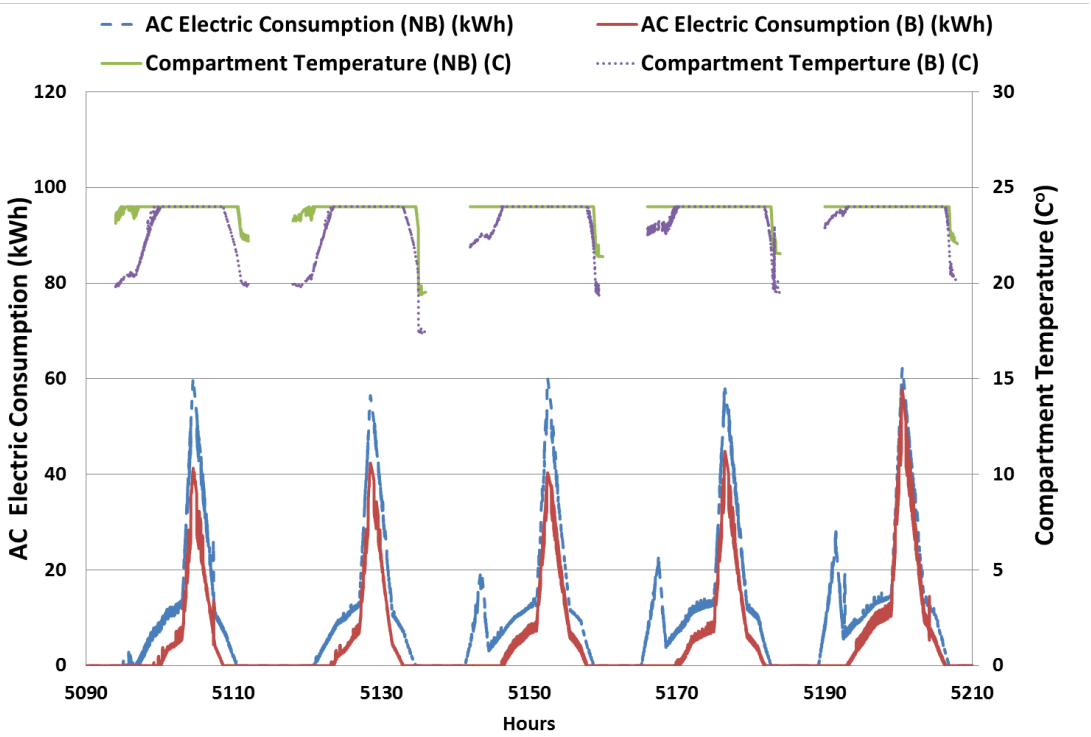

Figure 5.23: Air Conditioning (AC) Electrical consumption (W_{AC}) and Train Compartment Temperature for 5 days in August, for the year of 2013 for two scenarios: The current tunnels (NB), and tunnels equipped with vertical boreholes (B).

The air-conditioning consumption W_{AC} for the two scenarios is multiplied by the train traffic throughout the day between Queensway Station and Tottenham Court Road, then the results are multiplied by 2 to take into consideration the two tunnels that actually pass in the platforms in both directions. The total monthly air-conditioning electrical consumption for the trains in the Central Line between the 6 stations for the two scenarios is displayed in Figure 5.24. Air-conditioning is needed between April to November, where it is mostly used in the months of July and August, since they are the warmest month in the year. The boreholes manage to reduce W_{AC} by 60 % in both July & August, and eliminates the need for air-conditioning in April and November. The boreholes also reduce the annual electrical consumption for train air-conditioning by 60 % from 536160 kWh to 220,260 kWh. This saves 315,900 kWh of electricity annually which is equal to the annual electrical consumption of 77 houses, given that the average annual electricity domestic use is 4115 kWh per customer according to (DECC, 2015). This reduces carbon emissions by 125 tons of CO_2, since the carbon emission foot print of UK electricity production is 0.394 Kg CO_2/kWh (DECC, 2015).

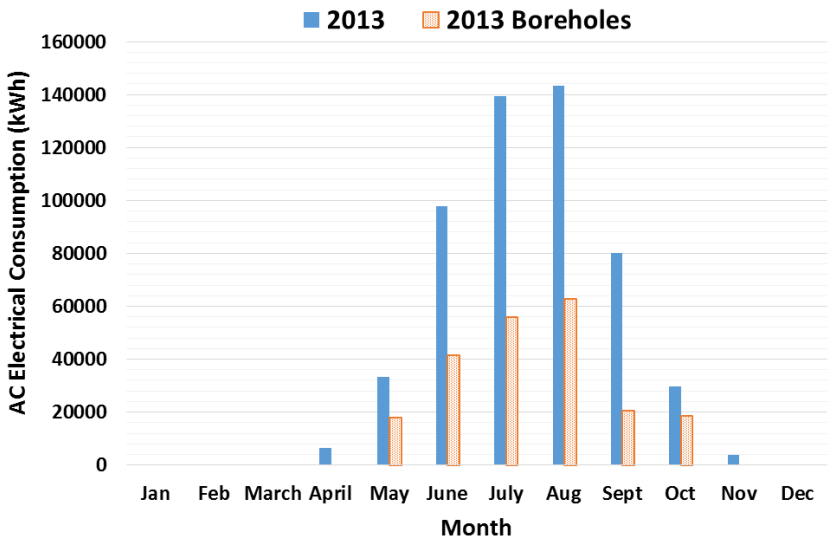

Figure 5.24: Monthly total air conditioning (AC) electrical consumption (WAC) for the trains between the 6 Central Line stations, for the year of 2013 for two scenarios: The current tunnels, and tunnels equipped with vertical boreholes.

The effect of the use of air-conditioning on the Central Line's environment is examined by comparing the resulting platform and tunnel temperatures for the two cases. The air temperature results of a single platform and tunnel section is used because they are equivalent to the other 6 platforms and tunnel sections in the model. The annual hourly frequency which T_{plat} would exceed 25 °C & 30 °C in the case train air-conditioning is used would increase by 222 hours (10 %) and 100 hours (35 %) respectively compared to not having on board train air-conditioning as seen in Table 5.8. This would further exacerbate the overheating problems in the platforms, where the gains in passenger comfort in the train compartment would come at an expense of passenger comfort in the platforms, because of the rejected heat from the train air-conditioning. The resulting simulated tunnel and platform temperatures are linearised and plotted versus the ambient outside air temperatures as seen in Figure 5.25. Train air-conditioning would lead to raising the Central Line's Tunnel and Platform temperatures by around 1 °C during summer where air-conditioning is mostly used (Figure 5.25).

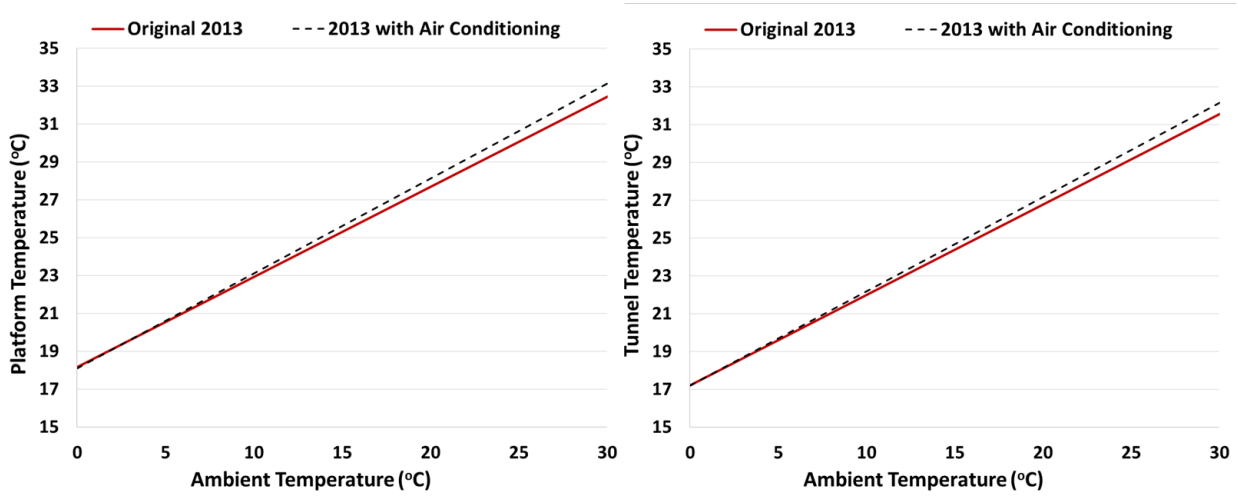

Figure 5.25: Central Line model simulated platform and tunnel air temperatures for the year of 2013 for two scenarios: The current trains, and trains equipped with air-conditioning.

5.5 Conclusion

Vertical closed loop ground boreholes were used to extract heat from the Central Line in the London Underground in order to provide cooling to the line's Tunnels & Platforms and district heating and cooling to the buildings above simultaneously. To determine the amount of heat extracted by the boreholes a 3D FEM (Finite Element Model) model of vertical ground boreholes was coupled with the 1D Central Line model. Retrofitting the Central Line with vertical geothermal closed loop boreholes on the scale of the City of London is investigated, where 6 stations in the Central Line are located and the tunnels pass under the roads. The buildings in the proximity of the tunnels were divided into 31 clusters, where the heating and cooling demand of the buildings was based on (Zhang et al., 2015b). The amount of heat extracted by the vertical boreholes next to the tunnels was compared with heat demand of the 31 clusters.

The vertical boreholes manage to cover a portion of the 31 clusters heat demand annually, where it covers the most for cluster 10 (29%) and least for cluster 16 (3.2%). The boreholes were also able to cover part of the total building monthly demand, where the percentage varies from 4.1% (January) to 74% (July) depending on the month, since the clusters heat demand is maximum during January and minimum during July. The amount of heat extracted by the boreholes, increases slightly during summer and decreases slightly during winter as a

result of variations in the Central Line tunnel temperatures, which provides a consistent and reliable amount of heat to the building clusters throughout the year. It was found that the boreholes can be run all days annually at full capacity, since the amount of heat extracted remains under the hourly heat demand all around the year, which would not lead to over supply from the vertical boreholes GSHPs. The amount of heat provided by the boreholes is less or equivalent to the minimum hourly heat demand for the month of July, which has the minimum hourly heat demand, for each of the 31 building clusters. Retrofitting the tunnels with verticals boreholes was found to reduce building heating carbon emissions by 1067 tons of CO_2 annually, when compared to gas boiler heating. This was found to be close to currently operating GSHP systems in (Blum et al., 2010). A life cycle analysis was performed on the Central Line BHE system which shown that it can reduce carbon emissions by o 31% annually, when compared to gas boiler heating. The Central Line GSHP system can benefit from the the Renewable Heat Incentive (the RHI) is a payment system in the UK for the generation of heat from renewable energy sources. The Central Line GSHP system can potentially benefit of 2.93 Million GBP per year for 7 years, which is a total of 20.51 Million GBP, as the UK government is paying 20.46 p GBP / kWh rate for GSHP systems as of April 1, 2018 (OFGEM, 2018). By examining the costs of existing GSHP system, the cost of implementing the BHE system for the 6 stations in the Central Line was shown to range between between 10.5 - 37.2 Million USD. Inorder to determine the accurate price several factors have to taken into consideration in future work: such as GSHP costs in the UK, GSHP contruction costs in heavily urbanized spaces, and the effect of the size of the GSHP system on the reduction of the costs.

The percentage of building heat demand provided by the partially insulated boreholes is close to the values of the heat only extracting boreholes described in the paragraph before. This is because the dimension of the borehole's section operating in heating only mode in the partially insulated boreholes is slightly smaller than the total length of the boreholes. As for the building clusters cooling demand, the partially insulated boreholes are able to cover part of the total building monthly demand, where the percentage varies from 21.3% to 6.3% depending on the month. During July, the building cooling demand is maximum, where the boreholes provide 21.3 % of the building cooling demand, compared to 6.3 % in May. The partially insulated vertical boreholes were found to provide a portion of the 31 clusters cooling demand annually, where they cover the least for cluster 10 (2.7%) and most for cluster 2 (26.3%). The hourly cooling demand for the clusters varies depending on the month, where

it is highest during the month of July, since it is dependent on the climate conditions. The section of the partially insulated boreholes that alternates between cooling and heating modes can be switched on and off depending on building cooling demand. During the hours where the cooling demand of the clusters exceeds the amount supplied by the boreholes, the borehole section injecting heat and providing cooling can be operated at full capacity.

The thermal comfort of passengers on board the train compartments & platforms was assessed for two scenarios: The current tunnels, and tunnels equipped with vertical boreholes. The boreholes manage to cool the tunnel by around 4 °C during the Central Line's opening times (6 am till 12 pm). The borehole cooling effect inside the tunnel also cools the compartments by 3-4 °C, since the train compartment temperatures are influenced by their surrounding tunnel temperature through direct air exchange. The tunnel air temperatures experience two sharp rises, the minor one for the morning peak, and the major one for the afternoon peak, where the underground experiences both high train and passenger traffic, but during the afternoon the ambient outer air temperatures are much higher than the morning. The vertical boreholes significantly reduces the hours T_{comp} and T_{plat} exceed the recommended temperatures for passenger comfort. The number of hours T_{comp} exceeds 26 °C decreases by 4.5 times from 1553 hours to 341 hours annually when the tunnels are equipped with boreholes. The number of hours T_{comp} exceeds 30 °C is also reduced from 158 to 31. In the platform, the number of hours T_{plat} exceeds 30 °C is reduced from 280 to 0 annually. Hence, the vertical boreholes manage to significantly mitigate over heating in the platforms and train compartments, by maintaining the platform temperatures below 30 °C, and reducing the annual hours T_{comp} & T_{plat} exceeds 26 °C and 25 °C respectively.

The 1D Central Line model was expanded to incorporate the 6 Central Line stations and modified to accommodate on board train carriage air-conditioning. The model is simulated for the year of 2013 for two scenarios: The current tunnels, and tunnels equipped with vertical boreholes. The boreholes reduced W_{AC} by 60 % in both July & August, and eliminated the need for air-conditioning in April and November in the Central Line. The boreholes also reduce the annual electrical consumption for train air-conditioning by 60 % from 536160 kWh to 220260 kWh saving 315900 kWh of electricity annually which is equivalent to the annual electrical consumption of 77 houses and 125 tons of CO_2. Train air-conditioning would raise the Central Line's tunnel and platform temperatures by around 1 °C. Consequently, the rejected heat from the train air-conditioning would further exacerbate the overheating

problems in the platforms, where the gains in passenger comfort in the train compartment would come at the expense of passenger comfort in the platforms.

Retrofitting the Central Line with geothermal vertical boreholes proved beneficial for simultaneously cooling the tunnels and platforms, while providing part of the surrounding building's heating and cooling demand. The boreholes also manage to enhance passenger comfort across their journey in the Central Line, where most of their time is spent in the platforms and train carriages. This solution can be applied to other deep and old lines in the London Underground, which were partly build under roads, particularly the Piccadilly, Bakerloo, and Northern Lines. GSHP combined with borehole thermal energy storage (BTES), can further enhance the storage capacity of the system and enable the system to provide cooling and heating to the buildings, where these system have been demonstrated across the world (Lanahan and Tabares-Velasco, 2017). This method can also be investigated in other deep and old lines suffering from overheating problems, such as the New York Subway, Saint Peterborough Metro and the Moscow Metro.

Chapter 6

Conclusion and Future Work

6.1 Conclusion

The primary context of this thesis was to address the overheating problems encountered by old and deep subway systems, most notably the London Underground, which causes passenger discomfort, increases the risks of heatstrokes, and disrupts services during summer (Ampofo et al., 2004a). Indeed, the London Underground, particularly the deep sections have become uncomfortable during summer due to its congestion and poorly ventilated tunnels. This thesis described modelling the climate of a representative section of a deep and old section of the London Underground, the Central Line in particular, using a 1D modelica based software called IDA Tunnel. The Central Line model is used to study the parameters that influence the London Underground environment, and understand the factors that characterizes the climate in other London Underground deep and old lines. The effects of projected climate change, passenger & train traffic increase, and modernization of trains on the climate of the Central Line were investigated. This thesis developed a 3D FEM (Finite Element Model) model to simulate the transient thermal interactions between the subway tunnels and the geothermal vertical boreholes using Comsol. A methodology is developed to co-simulate the 3D FEM borehole model transiently with a 1D subway line model, to asses the cooling impact of the boreholes on the climate of the subway's tunnels & platforms, and the passenger's thermal comfort. This thesis also, introduced a new concept of partially insulated borehole heat exchangers to enable the vertical boreholes to deliver heating and cooling to the building above the tunnels. The application of retrofitting a section of the Central Line with vertical geother-

mal closed loop boreholes in London is examined as a case study in this dissertation. The main aim of this thesis was to examine the potential of retrofitting old and deep subway lines with vertical geothermal boreholes in cooling old & deep subway lines to mitigate the subway's overheating problems and enhance passenger thermal comfort. The thesis also examined using the tunnel's wasted heat in the surrounding soil to provide district heating and cooling to the buildings above the tunnels.

6.1.1 1D Central Line model and parametric analysis

A representative section of a deep and old line in the London Underground was modelled using the 1D IDA tunnel software. The London Underground's Central line was selected as a representative case of a deep and old subway system that experiences overheating during London summer. Station building maps, rolling stock schematics, ventilation rates, and passenger traffic information for the Central Line were used to achieve a near realistic model of the London Underground's Central Line and the systems heat sources and sinks were identified and quantified. The Central Line model was simulated for the year of 2013 and verified using measured air temperature data for the tunnels and platforms obtained from Transport for London. The model was based on linearized air temperature data collected via Transport for London sensors in the tunnels and platforms as a form of a linear relationship between outside ambient temperatures and tunnel or platform temperatures. Transport for London only provided air temperature data, where the tunnels and platforms lacked adequate humidity and wind sensors. Thus, this limited our analysis of the Central Line IDA model to air temperature and prevented us from further calibrating our model to factor in humidity and wind speeds in the tunnel, although the Central Line model did output simulated humidity and wind speed in the tunnels and platforms modelled. Also, the Central Line IDA model simulation time step was 1 min to optimize simulation time, which wasn't able to capture the instantaneous second by second changes in temperature and wind speeds in the tunnels and platforms. it was shown that at peak times, braking contributes to approximately 61% of heat dissipation in the Central Line while passenger traffic in the station and trains combined contribute approximately to 34% of the total heat dissipation in the system, which correlated well with the results of (Ampofo et al., 2004a). However, it has to be pointed out that (Ampofo et al., 2004a) model is steady state and only modelled the tunnels and train carriages, while the IDA Central Line model is transient and has modelled the tunnel, train carriages,

platforms and station box. Also, Ampofo et al. (2004a) fixed the ambient outer air temperature to 27 °C, while this thesis simulated the Central Line over the year climate conditions between 0 °C and 30 °C, which gave a more detailed analysis of the thermal interactions in the subway system.

A parametric analysis was conducted on four major heat sources and sinks in the Central Line model to assess their influence on the Central Line climate. The analysis focused on summer conditions, where passengers experience discomfort due to elevated air temperatures. The ventilation rates were varied to asses their impact on the Central Line environment. Increasing the ventilation rates was found to lower the temperatures of the system slightly during summer, however it is constrained by outer ambient conditions, since high outside ambient conditions would result in high air temperatures within the London Underground system. Equipping the trains with regenerative braking of 20% and 40% have a slight effect in lowering the Central Line temperatures by 1 °C and 2 °C respectively during summer. However, it was found that the cooling benefit provided by 40% regenerative is negated by a +50 % increase in train traffic. The most prominent cooling effect in the system was achieved when soil temperatures at a distance of (0.4m) from the tunnel outer tunnel walls was lowered to 8 °C. This managed to cool the air temperatures of the platform and tunnels by 5 °C and 6 °C respectively. These results correlate well with (Ampofo et al., 2004c), which showed that that ground water cooling would result in the most effective cooling in the system, followed by applying regenerative braking, then increasing ventilation rates which had the least effect on cooling the London Underground tunnels among those three. The best option appears to be a combination of the cooling methods investigated in the parametric analysis.

The effects of climate change on the London Underground's environment was assessed to determine whether the upgrades in the London Underground's infrastructure will mitigate the overheating problems or at least preserve the status quo. The Central Line model was simulated between the years of 2013 and 2050, taking into consideration the projected passenger numbers, train traffic, infrastructure upgrades, and climate change. The introduction of new trains with regenerative braking will result in slightly cooling the Central Line by 0.5 °C during summer conditions, which maintains the current situation, since the temperature increase caused by climate change and passenger numbers & train traffic increase neutralizes the cooling benefits of regenerative braking. By 2050 the projected increase in train traffic,

passenger numbers, and outer ambient temperatures associated with climate change will overcome the benefits of the new trains making the Central Line warmer than it originally was in 2013 by 1.5 °C during summer, which will further exasperate the overheating problem. The future simulations of climate change considered two scenarios for the years of 2032 and 2050: Medium Emissions, and High Emissions. The Central Line model simulations showed no noticeable differences within the same year of 2032 and 2050 between the medium emission and high emission scenarios, because their climate profiles and annual median SAT temperatures differed slightly. These results agree with (BRE, 2004b), which concluded that passenger dissatisfaction is likely to increase due to climate change in the future unless adaptation measures are implemented.

The Central Line model was modified to study the parameters that influence the London Underground environment, and understand the factors that characterizes the climate in other London Underground deep and old lines. The climate conditions in the following deep lines in the London Underground was simulated: Northern Line, Bakerloo Line, and Jubilee Line. The modification of the Central Line model took into consideration each of the other deep line's distinct characteristics such as train type, train traffic, passenger numbers, tunnel diameters, and surrounding soil temperatures. The subway model simulation results for the Northern Line, Bakerloo Line, and Jubilee Line were compared and verified with measured data for the three deep lines obtained from Transport for London. The simulation results for these three deep lines were close to their corresponding measured data. However, for the 3 lines the model tended to estimate slightly cooler temperatures compared to measured data for winter conditions because train & local station heating was neglected, and slightly higher temperatures for the tunnels because cross tunnels were neglected in the model. Results have shown that high surrounding soil temperatures make the Bakerloo Line slightly warmer than the Central Line. A combination of brake regeneration & less train traffic & lower train speeds made the Northern Line cooler than the Central Line. Overall, tunnel temperatures in the Northern Line would remain cooler than the outer ambient temperatures in the summer even if the train speeds are increased to 100 km/hr, while the platform temperatures would rise above ambient temperatures. Also, it was shown that a combination of combination of lowering the soil boundary condition around the tunnels which emulates geothermal cooling and heat brake regeneration would successfully mitigate the overheating problems in the Bakerloo Line. The Jubilee is the coolest of the 4 lines modelled, because it combined larger tunnel diameters,

trains equipped with brake regeneration, and have the highest ventilation rates as a result of its modern infrastructure. The methodology used in modelling the Central Line can be utilized flexibly to model other deep lines across different cities and gain insight on the fundamentals behind their climate conditions.

6.1.2 3D Vertical Borehole Model and Optimization

A 3D FEM (finite element model) was developed using Comsol to model thermal transient interactions between the subway tunnels and closed loop vertical geothermal boreholes, to assess their effectiveness in cooling the Central Line's tunnels and platforms. The Central Line model, which was developed and validated in Chapter 3, is retrofitted with the vertical boreholes. The 1D Central Line and the 3D FEM borehole models were co-simulated, through exchanging outer tunnel wall and soil temperature profiles, until both models yield a similar outer tunnel wall temperature, which indicated that both models have converged to a single solution. The 1D - 3D co-simulation was found to convert within 11 iterations. The co-simulation time intervals was varied between 1 month and 3 month, and shown to yield equivalent results, which allows for co-simulating the two models with longer time intervals and a fewer total number of iterations.

The vertical boreholes manage to cool the tunnel and platform temperatures in the Central Line model by 5 °C and 4.5 °C respectively during summer conditions for the year of 2013. The 1D subway and 3D FEM borehole models were also co-simulated for the years of 2032 and 2050 taking into consideration climate change, projected passenger & train traffic increase, and modernization of the trains. The vertical boreholes were able to lower the air temperatures of the platforms and tunnels by around 3.9 °C & 4.3 °C respectively for the year of 2032, and by 4.1 °C & 4.7 °C respectively for the year of 2050. Thus, the boreholes will help in mitigating the overheating problems in the central line by significantly cooling the system currently and for the future years to come.

Results have shown that a single 100 m tunnel vertical borehole adjacent to the tunnels third year of operation heat extraction (9336 kWh) was 9% slightly below a stand-alone borehole (10177 kWh). This was because the boreholes next to the tunnels thermally interfered along the sides of the tunnel, reducing their performance slightly. This was a necessary compromise,

since the boreholes were placed as close as possible to the tunnel outer walls to better cool the London Underground tunnels. Different arrangements and distances of the vertical boreholes with respect to the tunnels are examined to achieve the best heat extraction and cooling in the tunnels and stations simultaneously. Results have shown that having parallel vertical boreholes at a distance of 20 cm from the outer tunnel walls at each side is the optimum borehole arrangement, since the closer the distance, the more heat will be extracted from the tunnels, which will consequently result in more cooling in the tunnels and stations.

A new concept of partially insulated boreholes was developed to address the issue of having low heat demand in the buildings during summer conditions, while the subway tunnels and stations require cooling. The main benefit of the partially insulated boreholes is that they are able to provide building heating during winter conditions, and both building cooling and heating simultaneously during summer conditions while cooling the London Underground. The partially insulated boreholes act as BTES thermal storage system, in which the ground is used as a medium to inject and extract heat. While BTES systems use an array of boreholes to inject and extract heat radially, the partially insulated boreholes can do this within the same borehole injecting and extracting heat at different depths, saving required borehole spacing. The optimum dimensions of the partially insulated borehole for a 100 m was found to be 30 m for the non-insulated section next to the tunnel which extracts heat all around the year (building heating), while the other 70 m section alternates between extracting heat during winter conditions between January & April and October & December, and injecting heat into the soil (building cooling) during summer conditions between May & September. A single 100 m partially insulated borehole can annually provide heating for 1.25 UK households and an additional 6700 kWh of building cooling, while the non-insulated borehole provides less building heating annually equivalent to 1 UK household during the third year of operation. These results provide a starting point to investigate the potential of using vertical boreholes to cool the older lines of the London Underground while providing district heating and cooling to the surrounding buildings above.

6.1.3 Multiple Benefits of Vertical Boreholes Underground and Overground

Retrofitting the Central Line with vertical geothermal closed loop boreholes in Central London is investigated. A section containing 6 stations in the Central Line is selected as a case study where the tunnels pass under the roads. To determine the amount of heat extracted by the boreholes the 1D - 3D co-simulation method, which was described in chapter 4 is used, where the 1D Central Line model was coupled with the FEM (Finite Element Model) model of vertical ground boreholes. The buildings in the proximity of the tunnels were divided into 31 clusters, where the heating and cooling demand of the buildings were obtained from (Zhang et al., 2015b). The length of the boreholes between each of the stations was adjusted such that priority was given to cooling the London Underground system, while maximizing the amount of heating and cooling provided, and reducing capital costs.

Results have shown that the vertical boreholes manage to cover part of the total cluster monthly heat demand where the percentage varies from 4.1% (January) to 74% (July) depending on the month, because the clusters heat demand is maximum during January and minimum during July. Also, the vertical boreholes manage to cover a portion of the 31 clusters heat demand annually, where it covers the most for cluster 10 (29%) and least for cluster 16 (3.2%). The amount of heat extracted remained under the hourly clusters heat demand all around the year. Thus, the vertical boreholes can be run all days annually at full capacity, without leading to heating over supply from the vertical boreholes GSHPs. During summer conditions, the amount of heat provided by the boreholes is less or equivalent to the minimum hourly heat demand for the month of July, which has the least hourly heat demand among the 12 month, for each of the 31 building clusters. The proposed GSHP system can benefit from the Domestic Renewable Heat Incentive (RHI) offered by the UK government for switching from conventional fossil fuel heating to renewable heating (OFGEM, 2018), where it can potentially generate 20.5 Million GBP over the period of 7 years, based on the feed in tariff system. Also, by considering life cycle of the GSHP, the BHEs in the Central Line will reduce CO_2 emissions by 869 CO_2 tons annually which is equivalent to 31% decrease compared to gas fired boilers based on the carbon emission foot print of UK electricity production of 0.394 Kg CO_2/kWh in the year 2015 (DECC, 2015). As the UK moves towards its renewable electricity generation share of 30 % of total electricity generation in 2020, then the GSHP systems

CO_2 emissions will further decrease, since the carbon emission foot print of UK electricity production will decrease.

The percentage of building heat demand provided by the partially insulated boreholes is close to the values of the heat only extracting boreholes. This is because the dimension of the boreholes section operating in heating only mode in the partially insulated boreholes is slightly smaller than the total length of the boreholes. The partially insulated vertical boreholes were found to provide a portion of the 31 clusters cooling demand annually, where they cover the least for cluster 10 (2.7%) and most for cluster 2 (26.3%). The partially insulated boreholes were able to cover part of the total building cluster cooling monthly demand where the percentage varies from 29.6% in May to 6.8% in July depending on the month. This depends on the building cooling demand which varies depending on the climate, where in the month of July it is maximum. The section of the partially insulated boreholes that alternates between cooling and heating modes can be switched on and off depending on cooling building demand. During the hours where the cooling demand of the clusters exceeds the amount supplied by the boreholes, the borehole section injecting heat and providing cooling can be operated at full capacity. The hourly cooling demand for the clusters varies depending on the month, where it is highest was during the month of July.

The thermal comfort of passengers on board the train compartments & platforms was assessed for two scenarios: The current tunnels, and tunnels equipped with vertical boreholes. The tunnel and train compartment air temperatures experience two sharp rises, the minor one for the morning peak, and the major one for the afternoon peak, where the London Underground experiences both high train and passenger traffic, but during the afternoon the ambient outer air temperatures are much higher than the morning. The vertical boreholes were able cool the tunnel by around 4 °C during the Central Line's opening times (6 am till 12 pm), which has been also shown in chapter 4. The vertical boreholes also manage to cool the compartments by 3-4 °C, since the train compartment temperatures are influenced by their surrounding tunnel temperature through direct air exchange. Consequently, the number of hours T_{comp} and T_{plat} exceed the recommended temperatures for passenger comfort is reduced. The Central Line simulations have shown that the number of hours T_{comp} exceeds 26 °C decreases by 4.5 times from 1553 hours to 341 hours annually when the tunnels are equipped with boreholes. Also, the number of hours T_{comp} exceeds 30 °C was also reduced by 5 times from 158 to 31. In the platform, the number of hours T_{plat} exceeds 30 °C is reduced from 280 to 0 annually.

Thus, the vertical boreholes could significantly mitigate the over heating in the platforms and train compartments, by reducing the annual hours T_{comp} & T_{plat} exceeds 26 °C and 25 °C respectively, maintaining the platform temperatures below 30 °C.

The Central Line Model was modified to accommodate on board train carriage cooling. The model is simulated for the year of 2013 for two scenarios: The current tunnels, and tunnels equipped with vertical boreholes. The vertical borehole's tunnel cooling eliminated the need for air-conditioning in April and November and reduced the air-conditioning electrical consumption W_{AC} by 60 % in both July & August in the Central Line. The vertical boreholes also reduced the annual electrical consumption for train air-conditioning by 60 % saving 315900 kWh of electricity annually which is equivalent to the average annual electrical consumption of 77 UK houses and 125 tons of CO_2. It was also shown that train air-conditioning would raise the Central Line's Tunnel and Platform temperatures by around 1 °C. Hence, the rejected heat from the train air condition would further exacerbate the overheating problems in the platforms.

Retrofitting the Central Line with geothermal vertical boreholes has been shown to provide multiple benefits underground and overground. The vertical boreholes were able to cool the tunnels and platforms, while providing part of the surrounding building's heating demand. The boreholes also manage to enhance passenger comfort across their journey in the Central Line, where most of their time is spent in the platforms and train carriages. The cost of implementing the BHE system for the 6 stations in the Central Line was shown to range between between 10.5 - 37.2 Million USD, where this is a very rough approximation and future work is required to accurately approximate the cost, taking into consideration the urban nature of London, and the scale of the project which could reduce costs (Sibbitt and McClenahan, 2015). Thus, the system has the potential to payback for its cost in less than 10 years, while benefiting the surrounding community and the passengers. This retrofitting solution can be applied to other deep and old lines in the London Underground, which were partly build under roads, particularly the Northern, Bakerloo, Piccadilly Lines.

6.2 Recommendations for future work

This thesis has successfully demonstrated the benefits of retrofitting old and deep subway stations with vertical geothermal boreholes from improving the passenger comfort to providing district cooling and heating to the buildings above the tunnels. Also, it has developed a methodology to transiently co-simulate a 1D subway model with a 3D FEM model of the vertical boreholes. This dissertation has also showcased a simplified method to model the environment in deep and old subway system within a reasonable simulation time, and has showcased the effect of climate change, passenger & traffic increase, and infrastructure upgrades on the subway environment. However, these models are not perfect and there are a number of ways they can be improved, and future work can be undertaken to gain more insight.

6.2.1 1D Central Line model

The Central line model managed to model the environment of the London Underground with good accuracy, however there is potential for improvement. The Central Line model neglected the cross tunnels between the westbound and eastbound tunnels, and also neglected on board train and areas of spot/localised heating in the station. These could be incorporated in the Central Line model if the detailed maps of the London Underground have been provided by Transport for London, and also the specifications & operational schedule of the train heating system. For now detailed maps of the London Underground are not easily obtained for reasons connected to national security. Also, the locations of the spot/localised heating in the station would require security access to the offices in the London Underground. Also, taking tunnel water seepage in the tunnels into consideration and the change of the surrounding tunnel soil properties would improve the accuracy of the Central Line model.

Transport for London did not have temperature sensors installed in the upper sections of the station, such as station entrances, escalators, and the walkways leading to the platforms. This limited the validation of the Central Line model to only the platforms and the tunnels, since only data on these were collected. A proposed future work is monitoring wind, humidity, and air temperature data across all the station through installing sensors and modeling the station using IDA tunnel, which would help in understanding the factors that influence the environment in multiple sections of the London Underground's station.

6.2.2 3D Vertical Borehole Model

The current 3D FEM borehole model adopted the cylindrical heat model which assumes a cylindrical borehole with infinite length buried in the ground, where the model's governing equation can be analytically solved through either a constant heat transfer rate across the borehole surface or a constant borehole surface temperature (Carslaw and Jeager, 1959), (Ingresoll and Plass, 1948) & (Hellstrom, 1991). This was valid and successful for the scope of this thesis, but this approach does not provide insight about the thermal interactions inside the borehole, which is important in investigating new designs of boreholes, such as the partially insulated boreholes. One suggested method to approach this, is through modifying the 3D vertical borehole model to include internal refrigerant flow within the boreholes. A major constraint on this approach is that it would yield unrealistic simulation times when the time scale is in years, as with the case of the 1D - 3D co-simulation methodology used in this thesis. With faster computers coming in the next couple of years, this method would become feasible, and is highly recommended.

The partially insulated boreholes is a concept that allows the flexible use of the boreholes next to the tunnels, as they would allow the same borehole to provide the cooling demand in the buildings, while also extracting heat from the tunnels simultaneously. This concept has not been applied before, so it has to be custom made. A future project would be constructing an actual experimental partially insulated borehole and comparing its performance to the simulated models.

The co-simulation between the 1D and the 3D model was computationally penalizing, so the model was setup efficiently in terms of symmetry, boundary conditions and mesh distribution. A method can be developed, such that the state space function of the borehole and tunnel interactions can be extracted from the 3D FEM borehole model, and integrated into the 1D subway model. Thus, the entire equations will get reduced to 1D equations within IDA tunnel, which would significantly reduce simulation times. However, currently the state space extraction method in COMSOL 5.0 is still limited to several points rather than entire domains, such as the entire borehole. With new versions of COMSOL being released in the future, state space extraction of complex geometry will be possible, and this method can be applied to optimize the simulation time in the borehole - subway tunnel simulation interactions.

6.2.3 Additional tunnel cooling methods and train air-conditioning

The use of naturally occurring seepage water from rainfall and the river Tyburn which runs beneath the station to provide air cooling is being trailed in the middle and lower concourse of the Victoria Station. The air cooling units use fans to exchange heat with the water. This method can be modified in which water from naturally occurring seepage in the ground can be circulated in pipes in the tunnels, resulting in cooling the subway system. IDA tunnel currently is unable to model this phenomena, since it is unable to transiently model the heat exchange between the water and the air in the tunnel. An interesting future work is modifying the subway model to incorporate this type of cooling, where an additional modelica based module can be coded into the existing model. The feasibility of this cooling method can be assessed, then compared to the vertical boreholes to determine which is more efficient in cooling the subway system.

6.2.4 Integrating the Central Line Vertical Boreholes with Buildings in London

This thesis has been successful in estimating the building district heating and cooling provided by the boreholes in a section of the Central Line in Central London. This method can be utilized in other deep and old lines suffering from overheating problems, such as the New York Subway, Saint Peterborough Metro and the Moscow Metro. However, there are some aspects that could be incorporated in future work to improve and build on this study. A comparison between the cost of installing the GSHP piping, and the recovery in investment period in savings compared to the exiting gas boilers would be of interest.

Another interesting future work would be to integrate the tunnel boreholes with other geothermal borehole studies such as (Zhang et al., 2015b), to examine the total amount of district heating and cooling provided by the boreholes around the buildings in addition to the boreholes next to the tunnels. The borehole arrangement in this city scale analysis can be modified to incorporate Borehole Energy Storage (BTES) system (Lanahan and Tabares-Velasco, 2017) next to the tunnels, which would further improve the efficiency of ground storage, increase the amount of district heating and cooling delivered, enhance the systems COP, and achieve thermal balance in the ground. The BTES system can be coupled with renewable energy, such

as the use of solar hot water panels to create hot water for storage in summer, and with solar panels to power the BTES mechanical components (AHGI, 2018). Since the land around the London Underground is restricted, we propose to modify the BHE arrangement in Figure 4.1 to Figure 6.1 inorder to incorporate BTES into the London Underground, while making sure that the thermal interference between the boreholes is minimal by keeping the distance between them at 6m apart (Figure 6.1). This new design can be co-simulated in COMSOL and 1D IDA Central Line model to asses the effectiveness of integrating the BTES system in providing cooling and heating to the buildings while cooling the London Underground tunnels.

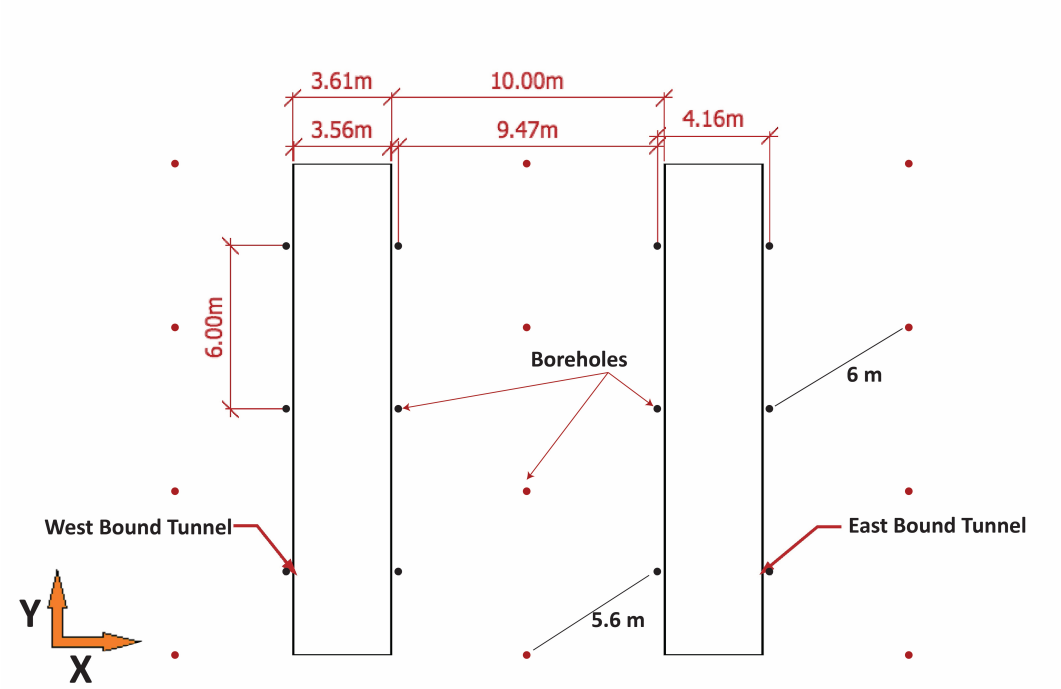

Figure 6.1: Schematic of the vertical borehole BTES arrangement and Central Line tunnels.

Also, in case of the presence of natural aquifers close to the tunnels in the London Underground, the application of Aquifer Thermal Energy Storage (ATES) (Lanahan and Tabares-Velasco, 2017) can also be investigated.

6.2.5 Passenger Thermal Comfort

This thesis evaluated the passenger's thermal comfort based on an extensive study and survey work conducted by (BRE, 2004a) which collaborated with Transport for London. This approach is appropriate for determining the general overall passenger comfort in the platform and the train carriages. However, this method doesn't provide a detailed and transient assessment of the passenger thermal comfort throughout their journey across their departure station till their arrival station. A future project could include the installation of sensors across the stations and train carriages to monitor the air temperature, wind speed and humidity. The 1D subway model can be coupled with the Fiala transient bio-heat model (Fiala et al., 2011) to simulate the passenger's thermal responses to the environmental conditions, as they are moving in the stations and trains (Figure 6.2). The passengers skin and core segmental temperatures outputted by the Fiala model can be used in a transient thermal comfort model such as the one developed by Zhang known as the UC Berkeley Multinode Thermal Comfort Model (Zhang, 2003). Thus, the transient thermal comfort for the passengers during their entire journey from the moment they walk into the station through taking the underground train then exiting at the destination station is assessed. Thermal imaging in the station and the train carriages can be used to validate the model and examine the passenger's thermal response in the London Underground's climate.

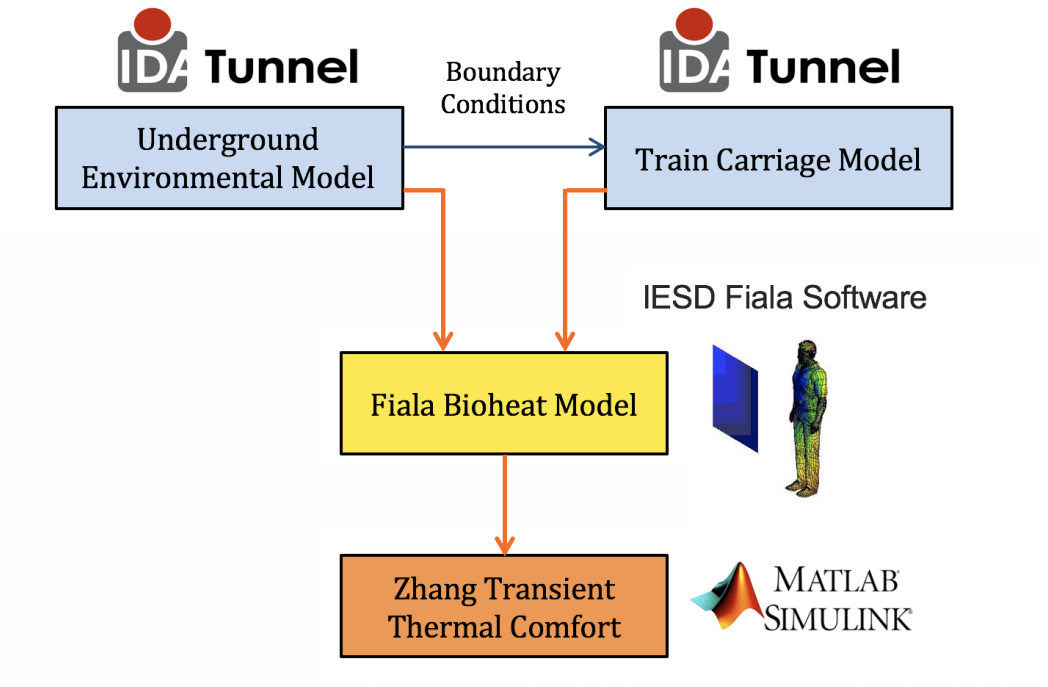

Figure 6.2: Flow chart for determining the transient thermal comfort for the passengers in the stations and train carriages using IDA Tunnel and Matlab.

Appendix A

IDA Fluid and Heat Models

A.1 Underground Model Geometrical Distribution

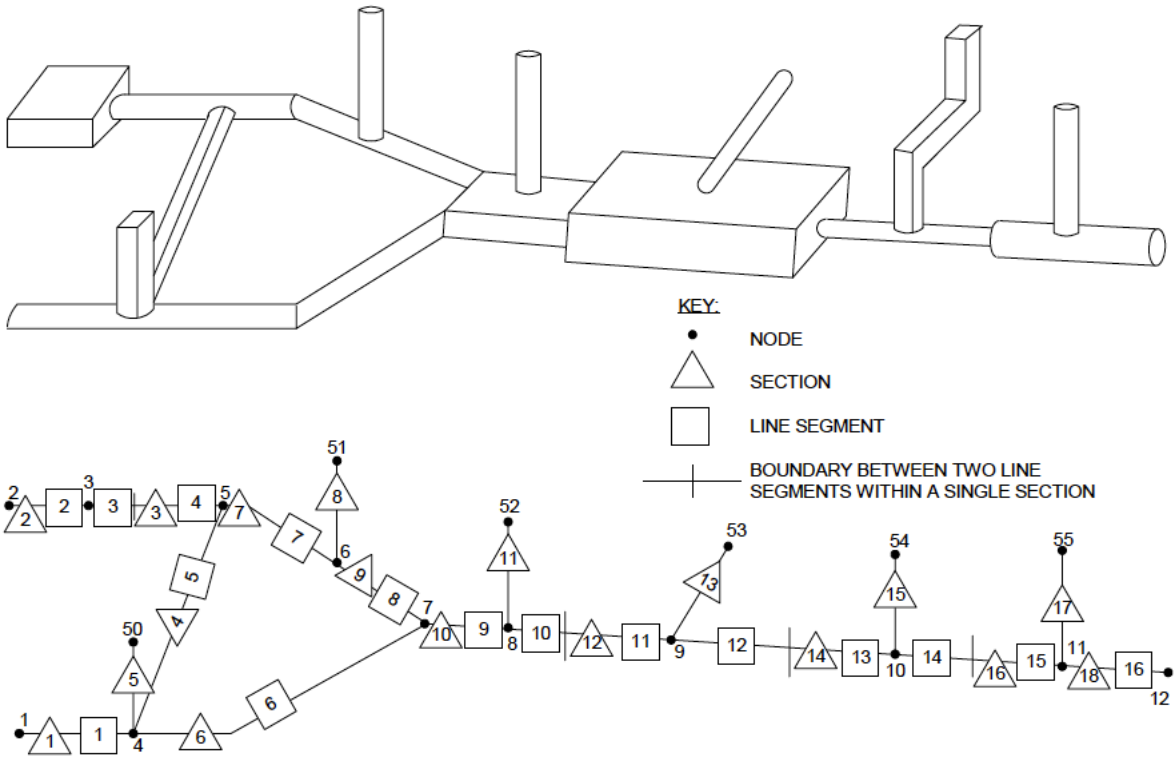

Figure A.1: Sample subway system and its corresponding schematic representation (SES, 2001).

A.2 Calculation of Major and Minor Head Loss

Energy is lost by the air flow in the tunnels due to head losses. In general there are two types of head losses which are the head losses due to viscous friction and head losses due to abrupt changes in the tunnel's geometry. The head loss due to friction between two points 1 and 2 in the flow is given as:

$$h_T = \frac{P_1 - P_2}{W} + \frac{{V_1}^2 - {V_2}^2}{2g} + z_1 - z_2 \tag{A.1}$$

The friction head h_f also referred as major head loss is determined by the use of the Dary-Weibach equation (Fox et al., 2004) which is:

$$h_l = f\frac{L}{d}\frac{V^2}{2g} \tag{A.2}$$

The Darcy-Weibach friction factor f is dependent on the Reynolds number Re and the surface roughness E of the surface, where these expressions are correlated in the moody chart (Figure A.2). The roughness of the tunnel in the underground depend on the average height of the protuberances found in the tunnel, such as signals, lights, tunnel ribs, and rail. details about determining the roughness of a tunnel filled with is found in (SES, 2001).

The second type of losses due to sudden changes in the tunnel geometry is called minor head losses and is represented as a velocity head of the fluid just before the sudden change in geometry. Minor head losses are irreversible head losses in the total head of a segment (Fox et al., 2004). The minor loss is expressed as a friction loss by calculating an equivalent length that the fluid has to travel to lose the same amount of energy as that of the sudden change in area or turn which is written as:

$$h_{lm} = f\frac{L}{d}\frac{V^2}{2g} = \frac{KV^2}{2g} \tag{A.3}$$

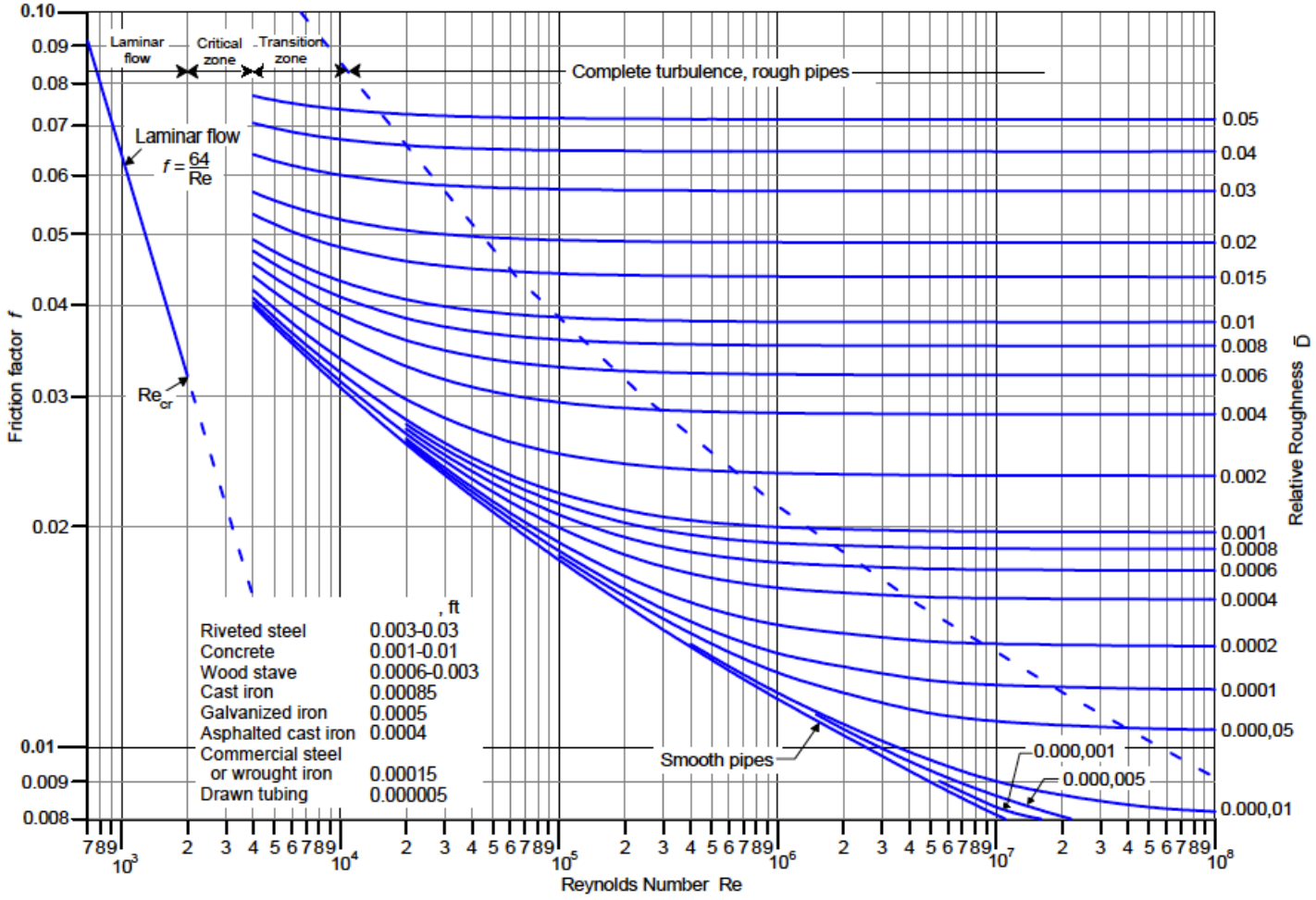

Figure A.2: Moody Diagram (Fox et al., 2004).

Where the minor head loss K coefficient depends on the geometry of the tunnel. Various tables provide the minor head loss through either the equivalent head or K for a variety of geometries, where some tables can be found in (Fox et al., 2004).

A.3 IDA Tunnel Airflow Equations

The flow equations for the stairs, halls, and passages within a station and ventilation shafts are equivalent except that the latter may have ventilation fans. Based on the section shown in Figure A.3 that has N segments and 2N nodes the flow equation is:

$$\frac{dQ_s}{dt}\sum_{i=1}^{N}\frac{L_t}{At} = -Q_s\left[(Q_s+|Q_s|)\sum_{i=1}^{N}\left[\frac{C^+_{Bt}+C^+_{Ft}}{4A_t^2}\right]-(Q_s-|Q_s|)\sum_{i=1}^{N}\left[\frac{C^-_{Bt}+C^-_{Ft}}{4A_t^2}\right]\right] + \Gamma_{S\alpha}(Q_S)+B_S+H_1-H_{2N} \tag{A.4}$$

Equation (A.4) also takes into consideration the ventilation fan operation and buoyancy through the terms $\Gamma_{S\alpha}(Q_S)$ and B_S respectively. The ventilation fan flow function is:

$$\Gamma_{S\alpha}(Q_S) = X_{\alpha_1}Q_S^3 + X_{\alpha_2}Q_S^2 + X_{\alpha_3}Q_S + X_{\alpha_4} \tag{A.5}$$

The method for calculating the X_α coefficients in equation (A.5) and a description of the ventilation fan's operation is provided in Appendix A.4. The expression for buoyancy in equation (A.3) is calculated as the difference in weight per unit area per unit mass between a column of the outside air having the stack height of the segment of interest and a similar column of air having the temperature of air inside the segment. The weight for the outer and inner air column is respectively:

$$W_o = \rho_0 g z_s = \frac{P_o g z_s}{RT_o} \tag{A.6}$$

$$W_s = \rho_s g z_s = \frac{P_o g z_s}{RT_s} \tag{A.7}$$

The Buoyancy function is calculated as:

$$B_s = \frac{W_o - W_s}{\rho_o} = (\frac{RT_o}{P_o})(\frac{P_o g z_s}{R})(\frac{1}{T_o}-\frac{1}{T_s}) = g z_s(1-\frac{T_o}{T_s}) \tag{A.8}$$

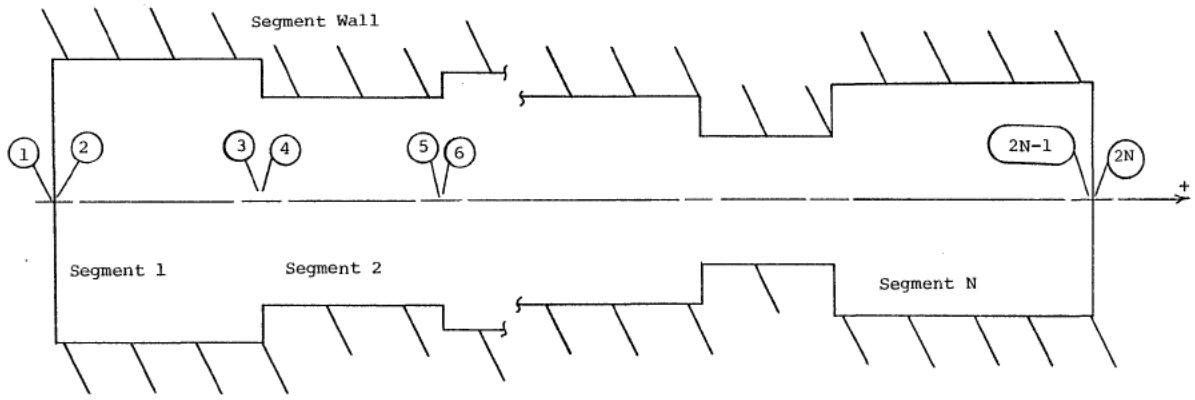

Figure A.3: Section subdivided into segments (SES, 2001).

The transient flow equation for an subway section of the rail tunnels can vary depending on several scenarios, where there could be a single train occupying a single segment, a train occupying several segments within a section, or two trains passing opposite to each other in a section. The model assumes that the train has similar front and rear shapes, so the drag coefficients are the same. For the case of a single train passing with velocity U_v in a segment as seen in Figure A.4, several control volumes are taken such that the air in front of the train is 23, the air between the train and the tunnel surface is 45, and the air behind the train is 67, while 1 and 8 are the boundaries of the segment that constitute nodes. The continuity equation 2.2 along with the mechanical energy equation 2.5 is applied consecutively, where details for the derivation can be found in (SES, 2001). The equation for the flow in a segment containing a train is:

$$\left[\frac{L_t - l_v}{A_t} + \frac{l_v}{A_t - a_v}\right]\frac{dQ_s}{d_t} = \frac{(K_{vB} + K_{vF})(A_t U_v - Q_s)^2}{2A_t^2} + \frac{f_t l_v P_t |(a_v U_v - Q_s)|(a_v U_v - Q_s)}{8(A_t - a_v)^3} + \frac{\lambda_v l_v P_v |(A_t U_v - Q_s)|(A_t U_v - Q_s)}{8(A_t - a_v)^3} + \frac{a_v l_v}{A_t - a_v}\frac{dU_v}{d_t} - \frac{f_t (L_t - l_v) P_t |Q_s| Q_s}{8A_t^3} + H_8 - H_1 - J_{12} - J_{78} \tag{A.9}$$

J_{12} and J_{78} represent the junction head losses between the points 1,2 and 7,8 respectively. K_{vF} and K_{vB} are dependent on the train blockage ratio in the tunnel which is $\sigma_t v = a_v/A_t$, and the direction of the flow with respect to the train. Typically the train is faster than the air, $U_v - V_t > 0$ the air will be moving towards the train in the control volume, so K_vF and K_vB are calculated respectively as:

$$K_{vF} = \frac{\sigma_{tv}(2 - \sigma_{tv})}{(1 - \sigma_{tv})^2} + \sigma_{tv} C_{DvF} \tag{A.10a}$$

$$K_{vB} = \frac{\sigma_{tv} C_{DvB}}{(1 - \sigma_{tv})^2} - \frac{2\sigma_t v}{(1 - \sigma_t v)} \tag{A.10b}$$

$$K_{vB} + K_{vF} = \frac{a_v^2 + a_v A_t C_{DvB}}{(A_t - a_v)^2} + \frac{a_v C_{DvF}}{A_t} \tag{A.10c}$$

Details for calculating the drag coefficients for the train C_{DvF} and C_{DvB} are found in Appendix B.5.

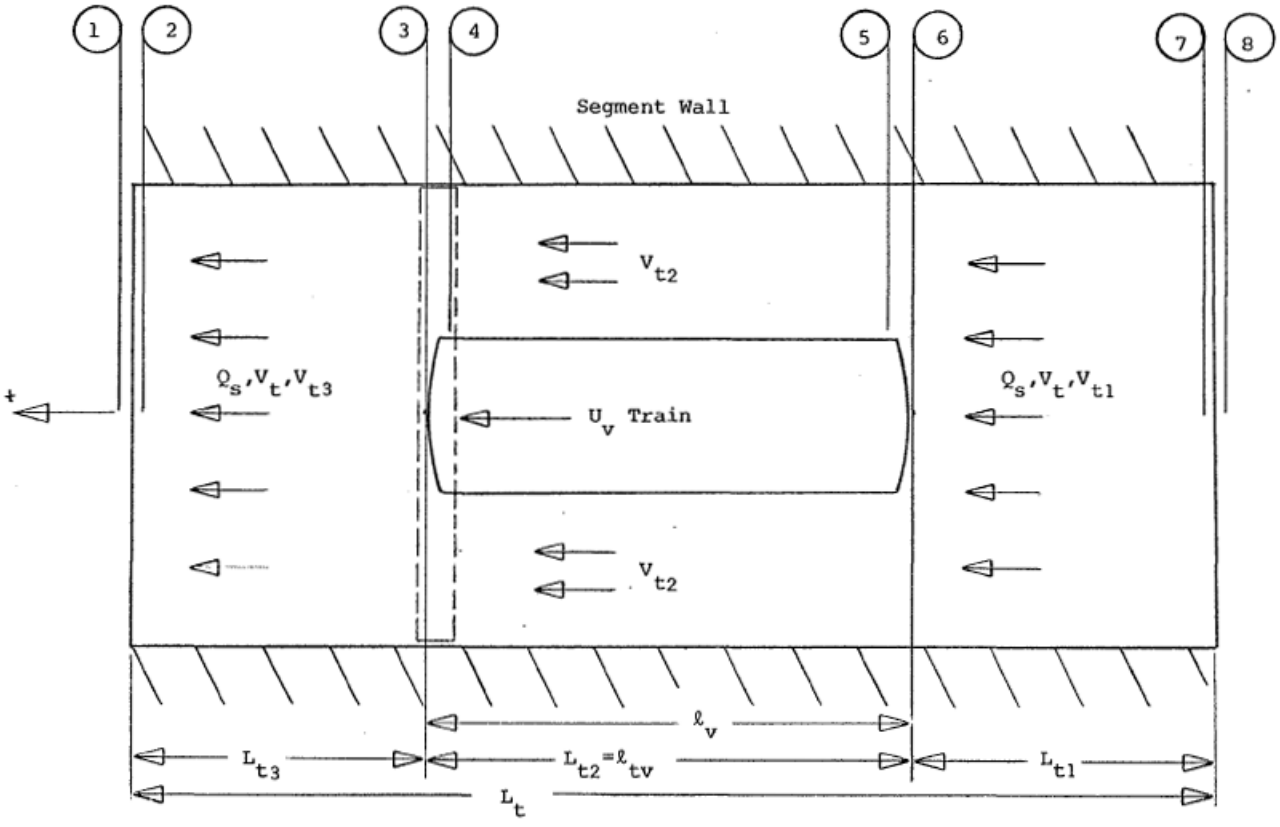

Figure A.4: A single train in a single segment (SES, 2001).

The method used for determining the flow equation in the previous case is used for the case of a single train passing through multiple segments within a section as described in Figure A.5. This case applies when the tunnel diameter changes as with the case of train arrivals and departures from the station. The flow equation for a train passing between three segments within a section is:

$$\frac{dQ_s}{dt}\sum_{t=1}^{3}\left[\frac{L_t - l_{tv}}{A_t} + \frac{l_{tv}}{A_t - a_v}\right] = \sum_{t=1}^{3}\left[\left[\frac{a_v l_{tv}}{A_t - a_v}\right]\frac{dU_v}{d_t} + \frac{f_t l_{tv} P_t |(a_v U_v - Q_s)|(a_v U_v - Q_s)}{8(A_t - a_v)^3}\right.$$
$$\left. + \frac{\lambda_v l_{tv} P_v |(A_t U_v - Q_s)|(A_t U_v - Q_s)}{8(A_t - a_v)^3}\right] - \frac{V_{31}^2}{2} + \frac{V_{32}^2}{2} + \frac{K_{vF}(U_v - V_{32})^2}{2} - \frac{V_{11}^2}{2} + \frac{V_{12}^2}{2} \quad \text{(A.11)}$$
$$+ \frac{K_{vB}(U_v - V_{11})^2}{2} - J_{1112} - J_{78} - J_{56} - J_{12} + H_{12} - H_1 - \sum_{t=1}^{3}\left[\frac{f_t(L_t - l_{tv})P_t|Q_s|Q_s}{8A_t^3}\right]$$

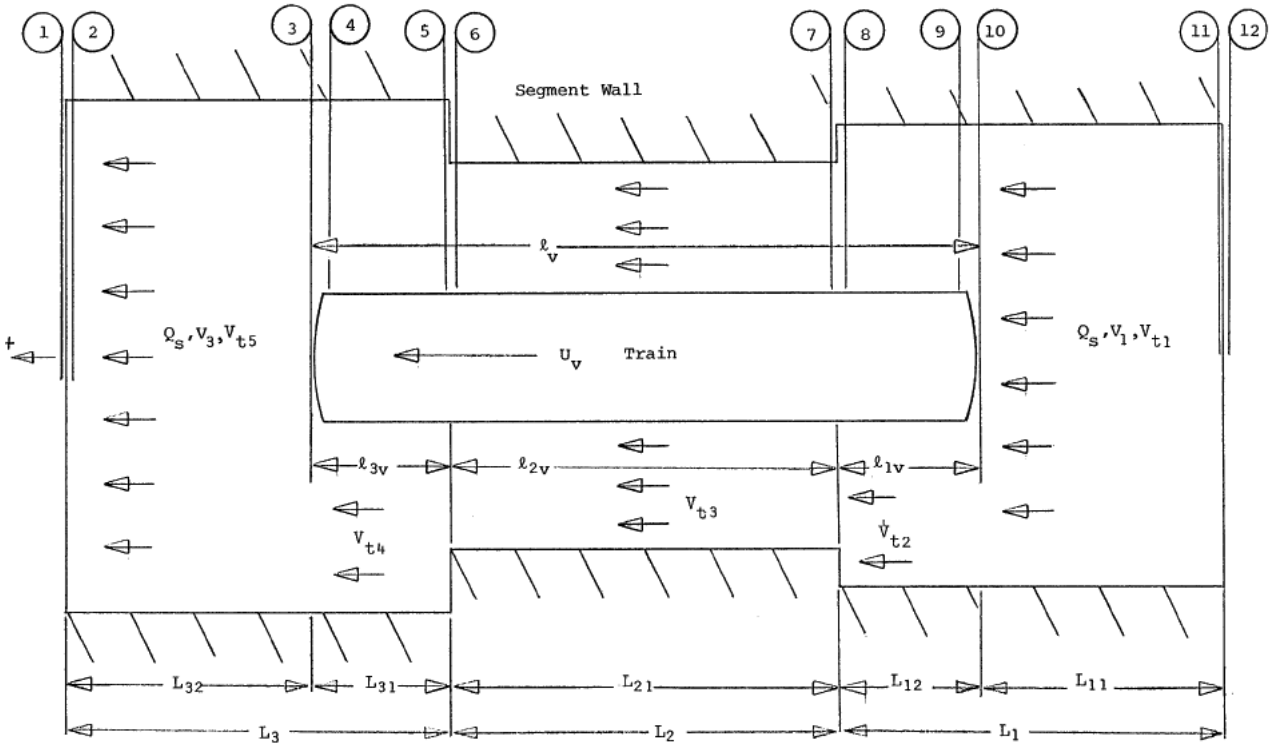

Figure A.5: Single train in multiple segments (SES, 2001).

Also K_{vF} and K_{vB} are calculated for $U_v - U_{32} > 0$ and $U_v - U_{11} > 0$ respectively as:

$$K_{vF} = \frac{a_v(2A_3 - a_v)}{(A_3 - a_v)^2} + \frac{a_v C_{DvF}}{A_3} \tag{A.12a}$$

$$K_{vB} = \frac{A_1 a_v C_{DvB}}{(A_1 - a_v)^2} - \frac{2a_v}{A_1 - a_v} \tag{A.12b}$$

Similarly for the case of two trains heading opposite to each other in a single segment, which occurs in double tracked subway rail systems in a single tunnel, the flow equation based on Figure A.6 is:

$$\begin{aligned}\frac{dQ_s}{dt}\sum_{t=1}^{5}\frac{L_{tr}}{A_{tr}} = -\sum_{t=1}^{5}\Big[\frac{f_{tr}L_{tr}P_t|V_{tr}|V_{tr}}{8A_{tr}}\Big] - \frac{\lambda_1 L_{t2}P_1|(V_{t2}-U_1)|(V_{t2}-U_1)}{8A_{t2}} - \frac{\lambda_1 L_{t3}P_1|(V_{t3}-U_1)|(V_{t3}-U_1}{8A_{t3}} \\ - \frac{\lambda_2 L_{t3}P_2|(V_{t3}-U_2)|(V_{t3}-U_2)}{8A_{t3}} - \frac{\lambda_2 L_{t4}P_2|(V_{t4}-U_2)|(V_{t4}-U_2)}{8A_{t4}} + \frac{a_1 L_{t2}}{A_{t2}}\frac{dU_1}{dt} + \frac{a_1 L_{t3}}{A_{t3}}\frac{dU_1}{dt} \\ + \frac{a_2 L_{t3}}{A_{t3}}\frac{dU_2}{dt} + \frac{a_2 L_{t4}}{A_{t4}}\frac{dU_2}{dt} + \frac{{V_{t5}}^2}{2} + \frac{K_{2F}(U_2 - V_{t5})^2}{2} + \frac{K_{1F}(U_1 - V_{t4})^2}{2} + \frac{K_{2B}(U_2 - V_{t2})^2}{2} \\ + \frac{K_{1B}(U_1 - V_{t1})^2}{2} + \frac{V_{t1}}{2} - J_{12} - J_{1112} + H_{12} -\end{aligned}$$

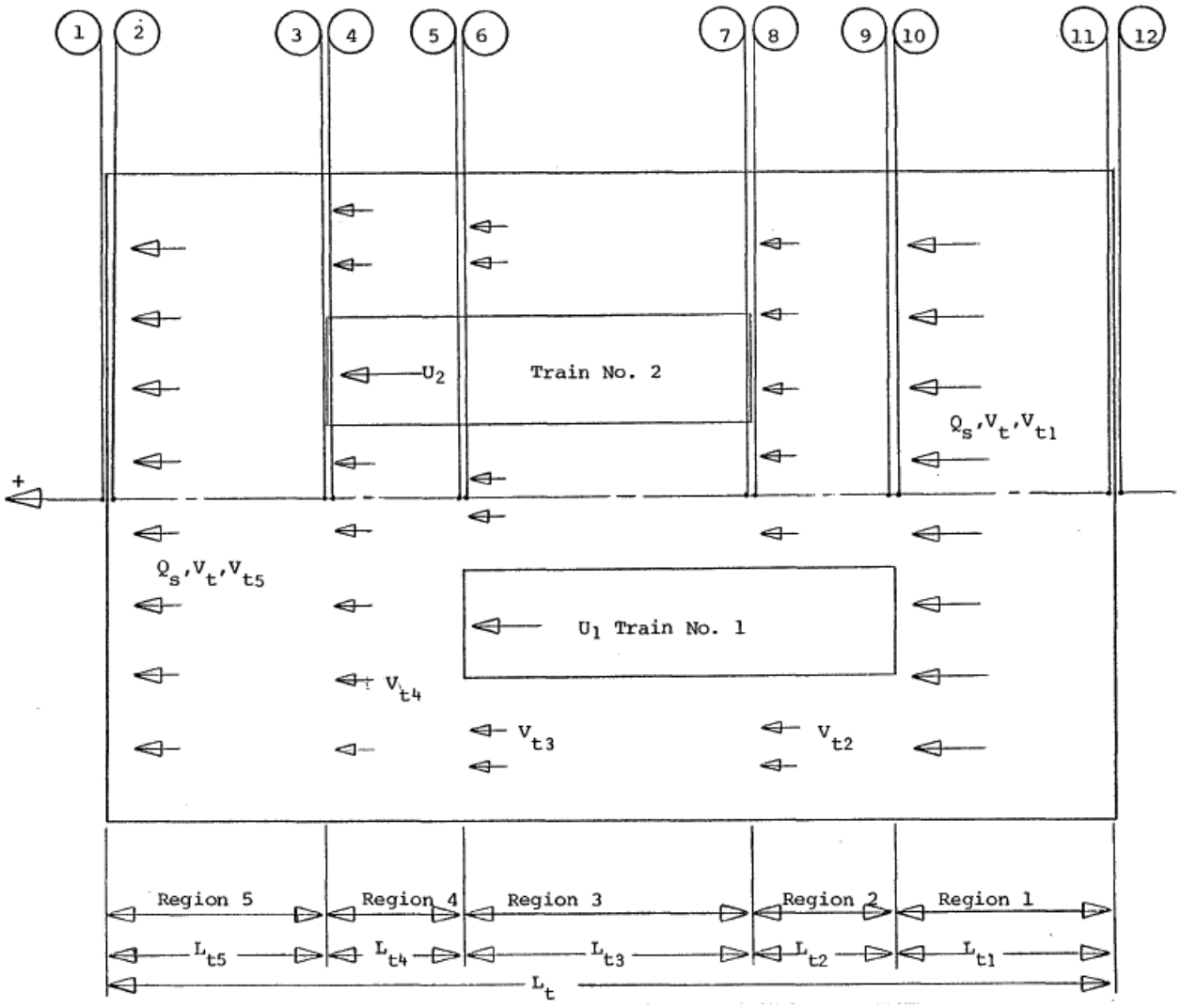

Figure A.6: Two trains in multiple segments (SES, 2001).

It is clear from the transient flow equations listed earlier that a large number of equations is required to calculate the flow rates in a subway system. This is because of the different situations that can arise as the trains are moving in the system, particularly in the case of a double track subway system. IDA Tunnel minimizes the number of equations by grouping the driving forces influencing the flows in each section into single terms and subdividing the segments into regions. This method is briefly described in this section, where detailed explanation with examples are found in (SES, 2001). For each region the changes in forcing and inertial functions are represented by ΔH and ΔZ respectively. These are summed for every region within a segment and for every segment such that $Z_s = \sum_{st}\sum_{tr} \Delta Z$ and $w_s = \sum_{st}\sum_{tr} \Delta H$. The entire system is divided into a set of loops, where each passes through the fewest number of sections and w_s for every loop are summed into Ω_N, where N is the number of loops. The equations are then grouped into a matrix system, where the algorithm for solving it is shown in Figure A.7. The matrix system is given as:

$$[Z]\left[\frac{dq}{dt}\right] = [\Omega] \tag{A.14}$$

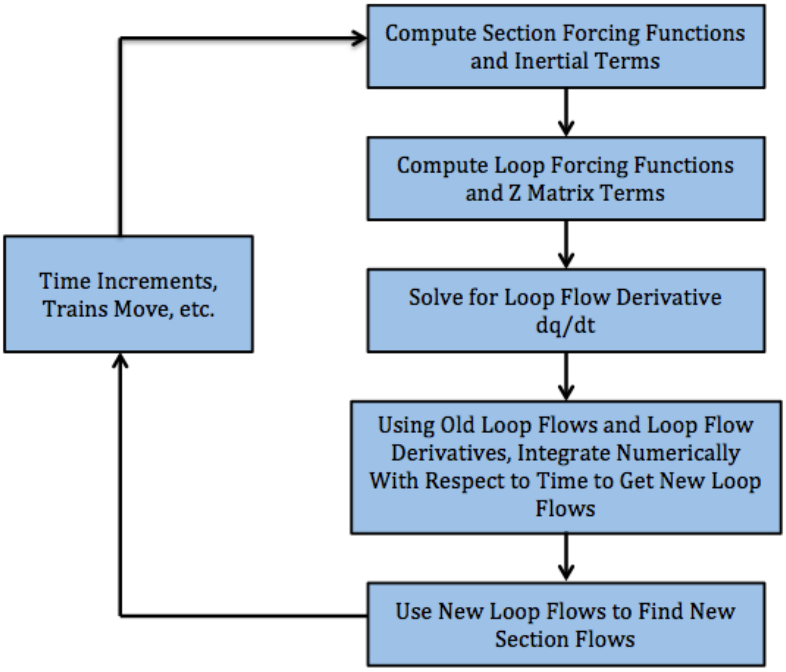

Figure A.7: Algorithm Schematic for Computing Section Airflows.

A.4 Fan Fit Curve

The fan forcing function coefficients $\Gamma(Q_s)$ are derived in this section. The fan's characteristic curve is typically expressed as the total pressure rise at the fan, over the air volume flow rate (Figure A.8). For the case of a bidirectional fan, a curve is usually provided for both supply and exhaust. Each curve is depicted by four points which are used to be fitted into a cubic polynomial.

$$H_1 = F_{\alpha 1}{Q_1}^3 + F_{\alpha 2}{Q_1}^2 + F_{\alpha 3}Q_1 + F_{\alpha 4} \tag{A.15a}$$

$$H_2 = F_{\alpha 1}{Q_2}^3 + F_{\alpha 2}{Q_2}^2 + F_{\alpha 3}Q_2 + F_{\alpha 4} \tag{A.15b}$$

$$H_3 = F_{\alpha 1}{Q_3}^3 + F_{\alpha 2}{Q_3}^2 + F_{\alpha 3}Q_3 + F_{\alpha 4} \tag{A.15c}$$

$$H_4 = F_{\alpha 1}{Q_4}^3 + F_{\alpha 2}{Q_4}^2 + F_{\alpha 3}Q_4 + F_{\alpha 4} \tag{A.15d}$$

Equations (A.15a), (A.15b), (A.15c), and (A.15d) are solved for $F_{\alpha 1}$, $F_{\alpha 2}$, $F_{\alpha 3}$ and $F_{\alpha 4}$ to get for the exhaust fan mode:

$$X_{\alpha 1} = F_{\alpha 1} \quad X_{\alpha 2} = F_{\alpha 2} \quad X_{\alpha 3} = F_{\alpha 3} \quad X_{\alpha 4} = F_{\alpha 4} \tag{A.16a}$$

as for the supply fan mode:

$$X_{\alpha 1} = F_{\alpha 1} \quad X_{\alpha 2} = -F_{\alpha 2} \quad X_{\alpha 3} = F_{\alpha 3} \quad X_{\alpha 4} = -F_{\alpha 4} \tag{A.16b}$$

A.5 Train Drag Coefficient

The aerodynamic drag for the train can be divided into three parts: the front or nose drag of the train, the drag from the back of the train, and the side drag including the roof and bottom. Figure A.9 shows the frontal train drag coefficient for several train shapes, which is used to calculate the nose drag. The darcy-weibach friction factor is used for the calculation of the skin friction coefficient for the sides, roof, and bottom; Experiments have shown that this value has an average of 0.012 for modern trains (Fox et al., 2004).

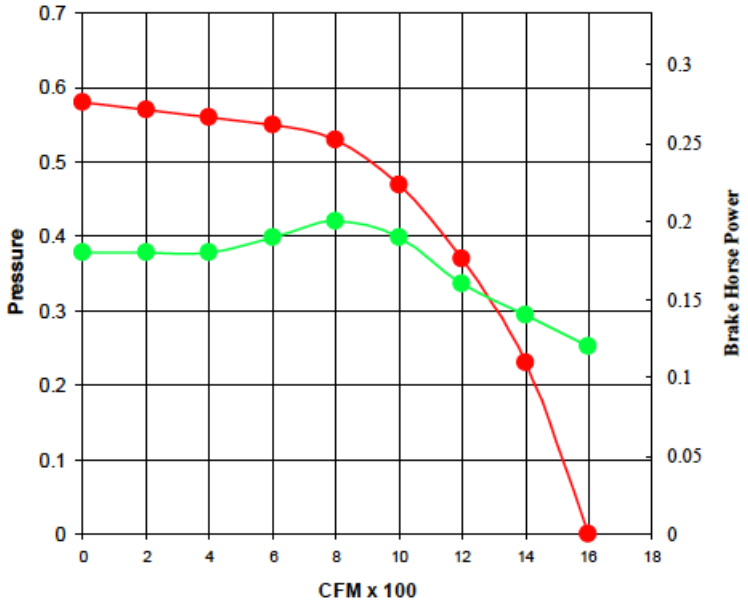

Figure A.8: Typical Fan Performance Curve, pressure in Inch Wg (Red) and Fan Brake Horse Power in hp (Green) (Fox et al., 2004).

The drag coefficient at the back of the train can be estimated using this formula (Harris, 1973):

$$C_{DvB} = 0.029(\frac{0.5\ell_v \lambda_v p_v}{a_v})^{-0.5} \tag{A.17}$$

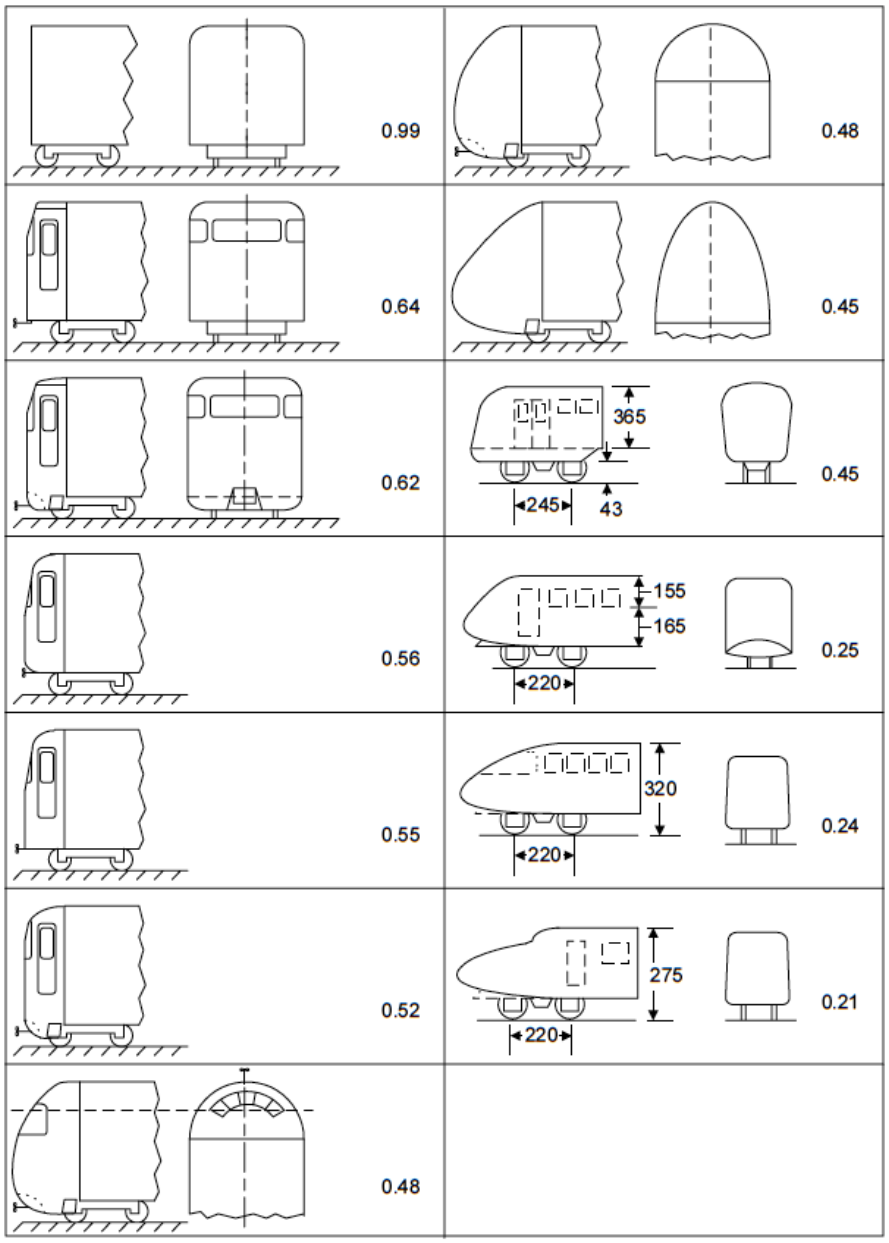

Figure A.9: Frontal train drag coefficient for several train shapes (SES, 2001).

A.6 Third and Fourth Rail Losses

The components of equation 2.12 that calculates the third and fourth rail losses are described. The resistance of the underground power distribution circuit is the summation of the resistance of the third and fourth, and the running rail (SES, 2001). Typical values for third and fourth

rail resistances are 12 milliohms per mile each, and 15 milliohms per mile for running rail. The kinetic energy of the trains is calculated as:

$$KE = WNnU^2 \tag{A.18}$$

The train losses due to aerodynamic drag are calculated as:

$$q_D = F_D d_a n \ \ where \ \ F_D = a\rho C_D \bar{U}^2 \tag{A.19}$$

The value of C_D is typically taken as 4 for most conditions.

The heat losses due to mechanical resistance is calculated as:

$$q_M = F_M d_a WNn \ \ where \ \ F_M = 2.6 + \frac{232}{W} + (11.1 * 10^{-4})\bar{U} \tag{A.20}$$

The starting resistor heat losses can be approximated without detailed knowledge of the train's motor characteristics. The train is assumed to undergo two transition steps to reach its operational velocity, where the heat dissipated in the first step is equal to that of the second step and the velocity used in the calculations is the transition speed of the the first and second steps shown in Figure A.10.

$$q_{step1} = KE_{step_1} + q_{Mstep1} \tag{A.21}$$

$$q_{Mstep1} = KE_{step_1} \frac{1 - \epsilon_m}{\epsilon_m} \tag{A.22}$$

The total starting losses for the two transition step is is equal to $q_{SR} = 2q_{step1}$
Therefore the total heat release from the train motors is given as:

$$q_{Mstep1} = (KE + q_D + q_M + q_{SR}) \frac{1 - \epsilon_m}{\epsilon_m} \tag{A.23}$$

Where the motor efficiency ϵ_m is taken as 90% if motor data is unavailable.

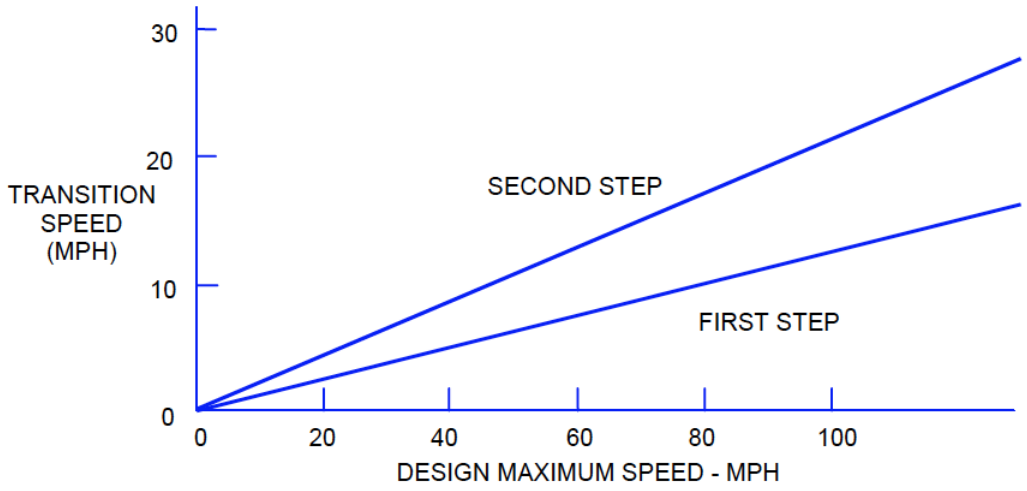

Figure A.10: Transitions speeds for underground cam-controlled train motors (SES, 2001).

A.7 Train Steady State Heat Sources

Heat is released by the condenser and compressor in a typical air-conditioning unit in the train, where it is calculated as:

$$q_{AC} = Rate_{AC} + W_{comp}(1 - EEF_{comp}) \tag{A.24}$$

The heat released by the train's pneumatic braking system is calculated as:

$$q_{aircomp} = P_c C_c \tag{A.25}$$

The heat released by the motor generation for train lightning and other electrical equipment is calculated as:

$$q_{m-g} = P_{m-g} C_{m-g} \tag{A.26}$$

Therefore the total heat released by the steady state heat sources in a train is given as:

$$q_{TOT} = q_{AC} + q_{aircomp} + q_{m-g} \tag{A.27}$$

A.8 Convection and Radiation Heat Transfer for Brake Resistor Grids

For radiation heat transfer, the resistor grids are assumed to be a grey body surrounded by a black enclosure that is at uniform temperature. The radiation emitted by the grids is assumed to be transmitted to the solid materials around it, which is the the tunnel surface and the train's under body, where this heat is considered to be instantaneously released to the tunnel air. By applying the Stefan-Boltzmann law, the resistor grid radiation heat transfer rate is:

$$Q_{rad} = A_r \varepsilon \sigma (T_g^4 - T_w^4) \tag{A.28}$$

The effective radiative surface area is equivalent to the total surface area of the grids multiplied by a shape factor with respect to its surrounding as seen in Figure A.11 which is given as:

$$A_r = 2(L_1 L_2 + L_2 L_3 + L_3 L_1) \tag{A.29}$$

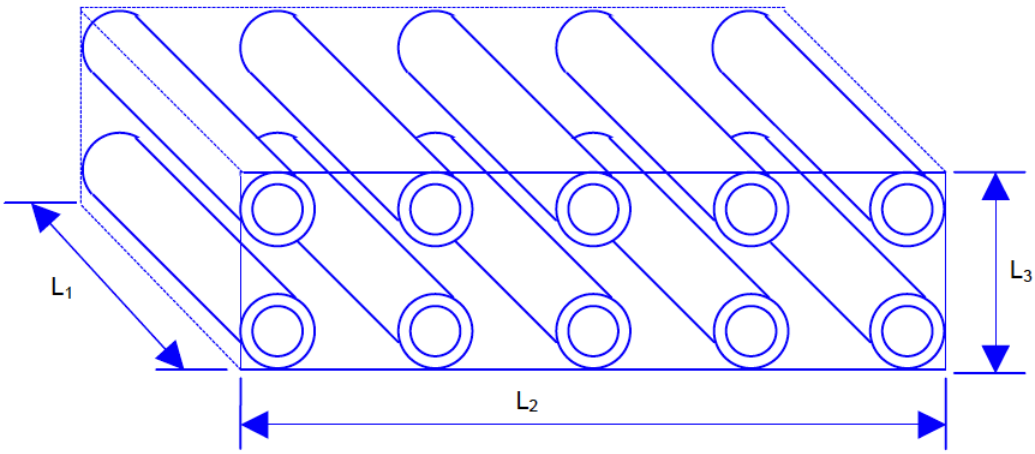

Figure A.11: Effective radiative surface area.

Convection heat transfer can occur by either forced convection or natural convection modes, where the heat transfer coefficients and conditions for both of these modes is found in Appendix B.7. Experimental field tests were used to calibrate the convective heat transfer

coefficients and adjust the formulas to correlate with experimental data (SES, 2001). The convective heat transfer is given as:

$$Q_{cov} = h_c A_c (T_g - T_a) \tag{A.30}$$

Where the effective convective area A_c for circular and rectangular shapes (Figure 2.15) is given respectively as:

$$A_c = \pi D_g L \tag{A.31}$$

$$A_c = 2(A+B)L \;\; where \;\; D_g = \frac{4(AB)}{2(A+B)} \tag{A.32}$$

Equations (A.29), (A.30), (A.31) and (A.32) shows the dependence of the resistor grid's thermal behavior on the temperature and velocity of the surrounding air in the tunnel and the electrical energy supplied to the grid. The instantaneous heat rejection rates for the resistor grids on board the trains are calculated using the air temperature and velocities supplied by the fluid and thermal subprograms of IDA Tunnel as well as the trains instantaneous energy consumption. It is assumed that each car of the train has two sets of resistor grids, where the first is for deceleration and the second for acceleration. Also, the grids are of the same type across the train, which implies that the heat rejection rate by the grids does not vary with location on the train. Thus, it is sufficient to compute the average temperature of one pair of deceleration and acceleration grids and equate the values for the grids on the train.

The model considers the resistor grids as point heat sources distributed uniformly over the length of the train, so the heat released by the deceleration and the acceleration grids are summed up and divided by the train's length. The energy rates into the deceleration grids are calculated using the rate of change of the train's kinetic and potential energy along with the aerodynamic drag and mechanical friction during the braking process. In reality, 90% of this energy goes into the resistor grids due to motor inefficiencies (RAE, 2007). On the other hand, the power into the acceleration grids is calculated by multiplying the square of the

supplied current with the grids resistance $P_{ga} = Ri^2$. Equation (2.13) is used in a first step of four Runge-Kutta numerical steps to calculate the new T_g. At the start of the simulation an initial value of T_g is computed, where the equations and methodology for these calculations are provided in Appendix A.9.

The forced convection model assumes that the resistor grids are in-line tube banks, where the air is flowing at variable rates. The flow is turbulent in nature and the average convective coefficient can be approximated using this expression (Holman, 2010):

$$\bar{h} = 0.33(\frac{K}{D_g})(\frac{\rho V_r D_g}{\mu})^{0.6}(Pr)^{0.3} \tag{A.33}$$

The above equation (A.33) is valid for both turbulent and transitional flow with $200 \leq \frac{\rho V_r D_g}{\mu} \leq 6000$ condition being satisfied.

The free convection model assumes that the elements of the resistor grid are tubes that are isolated from one another (Holman, 2010), where the average convection coefficient is calculated as:

$$\bar{h} = 0.53(\frac{K}{D_g})(Gr_D Pr)^{0.25} \tag{A.34}$$

$$Gr_D = \frac{\beta g {D_g}^3 \Delta T}{v^2} \tag{A.35}$$

Equation (A.35) is valid when the Grashof number ranges between $200 \leq Gr_D \leq 6000$. The range of the Grashof number at the resistor grids is well within the range of equation(A.35) during natural convection. In case there is mixed natural and forced conditions in which the conditions for equations (A.34) and (A.35) are both satisfied, the equation that has the highest convective coefficient is used.

A.9 Resister Grid Temperature Initialization

Several factors effect the temperature and thermal behavior of the train's resistor grids. The grid mass effects the number of train station stops required for the resistor grids to approach thermal equilibrium. The lower the mass of the grid, the lesser its heat storage capacity, and the lesser number of stops it would take to reach thermal equilibrium. Also, low mass resistor grids will experience more frequent fluctuations in temperature and heat transfer rate than higher mass counterparts. The train's kinetic energy will effect the decelerating resistor grid's thermal equilibrium temperature range (SES, 2001). Thus, the lighter or lower the top speed of the train, the lower the range for the resistor grid's temperature cycle. Also, the time interval for the one stop-journey cycle effects the resistor grid's temperature range in which the longer the cycle, the lower the temperature range and the lower the heat transfer rate, since it is dissipating the kinetic energy at a longer time interval. Experimental tests have shown that the effective mass of the grid is 50% greater than the mass of the active electrical resistance material (Brinckerhoff et al., 1976). Estimation of the average temperature of the deceleration resistor grids at thermal equilibrium is given by the following expression:

$$T_{G,E} = \frac{41.22 N_{cars} M V^2}{\bar{t} N_{cars} (A_C + A_R)} + T_{air} \tag{A.36}$$

Equation (A.36) can be rewritten as (A.37) in an iterative form to approximate the station to station deceleration resistor grid average temperature. This allows the calculation of the the resistor grid's average temperature as a function of the number of stops and the initial temperature prior to the first stop. After a sufficient number of iterations, the equilibrium temperature of the resistor grids is reached as seen in Figure A.12.

$$T_{G,n+1} = \frac{0.103(\frac{N_{cars}}{N_{pcars}}) M V^2 + 1.5 M_{DG} C_p T_{G,n} + 0.0025 (A_C + A_R) T_{air} t}{1.5 M_{DG} C_p + 0.0025 (A_C + A_R) t} \tag{A.37}$$

On the other hand, the heat rejected from the acceleration resistor grids is relatively small compared to the deceleration resistor grid. The acceleration grids can be initialized between the temperatures of 65 °C and 120 °C.

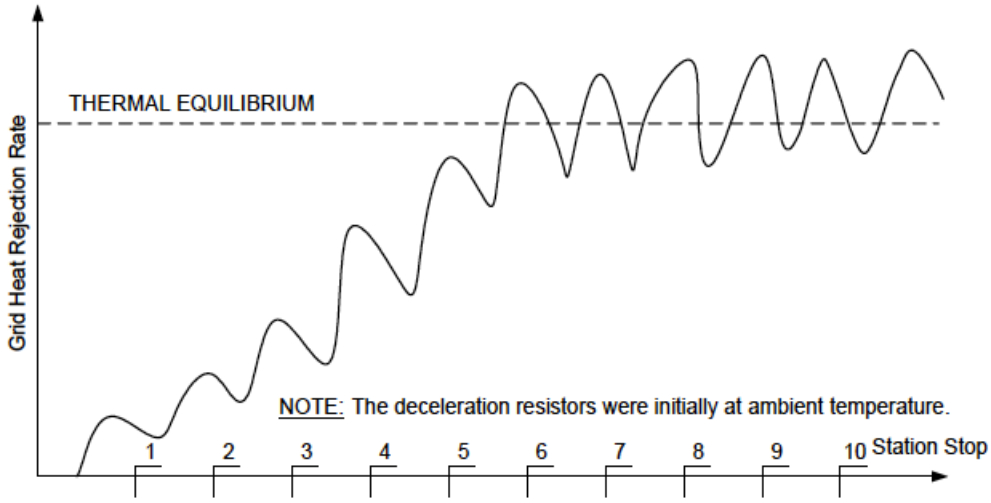

Figure A.12: Deceleration Resistor Grid Heat Rejection Pattern (SES, 2001).

A.10 IDA Temperature and Humidity Equations

Evaporation Model

Water seepage through the soil is a common phenomena particularly in areas that experience rain falls and are rich in water sources both underground and overground, and it is effected by several factors including soil type, rain fall, vegetation cover and temperature (Smethurst et al., 2012). Typical concrete mixtures used in the construction of the underground tunnels and stations have very small permeability to water (SES, 2001). The main cause of moisture in the underground system is due to water seepage through cracks and joints in the tunnel. This moisture exchanges heat with the tunnel air and contributes to the latent heat transfer through evaporation. The model assumes that the moisture supply to the evaporating surface is sufficient to maintain surface wetness and that the heat transfer with the evaporating surface occurs solely by convection while heat transfer with the tunnel wall and via radiation is assumed negligible. Moisture mass transfer rate to the surface balances the convective heat transfer such that the saturated surface temperature remains constant and equal to the wet bulb temperature. Based on these assumption the rate of evaporation is given as:

$$\lambda \dot{m} = h_c A_w (T_{DB} - T_{WB}) \tag{A.38}$$

Where A_w is the wetted surface area of the tunnel.

Temperature Model

As explained previously temperature in the subway system is computed based on subsegment divisions, where each one has a uniform cross sectional area, air temperature and wall temperature. From the air flow calculations the positive direction of the flow is determined such that the air flows from the backward boundary of the subsegment towards the forward boundary as seen in Figure A.13. Air having temperature T_{i-1} at subsegment $i-1$ enters subsegment i that has air temperature T_i, then enters subsegment $i+1$ that has temperature T_{i+1}.

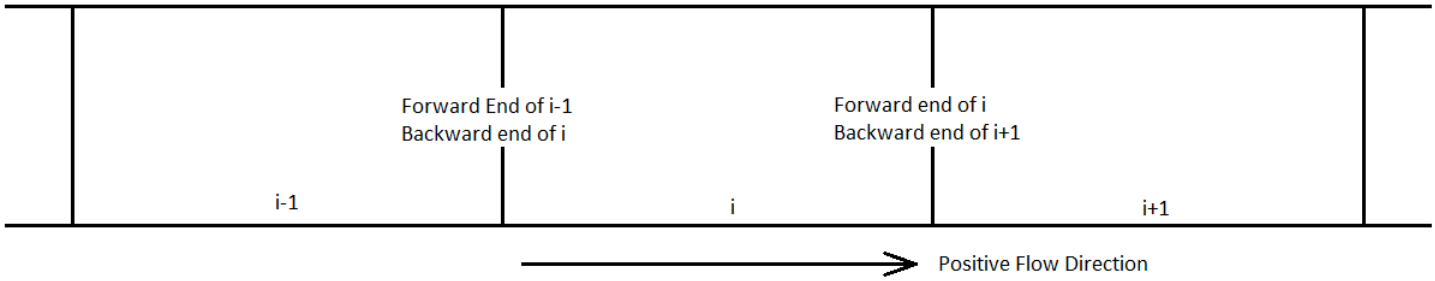

Figure A.13: Schematic of thermodynamic subsegments.

By performing an energy balance for a subsegment, a differential equation is developed that describes the temperature in subsegment i as a result of air flow entering and exiting the subsegment, heat exchanges with the tunnel surface, and heat added or removed due to heat sources and HVAC. The differential equation describing this energy balance is:

$$\frac{d}{dt}(M_i C_p T_i) = M_{p,i-1} C_p T_{i-1} + M_{p,i+1} C_p T_{i+1} - (M_{p,i} + M_{n,i}) C_p T_i + q_i - h_{wi} A_{wi} (T_i - T_{wi}) \tag{A.39}$$

Equation (A.39) is rewritten to give the rate of change of temperature in the subsegment by differentiating the left side terms:

$$\frac{dT_i}{dt} = \frac{M_{p,i-1} T_{i-1}}{M_i} + \frac{M_{n,i+1} T_{i+1}}{M_i} - \frac{(M_{p,i} + M_{n,i}) T_i}{M_i} + \frac{q_i}{M_i C_p} - \frac{h_{wi} A_{wi} (T_i - T_{wi})}{M_i C_p} - \frac{\frac{dM_i}{dt} T_i}{M_i} \tag{A.40}$$

Through integrating equation (A.40) the subsegment air temperature is calculated over a time step ΔT to give:

$$\int_t^{t+\Delta t} \frac{d}{dt}(M_i C_p T_i)dt = C_p \int_t^{t+\Delta t} M_{p,i-1}T_{i-1}dt + C_p \int_t^{t+\Delta t} M_{n,i+1}T_{i+1}dt - C_p \int_t^{t+\Delta t} (M_{p,i} + M_{n,i})T_i dt + \int_t^{t+\Delta t} q_i dt - \int_t^{t+\Delta t} h_{wi}A_{wi}(T_i - T_{wi})dt \quad (A.41)$$

The time interval ΔT is taken by the model to be the minimum time required for the air to flow through the subsegment, where the thermal equation about a subsegment is assumed at steady state.

Since computing the temperature across the subway system requires solving equation (A.40) for each subsegment simultaneously, a system of equations arranged within a dynamic thermal response matrix is used for these calculations. Inorder to develop the coefficients of this matrix equation the steady state assumption between the interval ΔT is taken, where equation (A.41) is rewritten as:

$$C_p \int_t^{t+\Delta t} M_{p,i-1}T_{i-1}dt + C_p \int_t^{t+\Delta t} M_{p,i+1}T_{i+1}dt - C_p \int_t^{t+\Delta t} (M_{p,i} + M_{n,i})T_i dt + \int_t^{t+\Delta t} q_i dt - \int_t^{t+\Delta t} h_{wi}A_{wi}(T_i - T_{wi})dt = 0 \quad (A.42)$$

Over the period ΔT a bar is added in the expressions of equation (A.42) that represents the time averaged values over that time interval:

$$C_p\overline{M_{p,i-1}T_{i-1}}\Delta t + C_p\overline{M_{n,i+1}T_{i+1}}\Delta t - C_p(\overline{M_{p,i}T_i} + \overline{M_{n,i}T_i})\Delta t + \overline{q_i}\Delta t - A_{wi}\overline{h_i T_i}\Delta t + A_{wi}\overline{h_i}T_{wi}\Delta t = 0 \quad (A.43)$$

The following expressions are developed:

$$X_i = \overline{M_{p,i}T_i} + \overline{M_{n,i}T_i}\ C_{2,i} = \frac{(\overline{M_{p,i}} + \overline{M_{n,i}})\overline{T_i}}{X_i}\ C_{3,i} = \frac{\overline{h_{c,i}T_i}}{\overline{h_{c,i}}\,\overline{T_i}}\ C_{4,i} = \frac{\overline{M_{p,i}T_i}}{X_i}\ C_{5,i} = \frac{\overline{M_{n,i}T_i}}{X_i} \quad (A.44)$$

The expressions above are equated in equation (A.43) to give:

$$[C_p C_{4,i-1}]X_{i-1} + \Big[- C_p - \frac{A_{wi} h_i C_{2,i} C_{3,i}}{(\overline{M_{p,i}} + \overline{M_{n,i}})} \Big] X_i + [C_p C_{5,i+1}]X_{i+1} = -\overline{q_i} - A_{wi}\overline{h_i} T_{wi} \quad \text{(A.45)}$$

$C_{2,i}$, $C_{3,i}$, $C_{4,i}$, $C_{5,i}$ in the equation are coefficients independent of the thermal changes in the underground system during Δt.

In the temperature model the subsegments are connected by nodes that are similar by nature to the ones connecting segments and sections. These thermal nodes are categorized into three categories, where each depends on the nature of the flow. Full flow mixing occurring in nodes is called type 1, while partial mixing might occur when we have four or more subsegments connected to a single node is Type 2. Type three consists of nodes that are joined to the atmosphere.

- **Mixing Node-Type 1**

  The equation that computes the air temperature for a type 1 node as seen in (Figure A.14) is given as:

$$\overline{M_{p,i} T_i} + \overline{M_{n,j} T_m} + \overline{M_{p,k} T_k} = \overline{T_N M_{p,i}} + \overline{T_N M_{n,j}} + \overline{T_N M_{p,k}} \quad \text{(A.46)}$$

  Substituting expressions of equation (A.44) in equation (A.45)

$$C_{4,i} X_i + C_{5,j} X_j + C_{4,k} X_k = X_N \;\; where \;\; X_N = \overline{T_N M_{p,i}} + \overline{T_N M_{n,j}} + \overline{T_N M_{p,k}} \quad \text{(A.47)}$$

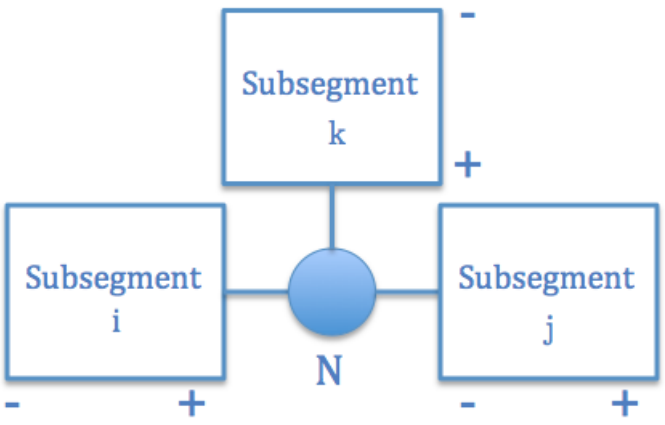

Figure A.14: Type 1 mixing node.

- **Partial Mixing Node-Type 2**

  For the case of partial mixing represented by four or more subsegments connected to a node, and the equations used for the matrix system for the case of five subsegments (Figure A.15) is given as:

$$C_{4,a}X_a + C_{5,b}X_b + C_{BA}X_B = X_A \tag{A.48a}$$

$$C_{5,d}X_d + C_{AB}X_A + C_{CB}X_C = X_B \tag{A.48b}$$

$$C_{4,f}X_f + C_{5,e}X_e + C_{BC}X_B = X_C \tag{A.48c}$$

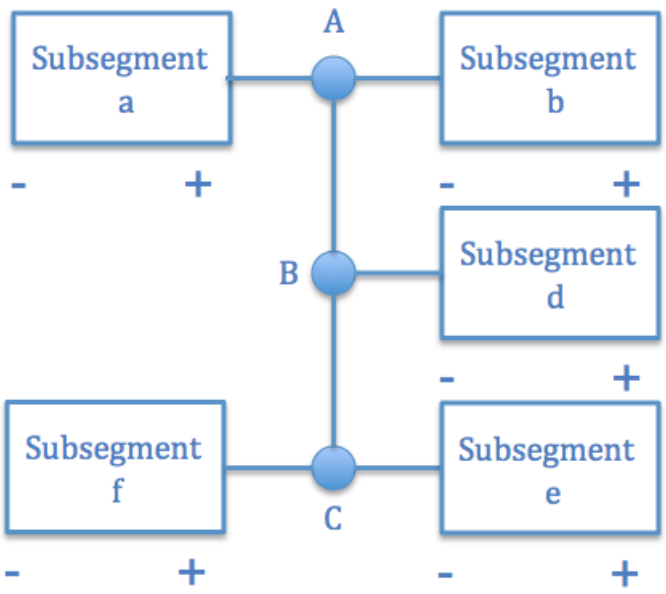

Figure A.15: Type 2 Partial mixing node with 5 subsegments and 3 subnodes A, B ,and C.

- **Boundary Node-Type 3**

  The thermal equation for the nodes connected to the subway system boundary to the outer air through vents and tunnel openings is given as:

$$X_N = \overline{M_N T_N} = \overline{M_N} T_N \tag{A.49}$$

The dynamic thermal response matrix is applied to a sample system shown in (Figure A.16) that is composed of five subsegments and four nodes. The subsegments are assigned the first equation location in the matrix followed by the nodes as displayed in Figure A.17. The first number of the subscripts on the matrix is for the equation number and the second one for the segment or node number.

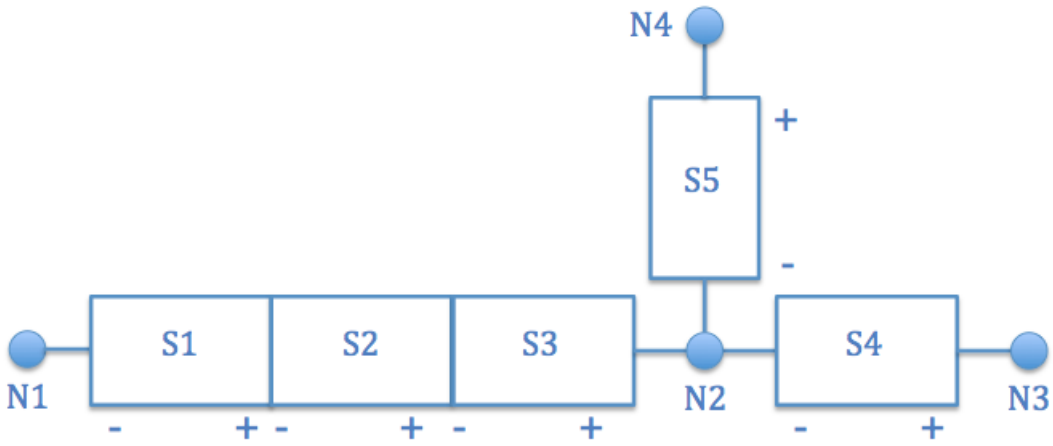

Figure A.16: Sample system for uncontrolled subsegments.

$$\begin{pmatrix} A_{11} & A_{12} & 0 & 0 & 0 & A_{16} & 0 & 0 & 0 \\ A_{21} & A_{22} & A_{23} & 0 & 0 & 0 & 0 & 0 & 0 \\ 0 & A_{32} & A_{33} & 0 & 0 & 0 & A_{37} & 0 & 0 \\ 0 & 0 & 0 & A_{44} & 0 & 0 & A_{47} & A_{48} & 0 \\ 0 & 0 & 0 & 0 & A_{55} & 0 & A_{57} & 0 & A_{59} \\ 0 & 0 & 0 & 0 & 0 & A_{66} & 0 & 0 & 0 \\ 0 & 0 & A_{73} & A_{74} & A_{75} & 0 & A_{77} & 0 & 0 \\ 0 & 0 & 0 & 0 & 0 & 0 & 0 & A_{88} & 0 \\ 0 & 0 & 0 & 0 & 0 & 0 & 0 & 0 & A_{99} \end{pmatrix} \begin{pmatrix} X_{S1} \\ X_{S2} \\ X_{S3} \\ X_{S4} \\ X_{S5} \\ X_{N1} \\ X_{N2} \\ X_{N3} \\ X_{N4} \end{pmatrix} = \begin{pmatrix} B_{S1} \\ B_{S2} \\ B_{S3} \\ B_{S4} \\ B_{S5} \\ B_{N1} \\ B_{N2} \\ B_{N3} \\ B_{N4} \end{pmatrix}$$

Figure A.17: The matrix elements of a dynamic thermal response matrix.

The thermal model also computes the quantity of sensible or latent heat that should be removed or added to maintain a zone in the subway system at a certain temperature and humidity. This is useful to size any ventilation, cooling or heating equipment in the underground. The subsegments can be either divided into uncontrolled zones and controlled zones which contain HVAC system and have temperature and humidity setpoints (Figure A.18). For calculating the required sensible load in a zone equation (A.39) is modified:

$$\begin{aligned} \frac{d}{dt}(M_i C_p T_i) = M_{p,i-1} C_p T_{i-1} + M_{n,i+1} C_p T_{i+1} - (M_{p,i} + M_{n,i}) C_p T_i + q_i \\ - h_{wi} A_{wi} (T_i - T_{wi}) + QAC_i \end{aligned} \tag{A.50}$$

Using the steady state approach over the time interval Δt discussed previously, equation (A.48) is developed for the case of a controlled zone to give:

$$\overline{QAC_i} = -C_p\overline{M_{p,i-1}T_{i-1}} - C_p\overline{M_{p,i+1}T_{i+1}} + C_p(\overline{M_{p,i}T_i} + \overline{M_{n,i}T_i}) - \overline{q_i} + A_{wi}\overline{h_iT_i} - A_{wi}\overline{h_i}T_{wi} \quad \text{(A.51)}$$

Where QAC_i is the amount of heat needed to be added or removed to subsegment i to maintain its temperature at the average temperature T_i over Δt

For the case of subsegment i that is bounded by environment controlled subsegments, equation (A.51) is modified such that T_D is the set point temperature in subsegment i:

$$\overline{QAC_i} = -C_p\overline{M_{p,i-1}T_{i-1}}\frac{T_D}{\overline{T_{i-1}}} - C_p\overline{M_{n,i+1}T_{i+1}}\frac{T_D}{\overline{T_{i+1}}} + C_p(\overline{M_{p,i}T_i} + \overline{M_{n,i}T_i})\frac{T_D}{\overline{T_i}} - \overline{q_i} + A_{wi}\overline{h_iT_i}\frac{T_D}{\overline{T_i}} - A_{wi}\overline{h_i}T_{wi} \quad \text{(A.52)}$$

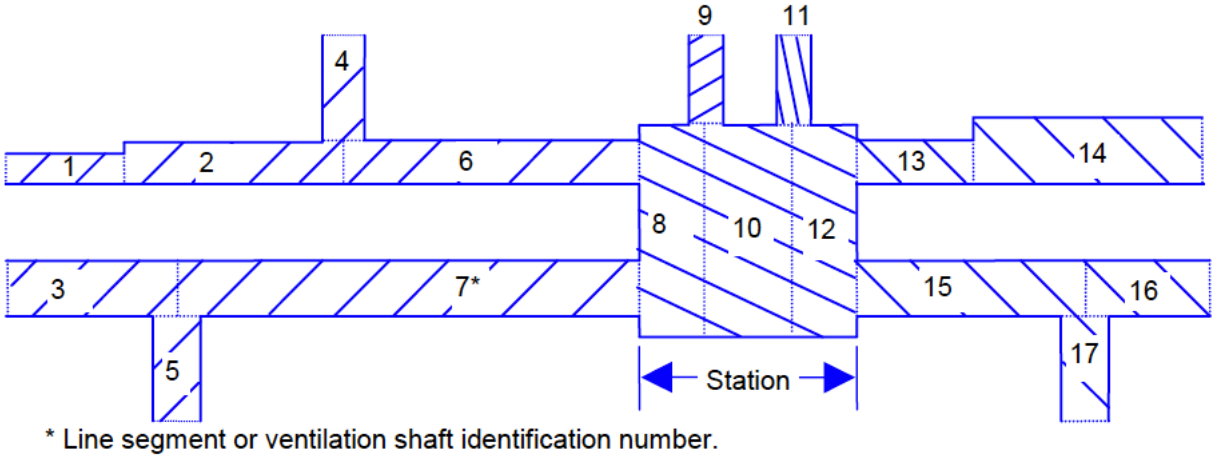

Figure A.18: Sample of environmental zones in a subway system where segments 8,10 and 12 are controlled zones and the remaining are uncontrolled (SES, 2001).

Humidity Model

The humidity model computes the specific humidity across the subway system where the assumptions are similar to the temperature model. Factors influencing the specific humidity in the subway include moisture vaporization, passengers, and HVAC systems. The humidity model adopts the same subway system geometrical components where a subsegment is the main building block. The transient equation for the specific humidity in a subsegment i (Figure A.13) is given as:

$$\frac{d}{dt}(M_iH_i) = M_{p,i-1}H_{i+1} + M_{n,i+1}H_{i+1} - (M_{p,i} + M_{n,i})H_i + w_i \quad \text{(A.53)}$$

Similar to the temperature model the humidity model solves the equations simultaneously and uses a four step Runge-Kutta numerical integration to determine the specific humidity. The

model also uses a dynamic thermal response matrix similar to the one shown in Figure A.17 to arrange the specific humidity equations. The equations of the humidity matrix equations are similar to the ones of the temperature equations, where $C_P T$ is replaced by H, q is replaced by w and h is set to zero throughout equations (A.42) to (A.48). For calculating the latent heat required to maintain a subsegment i at a setpoint specific humidity, equation (A.53) is modified to:

$$\frac{d}{dt}(M_i H_i) = M_{p,i-1} H_{i-1} + M_{n,i+1} - (M_{p,i} + M_{n,i}) H_i + w_i + WAC_i \tag{A.54}$$

Using the steady state approach over the time interval Δt discussed previously in the temperature model equation, (A.54) is developed for the case of a controlled zone to give:

$$\overline{WAC_i} = -\overline{M_{p,i-1} H_{i-1}} - \overline{M_{p,i+1} H_{i+1}} + (\overline{M_{p,i} H_i} + \overline{M_{n,i} H_i}) - \overline{w_i} \tag{A.55}$$

For the case of subsegment i that is bounded by environment controlled subsegments, equation (A.55) is modified such that H_D is the set point specific humidity in subsegment i:

$$\overline{WAC_i} = -\overline{M_{p,i-1} H_{i-1}} \frac{H_D}{\overline{H_{i-1}}} - \overline{M_{n,i+1} H_{i+1}} \frac{H_D}{\overline{H_{i+1}}} + (\overline{M_{p,i} H_i} + \overline{M_{n,i} H_i}) \frac{H_D}{\overline{H_i}} - \overline{w_i} \tag{A.56}$$

A.11 Thermodynamic Mixing in Nodes

- **Type 1 mixing node**

  The air flow's temperature and humidity leaving the node is calculated as the energy average of the temperature and humidity of the airflows entering the node. Type 1 mixing nodes are typically assigned to nodes connected to two or three subsegment, and can be expanded to encompass four or more segments. Based on Figure A.14, the mixing equation for type one nodes is developed as:

$$M_{p,i} T_i + M_{n,j} T_j + M_{p,k} T_k = T_N (M_{p,i} + M_{n,j} + M_{p,k}) \tag{A.57}$$

In case the airflow entering the node at a segment is negative, the flow rate into the node at that segment is set to zero. Thus, $M_{p,i}$, $M_{n,j}$ *and* $M_{p,k}$ are either positive or equal to zero. Equation (A.57) is integrated over the time interval Δt to give:

$$\int_t^{t+\Delta t} (M_{p,i}T_i + M_{n,j}T_j + M_{p,k}T_k)dt = \int_t^{t+\Delta t} T_N(M_{p,i} + M_{n,j} + M_{p,k})dt \qquad \text{(A.58)}$$

- **Type 2 partial mixing node** For the case where four or more subsegments are connected at a single node, the flow from one section sometimes might not fully mix with other air flow from the other subsegments. This might occur in tunnel to tunnel crossings and ventilation shafts that are connected to two separate tunnels. Type two nodes are divided into a set of three thermodynamic subnodes A, B , and C (Figure A.19), which are treated mathematically as a minor network within the node that links the adjoined subnodes in a way that reflects the actual mixing in the node. Each thermal subnode behaves individually as a type 1 mixing node and the air flows are computed in a similar manner. The aerodynamic model determines the flow direction and rate in each of the subsections, while the thermodynamic model applies the principle of continuity in each of the subnodes to determine the inter-subnode flows. The subnodes A, B and C form a flow network within the node and each of the subnodes are connected to the four or five subsegments as seen in Figure A.19.

  Based on Figure A.19, the equations for calculating the flow temperatures leaving the three subnodes are given as:

$$M_{p,a}T_a + M_{n,b}T_b + M_{BA}T_B = T_A(M_{p,a} + M_{n,b} + M_{BA}) \qquad \text{(A.59a)}$$

$$M_{n,d}T_d + M_{AB}T_A + M_{CB}T_C = T_B(M_{n,d} + M_{AB} + M_{CB}) \qquad \text{(A.59b)}$$

$$M_{p,f}T_f + M_{n,e}T_e + M_{BC}T_B = T_C(M_{p,f} + M_{n,e} + M_{BC}) \qquad \text{(A.59c)}$$

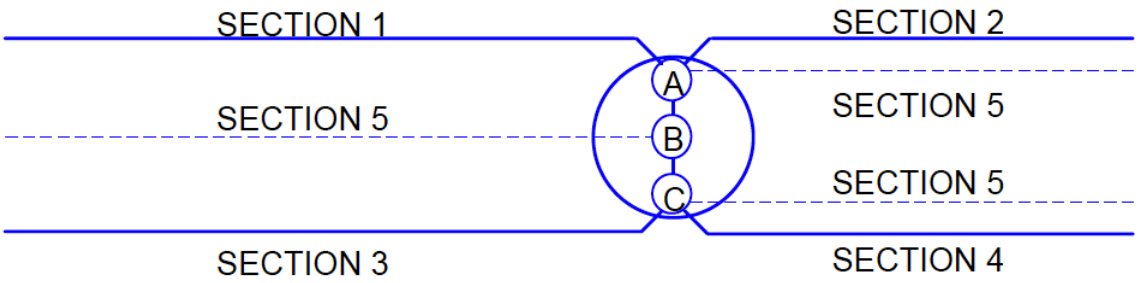

Figure A.19: A node divided into three thermal subnodes and connected to five segments (SES, 2001).

Equations (A.59a), (A.59b), and (A.59c) are integrated with respect to time over the time interval Δt to give:

$$\overline{M_{p,a}T_a} + \overline{M_{n,b}T_b} + \overline{M_{BA}T_B} = \overline{T_A M_{p,a}} + \overline{T_A M_{n,b}} + \overline{T_A M_{BA}} \tag{A.60a}$$

$$\overline{M_{n,d}T_d} + \overline{M_{AB}T_A} + \overline{M_{CB}T_C} = \overline{T_B M_{n,d}} + \overline{T_B M_{AB}} + \overline{T_B M_{CB}} \tag{A.60b}$$

$$\overline{M_{p,f}T_f} + \overline{M_{n,e}T_e} + \overline{M_{BC}T_B} = \overline{T_C M_{p,f}} + \overline{T_C M_{n,e}} + \overline{T_C M_{BC}} \tag{A.60c}$$

Where the expressions X_A, X_B and X_C are defined as:

$$X_A = \overline{T_A M_{p,a}} + \overline{T_A M_{n,b}} + \overline{T_A M_{BA}} \tag{A.61a}$$

$$X_B = \overline{T_B M_{n,d}} + \overline{T_B M_{AB}} + \overline{T_B M_{CB}} \tag{A.61b}$$

$$X_C = \overline{T_C M_{p,f}} + \overline{T_C M_{n,e}} + \overline{T_C M_{BC}} \tag{A.61c}$$

Equations (A.61a), (A.61b), and (A.61c) are rewritten into:

$$C_{4,a}X_a + C_{5,b}X_b + \frac{\overline{M_{BA}T_B}}{X_B}X_B = X_A \tag{A.62a}$$

$$C_{5,d}X_d + \frac{\overline{M_{AB}T_A}}{X_A}X_A + \frac{\overline{M_{CB}T_C}}{X_C}X_C = X_B \tag{A.62b}$$

$$C_{4,f}X_f + C_{5,e}X_e + \frac{\overline{M_{BC}T_B}}{X_B}X_B = X_C \tag{A.62c}$$

The following expressions are defined:

$$C_{BA} = \frac{\overline{M_{BA}T_B}}{\overline{T_B M_{n,d}} + \overline{T_B M_{AB}} + \overline{T_B M_{CB}}} \tag{A.63a}$$

$$C_{BC} = \frac{\overline{M_{BC}T_B}}{\overline{T_B M_{n,d}} + \overline{T_B M_{AB}} + \overline{T_B M_{CB}}} \tag{A.63b}$$

$$C_{AB} = \frac{\overline{M_{AB}T_A}}{\overline{T_A M_{p,a}} + \overline{T_A M_{n,b}} + \overline{T_A M_{BA}}} \tag{A.63c}$$

$$C_{CB} = \frac{\overline{M_{CB}T_C}}{\overline{T_C M_{p,f}} + \overline{T_C M_{n,e}} + \overline{T_C M_{BC}}} \tag{A.63d}$$

- **Type 3 boundary node** These are the nodes that are connected to one subsegment from one side and are bounded by the boundary conditions on the other side. The air that enters the subsegments from a type 3 node has the temperature and humidity specified in the boundary conditions.

A.12 Soil Heat Conduction Model Partial Differential Transient Equations

The partial differential transient equations describing the heat transfer across the two regions are:

$$\frac{\partial^2 T_1}{\partial r^2} + \frac{1}{r}\frac{\partial T_1}{\partial r} = \frac{1}{\alpha_1}\frac{\partial T_1}{\partial t} \tag{A.64a}$$

$$\frac{\partial^2 T_2}{\partial r^2} + \frac{1}{r}\frac{\partial T_2}{\partial r} = \frac{1}{\alpha_2}\frac{\partial T_2}{\partial t} \tag{A.64b}$$

Where the initial conditions are:

$$T_1(r, 0) = T_{ds} \tag{A.65a}$$

$$T_2(r, 0) = T_{ds} \tag{A.65b}$$

The system will have three boundary conditions, where the boundary condition at the wall-air interface is :

$$\overline{h}[T_{air} - T_1(R,T)] = -k_1 \frac{\partial T_1(R,T)}{\partial r} \tag{A.66a}$$

The boundary conditions at the wall-earth interface are:

$$T_1(R',t) = T_2(R',t) \tag{A.66b}$$

$$k_1 = \frac{\partial T_1(R',t)}{\partial r} = k_2 \frac{\partial T_2(R',t)}{\partial r} \tag{A.66c}$$

The boundary conditions at deep earth:

$$\lim_{r \to +\infty} T_2(r,t) = T_{ds} \tag{A.66d}$$

$$T_2(+\infty,t) = T_{ds} \tag{A.66e}$$

Equations (A.64a) and (A.64b) are simplified by applying the principle of superposition, where the heat conduction problem is divided into three sub problems such that the temperature for regions I and II is given as:

$$T_1 = T_{11} + T_{12} + T_{13} \tag{A.67a}$$

$$T_2 = T_{21} + T_{22} + T_{23} \tag{A.67b}$$

Where T_{11} is the transient component for the wall temperature, T_{12} the annual wall temperature component, and T_{13} the diurnal wall temperature component for region I. This applies for T_{21}, T_{22}, and T_{23} for the earth temperature in region II. The equations, initial, and boundary conditions for the three components in regions I and II are described.

- **Transient Component**

$$\frac{\partial^2 T_{11}}{\partial r^2} + \frac{1}{r}\frac{\partial T_{11}}{\partial r} = \frac{1}{\alpha_1}\frac{\partial T_{11}}{\partial t} \tag{A.68a}$$

$$\frac{\partial^2 T_{21}}{\partial r^2} + \frac{1}{r}\frac{\partial T_{21}}{\partial r} = \frac{1}{\alpha_2}\frac{\partial T_{21}}{\partial t} \tag{A.68b}$$

The initial conditions are:

$$T_{11}(r,0) = T_{ds} \tag{A.68c}$$

$$T_{21}(r,0) = T_{ds} \tag{A.68d}$$

The boundary conditions at the wall-air interface is:

$$\overline{h}[T_{ann.avg} - T_{11}(R,T)] = -k_1 \frac{\partial T_{11}(R,T)}{\partial r} \tag{A.68e}$$

The boundary conditions at the wall-earth interface is:

$$T_{11}(R',t) = T_{21}(R',t) \tag{A.68f}$$

$$k_1 = \frac{\partial T_{11}(R',t)}{\partial r} = k_2 \frac{\partial T_{21}(R',t)}{\partial r} \tag{A.68g}$$

The boundary conditions at deep earth:

$$T_{21}(+\infty,t) = T_{ds} \tag{A.68h}$$

- **Annual Periodic Component**

$$\frac{\partial^2 T_{12}}{\partial r^2} + \frac{1}{r}\frac{\partial T_{12}}{\partial r} = \frac{1}{\alpha_1}\frac{\partial T_{12}}{\partial t} \tag{A.69a}$$

$$\frac{\partial^2 T_{22}}{\partial r^2} + \frac{1}{r}\frac{\partial T_{22}}{\partial r} = \frac{1}{\alpha_2}\frac{\partial T_{22}}{\partial t} \tag{A.69b}$$

The initial conditions are:

$$T_{12}(r,0) = 0 \tag{A.69c}$$

$$T_{22}(r,0) = 0 \tag{A.69d}$$

The boundary conditions at the wall-air interface is:

$$\overline{h}[A_{ann.} sin(\omega_{an.} t) - T_{12}(R,T)] = -k_1 \frac{\partial T_{12}(R,T)}{\partial r} \tag{A.69e}$$

The boundary conditions at the wall-earth interface is:

$$T_{12}(R',t) = T_{22}(R',t) \tag{A.69f}$$

$$k_1 = \frac{\partial T_{12}(R',t)}{\partial r} = k_2 \frac{\partial T_{22}(R',t)}{\partial r} \tag{A.69g}$$

The boundary conditions at deep earth:

$$T_{22}(+\infty,t) = 0 \tag{A.69h}$$

- **Diurnal Periodic Component**

$$\frac{\partial^2 T_{13}}{\partial r^2} + \frac{1}{r}\frac{\partial T_{13}}{\partial r} = \frac{1}{\alpha_1}\frac{\partial T_{13}}{\partial t} \tag{A.70a}$$

$$\frac{\partial^2 T_{23}}{\partial r^2} + \frac{1}{r}\frac{\partial T_{23}}{\partial r} = \frac{1}{\alpha_2}\frac{\partial T_{23}}{\partial t} \tag{A.70b}$$

The initial conditions are:

$$T_{13}(r, 0) = 0 \tag{A.70c}$$

$$T_{23}(r, 0) = 0 \tag{A.70d}$$

The boundary conditions at the wall-air interface is:

$$\overline{h}[A_{di} sin(\omega_{di} t) - T_{13}(R, T)] = -k_1 \frac{\partial T_{13}(R, T)}{\partial r} \tag{A.70e}$$

The boundary conditions at the wall-earth interface is:

$$T_{13}(R', t) = T_{23}(R', t) \tag{A.70f}$$

$$k_1 = \frac{\partial T_{13}(R', t)}{\partial r} = k_2 \frac{\partial T_{23}(R', t)}{\partial r} \tag{A.70g}$$

The boundary conditions at deep earth:

$$T_{23}(+\infty, t) = 0 \tag{A.70h}$$

A.13 Heat and Mass Transfer between the Train Compartment and the Tunnel Equations

The air exchange rate through the train's doors R_d is approximated as a case of single side ventilation through open windows, in which the flow rate is given to be (Warren and Parkins, 1985) :

$$Q_D = 0.1 A_D U_L \tag{A.71}$$

The heat and mass transfer due to mixing between the internal and external air $Q_{V(i,e)}$ is calculated as:

$$Q_{V(i,e)} = \frac{R_a}{3600 V_c \rho_a c_a}(T_i - T_e) \tag{A.72}$$

The rate of heat generated inside the train carriage Q_g is the summation of the heat generated by the passengers Q_P and the lights Q_{lights}. Q_P depends on the number of passengers in the train and the percentage that is seated and standing since their metabolic rates vary. Q_{lights} depends on the quantity of lights and their heat release per unit. The interaction between occupants and the surrounding regarding heat and moisture is based on the three equations from ISO / DIS 7730 standards (IDA, 2013).

$$Q_{P(conv)} = S_P N_P 1.8(f_{cl}.h_{cl}(T_{cl} - T_{comp} + 0.0014 MET 58(34 - T_{comp})) \tag{A.73}$$

$$Q_{P(rad)} = 3.96x10^{-8} S_P N_P f_{cl}((T_{cl} + 273.15)^4 - (T_{comp} + 273.15)^4) \tag{A.74}$$

$$Q_P = Q_{P(conv)} + Q_{P(rad)} \tag{A.75}$$

The latent heat due to the mixing of the inner air with the outer air $Q_{L(i,e)}$ is calculated as:

$$Q_{L_{ie}} = \frac{R_a}{3600 V_c h_{fg}}(C_i - C_e) \tag{A.76}$$

The latent heat generated by the passengers depend on the amount of water vapor released by respiration, which is the rate at which humidity is added to the internal air C_g. A seated or standing person exhales an average of 0.72 grams of water per minute (Cain et al., 1989). The humidity ratio generated by the passengers in the carriage is calculated as:

$$C_g = \frac{0.72}{1000 V_c \rho_a} \tag{A.77}$$

The latent heat generated by the passengers $Q_{L(p,i)}$ is calculated as:

$$Q_{L(p,i)} = V_c h_{fg} C_g \tag{A.78}$$

Appendix B

Train Carriage Model

B.1 Rail Carriage Model

The convection heat transfer coefficient of the internal and external air with the train cover h_i and h_e depends on the type of convection. The convection can be natural, forced , or a mix between the two. The Nusselt number for forced convection is given for laminar and turbulent flows respectively as (Monteith, 1990):

$$Nu = 0.66Re^{0.5}Pr^{0.33} \tag{B.1a}$$

$$Nu = 0.036Re^{0.8}Pr^{0.33} \tag{B.1b}$$

The free convection coefficient for laminar and turbulent flow is given as:

$$Nu = 0.54(Gr.Pr)^{0.25} \tag{B.2a}$$

$$Nu = 0.15(Gr.Pr)^{0.33} \tag{B.2b}$$

In forced convection the flow and thickness of the laminar or turbulent boundary layer is related to the Reynolds number Re which is calculated as:

$$Re = \frac{\rho_a V_a L_c}{\mu_a} \tag{B.3}$$

In free convection the flow and the thickness of the laminar or turbulent boundary layer is related to the Grashof number Gr which is calculated as:

$$Gr = \frac{\beta.g.d^3.|T_{sd} - T_b|}{v'^2} \tag{B.4}$$

where T_{sd} is the solid surface temperature and T_b the bulk fluid temperature. The Prandtl number Pr for air at room temperature is 0.7.

To determine which convection type is occurring in the convective heat exchange, the ratio $\frac{Gr}{Re^2}$ is compared, where if it is > 15 natural convection occurs and if it is < 0.1 forced convection occurs and any value in between is considered mixed convection (Figure B.1). For mixed convection the Nusselt number for both forced and natural convection is calculated and the highest value is adopted. The convective heat coefficient is related to Nu by the following formula:

$$h = \frac{Nu.\lambda_a}{L} \tag{B.5}$$

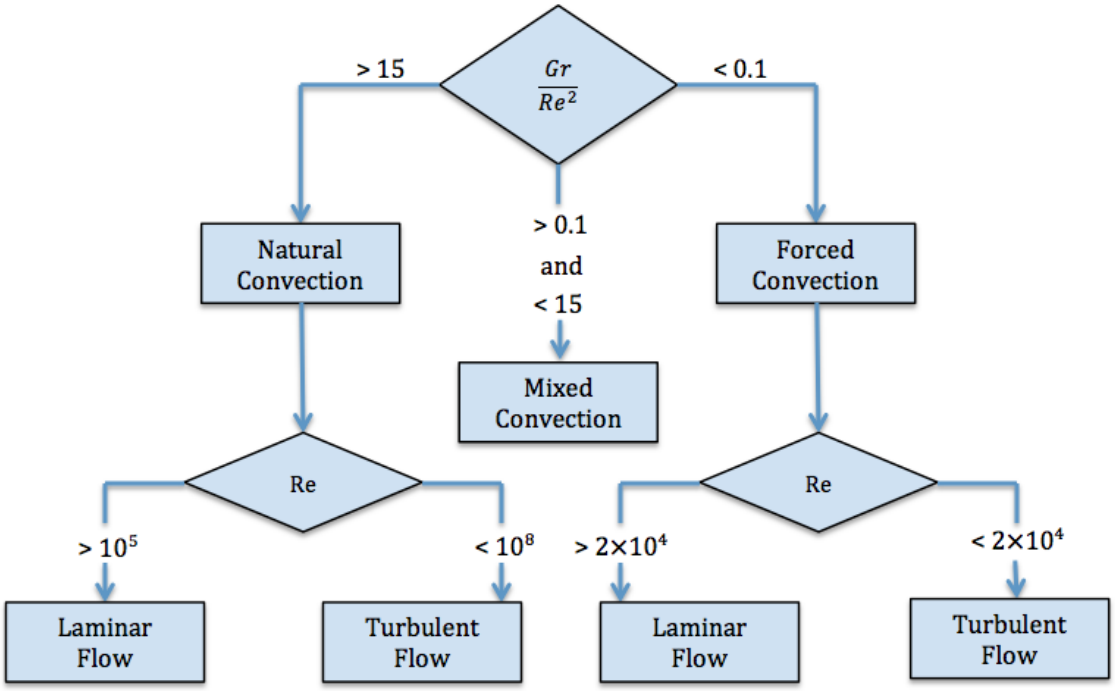

Figure B.1: Flow chart for determining convection mode and flow type (Monteith, 1990).

The convective heat transfer between the carriage's wall and window and the inner and external air $Q_{V(i,w)}$, $Q_{V(i,g)}$, $Q_{V(w,e)}$ and $Q_{V(g,e)}$ is given respectively as:

$$Q_{V(w,i)} = h_i A_w (T_w - T_i) \tag{B.6a}$$

$$Q_{V(g,i)} = h_i A_g (T_g - T_i) \tag{B.6b}$$

$$Q_{V(w,e)} = h_e A_w (T_w - T_e) \tag{B.6c}$$

$$Q_{V(g,e)} = h_e A_g (T_g - T_e) \tag{B.6d}$$

$c_w{}'$ and $c_g{}'$ are the heat capacities per unit area of the train wall and window respectively, which differ between one train and another depending on the type of the train.

In rare cases there is a probability of water condensing on the surface of the train cover, which happens if the temperature of the air is saturated and the cover's temperature is lower than the dupoint temperature of the air. The latent heat transfer by condensation on the wall $Q_{P(i,w)}$ and window $Q_{P(i,g)}$ is given as:

$$Q_{P(i,w)} = \frac{A_w h_{fg}}{c_{va}} Le^{-0.75} h_i (C_i - C_{isat}) \tag{B.7a}$$

$$Q_{P(i,g)} = \frac{A_g h_{fg}}{c_{va}} Le^{-0.75} h_i (C_i - C_{isat}) \tag{B.7b}$$

where C_i is the humidity of the internal air and C_{isat} is the saturated internal air humidity and c_{va} the heat capacity of humid air.

The most accurate methods to determine clothing ensemble resistances is through measurements on heated mannequins and on active subjects (ASHRAE, 2010). However, for practicality design tables provide an estimate of clothing ensemble resistances such as the one provided in Figure B.2. Clothing resistance value can be expressed in the unit clo with I_{cl} symbol associated with the resistance value in clo, where the relation between typical resistance unit and I_{cl} is $R_{cl} = 0.155 I_{cl}$. The clothing area factor f_{cl} that is used in the PMV equation is calculated as:

$$\mathrm{f}_{cl} = \begin{cases} 1.00 + 1.29 R_{cl} & \text{for } I_{cl} \leq 0.078\, m^2 C/W \\ 1.05 + 0.645 R_{cl} & \text{for } I_{cl} > 0.078\, m^2 C/W \end{cases} \tag{B.8}$$

The rate of work done during a physical activity is taken into consideration through the metabolic rate M and the mechanical work W done during the activity. However, W is neglected since its value is small compared to M. (ASHRAE, 2010) indicates shown that the ratio W/M is almost zero for most activities and it is unusual for it to reach more than 0.05 to 0.1. Metabolic rate varies depending on the person's activity and conditions (ASHRAE, 2010). Typically the metabolic rate is expressed in a unit called *met* where $1\,met = 58.1\,W/m^2$. The estimated metabolic rates per m^2 for a variety of activities is provided in Figure B.3 where it is multiplied by the average surface area of a person $A_D = 1.8\,m^2$ to get the overall metabolic rate.

Ensemble Description[a]	I_{cl} (clo)	I_t^b (clo)	f_{cl}	i_{cl}	i_m^b
Walking shorts, short-sleeved shirt	0.36	1.02	1.10	0.34	0.42
Trousers, short-sleeved shirt	0.57	1.20	1.15	0.36	0.43
Trousers, long-sleeved shirt	0.61	1.21	1.20	0.41	0.45
Same as above, plus suit jacket	0.96	1.54	1.23		
Same as above, plus vest and T-shirt	1.14	1.69	1.32	0.32	0.37
Trousers, long-sleeved shirt, long-sleeved sweater, T-shirt	1.01	1.56	1.28		
Same as above, plus suit jacket and long underwear bottoms	1.30	1.83	1.33		
Sweat pants, sweat shirt	0.74	1.35	1.19	0.41	0.45
Long-sleeved pajama top, long pajama trousers, short 3/4 sleeved robe, slippers (no socks)	0.96	1.50	1.32	0.37	0.41
Knee-length skirt, short-sleeved shirt, panty hose, sandals	0.54	1.10	1.26		
Knee-length skirt, long-sleeved shirt, full slip, panty hose	0.67	1.22	1.29		
Knee-length skirt, long-sleeved shirt, half slip, panty hose, long-sleeved sweater	1.10	1.59	1.46		
Same as above, replace sweater with suit jacket	1.04	1.60	1.30	0.35	0.40
Ankle-length skirt, long-sleeved shirt, suit jacket, panty hose	1.10	1.59	1.46		
Long-sleeved coveralls, T-shirt	0.72	1.30	1.23		
Overalls, long-sleeved shirt, T-shirt	0.89	1.46	1.27	0.35	0.40
Insulated coveralls, long-sleeved thermal underwear, long underwear bottoms	1.37	1.94	1.26	0.35	0.39

Figure B.2: Typical Insulation and permeability values for clothing ensembles (ASHRAE, 2010).

Activities

	W/m^2	met*
Resting		
Sleeping	40	0.7
Reclining	45	0.8
Seated, quiet	60	1.0
Standing, relaxed	70	1.2
Walking (on level surface)		
3.2 km/h (0.9 m/s)	115	2.0
4.3 km/h (1.2 m/s)	150	2.6
6.4 km/h (1.8 m/s)	220	3.8
Office Activities		
Reading, seated	55	1.0
Writing	60	1.0
Typing	65	1.1
Filing, seated	70	1.2
Filing, standing	80	1.4
Walking about	100	1.7
Lifting/packing	120	2.1
Driving/Flying		
Car	60 to 115	1.0 to 2.0
Aircraft, routine	70	1.2
Aircraft, instrument landing	105	1.8
Aircraft, combat	140	2.4
Heavy vehicle	185	3.2
Miscellaneous Occupational Activities		
Cooking	95 to 115	1.6 to 2.0
Housecleaning	115 to 200	2.0 to 3.4
Seated, heavy limb movement	130	2.2
Machine work		
sawing (table saw)	105	1.8
light (electrical industry)	115 to 140	2.0 to 2.4
heavy	235	4.0
Handling 50 kg bags	235	4.0
Pick and shovel work	235 to 280	4.0 to 4.8
Miscellaneous Leisure Activities		
Dancing, social	140 to 255	2.4 to 4.4
Calisthenics/exercise	175 to 235	3.0 to 4.0
Tennis, singles	210 to 270	3.6 to 4.0
Basketball	290 to 440	5.0 to 7.6
Wrestling, competitive	410 to 505	7.0 to 8.7

Figure B.3: Typical metabolic heat generation for various activities (ASHRAE, 2010).

The convective heat transfer is typically caused by air movement within the occupational space or that of the body. Several equations for calculating the convective heat transfer coefficient h_c for a variety of cases are provided in provided in Figure B.4, while the general equation by (Fanger, 1970a) is given as:

$$\mathrm{h}_c = \begin{cases} 2.38(T_{cl} - t_a)^{0.25} & \text{for } 2.38(T_{cl} - t_a)^{0.25} > 12.1\sqrt{v_{ar}} \\ 12.1\sqrt{v_{ar}} & \text{for } 2.38(T_{cl} - t_a)^{0.25} < 12.1\sqrt{v_{ar}} \end{cases} \quad \text{(B.9)}$$

The surface temperature of the clothing T_{cl} is calculated by the following equation (Fanger, 1970a) :

$$\mathrm{T}_{cl} = 35.7 - 0.028(M - W) - I_{cl}\Big[(3.96 * 10^{-8}) f_{cl}[(T_{cl} + 273)^4 - (\bar{t}_r + 273)^4 + f_{cl} h_c (T_{cl} - t_a)\Big] \quad \text{(B.10)}$$

Equation	Limits	Condition	Remarks/Sources
$h_c = 8.3V^{0.6}$ $h_c = 3.1$	$0.2 < V < 4.0$ $0 < V < 0.2$	Seated with moving air	Mitchell (1974)
$h_c = 2.7 + 8.7V^{0.67}$ $h_c = 5.1$	$0.15 < V < 1.5$ $0 < V < 0.15$	Reclining with moving air	Colin and Houdas (1967)
$h_c = 8.6V^{0.53}$	$0.5 < V < 2.0$	Walking in still air	V is walking speed (Nishi and Gagge 1970)
$h_c = 5.7(M - 0.8)^{0.39}$	$1.1 < M < 3.0$	Active in still air	Gagge et al. (1976)
$h_c = 6.5V^{0.39}$	$0.5 < V < 2.0$	Walking on treadmill in still air	V is treadmill speed (Nishi and Gagge 1970)
$h_c = 14.8V^{0.69}$ $h_c = 4.0$	$0.15 < V < 1.5$ $0 < V < 0.15$	Standing person in moving air	Developed from data presented by Seppanen et al. (1972)

Note: h_c in W/(m^2·K), V in m/s, and M in mets, where 1 met = 58.1 W/m^2.

Figure B.4: Equations for convection heat transfer coefficients (ASHRAE, 2010).

1992 Tube Stocks

Central line

Built by ABB Transportation, Derby 1991-1994
Entered service Central line 1993-1995
Maintained by: Metronet Rail BCV

Principal characteristics

Track gauge:	4ft 8½ ins/1435mm
Current system:	630V dc 3rd and 4th rail, floating earth
Types of vehicle:	Driving Motor (DM) – car type 'A' Non-Driving Motor (NDM) – car types 'B' or 'C' De-icing Non-Driving Motor (NDM) – car type 'D'
Formation per unit:	Two cars, formed A-B, B-C or B-D
Formation per train:	Eight cars, in any one of 36 combinations of A-B, B-C and B-D two car units, with 'A' type car always at outer ends.
Number of train:	85 eight-car trains.
Operation:	Fully Automatic (A.T.O.). Non-automatic driving (coded manual (A.T.P.)). Emergency driving (slow manual) Doors operated by the train operator in leading cab. One person operated.

Equipment details

Bodies:	Constructed by using welded aluminium extrusions. Pneumatically-operated sliding doors, externally hung. Exterior painted in London Underground corporate red, white and blue livery.
Bogies:	H-frame type bogies without headstocks, for welded steel-box section, built by Kawasaki Heavy Industries, Japan. Wheel diameter 700mm.
Couplers:	London Underground Automatic Wedgelock between units, semi-permanent bar between cars within a unit.
Traction system:	Brush Traction/ABB G.T.O. thyristor, dc chopper control with all axles motor by Brush Electrical Machines type LT130, frame-mounted traction motors with 21/136 gearbox ratio.
Compressors:	Westinghouse Type V.R.S.20 (reciprocating).
Brakes:	Fully blended dynamic regenerative rheostatic and E.P. brake with slip/slide protection. Automatic controlled spring applied, air-released parking brakes.
Auxiliary power supplies:	A.B.B./Brush Electrical Machines static converter, one per 2-car unit.
Main lighting:	Fluorescent tubes fed by inverters from 50V dc – 26 per car
Emergency lighting:	As main lighting, but remains lit when line supply fails. 4 fluorescent tubes per DM, 6 per NDM (additional to main lighting).

Figure B.5: 1992 tube stock train model technical details used for the Central Line: Part 1 (Tfl, 2007).

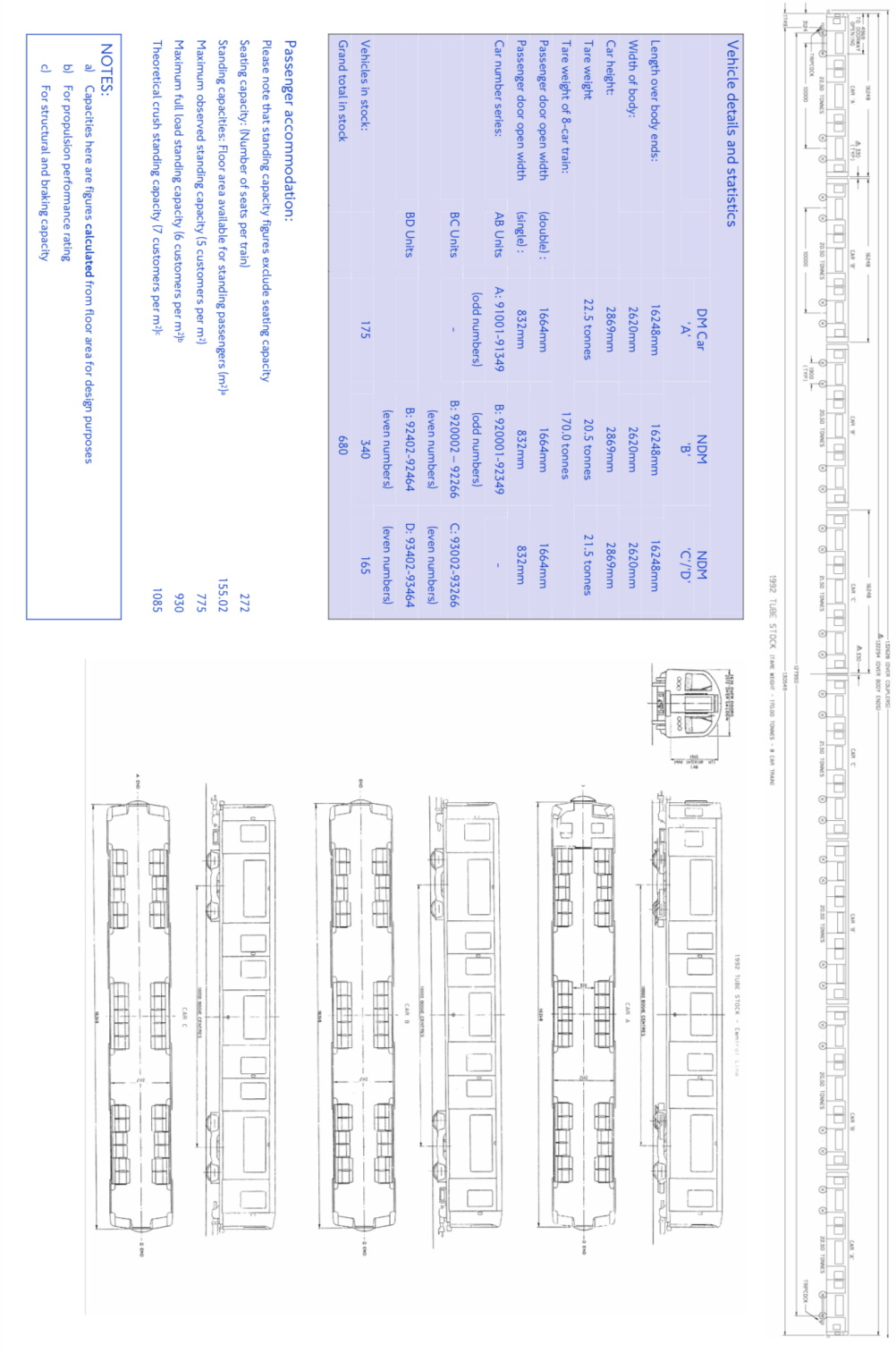

Vehicle details and statistics

	DM Car 'A'	NDM 'B'	NDM 'C'/'D'
Length over body ends:	16248mm	16248mm	16248mm
Width of body:	2620mm	2620mm	2620mm
Car height:	2869mm	2869mm	2869mm
Tare weight	22.5 tonnes	20.5 tonnes	21.5 tonnes
Tare weight of 8-car train:		170.0 tonnes	
Passenger door open width (double):	1664mm	1664mm	1664mm
Passenger door open width (single):	832mm	832mm	832mm
Car number series: AB Units	A: 91001-91349 (odd numbers)	B: 92001-92349 (odd numbers)	-
BC Units	-	B: 92002 – 92266 (even numbers)	C: 93002-93266 (even numbers)
BD Units		B: 92402-92464 (even numbers)	D: 93402-93464 (even numbers)
Vehicles in stock:	175	340	165
Grand total in stock		680	

Passenger accommodation:

Please note that standing capacity figures exclude seating capacity

Seating capacity: (Number of seats per train)	272
Standing capacities: Floor area available for standing passengers (m^2)[b]	155.02
Maximum observed standing capacity (5 customers per m^2)	775
Maximum full load standing capacity (6 customers per m^2)[b]	930
Theoretical crush standing capacity (7 customers per m^2)[c]	1085

NOTES:

a) Capacities here are figures **calculated** from floor area for design purposes

b) For propulsion performance rating

c) For structural and braking capacity

Figure B.6: 1992 tube stock train model technical details used for the Central Line: Part 2 (Tfl, 2007).

Bibliography

Adam, D. and Markiewicz, R. (2009). Energy from earth-coupled structures, foundations, tunnels and sewers. *Gotechnique*, 59(No. 3):229236.

AHGI (2018). Applied hydrology geothermal innovation. http://underground-energy.com/our-technology/btes/.

Aidbi, O., Kazeipour, A., Farhanieh, B., and Afshin, H., editors (2011). *Numerical Simulation of New Ventilation Approuch for Underground Stations*, volume 28.

Al-Khoury, R. and Bonnier, P. (2006). Efficient finite element formulation for geothermal heating systems. part ii: transient. *International Journal of Numerical Methods in Engineering*, 67(5):725 – 745.

Al-Khoury, R., Bonnier, P., and Brinkgreve, R. (2005). Efficient finite element formulation for geothermal heating systems Part I: steady state. *International Journal of Numerical Methods in Engineering*, 63(7):988 – 1013.

Ampofo, F., Maidment, G., and Missenden, J. (2003). Underground railway environment in the uk part 1: Review of thermal comfort. *Applied Thermal Engineering*, 24:611–631.

Ampofo, F., Maidment, G., and Missenden, J. (2004a). Underground railway environment in the UK Part 2: Investigation of heat load. *Applied Thermal Engineering*, 2:633–645.

Ampofo, F., Maidment, G., and Missenden, J. (2004b). Underground railway environment in the UK Part 2: Invetigation of heat load. *Applied Thermal Engineering*, 24:633–645.

Ampofo, F., Maidment, G., and Missenden, J. (2004c). Underground railway environment in the UK Part 3: Investigation of heat load. *Applied Thermal Engineering*, 2:63–645.

Arkell, B. P. and Darch, G. J. (2006). Impact of climate change on London's transport systems. Technical report, Atkins.

Arnfield, A. (2003). Two decades of urban climate research: A review of turbulence, exchanges of energy and water, and the urban heat island. *International Journal of Climatology*, 23:1–26.

ASHRAE (2002). Rail passenger vehicle guideline published by ashra. *HVAC*. ASHRAE 55-2013.

ASHRAE (2010). *ASHRAE HVAC applications Thermal Comfort*. ANSI/ASHRAE Standard 55.

ATOC (2014). Key train requirements. Technical Report Third Issue, Association of Train Operating Companies, London.

Bandos, T., Montero, A., Fernandez, E., Santander, J., Isidro, J., and Perez, J. (2009). Finite line source model for borehole heat exchangers: effect of vertical temperature variations. *Geothermics*, 38:263 – 270.

BBC (2006). Baking hot at baker street. `http://news.bbc.co.uk/1/hi/england/london/5191604.stm`.

Bell, C. and Watts, A. (1971). Thermal limits for industrial workers. *Med*, 28:259 264.

Bernier, M., Pinel, A., Labib, P., and Paillot, R. (2004). A multiple load aggregation algortihm for annual hourly simulations of gchp systems. *HVAC&R Res.*, 10:471–487.

Blum, P., Campillo, G., Munch, W., and Kolbel, T. (2010). Co2 savings of ground source heat pump systems a regional analysis. *Renewable Energy*, 35:122 – 127.

bombardier (2013). `http://www.bombardier.com/en/transportation/projects/`.

Booth, W. and Galliers, S. (2001). Quality environments for public transport buildings.

Botelle, M., Payne, K., and Redhead, B. (2010). Squeezing the heat out of London's tube. *Proceedings of the ICE Civil Engineering*, Volume 163(Issue 3):114 – 122.

Brandl, H. (2006). Energy foundation and other thermo-active ground structures. *Gotechnique*, 56(No. 2):81–122.

Brandl, H., Adam, D., Markiewicz, R., Utenberger, W., and Hofinger, H. (2010). Massivabsorbertechnologie zur erdwarmenutzung bei der wiener u-bahnlinie u2. *Ingenieur-und Architekten-Zeitschrift*, Vol. 155(No 7-9):10–12, 1–7.

BRE (2004a). Understanding thermal comfort on london underground trains and stations summer survey. Technical Report 211738, Building Research Establishment, London. Report by the Building Research Establishment for London Underground Limited.

BRE (2004b). Understanding thermal comfort on trains and stations. Technical Report 216996, London Underground Limited B.

Brinckerhoff, Parsons Associated Engineers, Quade Douglas Inc., Deleuw Cather, Company, and Kaiser Engineers (1976). Subway environmental design handbook, volume i. Technical report, Transit Development Corporation.

Burzynski, R., Crane, M., Yao, R., and Becerra, V. (2011). Heat demand analysis of residential development in London connected to district heating scheme. In *TSBE EngD Conference*, volume 5th. University of Reading.

Busby, J., Lewis, M., Reeves, H., and Lawley, R. (2009). Initial geological considerations before installing ground source heat pump systems. Technical report, British Geological Survey.

Cain, J. B., Livingstone, S. D., Nolan, R. W., and Keefe, A. A. (1989). Measurement of respiratory air temperature and calculation of respiratory heat loss when working at various ambient temperature. Technical report, Defense Research Establishment Ottawa, Ottawa, Canada.

Carslaw, H. S. and Jeager, J. C. (1959). *Conduction of Heat in Solids*. Oxford Press, Oxford, second edition edition.

Casasso, A. and Sethi, R. (2013). Efficiency of closed loop geothermal heat pumps: A sensitivity analysis. *Renewable Energy*, 62:737–746.

CIBSE (2012). *Energy Effeciency in Buildings*. The Chartered Institution of Building Services Engineering, London, third edition.

Colella, F., Rein, G., Borchiellini, R., Carvel, R., Torero, J., and Verda, V. (2009). Calculation and design of tunnel ventilation systems using a two-scale modelling approach. *Building and Environment*, 44:2357–2367.

Connolly, D., Lund, H., Mathiesen, B. V., and Leahy, M. (2010). A review of computer tools for analysing the integration of renewable energy into various energy systems. *Applied Energy*, 87:1059–1082.

Crossrail (2016). Europe's largest construction project. http://www.crossrail.co.uk/construction/.

Cui, P., Yang, H., and Fang, Z. H. (2006). Heat transfer analysis of ground heat exchangers with inclined boreholes. *Appl. Therm. Eng.*, 26:1169–1175.

Davies, J. V. (1912). Air resistance to trains in tube tunnels. *American Society of Civil Engineers*.

DECC (2011). *The Micro-Generation Installation Standard. MCS 022: Ground Heat Exchanger Lookup Tables. Supplementary Material to MIS 3005. Issue 1.0*. Department of Energy and Climate Change, London. page 21.

DECC (2013). Renewable heat incentive: Non-domestic scheme early tariff review. Technical report, Department of Energy and Climate Change, London.

DECC (2014a). Renewable heat incentive. http://www.energysavingtrust.org.uk/domestic/domestic/renewable-heat-incentive.

DECC (2014b). Renewable sources of energy, in: Digest of United Kingdom Energy Statistics (DUKES). Technical report, Department of Energy and Climate Change, London.

DECC (2015). National energy effeciency data framework. Technical report, Department of Energy and Climate Change, London.

DEFRA (2009). Climate change pojections. Technical report, Department for Environment, Food and Rural Affairs (DEFRA).

Di-Donna, A. and Laloui, L. (2014). Numerical analysis of the geotechnical behaviour of energy pile. *Numerical and Analytical Methods in Geomechanics*, 39:861 – 888.

Diao, N., Li, Q., and Fang, Z. . (2004). Heat transfer in ground heat exchangers with ground- water advection. *International Journal of Thermal Sciences*, 43:1203–1211.

Dierch, H., Bauer, D., Heidemann, W., Ruhaak, W., and Schatzl, P. C. G. e. (2011). Finite element modeling of borehole heat exchanger systems: Part 2. 37:1136 – 1147.

Diersch, H., Bauer, D., Heidemann, W., Ruhaak, W., and Schatzl, P. (2011). Finite element modeling of borehole heat exchanger systems: Part 1. *Fundementals of Computer Geoscience*, 37:1122–1135.

DTR (2009). Dundee tunnel research. `http://www.thermotun.com/`.

EC (2016). EU Climate Action. http://ec.europa.eu/clima/citizens/eu/index. Europian Commission.

Ellison, R., Woods, M., Allen, D., Forster, A., Pharoah, T., and King, C. (2004). Geology of london. Technical report, British Geological Survey. Special Memoir for 1:50000 Geological Sheets 256 (North London), 257 (Romford), 270 (Dartford) (England and Wales).

Elsayed, A. O. and Hariri, A. S. (2011). Effect of condenser air flow on the performance of split air conditioner. In *Low Energy Architecure*. World Renewable Energy Congress, LEA.

EQUA (2013). Road and rail tunnel ventilation and fire simulation software. Solna, Sweden.

Eskilson (1987). *Thermal Analysis of Heat Extraction Boreholes*. PhD thesis, University of Lund.

Fanger, P. O. (1970a). *Thermal Comfort*. McGraw-Hill, New York, USA.

Fanger, P. O. (1970b). *Thermal Comfort: Analysis and applications in environmental engineering*. McGraw Hill Book Company.

Fayegh, S. and Rosen, M. A. (2012). Modelling thermally interacting multiple boreholes with variable heating strength. In *World Sustainability Forum*, Oshawa, Ontario. 2nd World Sustainability Forum.

FEFLOW (2014). Element subsurface flow & transport simulation system. *White Papers*, 5.

Fiala, D., Havenish, G., Kampmann, B., and Jendritzky, G. (2011). Utci-fiala multi-node model of human heat transfer and temperature regulation. *International Journal of Biometeo- rology*, pages 1 – 13.

for London, T. (2013). Fit for the future. Technical report, Transport for London.

Fox, R. W., Mcdonald, A. T., and Pritchard, P. J. (2004). *Introduction to Fluid Mechanics*. Number 133. John Wiley & Sons, sixth edition.

Franzius, J. N. and Pralle, N. (2011). Turning segmental tunnels into sources of renewable energy. *Proceeding of ICE, Civil Engineering*, Vol. 164:35–40.

Fraunhofer (2014). Saving energy in subway stations. `http://www.fit.fraunhofer.de/en/presse/13-06-01.html`.

Fry, V. (2009). Lessons from london: regulation of open-loop ground source heat pumps in central london. *Quarterly Journal of Engineering Geology and Hydrogeology*, 42:325–34.

Garber, D., Choudhary, R., and Soga, K. (2013). Risk based lifetime costs assessment of a ground source heat pump (gshp) system design: Methodology and case study. *Building and Environment*, 60:66–80.

Gilbey, J., M., Duy, S., and Thompson, J. A. (2011). The potential for heat recovery from london underground stations and tunnels. In *CIBSE Technical Symposium*. CIBSE, Chartered Institution of Building Services Engineers.

GLA (2013). Londons zero carbon energy resource: Secondary heat.

Green, O. (1987). *The London Underground: An Illustrated History*. Ian Allan Publishing, 8th edition edition.

Griffiths, E. (2006). Baking hot at baker street. Internet.

Guan, X., Jiang, Y., and Yao, Y. (2007). Cfd simulation of a novel ventilation system of subway station in harbin. In *Building Simulation*. School of Municipal & Environmental Engineering, Harbin Institute of Technology.

Hammock, C. and Hammock, A. (2015). Underground thermal energy storage (utes).

Harris, G. L. (1973). *Aerodynamic Near Field of a Subway Train in Smooth and Rough Tunnels*. California Institute of Technology, Graduate Aeronautical Laboratories.

He, M. and Lam, H. (2017). *Study of Geothermal Seasonal Cooling Storage System with Energy Piles*. PhD thesis.

Headon, J., Banks, A., and Robinson, V. K. (2009). Regional distribution of ground temperature in the chalk aquifer of London, UK. *Quarterly Journal of Engineering Geology and Hydrogeology*, 1:313 – 323.

Hecht-Mendez, J., Giraldo-Molina, N., Blum, P., and Bayer, P. (2010). Evaluating mt3dms for heat transport simulation of closed geothermal systems. *Ground Water*, 48(5):741 – 756.

Hellstrom, G. (1991). *Thermal Analysis of Duct Storage Systems*. PhD thesis, University of Lund.

Hellstrom, G. and Sanner, B. (2000). *Earth energy designer: user manual version 2.0*.

Hikari, F., Ryuichi, I., and Takashi, I. (2004). Improvements on analytical modeling for vertical u-tube ground heat exchangers. *Geotherm. Resour Counc. Trans.*, 28:73–77.

Holman, J. P. (2010). *Heat Transfer*. McGraw-Hill, New York, USA.

Holzbecher, E. and Ruschel, H. (2014). Heat transfer in borehole heat exchangers from laminar to turbulent conditions. *COMSOL Conference*.

Hu, Z., Li, X., Zhao, X., Xiao, L., and Wu, W. (2008). Numerical analysis of factors affecting the range of heat transfer in earth surrounding three subways. *Mining Technology*, 18:67 – 71.

Huang, Y., Hong, T. H., and Kim, C. N. (2011). A numerical simulation of train induced unsteady airflow in a tunnel of seioul subway. *Mechanical Science and Technology*, 26(3):785–792.

Humphreys, M. and Nicol, J. (2002). The validity of ISO-PMV for predicting comfort votes in everyday thermal environments. *Energy Buildings*, 34:667684.

IDA (2006). Cooling the tube software comparison. Technical report, EQUA simulation AB.

IDA, T. (2013). *IDA Tunnel Application*. EQUA Simulation AB, Stockholm, Sweden, 1.1 edition.

Ingresoll, L. R. and Plass, H. J. (1948). *Theory of the ground pipe heat source for the heat pump*. Heating, Piping & Air Conditioning 20(7): 119-122.

IPlantE (2007). Rail engineering. Technical report, The Institution of Plant Engineers. Pages 9-11.

Jaffe, E. (2012). A brief history of air-conditioning on the New York subway. Internet. http://www.citylab.com/commute/2012/08/brief-history-air-conditioning-new-york-subway/2952/.

Juraeva, M., Ryu, K. J., Jeong, S.-H., and Song, D. J. (2013). Influence of mechanical ventilation-shaft connecting location on subway tunnel ventilation performance. *Wind Engineering and Industrial Aerodynamics*, 119:114–120.

Kavanaugh, S. P. (1995). A design method for commercial ground coupled heat pumps. *ASHREA Trans.*, 101:1088–1094.

Kavanaugh, S. P. and Rafferty, K. (1997). Ground-source heat pumps design of geothermalsystems for commercial and industrial buildings. Technical report, American Society of Heating, USA.

Ke, M.-T., Cheng, T.-C., and Wang, W.-P. (2002). Numerical simulation for optimizing the design of subway environmental control system. *Building and Environment*, 37:1139–1152.

Kennedy, W., Li, S., and ODwyer, T. (2000). *The development and testing of the subway environment: simulation version.*

Kim, J.-Y. and Kim, K.-Y. (2009). Effects of vent shaft location on the ventilation performance in a subway tunnel. *Wind Engineering and Industrial Aerodynamics*, 97:174–179.

KONE (2014). Energy calculation for machine room elevators. `http://download.kone.com/quick-energy/kone-quick-energy-2.swf?rdrsrc=/countries/SiteCollectionDocuments/quick20energy/KONE_Quick_Energy_2.swf&rdrtrg=http://download.kone.com/quick-energy/kone-quick-energy-2.swf`.

Lanahan, M. and Tabares-Velasco, P. (2017). Seasonal thermal-energy storage: A critical review on btes systems, modeling, and system design for higher system efficiency. *Energies.*

Langevin, C., Thorne, D., Dausman, A., Sukop, M., and W., G. (2008). *SEAWAT version 4: a computer program for simulation of multi-species solute and heat transport.*

Lapidus, L. and Pinder, G. F. (1982). *Numerical solution of differential equations in science and engineering.* Wiley & Sons.

Lee, K. (2013). Underground thermal energy storage. *In Underground Thermal Energy Storage*, pages 15 – 16.

Lei, T. (1993). Development of a computational model for a ground-coupled heat exchanger. *ASHRAE Transactions*, 99.

LU (2014). New tube for london. Technical report, London Underground, London.

LU (2015). Working timetable. Technical report, London Underground, London.

LUL (2013). Annual entries and exits. Technical report, London Underground Limited.

Lundh, M. and Dalenback, J. (2008). Swedish solar heated residential area with seasonal storage in rock: Initial evaluation. *Renewable Energy*, 33:703711.

Mangold, D., Schmidt, T., and Muller-Steinhagen, H. (2004). Seasonal thermal energy storage in Germany. *Structural Engineering International*, 14:230–232.

Mayor, o. L. (2015). London infrastructure plan 2050: Transport supporting paper. Technical report, mayor of London.

McClenahan, D., Gusdorf, J., Kokko, J., Thornton, J., and Wong, B. (2006). Seasonal storage of solar energy for space heat in a new community. *ACEEE Summer Study on Energy Efficiency in Buildings,*, pages 1 – 13. Okotoks, AB, Canada.

McNall, P., Jaax, J., Rohles, F., Nevins, R., and pringer, W. S. (1967). Thermal comfort (thermally neutral) conditions for three activity levels. *ASHRAE Trans.*, 73(1).

Mielke, P., Bauer, D., Homuth, S., E-Gotz, A., and Sass, I. (2014). Thermal effect of a borehole thermal energy store on the subsurface. *Geothermal Energy*, 2(5):1–15.

Molina-Giraldo, N., Blum, P., Zhu, K., Bayer, P., and Fang, Z. (2011). A moving finite line source model to simulate borehole heat exchangers with groundwater advection. *International Journal of Thermal Sciences*.

Monteith, J. L. ; Unsworth, M. H. (1990). *Principles of Environmental Physics*. Royal Meteorological Society.

Mott, M. (2010). Ea report 60121 r1. Technical report, Mott, Macdonnald.

Muraya, N., ONeal, D., and Heffington, W. (1996). Thermal interference of adjacent legs in a vertical u-tube heat exchanger for a ground-coupled heat pump. *ASHRAE Transactions*, 102(3980):1221.

NA (2014). A huge problem is threatening New York's subway system, and no one's talking about it. https://www.businessinsider.com.au/climate-change-will-ruin-the-nyc-subway-2014-12.

Nam, Y., Gao, X., Yoon, S., and Lee, K. (2015). Study on the performance of a ground source heat pump system assisted by solar thermal storage. *Energies*, 8:1337813394.

NASA (2016). Climate impacts. http://www.giss.nasa.gov/projects/impacts/.

Nevins, R., Rohles, F., Springer, W., and Feyerherm, A. (1966). A temperaturehumidity chart for thermal comfort of seated persons. *ASHRAE Trans.*, 72(1):283291.

Newman, T. (2009). The impact of adverse geological conditions on the design and construction of the thames water ring main in greater london. *Quarterly Journal of Engineering Geology and Hydrogeology*, 42:5–20.

Nicholson, D. P., Qing, C., de Silva, M., Winter, A., and Winterling, R. (2014). The design of thermal tunnel energy segments for crossrail. Technical report, Crossrail.

Nora, C., Shemin, G., and McCartney, J. S. (2016). Numerical modeling of a soil borehole thermal energy storage system. *Vadose Zone Journal*, 15(1):1–17.

NYCTA, Electric), G., and (WEC), W. E. C. (2010). An air conditioning study of the new york city transit system, part 1: A thermal system model and equipment valuation.

OFGEM (2018). Tariffs and payments: Domestic rhi. https://www.ofgem.gov.uk/environmental-programmes/domestic-rhi/about-domestic-rhi/changes-scheme.

OIIS (2002). *Thermal comfort on trains*. Cambridge Science Park, Milton road, Cambridge, CB4 0FH.

Palmer, J. and Cooper, I. (2013). United kingdom housing energy fact file. Technical report, Department of Energy and Climate Change, London.

Parker, J. (1972). Air-conditioning related to passenger environment. In MechE, editor, *Railway Division Conference on Passenger Environment*, page 58 63.

Paul, J. (2009). Geology and the london underground. *Geology Today*, 25(1):12–17.

Paul, J. D. (2016). High-resolution geological maps of central London, UK: Comparisons with the London Underground. *Geoscience Frontiers*, 7:273–286.

postglover (2016). Dynamic braking resistors, including those formerly from ipc. `http://www.postglover.com/dynamicbraking.html`.

Qi, H. (2015). *Thermal Performance of the Energy Geotechnical Structures*. PhD thesis, University of Cambridge, Cambridge.

Rad, F. and Fung, A. (2016). Solar community heating and cooling system with borehole thermal energy storage-Review of systems. *Renewable Sustainable Energy Reviews*, 60:15501561.

Rad, F., Fung, A., and Leong, W. (2013). Feasibility of combined solar thermal and ground source heat pump systems in cold climate. *Energy Building*, 61:224 – 232.

RAE (2007). The mathmatics of escalators in the london underground. Technical report, The Royal Academy of Engineering.

Rees, S. and He, M. (2013). A three-dimensional numerical model of borehole heat exchanger heat transfer and fluid flow. *Geothermics*, 46:1–13.

Reuss, M., Beuth, W., Schmidt, M., and Schoelkopf, W. (2015). Solar district heating with seasonal storage in attenkirchen. Technical report, Bavarian Center of Applied Energy Research: Garching, Germany.

Revesz, A., Chaer, I., Thompson, J., Mavroulidou, M., Gunn, M., and Maidment, G. (2016). Ground source heat pumps and their interactions with underground railway tunnels in an urban environment: A review. *Ground source heat pumps and their interactions with underground railway tunnels in an urban environment: A review*, 93:147 – 154.

Revez, A., Chaer, I., Thompson, J., Mavroulidou, M., Gunn, M., and Maidment, G. (2015). Ground source heat pumps and their interactions with underground railway tunnels in an urban environment: A review. *Applied Thermal Engineering*, 93:147 – 154.

Ritchie, I. (2016). Jubilee line mid line vents and escape shafts. http://www.ianritchiearchitects.co.uk/projects/bermondsey$_v ents$/.

Ryu, K. J., Juraeva, M., Jeong, S.-H., and Song, D. J. (2012). Ventilation effeciency in the subway environment for the indoor air quality. *Mechanical and Aerospace Engineering*, 6.

Saner, D., Juraske, R., Kubert, M., Philip, B., Hellweg, S., and Bayer, P. (2010). Is it only co2 that matters ? A life cycle perspective on shallow geothermal systems. *Renewables and Sustainable Energy*.

Sanner, B. (1999). *High Temperature Underground Thermal Energy Storage State-of-the-Art and Prospects*.

Schneider, M. and Moormann, C. (2010). GeoTU6 a geothermal research project for tunnels. *Tunnel*, pages 14–21.

SEAM4US (2014). `http://seam4us.eu/index.php?p=22`.

SES (2001). Subway environmental design handbook, volume ii/ ses version 4.1, part i user's manual. Technical report, Parsons Brinckerhoff Quade & Douglas, Inc.

Sibbet, B. (2012). The performance of a high solar fraction seasonal storage district heating systemfive years of operation. *Energy Procedia*, 30:856865.

Sibbitt, B. and McClenahan, D. (2015). Task 45 Large Systems: Seasonal Borehole Thermal Energy Storage - Guidlines for design and construction. Technical report, International Energy Agency (IEA): Solar Heating and Cooling Program.

Sliwa, T. and Rosen, M. (2015). Natural and artificial methods for regeneration of heat resources for borehole heat exchangers to enhance the sustainability of underground thermal storages: A review. *Sustainability*, 7:1310413125.

Smethurst, J. A., Clarke, D., and Powrei, W. (2012). Factors controlling the seasonal variation in soil water content and pore water pressures within a lightly vegetated clay slope. *Geotechnique*, 62(5):429–446.

Soga, K., , He, Q., , Rui, Y., and Nicholson, D. (2014). Some considerations for designing gshp coupled geotechnical structures based on a case study. *7th International Congress on Environmental Geotechnics*.

Solutions, G. (2014). Glass solutions. `http://www.aisglass.com/pvb_laminated.asp`.

Spitler, J. (2000a). GLHEPRO- A design tool for commercial building ground loop heat exchangers. *Proceedings of the fourth international heat pumps in cold climates conference*.

Spitler, J. D. (2000b). A design tool for commercial building ground loop heat exchangers. In *The Fourth International Heat Pumps in Cold Climates Conference*, Quebec.

Standing, J. and Burland, J. (2006). Unexpected tunneling volume losses in the Westminister area, London. *Geotechnique*.

Stauffer, F., Bayer, P., Blum, P., Kinzelbach, W., and Molina-Giraldo, N. (2013). *Thermal Use of Shallow Groundwater*. CRC Press.

Tfl (2007). *Rolling Stock Data Sheet*. Tfl, 2nd edition.

TfL (2011). Analyzing passengers' onward travel patterns. Technical report, TfL.

TfL (2013). *London Underground, Civil engineering common requirements: Category 1 Standard*.

Tfl (2014). `https://photolibrary.tfl.gov.uk/`.

TfL (2014). Tfl joins danone in giving out bottles of evian on the tube. https://tfl.gov.uk/info-for/media/press-releases/2014/july/tfl-joins-danone-in-giving-out-bottles-of-evian-on-the-tube.

TfL (2016a). A brief history of the under. https://tfl.gov.uk/corporate/about-tfl/culture-and-heritage/londons-transport-a-history/london-underground/a-brief-history-of-the-underground.

TfL (2016b). Facts & figures. https://tfl.gov.uk/corporate/about-tfl/what-we-do/london-underground/facts-and-figures.

Thompson, J. A., Maidment, G., and Missenden, J. F. (2006). Modelling low energy cooling strategies for underground railways. *Applied Energy*, 83:1152–1162.

Thornton, J., McDowell, T., Shonder, J., Hughes, P., Pahud, D., and Hellstrom, G. (1997). Residential vertical geothermal heat pump system models: calibration to data. *Transactions - American Society of Heating, Refrigerating and Air-Conditioning Engineers*, 103:660 – 674.

Toolbox, E. (2014). Engineering toolbox. `http://www.engineeringtoolbox.com/thermal-conductivity-d_429.html`.

Transit (2014). The bi-level coaches. `http://transit.toronto.on.ca/gotransit/2507.shtml`.

UITP (2014). World metro figures. Technical report, International Association of Public Transport.

Wagner, V., Blum, P., Kubert, M., and Bayer, M. (2013). Analytical approach to groundwater influenced thermal response tests of grouted borehole heat exchangers. *Geothermics*, 46:22–31.

Walker, J. B. (1970). *50 years of Rapid Transit, 1864-1914*. Arno Press and New York Times.

Wang, X., Zheng, M., Zhang, W., Zhang, S., and Yang, T. (2010). Experimental study of a solar-assisted ground-coupled heat pump system with solar seasonal thermal storage in severe cold areas. *Energy Building*, 42:21042110.

Warren, P. R. and Parkins, L. M. (1985). Single sided ventilation through open windows. In ASHRAE, editor, *Thermal Performance of Exterior Envelopes of Buildings*, volume 49, pages 209–228.

Water, T. (2013). Lul jubilee line tunnels. Technical report, Thames Water Utilities.

Webb, P. J., Amatya, B.and Soga, K. A. T., Davidson, C., and . Payne, P. (2009). Energy pile test at lambeth college, london: geotechnical and thermodynamic aspects of pile response to heat cycles. In *Gotechnique*, volume 59 of *Issue 3*, pages 237–248. Institution of Civil Engineers.

Westgate, S. and Gilby, M. (2007). Cooling the tube. Technical report, LURS (London Underground Rail Society).

Witte, H. (2013). Error analysis of thermal response tests. *Applied Energy*, 109:302 – 311.

Yavuzturk, C. (1999). *Modeling of vertical ground looop heat exchangers for ground source heat pump systems*. PhD thesis, Oklahoma State University.

Yi, M.and Yang, H., Diao, N., Liu, J., and Fang, Z. (2010). A new model and analytical ssolution for borehole and pile ground heat exchangers. *International Journal for Heat Mass Transfer*, 53:2593–601.

Yi, M., Ping, C., and Zhaohong, F. (2012). *Heat Transfer Modeling of the Ground Heat Exchangers for the Ground-Coupled Heat Pump Systems, Modeling and Optimization of Renewable Energy Systems*. Number ISBN: 978-953-51-0600-5. InTech.

Yuan, F. and You, S.-J. (2007). Cfd simulation and optimization of the ventilation for subway side-platform. *Tunneling and Underground Space Technology*, 22:474–482.

Yuandong, H. and GAO, W. (2010). A numercial study of the train induced unsteady airflow in a subway tunnel with natural ventilation ducts using the dynamic layering method. *Hydrodynamics*, 22(2):164–172.

Zeng, H. Y., Diao, N. R., and Fang, Z. (2002). A finite line-source model for boreholes in geothermal heat exchangers. *Heat Transf. Asian Res.*, 31:558–567.

Zhang, H. (2003). Human thermal sensation and comfort in transient and non-uniform thermal environments. California Digital Library.

Zhang, L., Xu, P., Mao, J., Tang, X., Li, Z., and Shi, J. (2015a). A low cost seasonal solar soil heat storage system for greenhouse heating: Design and pilot study. *Applied Energy*, 156:213222.

Zhang, Y., Choudhary, R., and Soga, K. (2015b). Influence of GSHP system design parameters on the geothermal application capacity and electricity consumption at city-scale for westminster, London. *Energy and Buildings*, 106:3–12.

Zheng, M., Fang, R., and Yu, Z. (2016). Life cycle assessment of residential heating systems: a comparison of distributed and centralized systems. *Energy Procedia*, 104:287 – 292.